PHASE CHANGE MATERIAL BASED HEAT SINK FOR THERMAL MANAGEMENT OF ELECTRONIC DEVICES

Ph.D. Thesis

By

ANUJ KUMAR

DEPARTMENT OF MECHANICAL ENGINEERING

INDIAN INSTITUTE OF TECHNOLOGY INDORE

OCTOBER 2021

PHASE CHANGE MATERIAL BASED HEAT SINK FOR THERMAL MANAGEMENT OF ELECTRONIC DEVICES

A THESIS

Submitted in partial fulfillment of the requirements for the award of the degree

of

DOCTOR OF PHILOSOPHY

by

ANUJ KUMAR

DEPARTMENT OF MECHANICAL ENGINEERING

INDIAN INSTITUTE OF TECHNOLOGY INDORE

OCTOBER 2021

INDIAN INSTITUTE OF TECHNOLOGY INDORE

CANDIDATE'S DECLARATION

I hereby certify that the work which is being presented in the thesis entitled **PHASE CHANGE MATERIAL BASED HEAT SINK FOR THERMAL MANAGEMENT OF ELECTRONIC DEVICES** in the partial fulfillment of the requirements for the award of the degree of **DOCTOR OF PHILOSOPHY** and submitted in the **DEPARTMENT OF MECHANICAL ENGINEERING, Indian Institute of Technology Indore**, is an authentic record of my own work carried out during the time period from July 2018 to July 2021 under the supervision of Dr. Santosh Kumar Sahu, Associate Professor, Indian Institute of Technology Indore and Dr. Shailesh Ishwarlal Kundalwal, Associate Professor, Indian Institute of Technology Indore.

The matter presented in this thesis has not been submitted by me for the award of any other degree of this or any other institute.

06/10/2021

Signature of the student with date
(Anuj Kumar)

This is to certify that the above statement made by the candidate is correct to the best of my/our knowledge.

06.10.2021
Signature of Thesis Supervisor #1 with date
(Dr. Santosh Kumar Sahu)

(DR. S. I. KUNDALWAL) **06.10.21**
Signature of Thesis Supervisor #2 with date
(Dr. Shailesh Ishwarlal Kundalwal)

Anuj Kumar has successfully given his/her Ph.D. Oral Examination held on March 07 2022

08.03.22
Signature of Thesis Supervisor #1 with date
(Dr. Santosh Kumar Sahu)

(DR. S. I. KUNDALWAL)
08.03.22
Signature of Thesis Supervisor #2 with date
(Dr. Shailesh Ishwarlal Kundalwal)

ACKNOWLEDGEMENTS

I would like to express my sincere gratitude to my supervisor, **Dr. Santosh Kumar Sahu**, Department of Mechanical Engineering, Indian Institute of Technology Indore, and **Dr. Shailesh Ishwarlal Kundalwal**, Department of Mechanical Engineering, Indian Institute of Technology Indore, for their valuable guidance, consistent effort and encouragement throughout my research work. I am very grateful to them for their support, motivation and enthusiasm provided to me during the course of this research. At many stages in the course of this research project, I benefited from their advice. Their careful editing contributed enormously to the production of this thesis.

I wish to express my gratitude to my Ph.D. progress committee members, **Dr. Shanmugam Dhinakaran,** Associate Professor, Department of Mechanical Engineering, Indian Institute of Technology Indore and **Dr. Prabhat Kumar Upadhyay,** Associate Professor, Department of Electrical Engineering, Indian Institute of Technology Indore for providing various technical inputs and valuable suggestions, which has greatly helped in shaping this thesis. I am also thankful to Head, DPGC convener, all faculty members and staff of the Department of Mechanical Engineering for their timely help and support throughout.

My sincere acknowledgement and respect to **Prof. Neelesh Kumar Jain,** Director (Officiating), Indian Institute of Technology Indore for providing me the opportunity to explore my research capabilities at **Indian Institute of Technology Indore**. I am grateful to him for providing me financial support to present my research work in International conferences within and outside India.

I am thankful to the **Department of Science and Technology (DST)**, Ministry of Science and Technology, India for the financial supports provided during the tenure of my PhD under the award of the **PROJECT DST/TMD/MES/2k17/65**. I acknowledge the **Ministry of Education (MoE),** India for providing support to purse my research.

I am thankful to **American Society of Mechanical Engineering (ASME),** USA, for the financial support to present my work in **POWER 2021** Virtual, Online conference.

I am thankful to the all the staff members of **Workshop, Advanced Manufacturing Processes lab,** Mechatronics and Instrumentation Laboratory and **Sophisticated Instrument Centre**

(SIC) for their extended effort during development of test facility, fabrication of test surfaces, and characterization at IIT Indore. Many thanks to **Mr. Arun Kumar Bhagwaniya**, Fluid Mechanics and Machinery Lab for his assistance for fabrication of test facility. I am thankful to all the members of **Central Library**, Indian Institute of Technology Indore for extended help during my Ph.D. work.

I owe a debt of gratitude to my seniors, lab mates, and colleague researchers in particular. **Mr. Rohit Kothari, Dr. Vishal Nirgude, Dr. Avadhesh K Sharma, Dr. Saurabh Yadav, Mr. Pushpanjay K. Singh, Dr. Mayank Modak, Dr. P. Maheandera Prabu, Dr. Hari Mohan, Dr. Dharmendra Panchariya, Mr. Jay Joshi, Mr. Pawan Sharma, Mr. Akhalesh Sharma, Mr. Pradeep Singh, Mr. Vivek Saxena, Mr. Jayanta Sutradhar, Mr. Pawankumar Singh, Mr. Rushikesh Vaidya, Mr. Ameya A. Chitre, Mr. Akash K. Singh**, Mr. Sai Praveen Surapu, Dr. Vijay Choyal, Dr. Ankit Rathi, Dr. Vijay K. Choyal, Dr. Kishor Shingare, Mr. Subhash Nehwal, Mr. Yogesh Andhale, Mr. Rajnish Modanwal, Mr. Madhur Gupta, Mr. Nitin Luhadia, Mr. Pradunmya Dutta, Mr. Kaushik Prince, Mr. Anupam Kumar, Mr. Vivek Rana, Mr. Pankaj Kumar, Mr. Bhavesh Chaudhary, Mr. M. Manikandan, Anas Ullah Khan, Mr. Shriprasad Chorghe, Mr. Manish Carpenter, Mr. Vishal Jagdale, Mr. Devashish Chorey, Mr. Abhinav Sharma, Mr. Pavan Gupta, Mr. S. Jayachandran, Mr. Ajinkya Sonawane, Mr. Vishal Kharka, Mr. Pravin Kumar, and Mr. Navdeep Srivastava for their cooperation during the course of my research.

I would like to express my sincere respect to **my parents** and **my late brother Birendra K. Shaw** for their love, care, and support they have provided to me throughout my life. Special thanks to **my brothers (Ravindra K. Shaw and Rahul K. Shaw), sisters (Nitu Shaw, and Chandani Shaw), and sister-in-law (Priyanka Shaw)** for their support and encouragements. I want to show my deepest love to my cute nephew **Anurag** and nieces **Ruhi, Rashi, Khushi, Nikita, Aradhya,** and **Ananya** for bringing happiness in my life.

Finally, I am thankful to all who directly or indirectly contributed, helped and supported me. I always learned and believed that I want to sum up in one line.

“The purpose of human life is to serve and to show compassion and the will to help others”

Finally, I would like to sign off with a very popular mantra.

ॐ असतो मा सद्गमय ।
तमसो मा ज्योतिर्गमय ।
मृत्योर्मा अमृतं गमय ।
ॐ शान्तिः शान्तिः शान्तिः ॥

Lead us from the unreal to the real
Lead us from darkness to light
Lead us from death to immortality.
Om peace, peace, peace.

Anuj Kumar

Dedicated to my family and friends

for their love, care and blessings

ABSTRACT

The present dissertation reports the theoretical and experimental studies on the thermal behavior of phase change materials (PCMs) during the melting and solidification process. The objective of the present investigation is to identify the best PCMs for thermal management application and study the thermal performance of PCM-based heat sinks with different thermal conductivity enhancers for thermal management of electronic components.

Initially, multi attribute decision making (MADM) technique is proposed to obtain the optimal PCM for the thermal management of electronic components. Three MADM techniques, namely technique for order of preference by similarity to ideal solution (TOPSIS), fuzzy TOPSIS, and VIKOR, are employed to estimate the best PCM. The analytic hierarchy process (AHP) method is employed to obtain the weight of the attributes used for PCM selection. Different types of PCMs, namely organic, inorganic, and eutectics with their important attributes as applicable for thermal management systems, are pre-screened for the analysis. Based on their properties, thirty PCMs and eleven attributes are considered for the analysis. The results show that MADM techniques such as TOPSIS, fuzzy TOIPSIS, and VIKOR can be used for the optimal selection of PCM.

In addition, thermal performance of various heat sink configurations involving different numbers of cavities (1, 4, 9, 16, 25, and 36), formed by cross plate fins arrangement, as applicable to thermal management of electronic components, are studied numerically by employing pressure-based finite volume method. Here, the mass and thermal capacity of each PCM-based heat sink configuration is kept the same for all the cases. The performance of various heat sink configurations is evaluated based on the transient temperature variation of the heat sink base, PCM melt fraction, average Nusselt number, and energy absorbed by PCM through both latent and sensible heat. The study also investigates the effect of various PCM materials on the thermal performance of heat sinks. The performance of the heat sink is found to increase with the increase

in number of cross fins. Efforts have also been made to investigate the hollow fins filled with PCM to characterize the heat transfer performance.

Furthermore, a test facility has been developed to evaluate the heat transfer performance of PCM-based heat sinks for thermal management of the electronic device. Tests are carried out to investigate the thermal performance of various PCM-based heat sinks involving without and with parallel plate fins, cross plate fins, circular pin fins, and square pin fins. Efforts have been made to incorporate copper oxide nanoparticles in PCM to estimate the effect of nano-enhanced PCM (NePCM) on thermal performance. In addition, the thermal performance of heat sinks is estimated with foam-PCM composite; both metallic (copper) and non-metallic (carbon) foam are used in the analysis. Effect of various input parameters such as heat flux, the volume fraction of thermal conductivity enhancer (TCE), the volume fraction of PCM, mass fraction of nanoparticles, and set point temperature (SPT) on the thermal performance of various heat sink configurations are studied through experimental investigation. Enhancement ratios are obtained for various heat sink configurations. The performance of various heat sinks is compared. It is found that the heat sink with carbon foam (CF)-PCM composite can be utilized for the effective cooling of electronic components.

***Keywords*:** *Thermal management, thermal energy storage, phase change materials, melting/solidification, melt fraction, heat sink, enhancement ratio, set point temperature, foam-PCM composite, nano-enhanced phase change material.*

TABLE OF CONTENTS

LIST OF FIGURES

LIST OF TABLES

NOMENCLATURE

English symbols

a_{ij}	Element of pairwise comparison matrix in Eq. (2.1)
A	Pairwise comparison matrix in Eq. (2.1)
A(∅)	Porosity function in Eq. (3.6)
A^*	Positive ideal solution in Eq. (2.13)
A'	Negative ideal solution in Eq. (2.13)
C_p	Specific heat at constant pressure *(J/kgK)*
C_i^*	Relative closeness index in Eq. (2.17)
d	PCM thickness (mm)
d_{ij}	Element of decision matrix in Eq. (2.11)
D	Decision matrix in Eq. (2.10)
E	Small computational constant in Eq. (3.6)
Fo	Fourier number, $\frac{\alpha t}{l_c^2}$
g	Acceleration due to gravity (m/s^2)
G	Thermal conductance (W/K)
h	Height of the fin (mm)
$\bar{h}$	Average surface heat transfer coefficient ($^{W}/_{m^2K}$)
H	Total enthalpy (J/kg)
J	Beneficial attribute in Eq. (2.14)
J'	Non-beneficial attribute in Eq. (2.14)
k	Thermal conductivity (W/mK)

l_c	Characteristics length (m)
L	Latent heat of PCM (J/kg)
m	Mass (kg)
M	Number of rows in Eq. (2.10)
n_{ij}	Elements of normalized matrix in Eq. (2.11)
N	Number of columns in Eq. (2.10)
$\overline{Nu}$	Average Nusselt number, $\frac{\bar{h} l_c}{k}$
p	Pressure (N/m^2)
P	Power (W)
q''	Heat flux (kW/m^2)
Q_{loss}	Heat loss (W)
R_i	Regret measure in Eq. (2.25)
$\vec{S}$	Momentum source term (N/m^3) in Eq. (3.3)
S_i	Utility measure in Eq. (2.24)
S_i^+	Distance from the positive ideal solution in Eq. (2.15)
S_i^-	Distance from the negative ideal solution in Eq. (2.16)
Ste^*	Modified Stefan number, $\frac{C_p q'' l_c}{kL}$
t	Time *(s)*
$t_{Cr\ with\ PCM}$	Time to reach critical SPT with PCM (s)
$t_{Cr\ without\ fins\ and\ PCM}$	Time to reach critical SPT without fins and PCM (s)
T	Temperature ($°C\ or\ K$)

ΔT	Temperature difference ($°C$ or K)
T_{max}	Maximum temperature after charging phase ($°C$ or K)
T_{amb}	Ambient temperature ($°C$ or K)
$\vec{\boldsymbol{u}}$	Velocity vector (m/s)
v	Weight for maximum group utility in Eq. (2.26)
V_f	Volume occupied by fins (mm^3) in Eq. (4.6)
V_{HS}	Volume of HS cavity (mm^3) in Eq. (4.6)
V_{PCM}	Volume of PCM (mm^3) in Eq. (4.6)
w_j	Weight of the attribute in Eq. (2.12)
Wt	Weight (N) in Eq. (4.5)
Z_{ij}	Element of weighted normalized matrix $Z_{ij} = [n_{ij}] \times [w_{j1}]$
Δz	Thickness of insulation in Eq. (4.1)

Greek symbols

α	Thermal diffusivity (m^2/s) in Eq. (3.17)
β	Thermal expansion coefficient, (K^{-1}) in Eq. (3.1)
γ	Copper oxide mass fraction in Eq. (4.2)
δ	Thermal capacity (J/K) in Eq. (4.10)
ε	Enhancement ratio in Eq. (4.9)
$\emptyset$	Melt fraction in Eq. (3.7)
φ	PCM volume fraction in Eq. (4.6)
ψ	Volume fraction of nanoparticles
ξ	Volume fraction of TCE in Eq. (4.7)

μ	Dynamic viscosity of PCM (kg/m-s)
ρ	Density of PCM (kg/m^3)
τ	Dimensionless time in Eq. (3.19)

Subscripts

abs	Absorbed
amb	Ambient
c	Characteristics
i, j	Row and column of a matrix in Eq. (2.1)
i	Initial
in	Input
ins	Insulation
l	Liquid
lat	Latent
m	Mean
ref	Reference
s	Solid
sen	Sensible
t	Total

Abbreviations

CF	Carbon foam
CoF	Copper foam

CRN	Corrosion
DSC	Differential scanning calorimeter
HS	Heat sink
HSNF	Heat sink with no fin
HSCPF	Heat sink with circular pin fin
HSRPF	Heat sink with rectangular plate pin fin
HSSPF	Heat sink with square pin fin
IM	Incongruent melting
LH	Latent heat
np	Nanoparticle
PCM	Phase change material
SC	Subcooling
SH	Specific heat(J/kgk)
SPT	Set point temperature
TS	Thermal stability
TCEs	Thermal conductivity enhancers
TOX	Toxicity

Chapter 1

Introduction and literature survey

1.1 General background

The invention of transistor during 1947 resulted in the miniaturization of electronic devices, subsequently increased the number of components per chip. The invention of an integrated circuit (IC) further enabled the increase in the number of devices per chip. Over the years, the electronic industry has been driven according to Moore's law, i.e., an increase in the number of transistors per silicon chip becomes double each year. Currently, the computer chip employs nearly 10 billion transistors with a characteristics length of ~ 10 nm housed in 500-1000 mm^2 area [1-2]. The invention of both transistor and the integrated circuit has increased the packaging density (number of components per chip) of the electronic components and led to the miniaturization of electronic devices. The advancements in transistor's performance, the reduction in chip area, higher processing speeds have led to higher heat generation, resulting in higher operating temperature of electronic components. Higher operating temperature of the electronic components for a longer period causes a rapid decrease in performance, efficiency, reliability, and early failure of critical components. It has been argued by the US air force that after 75 °C, the failure rate of electronic components due to overheating follows an exponential trend [3]. In addition, various studies report that 55% of modern electronic devices fail due to overheating [4-5]. In view of this, it is essential to develop an advanced thermal management system to maintain the peak performance, keep the temperature below the critical limits and enhance the reliability of modern electronic components.

1.2 Thermal management techniques

Efficient thermal management of electronic components plays a crucial role in the design of the component. The thermal management techniques for electronic components can be broadly classified into two categories such as active and passive cooling techniques, as shown in Fig 1.1 [6].

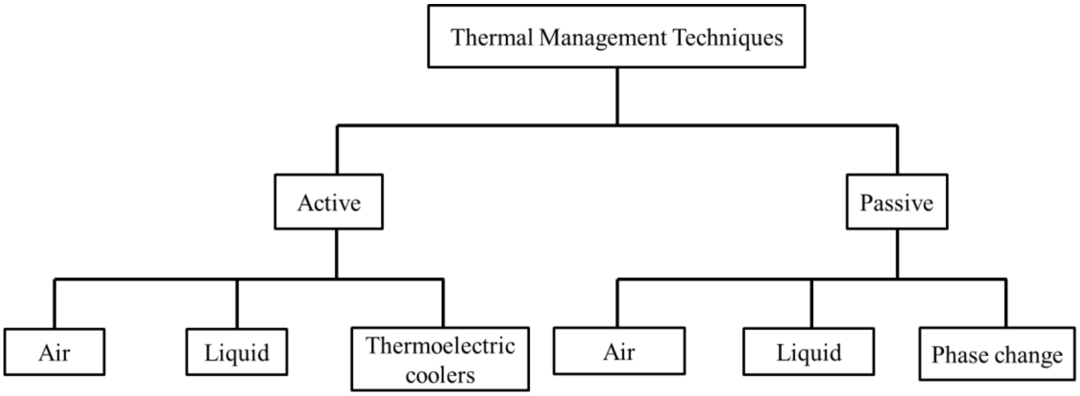

Fig. 1.1 Classification of thermal management techniques

1.2.1 Active cooling techniques

Active cooling techniques refer to cooling technologies that need an external power source to cool electronic devices. In this technique, the desired cooling effect is obtained by circulating the heat transfer fluid at a higher rate. It includes forced circulation of various fluids, including air and water. Also, one can use thermoelectric coolers (TECs) for cooling. The details are elaborate below.

Air cooling

Air is forced to flow over the heating surface with the help of a fan or blower to remove excessive heat from the hot surface (Fig. 1.2).

Fig. 1.2 Photographic view of active cooling module [8, 9]

Air cooling is commonly combined with a heat sink to achieve a faster heat dissipation rate. This cooling technique is generally used in chipsets, hard drives, computer cases, and CPUs to reduce temperature-related failures [7]. A large size fan is required to achieve a higher heat transfer rate [8, 9].

Liquid cooling

Liquid coolant is circulated through a tubing arrangement with the help of a pump in a closed-loop system to remove the heat from the hot surface. This cooling technique is used in cold plates mounted on the back side of the printed circuit board (PCB) containing a heat source. Liquid coolant present in a cold plate removes the heat generated by the source and transfers the heat energy to a secondary heat exchanger. Cooled liquid flows back to the cold plate with the help of a pump, and the cycle repeats during the process [8, 9]. The leakage of coolant is the major issue in this type of cooling.

Thermoelectric coolers (TECs)

The thermoelectric coolers (TEC) use semiconductor devices that utilize the Peltier effect to transfer heat from one surface to another surface. These devices are also known as Peltier coolers [9]. In order to cool the heat source, electrical power is provided to TECs, and the current starts flowing across two junctions. The flow of current between two terminals causes the temperature difference and results in a flow of heat from the source to sink through conduction. The TECs usually have long service life but are less efficient [10-12].

1.2.2 Passive cooling techniques

Passive cooling techniques do not have any rotating elements, and thus external power is not required for its operation [6]. In this technique, capillary or gravitational buoyancy forces circulate the heat transfer fluid. Also, extended surfaces provide more surface area and promote the heat transfer rate. Heat sinks, heat pipes, heat spreaders are some examples of passive cooling techniques.

Air cooling

Heat sinks and heat spreaders are examples of passive air cooling systems. Heat sinks are made of high thermal conductive materials such as copper and aluminum to minimize the temperature difference between the heat source and fin tip; they have protruding surfaces (fins) that increase the surface area (Fig. 1.3). Heat sinks are mounted over the heat-generating source; the heat is transferred to the heat sink by conduction. Subsequently, air takes heat from the heat sink and dissipates to the surrounding by convection and radiation [9]. The heat sink base and the top surface of the chip (heat source) are different; therefore, heat spreaders are used between the heat sink and heat source for higher heat dissipation. Heat spreaders are high thermal conductivity materials and act as heat exchangers with favorable geometry and surface area compared to the heat source [7, 8].

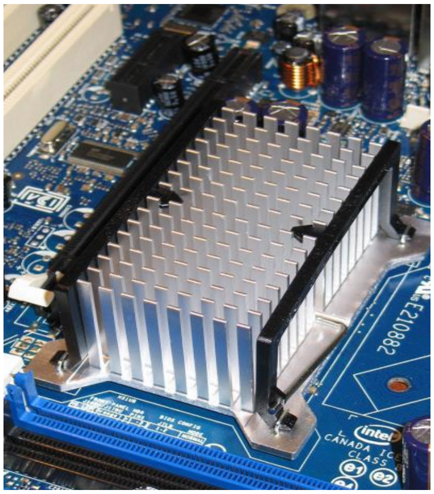

Fig. 1.3 Photographic view of heat sink module [7, 8]

Liquid cooling

Liquid coolant is used in various applications. Dielectric fluids such as silicon/mineral oil and synthetic/natural esters are widely used in various industrial applications, including cooling of high power transfer windings [13-15]. Dielectric fluids take the heat from the winding, and viscosity decreases, which enhances the flow rate leading to the increase in cooling efficiency. It may be noted that the cooling capacity of dielectric fluid decreases with time due to exponential temperature change [16]. Many a time, different fluids, including nanofluids, are used for cooling applications. Other heat transfer fluids, namely glycol-water mixture, hydrocarbon oils, refrigerants, and phase change fluids are used as coolants.

Phase change cooling

In the phase change cooling technique, the storage material takes the heat from the source and changes its phase. In general, the phase change can occur from liquid to vapor or solid to liquid during heat storage and vice versa during heat dissipation [17]. The storage materials used in this technique are known as phase change materials (PCMs).

Heat pipe or thermosyphon uses liquid-vapor phase change cooling technique to remove heat from the heat source. It consists of an evaporator that absorbs heat from the heat source and a condenser that dissipates heat to the surrounding (Fig. 1.4). The liquid present in the heat pipe takes heat from the source and changes its phase from liquid to vapor; subsequently, the generated vapor moves to the condenser region due to density and pressure differences and releases heat in the condenser while changing its phase from vapor to the liquid. The condensate returns to the evaporator region, and the entire cycle repeats [8, 9]. The liquid-vapor thermal storage technique is complex because of high pressure and large volume requirement.

The solid-liquid phase change process is another cooling technique in which no rotating part is involved in the process. In this technique, storage material takes heat from the source and changes its phase from solid to liquid [18]. This maintains the temperature of electronic devices near the melting temperature (isothermal phase change) of phase change material [18]. This process is called the melting or charging process. The PCM rejects heat to the surrounding by natural convection in the cooling/discharging process and again changes its phase from liquid to solid.

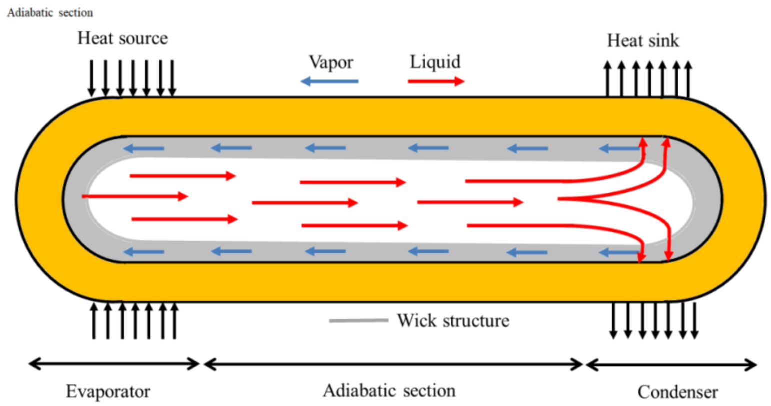

Fig. 1.4 Schematic of a heat pipe

1.2.3 Comparisons between active and passive cooling techniques

In an active cooling technique, external power is used to supply energy in the fluid, increasing fluid flow and heat transfer. In general, air or water is forced to circulate over the heat exchanging components to dissipate heat. However, these techniques need large space, regular maintenance, higher power requirement, and generate noise, resulting in higher operating costs [19-22]. On the other hand, passive thermal management techniques do not require any external power source to achieve the required cooling. Here, various forces such as capillary and gravity-induced buoyancy promote fluid circulation on the heat exchanging components. Table 1.1 shows the comparison among various available techniques [23].

Efforts have been made to use the combination of heat spreaders and heat sinks for thermal management applications. In such a case, the heat dissipation is limited due to lower natural convection inside the closed space. It may be noted that many a time, portable electronic devices tend to operate with higher temperatures for a certain time period followed by a rest period or lower temperature for improved response [24]. This occurs due to the power spikes, which increases the probability of failure of electronic devices. The constant increase in heat flux densities, harsher conditions, miniaturization, and ever-increasing performance requirements continue to challenge the thermal engineer. These continuous growths in electronics necessitate innovative thermal management techniques. The low heat generating portable electronic devices rejects heat in the range of 5-10W [22], and the heat flux varies in the range of

1.0- 3.5 kW/m^2. For high heat-generating electronic components, heat flux can be significant, and they can vary from 50 kW/m^2 for the printed circuit board to 20000 kW/m^2 for a semiconductor laser. The repetitive periodic heat source cycle includes a steady heat generation period followed by no heat generation period. Various modern electronic devices such as cellular phones, laptops, light-emitting diode (LED), digital cameras, notebooks, personal digital assistants (PDA), control systems in missiles, and avionics needs to be maintained in the temperature range of 40-60 °C for efficient working. As a result, novel cooling solutions, such as multiphase heat transfer technologies and other alternatives, are being developed to address the high heat flux issues in advanced modern electronic components. Passive air and liquid cooling techniques may not be suitable to remove heat under this situation due to the enhanced thermal cycling effect. However, phase change materials can absorb the excessive heat generated during spikes and dissipate during the rest period, and such arrangements can prevent the failure of electronic components [24].

Table 1.1 Comparison among various available techniques [23]

Parameters	Air	Liquid	Heat pipe	PCM
Ease of use	Easy	Difficult	Moderate	Easy
Life	≥ 20 years	3-5 years	≥ 20 years	≥ 20 years
Annual cost	Low	High	Moderate	Low
Integration	Easy	Difficult	Moderate	Easy
Efficiency	Low	High	High	High
Temperature drop	Small	Large	Large	Large
Temperature distribution	Uneven	Even	Moderate	Even
Maintenance	Easy	Difficult	Moderate	Easy

1.3 Phase change material

Phase change material (PCM) is a thermal energy storage material that usually undergoes phase change at certain temperatures and stores a large amount of heat in the form of latent heat. Generally, latent heat energy is absorbed by a material during various phase changes, namely solid-liquid and liquid-vapor. Although a larger amount of heat is stored during the liquid-vapor phase change process, this is not preferred due to larger volume change and higher pressure. In view of this, the solid-liquid phase change process is widely adopted for a thermal energy storage system for various industrial and engineering applications [25-26].

Fig. 1.5 illustrates the ideal working of a solid-liquid PCM-based cooling system. During the charging process, the heat dissipated by electronic components is absorbed by the PCM in the form of sensible heat, resulting in a temperature rise of PCM. When the temperature of the PCM reaches its melting temperature, it melts by absorbing latent heat, and the process continues till the complete melting of PCM, followed by an increase in PCM temperature due to a sensible heating process. During the discharging process, the same process occurs but in reverse order. Both the melting and solidification processes are assumed to be nearly isothermal.

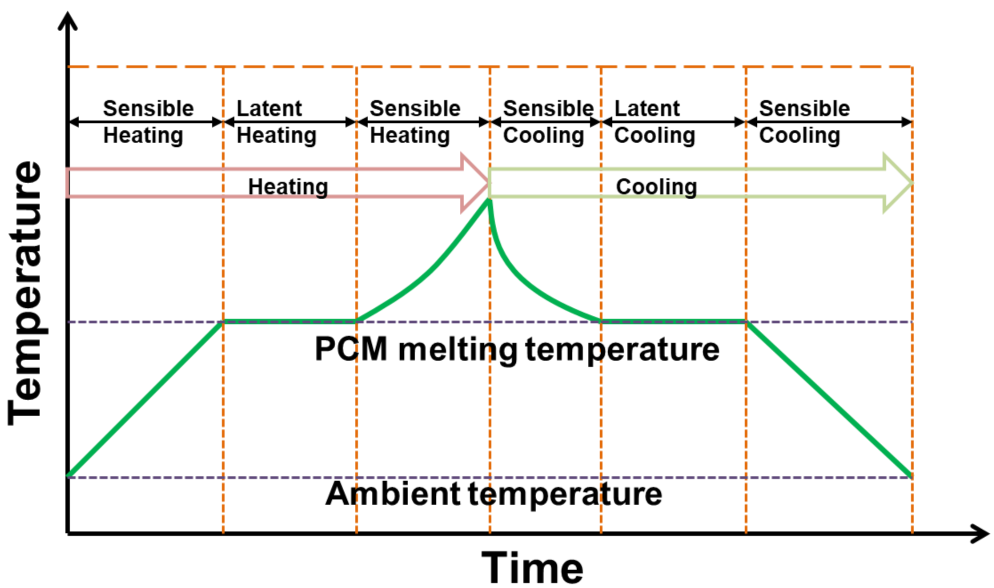

Fig. 1.5 Ideal heating and cooling curve of PCM-based thermal management system

1.3.1 Classification of PCMs

The PCMs are broadly classified into three categories: organic, inorganic, and eutectic, as shown in Fig. 1.6. The organic PCMs are classified into paraffin and non-paraffin compounds. Organic PCMs undergo phase change in temperature range varying between 15-130 °C [27] and exhibit very good thermal stability even at higher working temperature (500°C). These PCMs possess congruent melting, i.e., the composition of liquid and solid maintain the same composition, and charging and discharging occur repeatedly. The latent heat of fusion and the melting point of organic PCMs are found to increase with the increase in the length of the carbon chains, and they involve very little subcooling effect. Organic PCMs are non-corrosive, non-toxic, safe, reliable, recyclable, and less expensive. Because of these advantages, organic PCMs are widely used for thermal energy storage and thermal management applications. It may be noted that the thermal conductivity value of organic PCM is very poor. Inorganic PCMs (salts, salt hydrates, and metals) usually change their phase at a higher temperature compared to organic PCMs. Due to their higher latent heat of fusion and higher phase change temperature, they (especially salts) are used for large-scale industrial applications, including solar thermal energy systems [28]. However, their incongruent melting behavior prevents their use for thermal management applications [28]. This reduces the reversibility of the phase change process and heat storage ability. Also, the metallic salt exhibits higher weights. Although they possess higher thermal conductivity compared to organic PCMs, their high corrosive and toxic nature limits their applications.

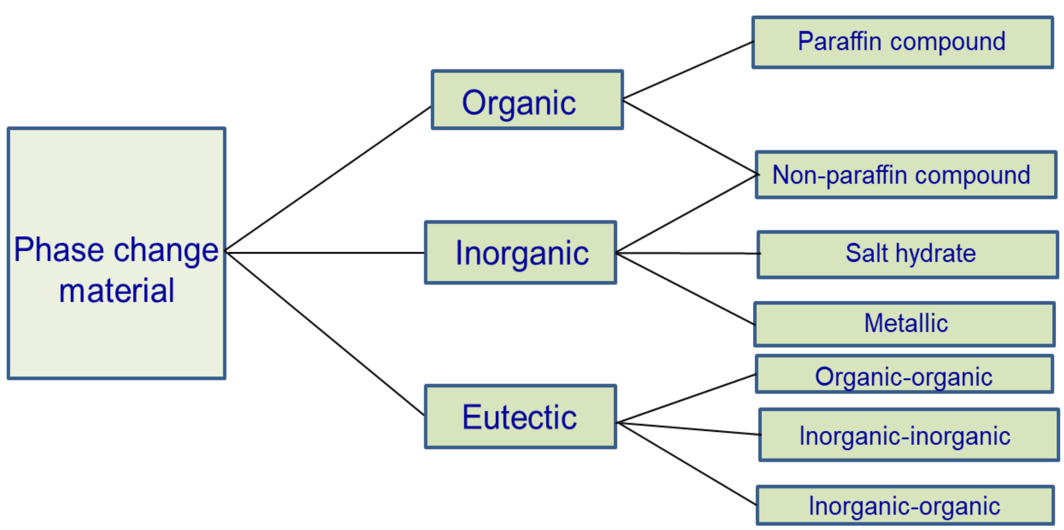

Fig. 1.6 Classification of PCMs

Eutectic PCMs are a mixture of two or more substances (organic/inorganic) with nearly same melting/solidification temperature. More studies are needed to analyze the thermophysical properties of these eutectics.

1.3.2 Selection of PCM

The selection of PCM for a specific application usually depends on its chemical and physical properties. For thermal management of electronic components, PCM is expected to possess the following properties [29, 30].

- The initiation of melting of PCM should take place at the design temperature, which must be lower than the safe working temperature of the electronic components.
- PCM should exhibit congruent melting behavior and must have a similar overall composition in both solid and liquid phases.
- In order to make the system lightweight, PCM should have a high value of latent heat of fusion and specific heat.
- In order to accelerate the charging and discharging rate, PCM should have a higher value of thermal conductivity.
- The volume expansion of PCM upon melting and vapor pressure should be very low to avoid the issue of confinement.
- The PCM should have a very low subcooling effect during solidification [31, 32].
- The PCM must be chemically and thermally stable and should be corrosion-free, non-explosive, and non-flammable.
- PCM should be easily available on a large scale, cost-effective, and recyclable.

It may be noted that a single PCM may not have all the properties mentioned above; for example, organic PCMs possess congruent melting but have lower thermal conductivity values. On the other hand, inorganic PCMs have higher thermal conductivity values but undergo incongruent melting. In such a case, one needs to employ the multi attribute decision making technique to select optimal PCM for thermal management applications.

1.3.3 Application of PCMs

The use of PCM in a different application has been reviewed by various authors and is summarized in Table 1.2. Due to the higher value of latent heat absorption capacity, PCMs are widely used in various engineering and industrial applications, including thermal management of photovoltaic panels, electronic components, electric vehicle batteries, buildings; also finds application in solar cookers, solar water heaters, and waste heat recovery. The applications of PCM are detailed below.

- Buildings: The building sector plays a major role in total energy consumption and emission of CO_2. In such a case, residential buildings can be designed to reduce energy consumption and control the indoor temperature automatically. The PCMs are used as a thermal energy storage system and help to moderate the indoor temperature.
- Solar energy: Solar energy is a renewable energy source that can be used for various applications. The efficient use of solar energy requires a storage medium that can facilitate the storage of excess energy, and PCM can efficiently store this energy in the form of latent and sensible heat. This energy can be used for different applications such as solar cooking, water heating, space heating, power generation, and drying of agricultural products.
- Satellite and spacecraft: Various critical components associated with remote sensing, satellite payloads, and spacecraft operate on repeated transient duty cycles, which generate a larger amount of heat. In such a case, PCM-based thermal management technique is required to control the excess temperature fluctuations of the components effectively.
- Transportation: The PCMs can be utilized to maintain the temperature of food products under certain limits and prevent the defrosting of frozen food. Also, the temperature of medical equipment can be controlled by using PCM material.
- Waste heat recovery: A large amount of energy is wasted when the heat energy is released to the surroundings in different sectors such as

residential, engineering, and transportation. In such a case, the PCM can be utilized to store this energy, and the same can be used for different applications.

- Thermal management: To improve the performance and reliability of the electric vehicle battery module, it is necessary to maintain the temperature of Li-ion batteries under a certain limit. Also, the reliability of electronic devices can be improved with the removal of excess heat from the electronic components. The utilization of PCM as the latent heat storage can increase the performance and reliability of Li-ion batteries and electronic components.

Table 1.2 Research and review studies on different applications of PCM

Applications	Source
Thermal management of battery modules	Osterman et al. [30], Nematpaur et al. [33], Asefi et al. [34]
Solar energy storage	Xu et al. [35], Liu et al. [36]
Satellite and spacecraft thermal control	Raj et al. [37], Kim et al. [38], Kansara et al. [39], Mulligan et al. [40]
PCM for cold thermal energy storage	Oro et al. [41]
Waster heat recovery	Gutierrez et al. [42], Nomura et al. [43], Shon et al. [44]
Thermal management of battery modules	Kim et al. [45], Siddique et al. [46], Jaguemont et al. [47]
Thermal management of electronic components	Sahoo et al. [48], Cai et al. [49],
Solar drying	Kant et al. [50]
Cooling of Photovoltaic modules	Islam et al. [51], Waqas et al. [52]

1.3.4 Limitation of PCMs

Many a time, the PCMs do not have all the desirable properties as reported in section 1.3.2. The limitations of PCMs can be summarized below.

- Low thermal conductivity: PCMs, especially organic, possess a low thermal conductivity value, which decreases the heat transfer rate. This slows down the charging and discharging rate of PCM, which affects the cooling performance. To counterbalance the lower value of thermal conductivity of PCM, it is necessary to introduce thermal conductivity enhancers (TCEs).

- Incongruent melting: The PCMs, especially inorganic and eutectics, are highly incongruent due to the presence of a large amount of hydrated salts. Due to this, PCM undergoes phase separation due to their different composition, reducing the reversibility of the phase change process and the storage efficiency. One can adopt mechanical stirring and encapsulation to avoid such issues.
- Supercooling: In the supercooling condition, the liquid PCM is cooled below its theoretical solidification/melting temperature while remaining in a liquid state; this occurs because of the poor nucleation rate in the PCM. This effect reduces the ability to retrieve the energy from the PCM. The phenomena of supercooling are more common in inorganic PCM.
- Thermal stability: For practical application, the PCM needs to undergo a large number of thermal cycles (melting/solidification) without losing its inherent properties. The degradation of thermo-physical properties of PCM over time is not desirable for any PCM. Therefore, PCM must be stable during different thermal cycles.

In addition, various issues such as corrosion of heat sink material, toxicity, and flammability are observed in PCMs that affect their use in thermal management applications. In general, organic PCMs are thermally stable, non-toxic, non-corrosive, possess little sub-cooling, and are available in the large temperature range [31, 32]. However, the major drawback of organic PCMs is their lower value of thermal conductivity [53]. To counterbalance the low thermal conductivity of PCM, various thermal conductivity enhancers, namely metallic fins, metallic/non-metallic nanoparticles, and metallic/non-metallic foams, are incorporated with PCM, and the details are elaborated in the subsequent sections.

1.4 Thermal conductivity enhancers

Currently, efforts have been made to develop compact and effective thermal management systems for electronic components. The PCM-based passive cooling technique is a very promising cooling technique due to its large latent heat storage capacity and nearly isothermal phase change behavior. This technique can be used for cooling various electronic devices such as laptops, cellular phones, power electronic equipment [54, 55], light-emitting diodes (LED), control systems in missiles [56, 57], and spacecraft [58, 59]. The organic PCMs, satisfy most of the ideal properties needed for thermal management of electronics; however, they exhibit a lower value of thermal conductivity, which results in slow melting and solidification. In order to promote the melting/solidification rate, various TCEs such as metallic extended surface (fins) [60-71], metallic/non-metallic nanoparticles [72-78], and metallic/non-metallic foams [79-84] are incorporated in the PCM. The details of TCE materials are elaborated below.

- Extended surface (fins): Integration of extended surface with PCM-based heat sink is the most convenient and effective way to enhance the effective thermal conductivity of the system and increase the heat transfer rate. This concept was first proposed by Abhat et al. [85] and subsequently implemented by Humphrey et al. [86]. The performance of a PCM-based heat sink depends on different parameters such as fin shape, fin size, number, height, and fins arrangement (parallel/staggered). The most common types of fins are plate and pin fins.
- Metallic/non-metallic nanoparticles: The addition of nanoparticles in PCM, termed as nano-enhanced PCM (NePCM), is considered the most effective way to enhance the thermal conductivity because of its light weight [87-90]. The thermal performance of such systems is found to depend on various parameters such as nanoparticle dispersion method, nanoparticle mass fraction, size, and type of particles. However, the addition of nanoparticles to the PCM increases the viscosity at higher nanoparticle concentrations, which suppresses the convection effect.
- Metallic/non-metallic foams: Among various TCEs, metallic/non-metallic foams in PCM integrated heat sink provide a higher surface area to volume ratio, good thermal conductivity, and considerable weight reduction [79-84]. Various metallic/non-metallic foams such as aluminum,

copper, nickel, and carbon are found to be most effective in enhancing the thermal performance of PCM-based heat sinks. The foams help to transport the heat from chips to the PCM through the webbed ligaments effectively. However, the performance depends on foam structure, types of foams and foam porosities, and pores per inch (PPI).

1.5 Review of literature

Various theoretical and experimental investigations have been carried out to enhance the thermal performance of PCM-based heat sinks. These include the selection of PCM for latent heat thermal energy storage and PCM-based passive cooling. Also, efforts have been made to analyze the effect of different TCEs such as fins, metallic/non-metallic nanoparticles, and metallic/non-metallic foams to augment the performance of PCM-based heat sinks. The studies relevant to the present dissertation are reported in the subsequent sections.

1.5.1 Theoretical investigation

In recent years, efforts have been made to propose novel PCM- based cooling systems that are compact, efficient, and economical. In such a case, among other parameters, selecting the best PCM plays a crucial role in designing PCM-based heat sinks. This section presents the studies pertaining to the optimal selection of PCM for thermal energy storage/thermal management systems. Also, the numerical studies pertaining to the thermal performance of PCM-based heat sinks are reported in this section.

Optimal selection of PCM

The selection of the best PCM for a specific application plays a crucial role in the design of PCM-based heat sinks. The PCM should possess various parameters such as adaptability, safety, reliability, and low cost for its use for a specific application. It is difficult to find the PCM that possesses all the ideal properties required for thermal management, as reported in section 1.3.2. In such a case, the engineer needs to consider various attributes to select the best PCM for a specific application. In view of this, various researchers used multi attribute decision making (MADM) techniques to select the best PCM for a specific application. The MADM technique can be employed to select the best material among various alternatives considering a large number of attributes or criteria. Numerous MADM techniques have been employed by various researchers to select the optimal material, sites, methods, manufacturing processes, and other engineering applications. These include ELimination and Choix Traduisant la Reality (elimination and choice expressing the reality) (ELECTRE), analytical hierarchy process (AHP), case-based reasoning (CBR), simple additive weighing (SAW), goal Programming (GP), VIseKriterijumska Optimizacija I Kompromisno Resenje (VIKOR), digital logic method (DLM), multi attribute utility theory (MAUT) and technique for order of preference by similarity to ideal solution (TOPSIS).

Barrenche et al. [93] carried out a detailed study to create a database that facilitates the selection of the most suitable PCM for domestic hot water applications in buildings. The authors considered more than 300 PCMs with phase change temperature varying between 50-150 °C. The cambridge engineering selector (CES) software proposed by Granta design [94] was utilized to select the best PCM. The software is a very intuitive tool for the design engineer to select the appropriate material for the specific application considering various alternatives and attributes. The new database is created based on two important properties of PCM, such as melting temperature and latent heat of fusion. The authors reported that PCM with melting temperature varying between 50-65 °C is suitable for domestic hot water (DHW) application and proposed that salt hydrate PCM are most suitable for the given application. Khare et al. [95] also utilized the CES material selection software to find out the suitable materials for a solid-state sensible heat storage system for higher operating temperature (>500 °C). The authors considered several factors such as thermal conductivity, energy density, mechanical strength, embodied energy, and greenhouse gas emission to select the suitable material. High-temperature composite materials such as alumina concrete and alumina-silicate are a promising group of sensible heat storage materials. Rathod and Kanzaria [96] employed a methodological concept to choose the best

PCM for thermal energy storage solar water systems. They employed TOPSIS and fuzzy TOPSIS techniques to estimate the best PCM among nine alternatives. The analytic hierarchy process (AHP) method is utilized to estimate the weight of the attributes. The authors considered six different attributes such as specific heat in the solid phase, specific heat in the liquid phase, latent heat of fusion, thermal conductivity, density, and the cost for the analysis. Based on the study, calcium chloride hexahydrate is found to be the best PCM among nine alternatives. The authors observed that TOPSIS method is the preferred solution in the material selection when precise performance ratings of the alternatives are known. At the same time, fuzzy TOPSIS is suitable when the performance rating of the alternatives is vague or inaccurate. The AHP method is a structured technique used to organize and analyze complex material selection problems based on mathematics and psychology. The selection of suitable PCM for the thermal comfort of vehicle interior space was carried out by Socaciu et al. [97] by employing AHP method. The PCMs were first short-listed based on the phase change temperature range varying between 0-30 °C, and the analysis was made by considering ten alternatives with seven different criteria. Thermal conductivity and latent heat of fusion were considered to be the most important criteria. They were assigned the highest weight (36.34 %), while the maximum operating temperature was provided the lowest weight (1.43 %). Based on the analysis, PCM-Hs01P is considered as the best material, followed by PCM-Hs29P and PCM-Hs22P for the application of vehicle thermal comfort. In another study, Socaciu et al. [98] utilized AHP method to select the best PCM for thermal comfort application in buildings. The PCM phase change temperature (PCT), density in the solid phase, specific heat capacity, latent heat capacity, and thermal conductivity are used as the selection criteria for the analysis. Total 8 PCMs such as Climsel C24, PlusIce S27, PlusIce S23, PlusIce A22H, PlusIce A26, Rubitherm RT27, Rubitherm RT28 HC, and Latest TM 25 T are considered as alternatives for comfort application in building. Based on the analysis, PlusIce S27 is found to be the best alternative for the given application, followed by PlusIce A22H, Climsel C24, and PlusIce S23. Efforts have been made by Rastogi et al. [99] to extend the MADM technique for ranking and selection of the best PCM for domestic heating, ventilation, and air-conditioning applications. The authors considered latent heat per unit volume and thermal inertia, i.e., thermal diffusivity, as a figure of merit subject to the Pareto optimality test. Subsequently, TOPSIS technique was employed to rank the PCM alternatives. A methodology was proposed to select the suitable PCM for hybrid electrical and thermal energy storage systems for different applications such as heating, cooling, and providing domestic hot water in residential buildings by Zsembinszki et al. [100]. A decision matrix based on qualitative attributes of the alternatives was used to select the most suitable PCM. The authors considered various attributes such as latent heat, melting temperature, cost, availability, and maximum working temperature for the analysis. A sensitivity analysis was performed to check the robustness of the decision matrix. The authors also performed experimental characterization of the best PCM to validate the model prediction. Results indicate that Rubitherm RT-4 is the most promising PCM for cooling applications, while RT 64-HC is found to be the best candidate for heating and domestic hot water applications. The selection of PCM plays a critical role in the efficient design and fabrication of electronic cooling systems. A hybrid MADM technique was proposed to select optimal PCM for thermal management application by Loganathan et al. [101]. The authors proposed hybrid MADM techniques involving fuzzy AHP, TOPSIS, VIKOR, and preference ranking organization method for enrichment evaluation (PROMETHEE) by considering ten alternatives and eight attributes. The weights obtained by AHP method were used as the input for TOPSIS and PROMETHEE to rank the material. The authors proposed the Rubitherm RT-80 as the best PCM among ten alternatives for thermal management applications. It is concluded that PROMETHEE and VIKOR techniques are suitable for handling similar problems and provide excellent results. The selection of optimal PCM for ground source heat pump (GSHP) integrated with PCM was studied using the MADM technique by Yang et al. [102]. Initially, a comprehensive appraisal index model is established, and subsequently, subjective and objective weights of the attributes are obtained by using AHP method. Later on, the pre-screened PCMs are ranked by employing the TOPSIS method, and $Ba(OH)_2.8H_2O$ is found to be the best PCM. The authors argued that the proposed method is simple and convenient to solve the PCM selection problem. In addition, studies are available on PCM selection by employing various MADM techniques for different applications and are summarized in Table 1.3.

Table 1.3 Studies available on selection of PCM for different applications

Authors	Applications	No. of alternatives	Temperature range (°C)	No. of attributes	Methods employed
Rathod et al. [96]	Solar domestic hot water system.	9	28-60	6	AHP and TOPSIS/fuzzy TOPSIS
Socaciua et al. [97]	Thermal comfort of the vehicle.	10	0-29	7	AHP
Socaciua et al. [98]	Thermal comfort in buildings.	8	22-28	5	AHP
Rastogi et al. [99]	Heating, ventilation, and air-conditioning.	35	17-25	7	TOPSIS
Zsembinszki et al. [100]	Energy storage for buildings.	25	50-68	4	MADM with characterizatio n
Loganathan et al. [101]	Cooling of electronics.	10	29-77	8	TOPSIS/VIK OR/PROMET HEE
Yang et al. [102]	Ground source heat pump integrated with PCTS.	8	65-80	13	AHP/ entropy, TOPSIS
Xu et al. [103]	Energy Storage for Solar air conditioning.	10	90-120	5	AHP
Xu et al. [104]	Energy storage for waste heat recovery.	10	21-25	5	AHP and TOPSIS
Wang et al. [105]	Low-temperature PCM for Energy Storage.	10	27-53	6	VIKOR

Numerical investigation

Numerous studies have been performed to analyze the thermal performance behavior of PCM integrated heat sinks through numerical investigation. The computational fluid dynamic (CFD) method with Ansys-fluent generally utilizes the enthalpy-porosity approach to model the melting and solidification of PCM. In this approach, the mushy region (partially solid) is treated as a porous medium where the porosity of each cell is defined by a term called melt fraction [106]. In the fully solidified region, the melt fraction becomes zero, and hence the velocity becomes zero in the region. Several numerical studies have been carried out by employing different TCEs such as extended surface (fins), nanoparticles, and foams to analyze the thermal performance of PCM-based heat sinks.

Nayak et al. [65] performed a numerical investigation to analyze the effect of three different types of TCEs such as plate fins, rod fins, and porous matrix. The performance of various thermal management modules with varying volume fractions of TCEs is analyzed through transient variation of heat source temperature. N-eicosane was used as the PCM. The TCE with thinner fins is found to improve the heat transfer performance. Also, the rod-type fins are found to maintain a more uniform temperature compared to the plate-type fins. Saha et al. [68] studied the effect of numerous parameters such as aspect ratio of heat sink enclosure, input heat flux, and different non-dimensional numbers (Fourier number, Rayleigh number, Nusselt number, and Stefan number) on the melting behavior of PCM inside heat sink. An effort has been made to develop correlations for Nusselt number as a function of Rayleigh number in various PCM-based heat sink enclosures (shallow, rectangular, and tall). Correlations are proposed for the Nusselt number as a function of characteristic length and Rayleigh number. Hosseinizadeh et al. [107] proposed both 2-D and 3-D numerical models to analyze the effect of various heat sink configurations (heat sink without fins and heat sink with fins) on the thermal performance for the cooling of electronic components. Effects of various parameters such as fin number, height, thickness, and heat input on the thermal performance are analyzed in their study. The heat input is varied between 25 to 45 W, and RT-80 is considered as PCM. An increase in the fin thickness is found to provide moderate improvement in thermal performance. After attaining the optimum value, a further increase in fin thickness does not show improvement in thermal performance. However, appreciable enhancement in thermal performance is noticed with the increase in the fin height and number. The effect of the height and width of plate fins on the melting rate of PCM was analyzed through numerical investigation by Bondareva et al. [108]. The heat transfer rate is found to increase with the decrease in fin width. The melting time of PCM is found to decrease by 16-18% and 37-40% with the increase in the fin length from 0.1 to 0.3 and 0.3 to 0.6, respectively. Arshad et al. [109] performed a numerical investigation to analyze the effect of fin thickness and heat input; the volume fraction of fins is considered as 9%, and n-eicosane is considered as PCM. The authors proposed correlations for melt fraction and modified Nusselt number as a function of Stefan number, Rayleigh number, and modified Fourier number.

Efforts have been made to study the thermal performance of PCM integrated heat sink by employing metallic/non-metallic nanoparticles as TCE inside PCM. Bondareva et al. [110] performed a numerical simulation to investigate the combined effect of fins and nanoparticles on conduction and convection heat transfer. It is concluded that the addition of alumina nanoparticles inside pure PCM accelerates the melting at the initial stage of melting due to enhancement in conduction heat transfer in solid and liquid PCM, while convection heat transfer dominates after the initiation of melting of PCM. The authors also observed that optimal nanoparticle concentration inside PCM is a function of heat input and fin height. Effect of copper oxide (CuO) nanoparticle concentration inside PCM integrated heat sink with and without fins and their effect on natural and forced convection heat transfer were analyzed by Sahoo et al. [87]. It is reported that the addition of CuO enhances the heat transfer from the chip. However, for heat sink with fins, the effect of nanoparticle concentration is not appreciable. Faraji et al. [111] performed a numerical simulation to analyze the melting heat transfer of NePCM (CuO as a nanoparticle, and n-eicosane as PCM) based thermal energy storage system by employing the enthalpy porosity method. The heat sink with

NePCM involving 4% volume fraction exhibits a reduction of 3 °C temperature compared to the PCM-based heat sink without nanoparticles. This may be due to the enhancement in thermal conductivity of PCM with the addition of nanoparticles. Dadvand et al. [112] studied the melting heat transfer behavior of NePCM inside a thermally insulated square enclosure involving a heated plate inside the enclosure. The effect of nanoparticle concentration and position of the heated plate on the melting rate of NePCM is analyzed in their study. Results are demonstrated in terms of isotherm and streamline contours, propagation of solid-liquid interface, and melting rate of PCM. For a fixed position of the hot plate, an increase in the volume fraction of nanoparticles increases the melting rate of NePCM. Also, the lowest and highest melting rate is achieved with the top and bottom position of the hot plate, respectively. Bayat et al. [113] performed a numerical simulation of a plate-fin heat sink by adding Al_2O_3 and CuO nanoparticles at various mass fractions. Performance of heat sink is also investigated for heat sink with and without PCM. It is reported that the addition of nanoparticles in pure PCM at a small percentage (2% by weight) improves the heat sink performance. Adding nanoparticles more than 2% by weight decreases the thermal performance due to high viscosity. The melting behavior of hybrid NePCMs (Al_2O_3/n-eicosane and CuO/n-eicosane) was studied numerically by Faraji et al. [114]. The combined effect of heat source position and inclination of the heat sink (rectangular and square geometry) is analyzed in their study. It is reported that when the heat source is placed on the center of the bottom surface, the heat sink geometry with a 90° inclination angle provides better heat transfer.

In addition, several numerical studies were performed by employing different metallic/non-metallic foams to improve the heat transfer performance of PCM-based thermal management module. The heat sink embedded with aluminum foam-PCM composite was studied numerically by Srivatsa et al. [115]. The effect of the porosity and pores per inch (PPI) of the aluminum foam on the natural convection current is analyzed in the study. It is observed that for constant porosity and higher PPI of aluminum foam, convection current is weaker, while for fixed PPI and higher porosity, convection current is stronger and maximum velocity is achieved. Also, the maximum velocity is observed when PCM is about to melt completely. The heat sink with foam-PCM composite is found to exhibit better thermal performance due to the increase in interfacial area between the heat sink and PCM. In addition to the experimental study, numerical simulations were performed by Marri et al. [116] to study the effect of porosity and PPI gradients of metal foam on the thermal performance of heat sink integrated with PCM. The solid-liquid phase change behavior of PCM in composite metal foam is studied during the charging and discharging process. It is reported that increasing the PPI density of metal foam from the bottom to the top, or reducing the porosity from the bottom to the top, improves the thermal performance of the heat sink compared to a heat sink with uniform porosity or uniform PPI density. The thermal performance is often evaluated by estimating the time to achieve the set point temperature. Metal foams are found to improve the thermal performance of a PCM-based heat sink by 4.4 times compared to a heat sink with pure PCM. Alshaer et al. [117] proposed a computational model to analyze the heat transfer characteristics of heat sink involving carbon foam-NePCM composite with RT-65 and MWCNT as PCM and nanoparticle, respectively. Results are shown in the form of isotherm contours, melt front propagation and module time-temperature variation for a fixed value of foam porosity. The effect of different foam porosity values (55, 65, and 75%) on the thermal performance is analyzed, and it is observed that the module temperature decreases with the decrease in foam porosity. For a lower porosity value (< 75%), the heat sink involving carbon foam-NePCM composite lowers the module temperature by 11.5%. The melting behavior of lauric acid as PCM inside porous metal foam (MF) was studied by Deng et al. [118]. To characterize the pore distribution, the fractal brownian motion is introduced. The effect of foam porosity and fractal dimension on thermal performance is studied in their investigation. The authors also analyzed the dynamic response of temperature and propagation of melt front. A higher melting rate and faster evolution of melt front are observed in foam-PCM composite compared to pure PCM. It is observed that, unlike pure PCM case, melt front in foam-PCM is not continuous, and various independent solid-liquid interfaces are formed, which leads to accelerate the melting rate and intensify the heat transfer. Sardari et al. [119] performed a numerical study with multiple segment foam-PCM composites to analyze the effect of various parameters such as pore density, porosity, and location of heat source on thermal performance. Copper foam is selected as a foam material, and RT-35 is utilized as PCM. The copper foam, in general, enhances the melting rate; the foam with low porosity performs better compared to foam with high porosity, and pore size does not significantly affect the melting rate. Various researchers have carried out numerical investigations to study the conjugate heat transfer behavior of PCM integrated heat sink involving different TCEs (fins, nanoparticles, and foams) and are summarized in Table 1.4.

Table 1.4 Summary of numerical studies on PCM-based heat sinks

Reference	Methods/Heat input	PCM used (M.P.)	Heat sink dimension (mm)	Observations
Bayat et al. [113]	Numerical (10-30 kWm^2)	Paraffin wax (41-45)	50×50×40	Temperature does not change much by adding nanoparticles.
Srivatsa et al. [115]	Numerical (6-12 W)	n-eicosane (36.5 °C)	80×62×25	Peak velocity of PCM in cross plate-fin HS is higher than foam embedded HS.
Alshaer et al. [117]	Numerical (30 W)	RT-65 (65)	52.4×40.2	The inclusion of MWCNT into foam/PCM composite reduces temperature by 11.5 %.
Yang et al. [120]	Numerical and experimental (80-320 W)	E-BiInSn (60.2 °C) Octadecanol (55.6 °C)	80×80×30	Metallic PCM exhibits much higher thermal conductivity than organic PCM.
Zehri et al. [121]	Numerical and experimental (0.24-1.00 W)	Paraffin wax (-)	-	Thermal conductivity enhanced by 54% with the addition of silver coatings.
Kalbasi et al. [122]	Numerical 5-10 kW/m^2	RT-27 (27)	Variable $W_0 = s_{opt} + 2t_f$ $10 \leq H \leq 30$	A correlation is proposed to find optimum fin numbers.
Sahoo et al. [123]	Numerical (-)	-	100×0.8	Temperature reduces with orthotropic fins.
Raj et al. [124]	Numerical and experimental (2-10 W)	FS-PCM (24.91)	65×35×65	Form stable PCM is suitable for thermal management.

1.5.2 Experimental investigation

In recent years, various researchers have made efforts to propose a PCM-based thermal management system to dissipate the excessive heat energy generated by compact and high-speed electronic components. Various experimental studies have been carried out to study the thermal performance of the PCM-based thermal management system. The effect of various heat sink configurations, types of TCEs (fins, nanoparticles, and foams), and their composites on the thermal performance have been analyzed. In addition, the effect of heat input, TCE volume fraction, PCM volume fraction, and the type of PCMs to stretch the operating time of electronic components have been analyzed by different researchers. The literature relevant to the thermal management of electronic components is elaborated below.

PCM with fins

Extended surface (fins) is considered the most convenient and effective way to augment the heat transfer rate. Numerous studies have been carried out on PCM-based heat sinks involving fins [126-132]. Ali et al. [126] studied the square and circular pin fin heat sink assembly filled with two different PCMs, namely, n-eicosane and paraffin wax. The thickness of square and circular pin fins are kept as 2 and 3 mm, respectively; the fin volume fraction is kept at 9%, and the input heat flux is varied in the range of 1.2-3.2 kW/m^2. At q''=1.6 and 2.0 kW/m^2, the enhancement in operating time is found to be 150 min and 210 min for n-eicosane and paraffin wax, respectively. Tests are conducted to investigate the effect of various heat flux values (q''=0.79-3.17 kW/m^2), PCM (n-eicosane) volume fraction, and different thicknesses (1, 2, and 3 mm) of square pin fin on the stretching the operating time of PCM-based heat sink as applicable to electronic components [127]. The TCE volume fraction is fixed at 9% in the study, and the heat sink is completely filled with PCM. The 2 mm, thick pin fin heat sink exhibits a higher operating time for various heat flux values. For 2 mm fin thickness, the enhancement ratio in operating time is found to be 2.0 and 4.0 for SPT values of 55 and 45 °C, respectively. In another study, Arshad et al. [128-129] examined the effect of pin fin-type (square, round), fin number, heat flux values (q''= 1.58-3.2 kW/m^2), PCM volume fraction, and different heat sink configurations on the thermal performance. For PCM volume fraction of unity, the heat sink involving round pin fins with 3 mm diameter and heat sink involving square pin fins with 2 mm thickness improves the operating time of electronic components. The maximum value of enhancement ratio in operating time is found to be 4.2 and 4.3 for round pin fin and square pin fin, respectively. Baby and Balaji [130] experimentally examined the effect of various heat sink configurations (no fin, 3 plate fins, and 72 pin fins) integrated with n-eicosane as PCM. The effect of different heat input values from the bottom side of the test section (2-7 W) are analyzed on the thermal performance for a constant amount of TCE volume fraction (9%). The heat sink with pin fins performs better compared to the heat sink with plate fins. The augmentation in operating time is found to be 18 for the pin finned heat sink to attain 45 °C at 7 W heat input. Ashraf et al. [131] carried out an experimental investigation to optimize the PCM-based heat sink configuration. Heat sinks with different pin fins (circular and square) and arrangements (staggered and inline), integrated with various PCMs (RT-54, RT-44, RT-35HC, SP-31, and n-eicosane) are considered for the analysis. The heat sink with circular and inline arrangement exhibits better thermal performance. Also, they reported that various PCMs such as PCM RT-54, n-eicosane, and SP-31 are found to be suitable for low heat input, while PCM RT-54 is the best candidate for higher heat flux requirements. Tests were conducted by Ali et al. [132] to optimize the heat transfer in PCM-based closed pack heat sink with different PCMs (n-eicosane, SP-31, RT-35HC, RT-44, RT-54, and paraffin) and various pin fin geometries (circular, rectangular, and triangular) as applicable for the cooling of electronic components. Based on the analysis, RT-44 HC is found to be the suitable PCM for the set point temperature (SPT) value of 60 °C. Triangular pin-fins are found to be the most effective pin-fin configuration for better heat transfer. Baby and Balaji [133] performed tests to analyze the effect of constant/intermittent heat inputs and PCM volume fraction on the heat transfer characteristics of PCM-based heat sink with plate-fins. Enhancement ratios for different SPTs are obtained to quantify the performance of each heat sink configuration. For SPT of 42°C and power level of 8 W, the operating time of PCM-based heat sink matrix is found to be more than four times compared to the heat sink involving plate-fin without PCM. Usman et al. [134] performed tests to analyze the thermal performance of PCM-based heat sinks involving triangular pin fin with different arrangements (staggered and inline), various PCMs (paraffin wax, RT-44, and RT-44HC), and PCM volume fractions. They concluded that a triangular pin fin heat sink is the most common design for cooling of electronic devices. Various experimental studies on PCM-based heat sink with fins are summarized in Table 1.5.

Table 1.5 Summary of experimental studies on PCM-based heat sink with fins

Reference	Methods/Heat input	PCM used (M.P.)	Heat sink dimension (mm^3)	Observations
Arshad et al. [129]	Experimental (1.58-3.174 kW/m^2)	Paraffin wax (56-58 °C)	114×114×25	The number of fins and the amount of PCM are important criteria for effectiveness.
Mahmoud et al. [135]	Experimental (3-5 W)	RT-42 (42 °C)	50×50×25	Cross fin arrangement performs better than parallel fin.
Kothari et al. [136]	Experimental (1.3-2.7 kW/m^2)	Paraffin wax (58-62 °C)	110×110×27	Operating time increases with fin number.
Kamkari et al. [137]	Experimental (Constant temperature, 55-70 °C)	Lauric acid (43.5-48.2)	120×120×50	The efficacy of the heat sink improves with an increase in the number of fins.
Yazici et al. [138]	Experimental (3.33 kW/m^2)	n-eicosane (35-37 °C)	100×48×34	The combined effect number of fins and the inclination were studied.
Fan et al. [139]	Experimental (60-120 W)	n-eicosane (37 °C) 1-hexadecanol (49 °C)	80×80×30	The maximum temperature rise with finned heat sink lowered by 10 °C.
Baby and Balaji [140]	Experimental (1.587-3.968 kW/m^2)	n-eicosane (36.5 °C) Paraffin wax (53-57)	80×62×25	Heat sink with pin fins is superior compared to a heat sink without fins.
Ali and Arshad [141]	Experimental (0.8-2.8 kW/m^2)	n-Eicosane (36.5 °C)	114×114×25	The result improved with the 3 mm pin fin.

PCM with nanoparticles

Various studies have been made to analyze the heat transfer characteristics of PCM-based systems incorporating different nanoparticles (metallic/non-metallic) [142-148]. The addition of nanoparticles inside the PCM is usually termed as nano-enhanced PCM (NePCM). Efforts have been made to analyze the heat transfer performance of NePCM (Al_2O_3 as nanoparticle and n-octadecane as PCM) inside the square vertical-cavity by Ho et al. [142]. Tests are conducted for a varied range of nanoparticle concentrations (0-10% by weight), a different value of Rayleigh numbers (1.71×10^6-5.67×10^7), and Stefan numbers (0.037-0.108). The natural convection heat transfer in the melting section degrades significantly with increasing mass fraction of nanoparticles. Sharma et al. [143] studied NePCM-based thermal management techniques to increase the electrical efficiency of building integrated concentrated photovoltaic (BICPV) modules, where RT-42 and CuO are used as PCM and nanoparticle, respectively. The thermal performance of NePCM based systems with no fin and micro-fins are analyzed and found that the micro-fins with PCM and micro-fins with NePCM exhibit a reduction in temperature by 10.7 °C and 12.5 °C, respectively. Both experimental and numerical studies were carried out by Bahiraraei et al. [144] to analyze the thermal performance of NePCM based thermal management systems. Different carbon-based nanoparticles such as graphene nano platelets (GNP), carbon nano fiber (CNF), and graphite nanopowder (GrP) are used with a different mass fraction (0.0, 2.5, 5.0, 7.5, and 10%). The results show that adding nanoparticles to PCM can increase conduction heat transfer while degrading the latent heat. However, it significantly increases the dynamic viscosity of composites that prevents natural convection current. An experimental study is performed by Alimohmmadi et al. [145] to investigate the effect of NePCM ($MnNO_3$ as PCM and Fe_3O_4 as nanoparticle) on the cooling of electronic components during free and forced convection heat transfer. The steady and transient behavior of electronic chip is simulated for a wide range of heat flux values (q''=1-4 kW/m^2). The inclusion of pure PCM and NePCM can lower the steady temperature of the electronic chip by 14°C and 10.5°C, respectively, compared to the heat sink with free and forced convection at q''= 4.0 kW/m^2. The effectiveness of composite PCM with graphene nano fillers on the transient performance of a hybrid thermal management system was investigated experimentally by Joseph et al. [146] for uniform and periodic pulsed heat loads. The authors concluded that for passive cooling mode, the heat sink with graphene-PCM composite reduces the maximum temperature by 6 °C during steady-state heating conditions compared to the heat sink under uniform thermal load. Also, for a hybrid cooling system, 23% increase in fan energy savings is achieved with a graphene-PCM composite heat sink compared to a heat sink with various periodic heat pulses. The thermal behavior of NePCM based heat sink with heat pipe was studied by Kumar et al. [147] for cooling of microprocessors. The NePCM-based systems increase the heat storage capacity, delay the sensible temperature rise, and maintain the temperature of the chipset at room temperature for a longer period of time. The combined effect of nanoparticle concentration with PCM in unfinned and finned heat sink for thermal management of electronic components was studied by Kothari et al. [148]. Tests are conducted for various nanoparticle concentrations (0, 2, 4, and 6%) at q''= 2 kW/m^2. The evolution and propagation of the NePCM melt front were studied through photographic observation. The highest reduction in melting time is found to be 9, 13, and 26% for NePCM-based unfinned, one finned, and three finned heat sinks, respectively. Various experimental studies on NePCM-based heat sink for thermal management applications are summarized in Table 1.6.

Table 1.6 Summary of experimental studies on NePCM-based heat sinks

Source	Methods/ Heat input	HS size (mm^3)	PCM (M.P., °C)/ Naonparticle (∅)	Observations
Ho et al. [142]	Experimental (40 °C)	HS with no fins 25×25×60	n-octadecane (25.1-26.5) Al_2O_3 (5.0, 10.0)	Increasing the nanoparticle in PCM degrade the natural convection.
Sharma et al. [143]	Experimental (0.8 W)	Without and with micro-fin 36×35×35	RT-42 (42) CuO (0.5)	NePCM for finned HS is not improving performance.
Joseph and Sajith [146]	Experimental (2.835-11.338 kW/m^2)	HS with 4 plate fins 42×42×32	Paraffin (59.6) Graphene (0.05 to 0.5 wt%)	Higher energy saving is obtained for HS with PCM-GR composite.
Farzanehnia et al. [149]	Experimental (2-6 kW/m^2)	HS with plate fins 73×68×44.5	Paraffin wax (40.22-46.92) MWCNT (0.2, 2.0)	The effect of NePCM is more pronounced after the melting.
Tariq et al. [150]	Experimental (0.86-2.4 kW/m^2)	HS with no fins 106×106×29	RT-44 HC (44) RT-64 HC (64) Graphene (0.002,0.005,0.008)	Graphene-based composite PCM shows enhancement in operating time.
Motahar et al. [151]	Experimental (0.74-1.98 kW/m^2)	HS with triangular plate fins 65×65×40	RT-42 (42) Carbon nanofibers 0.5, 2) TiO_2 (2, 4)	Adding carbon nanofibers and TiO_2 to RT-42 does not improve the thermal performance.
Alimohammadi et al. [152]	Experimental (1 to 5 kW/m^2)	HS with 4 plate fins 75×75 ×40	$Mn(No_3)_2$ (37) Fe_3O_4 (1 wt%)	Reduction in temperature with PCM and NePCM was observed compared to HS without fins for both forced and free convection.
Kothari et al. [153]	Experimental (2 kW/m^2)	Without and with 2 plate-fin 100×100 ×22	Paraffin wax (58-62) Al_2O_3 (0, 0.5, 4 and 6 wt%)	Addition of a small amount of nanoparticles in the PCM decreases the melting time.

PCM with metallic/non-metallic foam

In recent years, metallic/non-metallic foam attracted the attention of many researchers because of various advantages such as lightweight, high thermal conductivity, and stable properties [48]. Various experimental studies have been made to study the melting and solidification behavior of PCM-based heat sink with metallic/non-metallic foam for thermal management of electronic components. Baby and Balaji [84] conducted experiments on heat sink involving copper foam-PCM composite to investigate the effect of orientation on stretching the operating time of set point temperatures (SPTs) as applicable for electronic components. The maximum enhancement ratio is found to be 3 for SPT of 52 °C; the orientation is found to have no significant role on heat transfer performance. Rehman and Ali [154] carried out an experimental study to analyze the thermal performance of PCM-based heat sink with copper and iron-nickel foams as applicable for the cooling of low heat-generating electronic devices. The authors used RT 35-HC as PCM and aluminum as thermal conductivity enhancer (TCE). Studies have been made with various PCM-based heat sink composite with different PCM volume fractions (0.0, 0.6, 0.7, and 0.8) and copper foam with different porosity values (95% and 97%). The heat sink involving copper foam with 95% porosity and PCM volume fraction of 0.8 exhibits superior thermal performance. In another study, Rehman et al. [155] performed experiments on metallic foam (copper and nickel) based heat sink using RT-54HC as PCM for electronic cooling. The effect of PCM volume fraction (0.0, 0.6, 0.7, and 0.8) and different heat input values (8 to 24 W) on thermal performance were studied. It is reported that copper foam embedded with the PCM volume fraction of 0.8 reduces the base temperature by 26% compared to a heat sink with nickel foam without PCM. Thermal performance of various heat sink configurations such as heat sink with no PCM, heat sink with pure PCM, and heat sink involving PCM embedded with porous metal fiber sintered felt (PMFSF) with different values of porosity was studied by Wang et al. [156]. The inclusion of PMFSF is found to enhance the heat transfer in PCM and leads to a lower surface temperature. Alshaer et al. [157] performed tests on different heat sink configurations such as heat sink with carbon foam (CF), CF-PCM composite, and CF-NePCM composite; the multi-wall carbon nanotubes (MWCNTS) and RT-65 are used as nanoparticle and PCM, respectively. The authors used different types of CFs such as CF-20 and KL1-250 with thermal conductivity of 3.1 and 40 W/m-k, respectively. The KL1-250 based heat sink exhibits better heat transfer performance compared to the heat sink with CF-20, while the inclusion of MWCNTs exhibits better performance with heat sink involving CF-20 compared to the heat sink with KL1-250. In another study, Alshaer et al. [158] studied the thermal performance of heat sink with CF-NePCM composite where MWCNTs and RT-65 are used as nanoparticle and PCM, respectively. It is revealed that temperature pulse is dampened for heat sink with CF-NePCM composite. Iasiello et al. [159] performed an experimental and numerical investigation to analyze the thermal performance of heat sink with aluminum foam embedded with PCM for a thermal energy storage system. The effect of various parameters such as heat flux, foam porosity, PPI, and orientation of storage unit on the thermal performance is analyzed. It is observed that liquid phase convection strongly affects the melting front position. Various studies that report the foam-PCM composite for thermal management applications are summarized in Table 1.7.

Table 1.7 Summary of experimental studies on foam-PCM based heat sinks

Source	Types foam used (Porosity %)	Foam K (W/m-K)	PCM (M.P., ^{o}C)	Observations
Zehri et al. [121]	Graphene foam (99.6)	- (1.3)	Paraffin wax (-)	Thermal conductivity of graphene foam enhanced by 54% with the addition of silver coating by sintering silver nanoparticles.
Alshaer et al. [157]	Carbon foam (88, 89.6)	CF-20-(3.1) KL1-250-40	RT-65 (65)	KL1-250 based module shows lower operating temperature compared to CF-20 based module.
Lafidi et al. [160]	Aluminum foam (93.9)	ERG Al Foam (5)	Paraffin wax (25.5-28.9)	The steady-state temperature in high porosity reaches faster compared to low porosity foam.
Zhu et al. [161]	Copper foam	-	RT-40 (40)	Copper foam with 75% filling height in the heat sink is more economical than 100 % filling.

Gimenez et al. [162]	Graphite foam (82, 70, 72)	KFoam L1 250 (40) KFoam L1 (60) KFoam D1 (110) PocoFoam (135)	$NaNo_3$ (306)	The addition of thermally conductive grease at the heat exchanger and TES interface is not possible due to high temperature constraints.
Kothari et al. [163]	Copper foam (90)	Nanoshel LLC (10)	Paraffin wax (58-62)	Heat sink with fin and PCM-metal foam composites gives better heat transfer performance.

1.6 Scope of present investigation

The literature review presents the thermal performance of PCM-based heat sink configurations through theoretical and experimental investigation. These include various MADM techniques to select the best PCM. Also, the studies pertaining to the thermal performance of various heat sink configurations such as PCM-based heat sink with fins, nanoparticles, and metallic/nonmetallic foams have been discussed in the previous sections. The effect of several parameters such as heat flux values, heat sink configurations, the volume fraction of PCM and TCEs, types of TCEs, on the thermal performance has been investigated. Most of the authors reported the thermal performance parameters in terms of time required to attain the set point temperature (SPT), Nusselt number variation, the temperature distribution in PCM, temperature variation on the base of the heat sink, energy storage capacity, and PCM melt fraction. However, several issues pertaining to thermal management of PCM-based heat sink modules need further investigation and are elaborated below.

a) The selection of the best PCM for a specific application plays a crucial role in the design of PCM-based heat sinks. The PCM should possess various parameters such as adaptability, safety, reliability, and low cost for its use for a specific application. The selection of optimal PCM employing various MADM techniques, especially for thermal management systems, has not been reported in the literature extensively.

b) The thermal performance of a PCM-based heat sink can be enhanced because of numerous parameters such as increase in the number of fins, the height of the fin, and increase in PCM volume. Different fin arrangements with an increase in surface area density can be adopted to enhance thermal performance for a given weight of fin materials. In view of this, various configurations, including the cross plate fins, can be investigated to examine the melting behavior and thermal performance of PCM-based heat sinks through numerical investigations.

c) It may be noted that the increase in these parameters (number of fins, height of the fin, and PCM volume) increases the overall thermal conductivity, thermal capacity, and latent heat capacity of the system and leads to improvement of thermal performance. Most of the earlier studies focus on heat sink configurations that consider different mass for different heat sink configurations. Efforts need to be made to analyze the thermal performance of various heat sink configurations keeping the mass constant for cross plate fin arrangements. The natural convection effect, number of conduction paths, and surface area density need further investigation to understand the heat transfer performance of PCM-based heat sinks.

d) Numerous studies are available on solid pin fin heat sink; however, study on the hollow fins is limited in the literature. Different types of hollow fins can be analyzed to study the thermal performance of PCM-based heat sinks for the thermal management of electronic components.

e) The influence of convection, induced due to density difference during the melting, evolution of melt front, melting pattern, and isotherm contours need to be analyzed in more detail to understand the thermal performance of PCM.

f) Limited studies are available that report the thermal performance of various NePCM-based heat sinks involving different pin fin geometry (circular and square) and CuO-based NePCM with a varied range of nanoparticle concentrations and different heat loads.

g) The heat sink embedded with TCEs such as high thermal conductivity foams (metallic, non-metallic) impregnated with PCM is found to exhibit better thermal performance. Limited studies have been made that report the thermal performance of heat sink embedded with carbon/copper foam impregnated with PCM for a wide range of input heat flux values and different volume fractions of TCE.

h) Characterization of PCM and various thermal conductivity enhancers such as fins, nanoparticles, and foams is necessary to predict the heat transfer behavior of the thermal management module. Limited studies are available that report the thermophysical properties such as thermal conductivity, specific heat, latent heat of PCM and NePCM and morphological characteristics of TCE material (fins and foams).

The present work aims to address the above-mentioned issues pertaining to the thermal performance of PCM integrated heat sink for cooling application of electronic components. Here, efforts have been made to select the best PCM for thermal management of electronic components by employing TOPSIS and the fuzzy TOPSIS method. The thermal performance of various PCM-based heat sink configurations with different TCEs (nanoparticles, fins, metal foams) is studied through experimental investigation. Also, numerical simulation has been made to analyze the effect of heat flux and fin geometry on thermal performance. In addition, the melting and solidification of PCM inside various heat sink configurations are studied in the present dissertation. Efforts have been made to analyze the effect of various input parameters such as a wide range of heat flux values, different types of TCEs and heat sink configurations, types of PCM, and SPT on heat sink thermal performance. Results are analyzed in terms of various performance parameters such as time required to reach various SPTs during the melting and solidification process, enhancement ratio, latent heat duration, thermal conductance, thermal capacity, and Nusselt number variation with time. The organization of the thesis is as follows:

Chapter 1: This chapter introduces various active and passive thermal management techniques for cooling of electronic components and discusses the classification and application of PCMs. In addition, the brief introduction, selection, and application of PCM have been presented. Studies pertaining to PCM selection and the use of PCM-based heat sinks involving thermal conductivity enhancers (TCE) for thermal management techniques have been discussed. Finally, the scope of the present investigation is highlighted.

Chapter 2: Here, various MADM techniques (TOPSIS and fuzzy TOPSIS) have been employed to select the best PCM among 30 pre-screened PCMs. Pre-screened PCMs have melting temperatures in the range of 28-58 °C. A total of 11 attributes are used for the selection of the best PCM for the thermal management of electronic components. The AHP technique is utilized to determine the weight of the attributes. Results are also compared with another MADM technique 'VIKOR' method.

Chapter 3: In this chapter, the thermal performance of PCM-based cross plate fin heat sinks with various cavities is analyzed through numerical investigation. Here, the performance of various heat sink configurations is evaluated based on the transient variation of heat sink base temperature, PCM melt fraction, average Nusselt number, energy absorbed by PCM through both latent and sensible heat, solid-liquid interface propagation, and isotherm contours. The performance of commercially available PCM is also analyzed. Efforts have also been made to analyze the thermal performance of solid and hollow pin fin heat sink filled with PCM.

Chapter 4: This chapter reports three different experimental studies pertaining to analyze the thermal performance of heat sinks for thermal management applications. The first problem reports the thermal performance of PCM-based cross-plate fins arrangement heat sinks with various cavities. The second problem discusses the thermal performance of various heat sink configurations such as heat sink with no fin, 4 plate fins, 132 circular pin fins, and 225 square pin fins integrated with pure PCM and NePCM. In the next problem, the thermal performance of PCM-based heat sinks with high thermal conductivity carbon and copper foams are discussed. The effect of PCM volume fraction, input heat flux, TCE volume fraction, SPTs on the thermal performance of PCM integrated heat sink is elaborated in this chapter.

Chapter 5: This chapter presents the conclusions obtained from the present study involving both theoretical and experimental investigations followed by the scope of further investigation.

Chapter 2

Selection of phase change material for thermal management of electronic devices

2.1 General background

Literature review reveals that the selection of PCM plays an important role for thermal management of electronic components. For a given application, the selection of suitable PCM is difficult because of numerous conflicting attributes. In such a case, the designer needs to consider all possible alternatives and evaluate them considering various conflicting criteria or attributes. Various studies have been made to select the best PCM for different applications such as domestic solar water heater systems, waste heat recovery, thermal comfort of vehicle occupants, and energy storage for heating/cooling of residential buildings [96-105]. Most of these studies consider either a smaller number of alternatives or attributes. The optimal selection of PCM, especially for thermal management of electronic components, has not been reported extensively in the literature. Furthermore, the selection of the best PCM by considering a large number of attributes and alternatives has not been reported in the literature. It is argued that the best choice of the material can be obtained by considering a large number of attributes and alternatives in the analysis.

Here, an effort has been made to consider various alternatives and attributes, and the multi attribute decision making (MADM) approach is employed to rank and select the best PCM for thermal management of electronic devices. Initially, different types of PCMs, namely organic, inorganic, and eutectics, are pre-screened; the important attributes applicable for thermal management are considered for the analysis. Among various PCMs, thirty PCMs based on the phase transition temperature (28-58 °C) and eleven attributes are considered for the analysis. The weight of the attributes is obtained by using analytic hierarchy process (AHP) methodology. Various MADM techniques such as technique for order of preference by similarity to ideal solution (TOPSIS), fuzzy TOPSIS, and

VIKOR method are employed to select the best PCM for the efficient design of thermal management module.

2.2 Pre-screening of PCM

Thermal energy is stored as latent heat when the PCM undergoes the phase transition. Although numerous PCMs, including organic, inorganic, and eutectic, are available, only limited PCMs can be used for thermal management applications. Apart from various properties, PCMs are usually selected on the basis of melting temperature and the latent heat absorption capacity. PCM must possess suitable thermophysical and chemical properties for the real application and should be non-hazardous and non-corrosive in nature. Every PCM possesses certain unique properties, and the researchers must choose the best PCM from the host of alternatives based on certain properties or prior experience. It may be noted that there are no standard guidelines to select optimal PCM considering all properties. The dependency of one or more properties of PCM with various alternatives makes the PCM selection a multi attribute decision making (MADM) problem. A brief description of various properties of different categories of PCMs (organic, inorganic, and eutectic) is elaborated below.

2.2.1 Organic PCM

Many studies have been made on organic materials such as alkanes and paraffin or waxes [164-170]. These materials are usually polymers with long-chain molecules mostly made of carbon and hydrogen and can be used as PCM. Organic PCMs with alkane-based alloys are thermo adjustable. The latent heat of fusion and melting point rise with the length of the carbon chains, and they have very little subcooling effect. These materials change phase above 0 °C and exhibit a higher order of crystallinity. Organic PCMs include octadecane, hexadecane, paraffin, fatty acid/esters. Organic PCMs exhibit certain advantages such as congruent melting, less supercooling, higher heat of fusion, chemically and thermally stable, recyclable, and are available in a wide temperature range. On the contrary, they exhibit certain disadvantages: lower thermal conductivity, low latent heat storage capacity on a volumetric basis, and flammability (depending on containment). The properties of organic PCMs available in the selected temperature range (8-118 °C) are summarized in Table 2.1.

Table 2.1 Organic substance with potential use as PCM [23, 171, 172]

S. No.	PCM	T_m (°C)	L (kJ/kg)	k (W/mK)	ρ (kg/m^3)
1	Polyglycol E400	8	99.6	0.187	1125
2	Dimethyl-sulfoxide	16.5	85.7	-	1009
3	Polyglycol E600	22	127.2	0.189	1126
4	Paraffin C_{16}–C_{18}	20-22	152	-	-
5	Paraffin C_{13}–C_{24}	22-24	189	0.21	-
6	RT 21	21	155	0.20	-
7	OM 18	18	167	906	0.182
8	SaveE OM 30	30	200	0.154	901
9	Capric acid	32	152.7	0.153	945
10	Sav*E* OM 55	55	210	0.13	840
11	Polyglycol E6000	66	190	-	1085
12	PEG 1000	37	150	0.152	1109
13	Pure Temp 28	28	190	0.2	900
14	Pure Temp 37	37	210	0.2	880
15	Lauric acid	44.2	211.6	0.147	934.5
16	Pure Temp 48	48	230	0.2	860
17	Pure Temp 58	58	225	0.2	850
18	RT 35	35	160	0.2	815
19	RT 44 HC	44	250	0.2	750
20	Heneicosane	42.2	201	0.154	791
21	Paraffin wax	58	193.2	0.21	900
22	A 37	37	235	0.18	810
23	A 50	50	218	0.15	810
24	n- octadecane	28	241	0.27	780
25	Eicosane	36	247	0.15	785
26	Biphenyl	71	119.2	-	991
27	Propionamide	79	168.2	-	-
28	Erythritol	118	339.8	0.326	1300
29	p-bromofenol	63.5	86	0.5	900
30	RT 65	65	150	0.20	880
31	OM 65	65	183	0.19	924
32	Paraffin C_{21}–C_{50}	66-68	189	0.21	0.930

2.2.2 Inorganic PCM

Inorganic PCMs are mainly classified into two broad categories; the first category includes the salts and their hydrates, while the second category includes metals and their alloys. Compared to organic PCMs, inorganic PCMs usually exhibit higher thermal conductivity and higher storage capacity. The latent heat capacities of inorganic PCMs are approximately two times higher compared to organic PCMs. Therefore, inorganic PCMs find a potential candidate in different sectors, including thermal energy storage, particularly in medium to high-temperature applications. However, inorganic PCMs (salts and salt hydrates) can also suffer from phase segregation and supercooling that affect the energy storage capacity. Inorganic PCMs exhibit certain advantages such as higher volumetric latent heat capacity, higher thermal conductivity, sharp phase change temperature, low cost, non-flammable, and easy availability. While, these PCMs show certain disadvantages such as high volume expansion upon melting, segregation, lack of thermal stability, corrosive and supercooling effect. The properties of inorganic PCM are summarized in Table 2.2 [23, 173, 174].

Table 2.2 Inorganic substance with potential use as PCM [23, 173, 174]

S. No.	PCM	T_m (°C)	L (kJ/kg)	k (W/mK)	ρ (kg/m^3)
1	$LiClO_3.3H2O$	8.1	253	-	1720
2	Mn(NO3)2.6H2O	25.8	125.9	-	1738
3	SaveE HS 34	34	150	0.485	1915
4	ClimSel C 48	48	180	0.645	1300
5	ClimSel C 32	32	160	0.92	1400
6	ClimSel C 28	28	170	0.85	1400
7	Climsel C58	58	288.5	0.6	1460
8	$CaCl_2.6H_2O$	29.7	174.4	0.824	1649
9	$LiNo_3.3H_2O$	30	296	0.702	1500
10	Na2SO4. 10 H2O	32.4	254	0.544	1485
11	Latest 29 T	29	175	1	1490
12	Latest 36 S	36	260	0.6	1450
13	S 30	30	190	0.48	1304
14	S 34	34	115	0.52	2100
15	S 44	44	100	0.43	1584
16	$Na_2P_2O_7{\cdot}10H2O$	70	184	-	-
17	$Ba(OH)_2.8H2O$	78	265.7	0.653	1937
18	$Mg(NO3)_2.6H2O$	89	162.8	0.611	1640
19	$(NH_4)Al(SO_4).6H2O$	95	269	-	-
20	$MgCl_2.6H2O$	117	168.6	0.598	1569

2.2.3 Eutectic mixture

A eutectic mixture is made up of two or more components that have the same melting point. The mixtures are fabricated with additives such as corrosion inhibitors and microbiocides based on the requirement and nucleating agents to reduce supercooling. One of the most important characteristics of eutectics is their capability to melt/freeze congruently without phase segregation. Eutectic PCMs are generally classified as organic-organic (organic eutectics), inorganic-inorganic (inorganic eutectics), and inorganic-organic compounds. Organic eutectics possess a lower melting temperature and possess higher heat of fusion compared to inorganic eutectics. In view of this, they are found to be suitable for thermal energy storage at a lower temperature. The sharp melting point temperature and higher volumetric energy storage capacity are the main advantages of eutectic PCMs. It may be noted that limited test data are available on thermophysical properties of eutectic PCMs; the properties of some of the eutectic PCMs are summarized in Table 2.3.

Table 2.3 Eutectics with potential use as PCM [23]

S. No.	PCM	T_m (°C)	L (kJ/kg)	k (W/mk)	ρ (kg/m^3)
1	66.6% $CaCl_2.6H_2O$+ 33:3% $MgCl_2$.6H2O	25	127	-	1590
2	48% $CaCl_2$+4:3% NaCl+ 0:4% KCl+ 47:3% H2O	26.8	188	-	1640
3	14% $LiNO_3$+ 86% $Mg(NO_3)_2$.6H2O	72	>180	-	1610
4	66.6% urea+33:4% NH_4Br	76	161	0.649	1548

2.3 Multi attribute decision making (MADM) techniques for selection of PCM

The selection of optimal material for any product design and development is crucial for efficient performance. The multi attribute decision making (MADM) techniques can select the optimal material among various alternatives considering a large number of attributes or criteria. Numerous MADM techniques have been used by various researchers to select the optimal material, sites, methods, manufacturing processes, and other engineering applications [96, 175-180]. These include ELimination and Choix Traduisant la Reality (elimination and choice expressing the reality) (ELECTRE), analytical hierarchy process (AHP), simple additive weighing (SAW), goal programming (GP), case-based reasoning (CBR), simple additive weighing (SAW), processing technique of ratings for ranking of alternatives (PROTERRA), VIseKriterijumska Optimizacija I Kompromisno Resenje (VIKOR), method detection limit (MDL), multi attribute utility theory (MAUT) and technique for order of preference by similarity to ideal solution (TOPSIS). In the present study, three MADM methods, namely TOPSIS, fuzzy TOPSIS, and VIKOR technique, are used to determine optimal PCM for thermal management of electronic components. Table 2.4 presents the advantages, disadvantages, and applications of various MADM techniques used for the material selection.

Table 2.4 Advantages and disadvantages of various MADM methods

Methods	Advantages	Disadvantages	Application
ELECTRE	It accounts for uncertainty and vagueness.	Process and outcomes are difficult to explain in layman's terms.	Energy, economic, water management, transportation, and environmental problems.
AHP	Easy to apply, no data-intensive, scalable, and hierarchy structure can easily adjust to many problems.	Problem of rank reversal and can lead to inconsistencies between ranking and attributes.	Resource management, public policy, corporate policy and strategy, political planning and strategy.
CBR	Can improve over time, no intensive data requires, little maintenance.	Requires too many cases, sensitive to inconsistent data.	Business, medicine, vehicle insurance, and engineering design.
SAW	Intuitive to decision makers, no complex computer programme.	Results obtained may not be logical.	Business and water management.
GP	Ability to handle large-scale problems can also produce an infinite alternative.	Needs to be used in combination with other MADM methods.	Scheduling health care, water reservoir management, Scheduling healthcare, energy planning, and wildlife management.
VIKOR	Simple, smaller steps, determine the weight stability interval.	Compromise between pessimistic and expected solution.	Ranking of investment project, lean tool selection.
MAUT	Takes uncertainty into account.	Lots of input is required.	Agriculture, Energy management, and water management.
TOPSIS	Easy to use, number of steps remain same regardless of alternatives.	Difficult to weight and keep consistency of judgment.	Supply chain management, business and marketing, engineering and manufacturing system, and water resource management.

Evaluation of the weight of the attributes plays an important role in the material selection problem employing MADM technique. All possible attributes should be considered in the material selection. Analytic hierarchy process (AHP) is usually used to estimate the weight of the important attributes considered for PCM selection. The mathematical formulation of AHP, TOPSIS, fuzzy TOPSIS, and VIKOR methodology are presented in the subsequent sections.

2.3.1 Analytic hierarchy process for evaluation of the weight of the attributes

The AHP method is a structured technique to formulate and analyze complicated decision making problems based on psychology and thinking. Thomas L. Saaty first invented this innovative technique in 1970 [181]. AHP has been extensively employed to solve complex decision making problems [182-184]. It depicts the procedure to estimate the relative importance of a host of attributes or criteria in a decision making problem. One of the main advantages of AHP method over other MADM methods is that it incorporates judgment on intangible qualitative attributes apart from tangible quantitative attributes. This technique utilizes three principles such as developing the structure of the model, judging the decision maker's evaluations by pairwise comparison of the alternative as well as an attribute, and using the eigen vector method to find the weight of the attributes. In the very first step, a complicated decision making problem is formulated as a hierarchy, and this complex decision making problem is then transformed into a simple hierarchy of interdependent elements involving alternatives and attributes. This hierarchy is comprised of three levels: principal objective at the top, attributes considered at the intermediate, and alternatives at the bottom level [185]. Fig. 2.1 describes the proposed hierarchical model based on AHP. Here, C1, C2… C11 are different attributes used in the PCM selection and A1, A2… A30 are different alternatives of PCM.

The comparison between alternatives and attributes is made in the second step. Here, first, the problem is disintegrated, and the hierarchy is formed; later on, the relative importance of the attributes is determined by employing the prioritization process within each level. The pairwise comparison employing a scale of relative importance begins at the intermediate level and ends at the bottom level. Here, multiple pairwise comparisons of the attributes are made based on 1-9 point scale (Table 2.5).

At the last stage, mathematical computation has been made to normalize the matrix, and subsequently, relative weights are evaluated for each attribute. The consistency of the decision makers and also of the whole hierarchy is checked by using a consistency evaluation technique [186]. Various steps involved in the AHP technique are detailed below.

Step 1: Develop the pairwise comparison matrix employing a relative importance scale. The comparison matrix reveals the decision maker's judgment pertaining to the relative importance of the attributes. If C = {Cj | j= 1, 2, 3…, n} are the set of an attribute, pairwise comparison of n attributes can be written in the matrix (n×n) form A (Eq. 2.1). Each element a_{ij} (i,j= 1,2,3…,n) of matrix A represents the relative importance of i^{th} attribute with respect to the j^{th} attribute. It should be noted that matrix A is always a square matrix, and each element of its principal diagonal will be assigned a value of 1. Since attributes compared with themselves are assigned to unity value.

$$A = \begin{bmatrix} 1 & a_{12} & a_{13} & \dots & a_{1n} \\ a_{21} & 1 & a_{23} & \dots & a_{2n} \\ a_{31} & a_{32} & 1 & \dots & a_{3n} \\ \dots & \dots & \dots & \dots & \dots \\ a_{n1} & a_{n2} & a_{n3} & \dots & 1 \end{bmatrix} \qquad a_{ij}=1/a_{ji} \text{ and } a_{ji}\neq 0 \qquad (2.1)$$

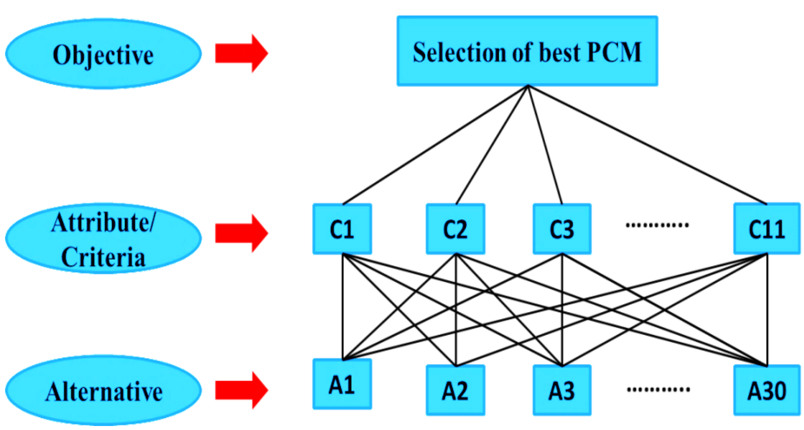

Fig. 2.1 Proposed model based on AHP

Step 2: Here, relative normalized weights of each attribute are obtained by taking the geometric mean of ith row and then normalizing the geometric mean for corresponding attributes according to Eq. 2.2-2.3. Here n denotes the number of attributes or criteria utilized for material selection.

$$GM_i = \{a_{i1} \times a_{i2} \times a_{i3} \times \dots . \times a_{in}\}^{1/n} \tag{2.2}$$

$$W_i = \frac{GM_i}{\sum_{j=1}^{j=n} GM_i} \tag{2.3}$$

Here, W_i represents the relative weight of the i^{th} attributes. Now, we have to follow steps 3-8 to examine the consistency of pairwise comparison matrix A.

Table 2.5 Relative importance of the attribute (i over j) points [187]

Description (i over j)	Relative importance (a_{ij})
Equal importance	1
Moderate importance	3
Strong importance	5
Very strong importance	7
Extremely importance	9
Intermediate values	2,4,6,8

Step 3: Obtain the matrix 'M' such that

$$M = A \times W, \qquad \text{Where, } W = (W_1, W_2, W_3, \dots, W_n)^T \tag{2.4}$$

$$M = A \times W = \begin{bmatrix} 1 & a_{12} & a_{13} & \dots & a_{1n} \\ a_{21} & 1 & a_{23} & \dots & a_{2n} \\ a_{31} & a_{32} & 1 & \dots & a_{3n} \\ \dots & \dots & \dots & \dots & \dots \\ a_{n1} & a_{n2} & a_{n3} & \dots & 1 \end{bmatrix} \begin{bmatrix} W_1 \\ W_2 \\ W_3 \\ \dots \\ W_n \end{bmatrix} = \begin{bmatrix} C_1 \\ C_2 \\ C_3 \\ \dots \\ C_4 \end{bmatrix} \tag{2.5}$$

Where matrix *M* represents an n-dimensional column vector and describes the sum of the weighted values for the importance degrees of alternative.

Step 4: Here, consistency values (*CV*) for a host of alternatives can be evaluated as:

$$CV_i = \frac{C_i}{W_i} \tag{2.6}$$

Step 5: In this step, the eigen value (λ_{max}) representing the mean of the consistency values can be obtained by the following expression.

$$\lambda_{max} = \frac{\sum_{i=1}^{n} CV_i}{n} \tag{2.7}$$

Step 6: Estimate the consistency index (*CI*), which is expressed as

$$CI = \frac{(\lambda_{max} - n)}{n - 1} \tag{2.8}$$

It may be noted that consistency plays a key role in AHP method. The output of the AHP relies on the consistency index value as it describes the degree of consistency during the pairwise comparison of the attributes.

Step 7: Obtain the random index (*RI*). Random index depends upon the number of attributes used for the material selection problem and can be obtained using Table 2.6 [181].

Step 8: Calculate the consistency ratio (*CR*).

$$CR = \frac{CI}{RI} \text{ ; where } RI = \frac{1.987(n-2)}{n} \tag{2.9}$$

Where n represents the number of attributes, the upper limit of *CR* should not exceed the value 0.1. If the *CR* value exceeds 0.1, the same procedure must be repeated until we get the *CR* value less than 0.1. The measurement of consistency reflects the decision maker's experience and analytical thinking in material selection problems.

Table 2.6 Random Index (RI) values [181].

Criteria	RI	Criteria	RI
3	0.52	8	1.4
4	0 .89	9	1.45
5	1.11	10	1.49
6	1.25	11	1.63
7	1.35	12	1.66

2.3.2 Technique for order of preference by similarity to ideal solution (TOPSIS)

TOPSIS is a MADM tool for structuring and solving complex decision making problems involving multiple attributes or criteria. It was first introduced by Hwang & Yoon (1981) [188]. The methodology plays a crucial role in finding the best alternative among several alternatives with multiple attributes usually conflicting in nature. Among various MADM methods, TOPSIS has great potential to deal with complex material selection problems since it facilitates both quantitative and qualitative attributes together. The technique selects the best alternative among a finite set of alternatives that is closest to the ideal solution and farthest from the non-ideal solution [189]. The ideal solutions are one that helps in maximizing the beneficial attributes (higher value is better) and minimizes the cost attribute (a lower value is better). On the contrary, non-ideal solutions minimize the beneficial attributes and maximize the cost attributes. It should be noted that we always desire a higher value of the beneficial attribute and a lower value of the cost attribute to optimize the material selection problem. TOPSIS can be used in an array of disciplines due to the following advantages [190-191].

(1) Systematic, simple, and comprehensible in concept,

(2) Ease of computation even if a problem is complex in nature.

(3) It can quantify the solution and incorporates both qualitative and quantitative attributes.

Fig. 2.2 shows the proposed model of PCM selection for a thermal management system.

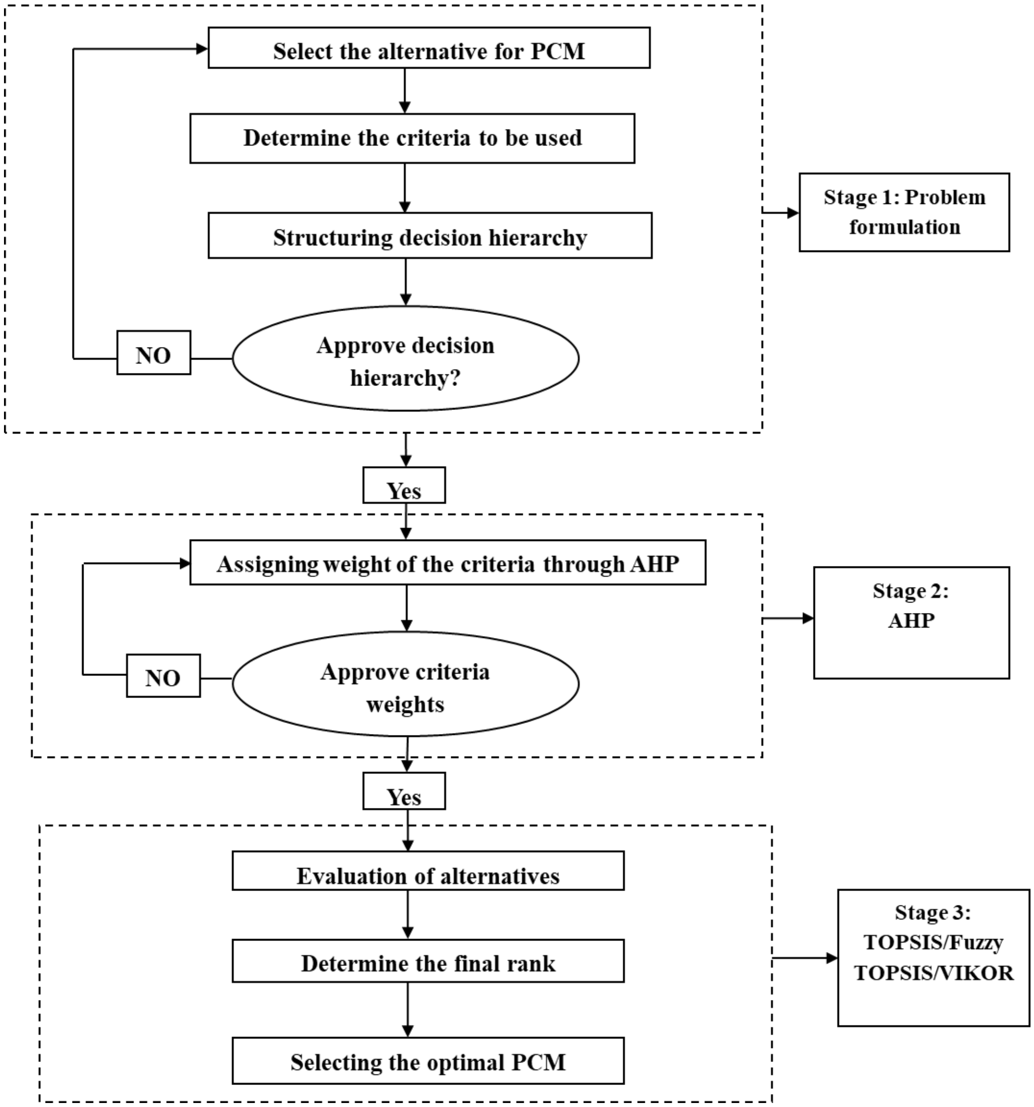

Fig. 2.2 Schematic diagram of the proposed model for PCM selection

Various steps associated with the TOPSIS methodology are illustrated below.

Step 1: A decision matrix $[D]_{M\times N}$ is developed, in which M1, M2, M3,..., M_n represent the number of alternatives and N_1, N_2, N_3,…, N_n represent the number of criteria or attributes of the alternatives. An element d_{ij} of the decision matrix represents the performance rating of the i^{th} alternative corresponding to the j^{th} attribute, as shown in Eq. 2.10. Here, W_1, W_2, W_3…, W_n is the corresponding weight of each attribute that can be obtained using the AHP method.

$$
D = \begin{array}{c c}
 & \begin{array}{ccccc} N_1 & N_2 & N_3 & - & N_n \\ W_1 & W_2 & W_3 & - & W_n \end{array} \\
\begin{array}{c} M_1 \\ M_2 \\ M_3 \\ - \\ - \\ M_n \end{array} & \begin{bmatrix} d_{11} & d_{12} & d_{13} & - & d_{1n} \\ d_{21} & d_{22} & d_{23} & - & d_{2n} \\ d_{31} & d_{32} & d_{33} & - & d_{3n} \\ - & - & - & - & - \\ - & - & - & - & - \\ d_{m1} & d_{m2} & d_{m3} & - & d_{mn} \end{bmatrix}
\end{array} \tag{2.10}
$$

The AHP considers qualitative and quantitative attributes for the analysis. Initially, the qualitative attributes are considered as a linguistic term. The linguistic variables are transformed into the fuzzy number by employing a suitable conversion scale [192-194]. Different conversion scales such as nine-point [187] and eleven-point scales [96] can be employed to convert the linguistic term into the corresponding fuzzy number. The present study considers an eleven-point conversion scale for the analysis. The transformation of qualitative attributes into quantitative attributes by employing the eleven-point conversion scale is summarized in Table 2.7 [96]. After obtaining the fuzzy numbers, the remaining calculation is followed in the same fashion as the quantitative attributes.

Step 2: Here, each element of the decision matrix is normalized by converting it into a particular scale 0 to 1. Hence, each element of the decision matrix (n_{ij}) is obtained by the following expression.

$$
n_{ij} = {d_{ij}} \Big/ {\left(\sum_{i=1}^{m} d_{ij}^2\right)^{1/2}} \quad Where\ i = 1,2,\dots,m\ and\ j = 1,2,\dots,n \tag{2.11}
$$

Step 3: In this step, the weighted normalized matrix (Z) is determined by taking the product of the elements of the normalized decision matrix with their corresponding associated weights. This provides comparable values of each attribute. Each element of this matrix is defined as:

$$
Z = [z_{ij}] = [n_{ij}] \times [w_{j1}] \quad Where\ i = 1,2,\dots,m\ and\ j = 1,2,\dots,n \tag{2.12}
$$

Where, z_{ij} represent the element of the weighted normalized matrix. It may be noted that the weight W_j is obtained from AHP technique.

Step 4: In step 4, we obtain positive ideal solutions $A*$ and negative ideal solutions A'. Here, $A*$ is obtained by selecting the maximum value from beneficial attributes and minimum value from non-beneficial attributes, and A' is obtained by selecting the minimum value from beneficial attributes and maximum value from non-beneficial attributes as reported in Eq. 2.13.

$$\begin{aligned} A^* &= \{Z_1^*, Z_{2,}^* \dots \dots \dots, Z_n^*\} \\ A' &= \{Z_1', Z_{2,}' \dots \dots \dots, Z_n'\} \end{aligned} \tag{2.13}$$

Where, Z_j^* and Z_j' are obtained from Eq. 2.14.

$$\begin{aligned} Z_j^* &= \{\max(Z_{ij})\ if\ j \in J\ ; \min(Z_{ij})\ \ if\ j \in J'\} \\ Z_j' &= \{\min(Z_{ij})\ if\ j \in J\ ; \max\ (Z_{ij})\ \ if\ j \in J'\} \end{aligned} \tag{2.14}$$

Here, J belongs to beneficial attributes (larger the better type) and J' belongs to non-beneficial attributes (smaller, the better type).

Step 5: Now, the distance from positive ideal solutions S_i^+ and negative ideal solutions S_i^- are obtained. An N-dimensional Euclidean distance approach is utilized to obtain the distance of each alternative from the positive and negative ideal solution. According to N-dimensional Euclidean S_i^+ is evaluated as:

$$S_i^+ = \left[\sum_{j=1}^{n} \left(z_{ij} - z_i^*\right)^2\right]^{1/2} \dots (i = 1,2, \dots m) \tag{2.15}$$

While (S_i^-) is estimated as:

$$S_i^- = \left[\sum_{j=1}^{n} \left(z_{ij} - z'_i\right)^2\right]^{1/2} \dots (i = 1,2, \dots, m) \tag{2.16}$$

Step 6: Here, the relative closeness index (C_i^*) is obtained using Eq. 2.17.

$$C_i^* = \frac{S_i^-}{S_i^- + S_i^+} \tag{2.17}$$

Step 7: The alternative which scores the highest value of the relative closeness index C_i^* can be considered as the best alternative. One can put the alternatives in descending order according to their relative closeness index value.

Step 8: Take the final decision based on the user's consideration and practical application. It should be noted that users should consider all the possible attributes that may affect the problem of material selection.

Table 2.7 Values of material selection attribute based on 11 point scale [96]

Linguistic term of the attributes	Crisp score
Exceptionally low (ExL)	0.045
Extremely low (EL)	0 .135
Very low (VL)	0.255
Low (L)	0.355
Below average (BA)	0.410
Average (A)	0.500
Above average (AA)	0.590
High (H)	0.665
Very high (VH)	0.745
Extremely high (EH)	0.865
Exceptionally high (ExH)	0.955

2.3.3 Fuzzy TOPSIS

TOPSIS technique is employed to obtain the solution of ranking problems in real conditions. In certain cases, one needs to obtain a solution by considering both ranking and justification aspects of the problem. Many a time, personal judgments are quantified with a crisp score to tackle the qualitative attributes of the problem. Very often, it is challenging to assign an explicit value of performance rating to the alternative described by qualitative attributes. In such a case, one can employ a fuzzy technique to allocate the relative importance of the attributes by using fuzzy numbers instead of precise numbers. Therefore, the fuzzy TOPSIS technique is developed to address situations involving both ranking and justification problems. The definitions pertaining to the fuzzy theory are elaborated below.

Definition 1 A fuzzy set $\tilde{A}$ in a universe of monologue X is represented by a participation function $\mu_{\tilde{A}}(x)$ which accomplices with each element x in X, a real number in the interval [0, 1]. The functional value $\mu_{\tilde{A}}(x)$ is termed as the grade of membership of x in $\tilde{A}$ [187]. The triangular fuzzy environment is used in the present evaluation model. A triangular fuzzy number ã is represented by a triplet (a_1, a_2, a_3) (Fig. 2.3) and membership function $\mu_{\tilde{a}}(x)$ can be evaluated using the following expression [96].

$$\mu_{\tilde{a}}(x) = \begin{cases} 0; & x < a_1 \\ \dfrac{x - a_1}{a_2 - a_1}; & a_1 < x \le a_2 \\ \dfrac{a_3 - x}{a_3 - a_2}; & a_2 < x \le a_3 \\ 0; & x > a_3 \end{cases} \tag{2.18}$$

Definition 2 Let ã = (a_1, a_2, a_3) and $\tilde{b}$ = (b_1, b_2, b_3) are two fuzzy triangular numbers, hence the vertex method is utilized to obtain the separation between these two and is expressed as:

$$(\tilde{a},\tilde{b}) = \sqrt{\frac{1}{3}[(a_1 - b_1)^2 + (a_2 - b_2)^2 + (a_3 - b_3)^2]} \tag{2.19}$$

It may be noted that the basic operational law of two fuzzy triangular numbers can be evaluated as below [187].

$$\begin{aligned} &\tilde{a} + \tilde{b} = (a_1 + b_{1,} a_2 + b_{2,} a_3 + b_3) \quad \text{For addition} \\ &\tilde{a} \times \tilde{b} = (a_1 \times b_{1,} a_2 \times b_{2,} a_3 \times b_{3,}) \quad \text{For multiplication} \end{aligned} \tag{2.20}$$

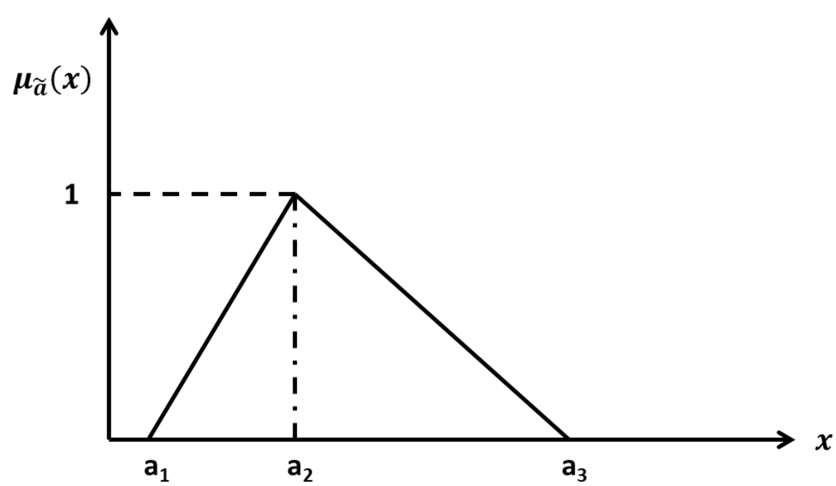

Fig. 2.3 Triangular fuzzy number $\tilde{a}$ [96]

Various steps involved in the fuzzy TOPSIS technique are elaborated below.

Step 1: Here, the linguistic values (d_{ij}, i = 1,2,3,…,m, and j = 1,2,3, …, n) are selected for each alternative corresponding to each attributes. In this approach, no normalization is needed to achieve the normalized triangular fuzzy numbers within 0 and 1.

Step 2: Obtain the weighted normalized fuzzy decision matrix.

Step 3: Estimate the positive ideal solution A^* and negative ideal solution A'. The fuzzy positive ideal and negative ideal solution can be obtained following the procedure as expressed in Eq. 2.13-2.14.

Step 4: The separation (distance) measures S_i^+ and S_i^- can be obtained by using Eq. 2.21-2.22.

$$S_i^+ = \sum_{j=1}^{n} d(\tilde{z}_{ij}, \tilde{z}_i^*) \qquad i = 1,2, \ldots\ldots, m \tag{2.21}$$

$$S_i^- = \sum_{j=1}^{n} d(\tilde{z}_{ij}, \tilde{z}_i') \qquad i = 1,2, \ldots\ldots, m \tag{2.22}$$

Step 5: Determine the relative closeness index to the ideal solution C_i^*. This can be obtained using Eq. 2.23.

$$C_i^* = \frac{S_i^-}{S_i^- + S_i^+} \tag{2.23}$$

Step 6: List the alternative involving maximum C_i^* as the optimal material and rank the alternatives in descending order of C_i^* value.

2.3.4 Vise Kriterijumska Optimizacija Kompromisno Resenje (VIKOR) method

The name VIKOR is derived from the Serbian language VIKOR (VIseKriterijumska Optimizacija I Kompromisno Resenje), which means multi attribute optimization and compromise solution. The technique is employed for selecting the best alternative by determining the compromise solution with conflicting attributes/criteria. By taking into account the relative value of each attribute, the approach proposes an aggregating function that reflects the distance from the ideal solution. One of the distinguishing features of the VIKOR method is that it aggregates the function in such a way that solution is always closest to the optimum solutions, whereas, in TOPSIS, the relative closeness index of the solution is not always close to the ideal solution. The basic compromise algorithm in the VIKOR method can be explained in the following steps [195-196].

Step 1: Create decision matrix $[A]_{M\times N}$, where M1, M2, M3,..., M_n represent the number of alternatives and N_1, N_2, N_3,…, N_n represent the number of attributes of the alternatives similar to the decision matrix used in TOPSIS methodology. The performance rating of the i^{th} alternative corresponding to the j^{th} attribute is represented by element a_{ij} of the decision matrix (Eq. 2.10). The corresponding weightage of each attribute is denoted by W_1, W_2, W_3…, W_n that is obtained by employing AHP method.

Step 2: Obtain normalized and weighted normalized matrix following Eq. 2.11-2.22.

Step 3: From the initial decision matrix, identify the best $(a_{ij})_{max}$ and worst $(a_{ij)min}$ of each attribute.

Step 4: Calculate the utility measure (S_i) and regret measure (R_i) using the following expressions.

$$S_i = L_{1,i} = \sum_{j=1}^{n} \frac{w_j\left[(a_{ij})_{max} - a_{ij}\right]}{\left[(a_{ij})_{max} - (a_{ij})_{min}\right]} \text{ for beneficial attribute}$$

$$S_i = L_{1,i} = \sum_{j=1}^{n} \frac{w_j\left[a_{ij} - (a_{ij})_{min}\right]}{\left[(a_{ij})_{max} - (a_{ij})_{min}\right]} \text{ for non-beneficial attribute} \tag{2.24}$$

$$R_i = L_{\infty,i} = \text{Max}^{\text{m}} \text{ of } \frac{w_j\left[(a_{ij})_{max} - a_{ij}\right]}{\left[(a_{ij})_{max} - (a_{ij})_{min}\right]} \text{ for beneficial attribute}$$

$$R_i = L_{\infty,i} = \text{Max}^{\text{m}} \text{ of } \frac{w_j\left[a_{ij} - (a_{ij})_{min}\right]}{\left[(a_{ij})_{max} - (a_{ij})_{min}\right]} \text{ for non-beneficial attribute} \tag{2.25}$$

Step 5: Calculate the Q_i value.

$$Q_i = v\left[\frac{S_i - S_{min}}{S_{max} - S_{min}}\right] + (1 - v)\left[\frac{R_i - R_{min}}{R_{max} - R_{min}}\right] \tag{2.26}$$

Here, v is the weight for the maximum group utility, and (1-v) is the weight of individual regret. The value of v may vary between 0 and 1. Here, the value of v is considered as 0.5, and this value has been adopted in most of the previous studies [195-197].

Step 6: Arrange the alternative in decreasing order of Q_i value; the best alternative is one that exhibits minimum Q_i value.

2.4 Results and discussion

The selection of optimal PCM for thermal management needs to be made by considering a large number of alternatives for PCM. The selection of the best possible PCMs for thermal management is necessary for the lifelong success of PCM-based heat sink modules. There should not be single criteria for the selection of PCMs. As the melting temperature of the PCM must be close to the heating temperature of the electronic components, it is treated to be the only criteria for PCM pre-screening. In general, the PCM that possesses the melting temperature within 28-58 °C is considered for thermal management of electronic components [135]. Here, a total of thirty alternatives of PCMs evaluated from pre-screening based on the melting temperature range are taken for the analysis. Total eleven attributes are considered for the analysis. Three basic stages have been followed for the selection of the best PCM. These include identification of the criteria or attributes of the alternatives, evaluation of the weight of the attributes, and ranking of alternatives by employing the TOPSIS, fuzzy TOPSIS, and VIKOR methods.

Identification of the attributes for selection of PCM

Numerous properties namely, thermophysical (latent heat, specific heat, thermal conductivity), physical (density, volume and expansion upon melting), kinetic (subcooling, incongruent melting), chemical (thermal stability, corrosiveness, toxicity), and economic (cost) are found to play a significant role during the selection of PCM. Latent heat and specific heat of the PCM are the important attributes that must be considered for the PCM selection problem.

Former properties mean PCM can store more heat during the phase change while keeping the heat sink at a constant temperature. While the latter means it can store more sensible heat for the same temperature difference. High latent and specific heat makes the thermal storage density as great as possible. Thermal conductivity is also one of the important parameters that need to be considered during PCM selection. This characteristic enables heat absorption or release at a low-temperature gradient, resulting in a faster heat storage/release rate of the system. As a result, this characteristic has the potential to improve system efficiency. The desired thermophysical properties of the PCMs for thermal management applications are:

- The melting temperature of the PCM must be below the critical temperature of the electronic components.
- Must have high latent heat of fusion and specific heat.
- High thermal conductivity in both solid and liquid phases.

To reduce the size of the storage containers and the amount of PCM utilized, the latent heat per unit volume of the material should be high, while increased specific heat and thermal conductivity would provide greater sensible energy storage capacity and heat transfer. The desired physical properties of the PCMs are:

- High density.
- Small volume expansion upon melting.

In addition to high latent heat specific heat and thermal conductivity, larger density means that the heat storage capacity per unit volume of PCM is high; this contributes to reducing container costs. Further, it should be noted volume expansion upon melting of PCM should be low negligible. A small volume expansion of the PCM means that a simpler type of thermal management system can be adopted for the system, and a large heat transfer rate can be guaranteed. The important kinetic properties of PCMs are:

- Less or no incongruent melting.
- Less or no subcooling effect.

PCM must melt congruently to prevent irreversible segregation, which leads to loss of energy storage capacity with the cycling. The phase change material should have a consistent chemical composition in different phase states, which can help avoid phase separation phenomena caused by density differences between the solid and liquid states. Furthermore, one of the most essential properties of PCMs is that they have a good rate of nucleation and crystallization and little or no subcooling. Subcooling is particularly problematic for PCM like salt-hydrates, as it obstructs or entirely prevents energy storage. The important chemical properties of PCM for thermal management applications should be:

- Chemically and thermally stable.
- Compatible with the container.
- No toxicity.

There should be no segregation, chemical decomposition, or other side effects when repeatedly cycling through the heat absorption and release processes. This ensures long-term minimal attenuation of the heat storage capacity and improves the reliability of the system. The contamination problems must be avoided with the material for long-term application. Furthermore, PCM must be highly resistant to corrosion and less toxic for safety measures. This means that the PCM is compatible with a variety of packaging materials, making the container material selection easy and lower cost. Also, the material should be non-toxic, non-flammable, non-explosive and safe to use. Finally, PCM used for thermal management must be easily available at a lower price.

The present study considers thirty alternatives with eleven attributes, and the performance ratings are depicted in Table 2.8. Here, the attributes, namely latent heat (LH), specific heat (SH), thermal conductivity (k), density (ρ), are considered to be quantitative attributes. Other attributes such as subcooling (SC), thermal stability (TS), incongruent melting (IM), corrosion (CRN), toxicity (TOX), volume expansion (VE), and cost are considered to be qualitative attributes. The conversion from qualitative to quantitative attributes is made by employing material selection attributes values proposed in Table 2.7. The properties of the pre-screened PCM with their crisp scores are presented in Table 2.9.

Estimation of the weight of the attributes

Table 2.9 is also termed as a decision matrix. After forming the decision matrix weight of each attribute is determined by utilizing AHP technique. In this technique, a pairwise comparison matrix is formulated utilizing the scale presented in Table 2.5. The normalized weights of each attribute are estimated by employing the procedure elaborated in the previous section 2.3.1 and are summarized in Table 2.10. Fig. 2.4 represents the comparison of the weight of the attributes evaluated from this technique. Based on the AHP methodology, various attributes such as latent heat, thermal conductivity, density, and incongruent melting are calculated as the four most important attributes for a thermal management system. The consistency ratio is found to be 0.095, which is less than 0.1. Therefore, weights are considered to be logical and consistent, and they can be utilized for the optimal selection of PCM.

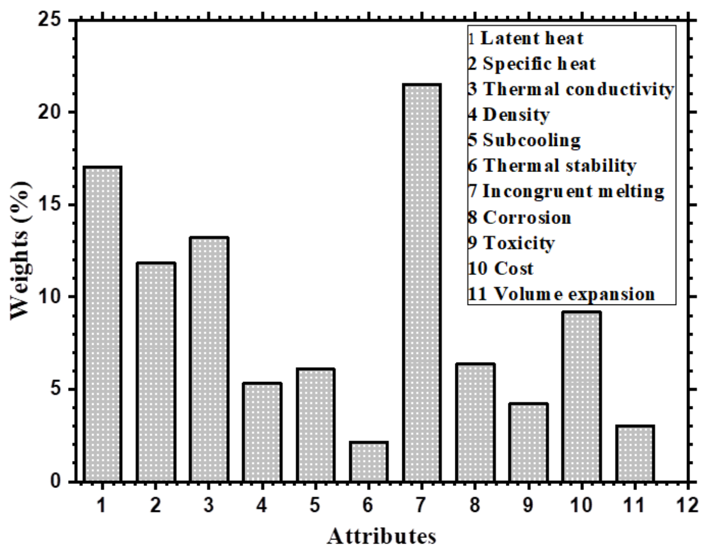

Fig. 2.4 Weight for the attributes obtained from AHP method

Table 2.8 Properties of pre-screened PCM materials

S. No.	PCM	LH (kJ/kg)	SH (J/kgK)	k (W/mK)	ρ (kg/m^3)	SC	TS	IM	CRN	TOX	cost	VE
1	saveE HS 34	150	2400	0.485	1915	L	H	L	L	L	EH	L
2	saveE OM30	200	2600	0.154	901	VL	VH	VL	VL	VL	VH	H
3	sav*E* OM 55	210	3050	0.130	840	VL	VH	VL	VL	VL	VH	H
4	PEG 1000	150	2142	0.152	1109	L	H	L	L	L	H	VL
5	ClimSel C 48	180	3600	0.645	1300	EH	EL	EH	EH	EH	L	VL
6	ClimSel C 32	160	3600	0.920	1400	EH	EL	EH	EH	EH	L	VL
7	ClimSel C 28	170	3600	0.850	1400	EH	EL	EH	EH	EH	L	VL
8	Climsel C58	288.5	1890	0.600	1460	EH	EL	EH	EH	EH	L	VL
9	Pure Temp 28	190	2440	0.200	900	VL	VH	VL	VL	VL	H	VL
10	Pure Temp 37	210	2420	0.200	880	VL	VH	VL	VL	VL	H	EH
11	Pure Temp 48	230	2185	0.200	860	VL	VH	VL	VL	VL	H	EH
12	Pure Temp 58	225	2590	0.200	850	VL	VH	VL	VL	VL	H	EH
13	$CaCl_2.6H_2O$	174.4	1690	0.824	1649	EH	EL	EH	EH	EH	L	VL
14	$LiNo_3.3H_2O$	296	2275	0.702	1500	EH	EL	EH	EH	EH	L	VL
15	Na2SO4. 10 H2O	254	2776	0.544	1485	EH	EL	EH	EH	EH	L	VL
16	Latest 29 T	175	2000	1.000	1490	H	L	H	H	H	H	L
17	Latest 36 S	260	2000	0.600	1450	H	L	H	H	H	H	L
18	S 30	190	1900	0.480	1304	VH	VL	VH	VH	VH	L	VL
19	S 34	115	2100	0.520	2100	VH	VL	VH	VH	VH	L	VL
20	S 44	100	1610	0.430	1584	VH	VL	VH	VH	VH	L	VL
21	RT 35	160	2000	0.20	815	EL	EH	EL	EL	EL	VL	H
22	RT 44 HC	250	2000	0.200	750	EL	EH	EL	EL	EL	VL	H
23	Capric acid	152.7	2090	0.153	945	L	H	L	L	L	EH	EH
24	Heneicosane	201	2500	0.154	791	VL	VH	VL	VL	VL	EH	VH
25	lauric acid	211.6	2015	0.147	934.5	L	H	L	L	L	EH	EH
26	Paraffin wax	193.2	2890	0.210	900	EL	EH	EL	EL	EL	EL	VL
27	A 37	235	2850	0.180	810	VL	VH	VL	VL	VL	L	VH
28	A 50	218	2150	0.150	810	VL	VH	VL	VL	VL	L	VH
29	n- octadecane	241	2050	0.270	780	VL	VH	VL	VL	VL	L	VH
30	n-eicosane	247	2460	0.150	785	VL	VH	VL	VL	VL	L	H

Table 2.9 Performance rating of the PCMs with a crisp fuzzy score

PCM No.	LH (kJ/kg)	SH (J/kgK)	K (W/mK)	ρ (kg/m^3)	SC	TS	IM	CRN	TOX	cost	VE
1	150	2400	0.485	1915	0.335	0.665	0.335	0.335	0.335	0.865	0.335
2	200	2600	0.154	901	0.255	0.745	0.255	0.255	0.255	0.745	0.665
3	210	3050	0.130	840	0.255	0.745	0.255	0.255	0.255	0.745	0.665
4	150	2142	0.152	1109	0.335	0.665	0.335	0.335	0.335	0.665	0.255
5	180	3600	0.645	1300	0.865	0.135	0.865	0.865	0.865	0.335	0.255
6	160	3600	0.920	1400	0.865	0.135	0.865	0.865	0.865	0.335	0.255
7	170	3600	0.850	1400	0.865	0.135	0.865	0.865	0.865	0.335	0.255
8	288.5	1890	0.600	1460	0.865	0.135	0.865	0.865	0.865	0.335	0.255
9	190	2440	0.200	900	0.255	0.745	0.255	0.255	0.255	0.665	0.255
10	210	2420	0.200	880	0.255	0.745	0.255	0.255	0.255	0.665	0.865
11	230	2185	0.200	860	0.255	0.745	0.255	0.255	0.255	0.665	0.865
12	225	2590	0.200	850	0.255	0.745	0.255	0.255	0.255	0.665	0.865
13	174.4	1690	0.824	1649	0.865	0.135	0.865	0.865	0.865	0.335	0.255
14	296	2275	0.702	1500	0.865	0.135	0.865	0.865	0.865	0.335	0.255
15	254	2776	0.544	1485	0.865	0.135	0.865	0.865	0.865	0.335	0.255
16	175	2000	1.000	1490	0.665	0.335	0.665	0.665	0.665	0.665	0.335
17	260	2000	0.600	1450	0.665	0.335	0.665	0.665	0.665	0.665	0.335
18	190	1900	0.480	1304	0.745	0.255	0.745	0.745	0.745	0.335	0.255
19	115	2100	0.520	2100	0.745	0.255	0.745	0.745	0.745	0.335	0.255
20	100	1610	0.430	1584	0.745	0.255	0.745	0.745	0.745	0.335	0.255
21	160	2000	0.200	815	0.135	0.865	0.135	0.135	0.135	0.255	0.665
22	250	2000	0.200	750	0.135	0.865	0.135	0.135	0.135	0.255	0.665
23	152.7	2090	0.153	945	0.335	0.665	0.335	0.335	0.335	0.865	0.865
24	201	2500	0.154	791	0.255	0.745	0.255	0.255	0.255	0.865	0.745
25	211.6	2015	0.147	934.5	0.335	0.665	0.335	0.335	0.335	0.865	0.865
26	193.2	2890	0.210	900	0.135	0.865	0.135	0.135	0.135	0.865	0.255
27	235	2850	0.180	810	0.255	0.745	0.255	0.255	0.255	0.335	0.745
28	218	2150	0.150	810	0.255	0.745	0.255	0.255	0.255	0.335	0.745
29	241	2050	0.270	780	0.255	0.745	0.255	0.255	0.255	0.335	0.745
30	247	2460	0.150	785	0.255	0.745	0.255	0.255	0.255	0.335	0.665

Table 2.10 Results obtained from AHP method

Criteria	Weights	λ_{max}, CI, RI	CR
Latent heat	0.177		
Specific heat	0.119	λ_{max}=12.560	
Thermal conductivity	0.134		
Density	0.050	CI = 0.156	
Subcooling	0.058		
Thermal stability	0.018	RI = 1.630	CR = 0.095
Incongruent melting	0.228		
Corrosion	0.060		
Toxicity	0.039		
cost	0.090		
Volume expansion	0.027		

Estimation of alternatives using TOPSIS method

The performance rating of the alternative (Table 2.9) can also be used as a decision matrix for TOPSIS calculation. Each element of the decision matrix is normalized using Eq. 2.11. The normalized weight of each attribute, estimated using the steps explained in section 2.3.1, is summarized in Table 2.10. Subsequently, the normalized matrix is obtained and is shown in Table 2.11. The weighted normalized matrix is then determined following Eq. 2.12. The positive ideal solutions and negative ideal solutions are obtained by using the Eqs 2.13-2.14.

The final ranking of the alternatives is estimated by utilizing steps 5-8 as detailed in section 2.3.2 and the results obtained are presented in Table 2.12. The final ranking of the alternatives are obtained based on the relative closeness to the ideal solution value (C_i^*). Based on the C_i^* value alternative materials are listed in descending order (Table 2.13). Here, RT 44 HC can be selected as the best alternative for thermal management of electronic components, followed by RT 35, Paraffin wax, n-eicosane, and A-37 considering eleven attributes. It may be noted that the new attributes (if any) discovered can be incorporated into the model to enhance the efficiency of the problem. In addition to this, efforts have been made to employ a fuzzy TOPSIS and VIKOR method to evaluate an optimal selection of PCMs. The details of the technique and the results obtained by these methods are compared in the subsequent section.

Estimation of alternatives using fuzzy TOPSIS method

The fuzzy TOPSIS approach also utilizes the decision matrix (Table 2.9). One needs to convert performance rating into fuzzy qualitative variables at this juncture, as reported in section 2.3.3. This yields the normalized value of performance rating within the range of (0-1). The normalized ratings of each element of the decision matrix are obtained by utilizing the following expression.

$$r_{ij} = \frac{[d_{ij} - min(d_{ij})]}{[max(d_{ij}) - min(d_{ij})]} \qquad \text{for beneficial criteria}$$

$$r_{ij} = \frac{[max(d_{ij})] - d_{ij}}{[max(d_{ij}) - min(d_{ij})]} \qquad \text{for non-beneficial criteria} \tag{2.27}$$

Using equation 2.27, the normalized matrix is obtained and is summarized in Table 2.14. The weights of the attributes are also presented in Table 2.14. Further, the decision matrix can be estimated using the membership function of fuzzy qualitative variables, as depicted in Fig. 2.5. The triangular numbers associated with the fuzzy variables are presented in Table 2.15. Hence, Table 2.14 is converted to Table 2.16 to form the decision matrix with fuzzy linguistic variables.

Table 2.11 Normalized matrix for TOPSIS analysis

PCM No.	LH	SH	K	ρ	SC	TS	IM	CRN	TOX	cost	VE
1	0.133	0.179	0.188	0.288	0.112	0.204	0.112	0.112	0.112	0.278	0.11
2	0.177	0.194	0.06	0.136	0.085	0.228	0.085	0.085	0.085	0.240	0.217
3	0.186	0.227	0.05	0.126	0.085	0.228	0.085	0.085	0.085	0.240	0.217
4	0.133	0.159	0.059	0.167	0.112	0.204	0.112	0.112	0.112	0.214	0.083
5	0.160	0.268	0.25	0.196	0.288	0.041	0.288	0.288	0.288	0.108	0.083
6	0.142	0.268	0.357	0.211	0.288	0.041	0.288	0.288	0.288	0.108	0.083
7	0.151	0.268	0.33	0.211	0.288	0.041	0.288	0.288	0.288	0.108	0.083
8	0.256	0.141	0.233	0.22	0.288	0.041	0.288	0.288	0.288	0.108	0.083
9	0.168	0.182	0.078	0.136	0.085	0.228	0.085	0.085	0.085	0.214	0.083
10	0.186	0.180	0.078	0.132	0.085	0.228	0.085	0.085	0.085	0.214	0.283
11	0.204	0.163	0.078	0.129	0.085	0.228	0.085	0.085	0.085	0.214	0.283
12	0.200	0.193	0.078	0.128	0.085	0.228	0.085	0.085	0.085	0.214	0.283
13	0.155	0.126	0.32	0.248	0.288	0.041	0.288	0.288	0.288	0.108	0.083
14	0.262	0.169	0.272	0.226	0.288	0.041	0.288	0.288	0.288	0.108	0.083
15	0.225	0.207	0.211	0.224	0.288	0.041	0.288	0.288	0.288	0.108	0.083
16	0.155	0.149	0.388	0.224	0.222	0.103	0.222	0.222	0.222	0.214	0.110
17	0.231	0.149	0.233	0.218	0.222	0.103	0.222	0.222	0.222	0.214	0.110
18	0.168	0.141	0.186	0.196	0.248	0.078	0.248	0.248	0.248	0.108	0.083
19	0.102	0.156	0.202	0.316	0.248	0.078	0.248	0.248	0.248	0.108	0.083
20	0.089	0.12	0.167	0.238	0.248	0.078	0.248	0.248	0.248	0.108	0.083
21	0.142	0.149	0.078	0.123	0.045	0.265	0.045	0.045	0.045	0.082	0.217
22	0.222	0.149	0.078	0.113	0.045	0.265	0.045	0.045	0.045	0.082	0.217
23	0.135	0.156	0.059	0.142	0.112	0.204	0.112	0.112	0.112	0.278	0.283
24	0.178	0.186	0.06	0.119	0.085	0.228	0.085	0.085	0.085	0.278	0.244
25	0.188	0.15	0.057	0.141	0.112	0.204	0.112	0.112	0.112	0.278	0.283
26	0.171	0.215	0.081	0.135	0.045	0.265	0.045	0.045	0.045	0.278	0.083
27	0.208	0.212	0.070	0.122	0.085	0.228	0.085	0.085	0.085	0.108	0.244
28	0.193	0.160	0.058	0.122	0.085	0.228	0.085	0.085	0.085	0.108	0.244
29	0.214	0.153	0.105	0.117	0.085	0.228	0.085	0.085	0.085	0.108	0.244
30	0.219	0.183	0.058	0.118	0.085	0.228	0.085	0.085	0.085	0.108	0.217

Table 2.12 Summary of results obtained from TOPSIS analysis

PCM	LH	SH	K	ρ	SC	TS	IM	CRN	TOX	cost	VE	C_i^*
1	0.023	0.021	0.025	0.014	0.006	0.004	0.025	0.007	0.004	0.025	0.003	0.2362
2	0.031	0.023	0.008	0.007	0.005	0.004	0.019	0.005	0.003	0.022	0.006	0.2544
3	0.033	0.027	0.007	0.006	0.005	0.004	0.019	0.005	0.003	0.022	0.006	0.2603
4	0.024	0.019	0.008	0.008	0.006	0.004	0.025	0.007	0.004	0.019	0.002	0.2149
5	0.028	0.032	0.034	0.010	0.017	0.001	0.066	0.017	0.011	0.010	0.002	0.1790
6	0.025	0.032	0.048	0.010	0.017	0.001	0.066	0.017	0.011	0.010	0.002	0.2281
7	0.027	0.032	0.044	0.010	0.017	0.001	0.066	0.017	0.011	0.010	0.002	0.2156
8	0.045	0.017	0.031	0.011	0.017	0.001	0.066	0.017	0.011	0.010	0.002	0.1966
9	0.03	0.022	0.01	0.007	0.005	0.004	0.019	0.005	0.003	0.019	0.002	0.2542
10	0.033	0.021	0.01	0.007	0.005	0.004	0.019	0.005	0.003	0.019	0.008	0.2573
11	0.036	0.019	0.01	0.006	0.005	0.004	0.019	0.005	0.003	0.019	0.008	0.2614
12	0.035	0.023	0.01	0.006	0.005	0.004	0.019	0.005	0.003	0.019	0.008	0.2622
13	0.027	0.015	0.043	0.012	0.017	0.001	0.066	0.017	0.011	0.010	0.002	0.1955
14	0.046	0.020	0.037	0.011	0.017	0.001	0.066	0.017	0.011	0.010	0.002	0.2176
15	0.040	0.025	0.028	0.011	0.017	0.001	0.066	0.017	0.011	0.010	0.002	0.1779
16	0.027	0.018	0.052	0.011	0.013	0.002	0.051	0.013	0.009	0.019	0.003	0.2392
17	0.041	0.018	0.031	0.011	0.013	0.002	0.051	0.013	0.009	0.019	0.003	0.1886
18	0.030	0.017	0.025	0.010	0.014	0.001	0.057	0.015	0.010	0.010	0.002	0.1421
19	0.018	0.019	0.027	0.016	0.014	0.001	0.057	0.015	0.010	0.010	0.002	0.1407
20	0.016	0.014	0.022	0.012	0.014	0.001	0.057	0.015	0.010	0.010	0.002	0.1187
21	0.025	0.018	0.010	0.006	0.003	0.005	0.010	0.003	0.002	0.007	0.006	0.3032
22	0.039	0.018	0.010	0.006	0.003	0.005	0.010	0.003	0.002	0.007	0.006	0.3208
23	0.024	0.018	0.008	0.007	0.006	0.004	0.025	0.007	0.004	0.025	0.008	0.2112
24	0.032	0.022	0.008	0.006	0.005	0.004	0.019	0.005	0.003	0.025	0.007	0.2531
25	0.033	0.018	0.008	0.007	0.006	0.004	0.025	0.007	0.004	0.025	0.008	0.2235
26	0.030	0.026	0.011	0.007	0.003	0.005	0.010	0.003	0.002	0.025	0.002	0.3018
27	0.037	0.025	0.009	0.006	0.005	0.004	0.019	0.005	0.003	0.010	0.007	0.2754
28	0.034	0.019	0.008	0.006	0.005	0.004	0.019	0.005	0.003	0.010	0.007	0.2661
29	0.038	0.018	0.014	0.006	0.005	0.004	0.019	0.005	0.003	0.010	0.007	0.2750
30	0.039	0.022	0.008	0.006	0.005	0.004	0.019	0.005	0.003	0.010	0.006	0.2758

Table 2.13 Alternatives arranged in descending order of C_i^* value

PCM	Ranking	PCM	Ranking	PCM	Ranking
RT 44 HC	1	Pure Temp 37	11	PEG 1000	21
RT 35	2	SavE OM 30	12	Capric acid	22
Paraffin wax	3	Pure Temp 28	13	Climsel C58	23
n-eicosane	4	Heneicosane	14	$CaCl_2.6H_2O$	24
A 37	5	Latest 29 T	15	Latest 36 S	25
n- octadecane	6	SavE HS 34	16	Climsel C 48	26
A 50	7	ClimSel C 32	17	Na2SO4. 10 H2O	27
Pure Temp 58	8	Lauric acid	18	S 30	28
Pure Temp 48	9	$LiNo_3.3H_2O$	19	S 34	29
SavE OM 55	10	Climsel C 28	20	S 44	30

Table 2.14 Normalized decision matrix for fuzzy TOPSIS analysis

PCM	LH	SH	K	ρ	SC	TS	IM	CRN	TOX	cost	VE
1	0.26	0.4	0.41	0.86	0.73	0.73	0.73	0.73	0.73	0.00	0.87
2	0.51	0.5	0.03	0.11	0.84	0.84	0.84	0.84	0.84	0.20	0.33
3	0.56	0.72	0.00	0.07	0.84	0.84	0.84	0.84	0.84	0.20	0.33
4	0.26	0.27	0.03	0.27	0.73	0.73	0.73	0.73	0.73	0.33	1.00
5	0.41	1.00	0.59	0.41	0.00	0.00	0.00	0.00	0.00	0.87	1.00
6	0.31	1.00	0.91	0.48	0.00	0.00	0.00	0.00	0.00	0.87	1.00
7	0.36	1.00	0.83	0.48	0.00	0.00	0.00	0.00	0.00	0.87	1.00
8	0.96	0.14	0.54	0.53	0.00	0.00	0.00	0.00	0.00	0.87	1.00
9	0.46	0.42	0.08	0.11	0.84	0.84	0.84	0.84	0.84	0.33	1.00
10	0.56	0.41	0.08	0.1	0.84	0.84	0.84	0.84	0.84	0.33	0.00
11	0.66	0.29	0.08	0.08	0.84	0.84	0.84	0.84	0.84	0.33	0.00
12	0.64	0.49	0.08	0.07	0.84	0.84	0.84	0.84	0.84	0.33	0.00
13	0.38	0.04	0.80	0.67	0.00	0.00	0.00	0.00	0.00	0.87	1.00
14	1.00	0.33	0.66	0.56	0.00	0.00	0.00	0.00	0.00	0.87	1.00
15	0.79	0.59	0.48	0.54	0.00	0.00	0.00	0.00	0.00	0.87	1.00
16	0.38	0.20	1.00	0.55	0.27	0.27	0.27	0.27	0.27	0.33	0.87
17	0.82	0.20	0.54	0.52	0.27	0.27	0.27	0.27	0.27	0.33	0.87
18	0.46	0.15	0.40	0.41	0.16	0.16	0.16	0.16	0.16	0.87	1.00
19	0.08	0.25	0.45	1.00	0.16	0.16	0.16	0.16	0.16	0.87	1.00
20	0.00	0.00	0.34	0.62	0.16	0.16	0.16	0.16	0.16	0.87	1.00
21	0.31	0.20	0.08	0.05	1.00	1.00	1.00	1.00	1.00	1.00	0.33
22	0.77	0.20	0.08	0.00	1.00	1.00	1.00	1.00	1.00	1.00	0.33
23	0.27	0.24	0.03	0.14	0.73	0.73	0.73	0.73	0.73	0.00	0.00
24	0.52	0.45	0.03	0.03	0.84	0.84	0.84	0.84	0.84	0.00	0.20
25	0.57	0.20	0.02	0.14	0.73	0.73	0.73	0.73	0.73	0.00	0.00
26	0.48	0.64	0.09	0.11	1.00	1.00	1.00	1.00	1.00	0.00	1.00
27	0.69	0.62	0.06	0.04	0.84	0.84	0.84	0.84	0.84	0.87	0.20
28	0.6	0.27	0.02	0.04	0.84	0.84	0.84	0.84	0.84	0.87	0.20
29	0.72	0.22	0.16	0.02	0.84	0.84	0.84	0.84	0.84	0.87	0.20
30	0.75	0.43	0.02	0.03	0.84	0.84	0.84	0.84	0.84	0.87	0.33
Weight	0.18	0.12	0.13	0.05	0.06	0.02	0.23	0.06	0.04	0.09	0.03

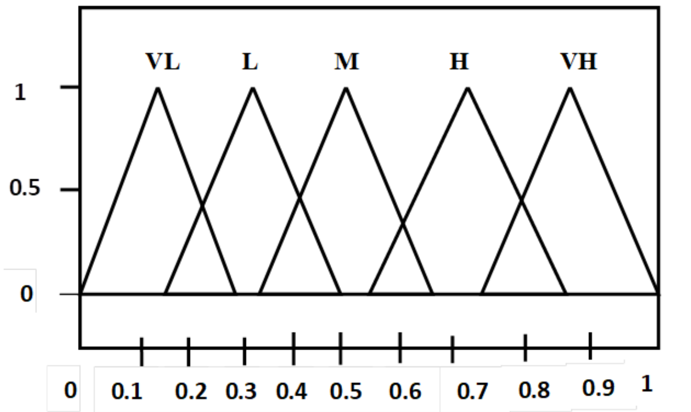

Fig. 2.5 Fuzzy triangular membership functions [96]

Table 2.15 Transformation for fuzzy membership functions [96]

Linguistic variables	Fuzzy numbers
Very low (VL)	(0.00, 0.10, 0.25)
Low (L)	(0.15, 0.30, 0.45)
Medium (M)	(0..35, 0.50, 0.65)
High (H)	(0.55, 0.70, 0.85)
Very high (VH)	(0.75, 0.90, 1.00)

The fuzzy linguistic variable is then converted into fuzzy triangular numbers. Furthermore, the fuzzy weighted decision matrix is obtained, and various steps (3-5), as explained in section (2.3.3), are followed to evaluate the final ranking of the alternatives. The value of C_i^* are used to list out the best alternatives, and the same are summarized in Table 2.17. The top five alternatives obtained from fuzzy TOPSIS analysis for thermal management of electronic components are found to be paraffin wax, RT 44 HC, A 37, n- eicosane, and A50.

Table 2.16 Decision matrix with fuzzy linguistic variables

PCM No.	LH	SH	K	ρ	SC	TS	IM	CRN	TOX	cost	VE
1	L	L	L	VH	H	H	H	H	H	VL	VH
2	M	M	VL	VL	H	H	H	H	H	VL	L
3	M	H	VL	VL	H	H	H	H	H	VL	L
4	L	L	VL	L	H	H	H	H	H	L	VH
5	L	VH	M	L	VL	VL	VL	VL	VL	VH	VH
6	L	VH	VH	M	VL	VL	VL	VL	VL	VH	VH
7	L	VH	H	M	VL	VL	VL	VL	VL	VH	VH
8	VH	VL	M	M	VL	VL	VL	VL	VL	VH	VH
9	M	M	VL	VL	H	H	H	H	H	L	VH
10	M	L	VL	VL	H	H	H	H	H	L	VL
11	M	L	VL	VL	H	H	H	H	H	L	VL
12	M	M	VL	VL	H	H	H	H	H	L	VL
13	L	VL	H	H	VL	VL	VL	VL	VL	VH	VH
14	VH	L	H	M	VL	VL	VL	VL	VL	VH	VH
15	H	M	M	M	VL	VL	VL	VL	VL	VH	VH
16	L	VL	H	M	L	L	L	L	L	L	VH
17	H	VL	M	M	L	L	L	L	L	L	VH
18	M	VL	L	L	VL	VL	VL	VL	VL	VH	VH
19	VL	VL	L	VH	VL	VL	VL	VL	VL	VH	VH
20	VL	VL	L	M	VL	VL	VL	VL	VL	VH	VH
21	L	VL	VL	VL	VH	VH	VH	VH	VH	VH	L
22	H	VL	VL	VL	VH	VH	VH	VH	VH	VH	L
23	L	VL	VL	VL	H	H	H	H	H	VL	VL
24	M	L	VL	VL	H	H	H	H	H	VL	VL
25	M	VL	VL	VL	H	H	H	H	H	VL	VL
26	M	M	VL	VL	VH	VH	VH	VH	VH	L	VH
27	H	M	VL	VL	H	H	H	H	H	VH	VL
28	H	L	VL	VL	H	H	H	H	H	VH	VL
29	H	VL	VL	VL	H	H	H	H	H	VH	VL
30	H	L	VL	VL	H	H	H	H	H	VH	L
Final weight	H	M	M	VL	VL	VL	VH	VL	VL	VL	VL

Table 2.17 Alternatives arranged in descending order of C_i^* value

PCM	Ranking	PCM	Ranking	PCM	Ranking
Paraffin wax	1	Save OM 30	11	Na2SO4. 10 H2O	21
RT 44 HC	2	Pure Temp 58	11	Latest 36 S	22
A 37	3	PEG 1000	13	Climsel C 58	23
n-eicosane	4	Pure Temp 37	14	Capric acid	24
A 50	5	Pure Temp 48	14	Climsel C 48	25
Pure Temp 28	6	Heneicosane	16	Latest 29 T	26
Sav*E* OM 55	7	$LiNo_3.3H_2O$	17	$CaCl_2.6H_2O$	27
SavE HS 34	8	Climsel C 32	18	S 30	28
n-octadecene	9	Lauric acid	19	S 34	29
R-T35	10	Climsel C 28	20	S 44	30

Estimation of alternatives using VIKOR method

Here, similar to TOPSIS and fuzzy TOPSIS method decision matrix is constructed as presented in Table 2.9. The decision matrix is then normalized, and the weighted normalized matrix is obtained following the procedure explained in section 2.3.4. The utility measures (S_i) and regret measures (R_i) are obtained using Eq. 2.24-2.25. Finally, the Q_i value is obtained and presented in Table 2.18. Based on Q_i value, PCMs are ranked and presented in Table 2.19. According to the VIKOR method, the top PCM for thermal management applications are RT 44 HC, A 37, n-octadecene, n-eicosane, RT 35, and paraffin wax.

Table 2.18 Results of VIKOR methodology

PCM	S_i	R_i	Q_i
1	0.494	0.132	0.279
2	0.478	0.131	0.216
3	0.448	0.134	0.189
4	0.557	0.132	0.313
5	0.604	0.228	0.579
6	0.576	0.228	0.546
7	0.578	0.228	0.548
8	0.609	0.228	0.585
9	0.460	0.123	0.179
10	0.470	0.123	0.191
11	0.467	0.123	0.187
12	0.448	0.123	0.165
13	0.683	0.228	0.672
14	0.562	0.228	0.529
15	0.595	0.228	0.568
16	0.584	0.166	0.418
17	0.571	0.166	0.402
18	0.656	0.191	0.557
19	0.676	0.191	0.581
20	0.752	0.191	0.671
21	0.407	0.123	0.117
22	0.328	0.123	0.024
23	0.620	0.131	0.384
24	0.508	0.131	0.252
25	0.573	0.132	0.330
26	0.392	0.122	0.096
27	0.374	0.127	0.084
28	0.435	0.131	0.167
29	0.403	0.113	0.088
30	0.388	0.131	0.111

Table 2.19 Alternatives arranged based on Q_i value

PCM	Ranking	PCM	Ranking	PCM	Ranking
RT 44 HC	1	Save OM 55	11	$LiNO_3$. 3H2O	21
A 37	2	Pure Temp 37	12	Climsel 32	22
n-octadecene	3	Save OM 30	13	Climsel C 28	23
Paraffin wax	4	Heneicosane	14	S 30	24
n-eicosane	5	Save HS 34	15	Na2SO4. 10 H2O	25
RT 35	6	PEG 1000	16	Climsel C 48	26
Pure Temp 58	7	Lauric acid	17	S 34	27
A 50	8	Capric acid	18	Climsel C 58	28
Pure Temp 28	9	Latest 36 S	19	S 44	29
Pure Temp 48	10	Latest 29 T	20	$CaCl_2.6H_2O$	30

It may be noted that each method (TOPSIS, fuzzy TOPSIS, and VIKOR) yields RT 44 HC and paraffin wax as the best PCM for thermal management of electronic devices. In addition to this, some of the top selected PCMs employing various MADM techniques for thermal management applications are RT 35, A 37, n-eicosane, n-octadecene, and A 50. Fig. 2.6 presents the comparison of ranking from these three methods. This shows the validation of these models. However, the preference may change after the top spot. Although there are small variations in the ranking as obtained using these three methods, there is a high-rank correlation between these three methods. A similar validation procedure has been adopted by Rathod et al. [96] in the selection of phase change materials for solar water system applications. The authors employed TOPSIS and fuzzy TOPSIS methods and obtained calcium chloride hexahydrate as the best PCM with both the methods for the given application.

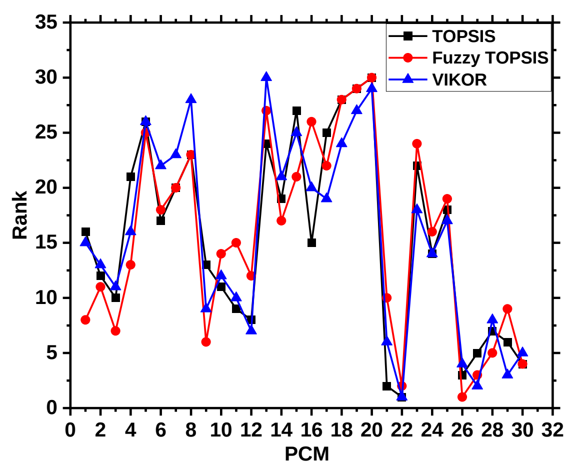

Fig. 2.6 Comparative ranking of PCM using different MADM techniques

2.5 Concluding remarks

In this study, a novel multi attribute decision making (MADM) model is proposed to select the best PCM among various PCMs for thermal management applications. The model considers various alternatives and attributes for the analysis.

Here, a selection system and model based on the AHP, TOPSIS, fuzzy TOPSIS, and VIKOR methods were proposed for the selection of PCM to use in a thermal management system. The AHP technique is utilized to determine the weight of the attributes. The present study considers 30 PCMs with melting temperatures varying between 28-58 °C and 11 attributes for the analysis. The model is validated, and results are found to be in good agreement with the existing studies. Based on the analysis, it is recommended to use organic PCMs for the thermal management of electronic components. In general, TOPSIS, fuzzy TOPSIS, and VIKOR methods, along with AHP, can play a crucial role in narrowing down the wrong selection of PCM for the given application. The present study provides a general procedure for diverse material selection problems. The methodology proposed can consider any number of qualitative and/or quantitative attributes simultaneously and helps to obtain the rank of the alternatives.

The present study considers both quantitative and qualitative attributes for the analysis. In summary, the methodology is simple, logical, and convenient to use compared to other MADM methods.

Chapter 3

Numerical investigation on the thermal performance of PCM-based heat sink with various fin configurations

3.1 General background

The design and development of the thermal management system play a crucial role in preventing the overheating and failure of electronic components because of higher power density. The latent heat thermal energy storage system (LHTESS) incorporating PCMs is found to be successful in extending the overheating time of critical components in electronic devices. However, the organic PCMs usually have lower thermal conductivity values (0.1-0.3 W/m-K), which decreases the rate of heat absorption and release [198]. Numerous studies have been made that report the enhancement of the thermal performance of heat sink by employing fins in the PCM-based heat sink module [65, 107, 130, 135, 141, 199-201]. The thermal performance of a PCM-based heat sink is found to depend on numerous parameters such as the number of fins, the height of the fin, and PCM volume fraction [65, 107, 130, 135]. Most of the previous studies consider different mass for different heat sink configurations. Also, the studies mostly consider parallel plate-fin arrangement based heat sinks. Nevertheless, not a single study has been reported to analyze the heat transfer performance of PCM-based heat sink with cross plate fins through numerical investigation. In addition, it is essential to study the influence of convection, induced due to density difference, during the melting of PCM, evolution of melt front, melting pattern, and isotherm contour; this can be achieved in more detail through numerical investigation [202].

The present study reports the three-dimensional numerical investigation of PCM-based cross plate fin heat sink to analyze the thermal performance and phase change phenomena during the melting of PCM. Here, the heat sink assembly involving cross plate fins with a different number of cavities (1, 4, 9, 16, 25, and 36) is studied; the thickness of fins and wall is varied to ensure the constant value of mass and thermal capacity of heat sink module. The performance of various heat sink configurations is evaluated based on the transient temperature variation of the heat sink base, PCM melt fraction, average Nusselt number, and energy absorbed by PCM during both latent and sensible heat stages.

In order to reduce the weight of the systems, many a time, hollow fins of different configurations are used to analyze the thermal performance of heat sink modules. Such studies have not been reported extensively in the literature. Here, an effort has been made to analyze the thermal performance of PCM-based heat sinks involving hollow fins with different configurations (circular and square). The heat transfer performance is analyzed through variation in the heat sink base temperature, melt fractions, solid-liquid interface, and maximum velocity distributions during melting of PCM for a varied range of heat flux values ($q'' =$1.5-2.0 kW/m^2).

3.2 Numerical modeling to estimate the thermal performance of PCM-based heat sink with cross plate fins

Here, efforts have been made to analyze the thermal performance of heat sink modules with cross plate fins for a varied range of heat flux values through numerical investigation. The details of the physical model, governing equation, boundary condition, solution scheme, and results obtained from the model are presented in subsequent sections.

3.2.1 Physical model

The isometric view of the physical model with different numbers of cross plate fin heat sink forming different cavities is depicted in Fig. 3.1. The overall size of the heat sink is kept constant (100×100×25 mm^3). Table 3.1 depicts the dimension of heat sink configurations used in this study. The fin volume fraction is kept at 6.60 % for all the cases, while the thickness of the wall and fin material is varied in different heat sink configurations. Here, the material of the heat sink and fins are chosen as aluminum because of its lightweight (ρ=2719 kg/m^3), higher thermal conductivity (k=202.4 W/m-K), and high specific heat value (C_p=871 J/kg-K). The thermodynamic representation of one of the models (16 cavities heat sink) is presented in Fig. 3.2. Here, the square heat sink ($L \times W$=100×100 mm^2) with the base thickness (t_b =2 mm) and height (H=25 mm) is considered as constant for all six designs of the heat sink. Here, t_w, t_f, h**,** and d represent the thickness of the wall, thickness of the fin, height of the PCM element, and size of the PCM storage cavity, respectively, and are selected in such a way that mass and heat capacity of each thermal storage unit remain constant. Constant heat flux is applied on the bottom surface of the heat sink, while the top surface and side walls of the heat sink are considered to be thermally insulated. Commercially available paraffin wax (melting point = 58-62°C [203]) obtained as best PCM from fuzzy TOPSIS method is selected as PCM for storing thermal energy due to its various favorable thermophysical properties.

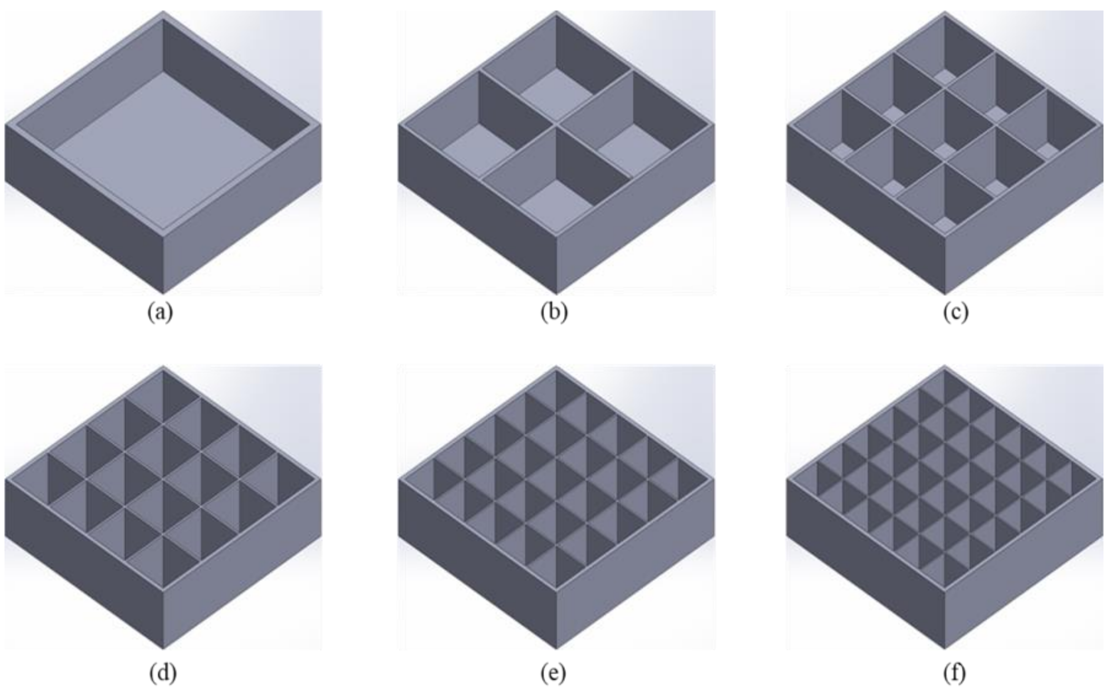

Fig. 3.1 Isometric views of various heat sink configurations used for numerical study: (a) 1 cavity (b) 4 cavities (c) 9 cavities (d) 16 cavities (e) 25 cavities (f) 36 cavities

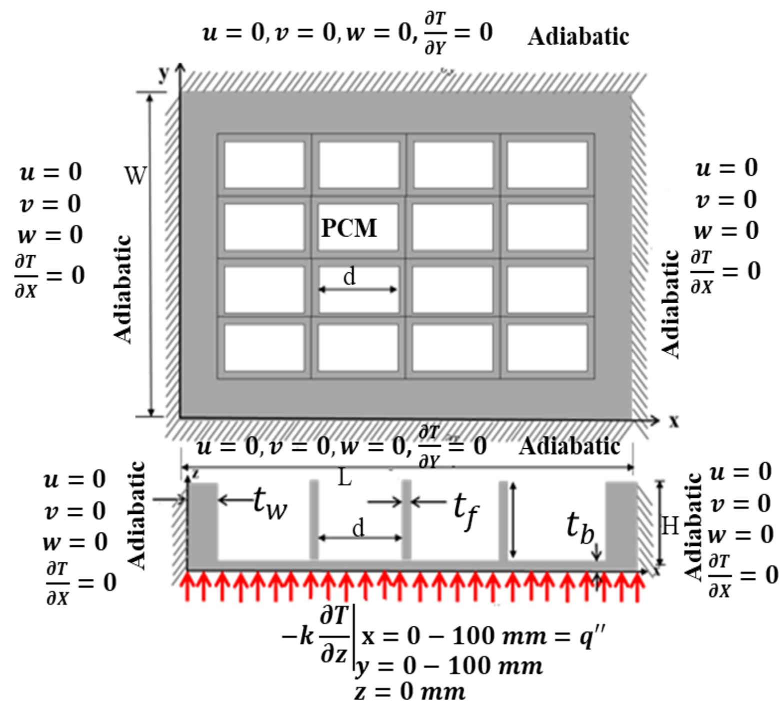

Fig. 3.2 Thermodynamic representation of the computational domain (16 cavities heat sink)

Table 3.1 Dimensions of heat sink and cross fins

Heat sink	Dimension ($L \times W \times H$ mm^3)	t_b (mm)	t_w (mm)	t_f (mm)	Cavity ($d \times d \times h$ mm^3)
1 cavity (No fin)	100×100×25	2	3.5	-	93×93×23
4 cavities (1×1fin)	100×100×25	2	2	2.00	47×47×23
9 cavities (2×2 fin)	100×100×25	2	2	1.50	31×31×23
16 cavities (3×3 fin)	100×100×25	2	2	1.00	23.25×23.25×23
25 cavities (4×4 fin)	100×100×25	2	2	0.75	18.6×18.6×23
36 cavities (5×5 fin)	100×100×25	2	2	0.60	15.5×15.5×23

3.2.2 Mathematical model and computational procedure

The enthalpy-porosity approach [106-204] is utilized to model the phase change phenomena of PCM during melting. In this approach, the energy equation involving enthalpy variation, which accounts for the phase change process of

PCM melting, is considered for the analysis. The computational domain of the physical model is assumed to be a porous medium. The porosity value of an individual cell is defined by a term called melt fraction ($\emptyset$) which helps in tracking the melting of PCM. The value of $\emptyset$=0 indicates a solid-state of PCM, while $\emptyset$=1 corresponds to fully melted PCM. The following are the necessary assumptions used to solve the present numerical model of the PCM-based heat sink assembly:

a) Three-dimensional and unsteady state.
b) The flow of the molten PCM is Newtonian, laminar, and incompressible with negligible viscous dissipation.
c) Heat transfer through radiation is not accounted for.
d) The expansion of PCM upon melting is not considered [115, 202]
e) The PCM and aluminum are pure with constant thermophysical properties. Also, the thermophysical properties of PCM are considered to be phase-independent.

In order to activate natural convection, the Boussinesq approximation is applied in the momentum equation.

$$\rho = \frac{\rho_l}{(\beta(T - T_l) + 1)} \tag{3.1}$$

Where, ρ_l and β is the density of molten PCM at melting temperature and coefficient of thermal expansion, respectively.

Based on the preceding assumptions, the governing equations (mass, momentum, and energy) for PCM-based LHTESS can be expressed as [202].

Continuity equation:

$$\frac{\partial \rho}{\partial t} + \nabla \cdot (\rho \vec{\boldsymbol{u}}) = 0 \tag{3.2}$$

Momentum equation:

$$\frac{\partial (\rho \vec{\boldsymbol{u}})}{\partial t} + \nabla \cdot (\rho \vec{\boldsymbol{u}} \vec{\boldsymbol{u}}) = \mu \nabla^2 \vec{\boldsymbol{u}} - \nabla p + \rho \vec{\boldsymbol{g}} + \vec{\boldsymbol{S}} \tag{3.3}$$

Energy equation:

$$\frac{\partial}{\partial t}(\rho H) + \nabla \cdot (\rho \vec{\boldsymbol{u}} H) = \nabla \cdot (k \nabla T) \tag{3.4}$$

Where ρ is the density, $\boldsymbol{u}$, k, and, μ are the velocity, thermal conductivity, and dynamic viscosity, respectively and $\vec{\boldsymbol{S}}$ denotes the momentum source term, which is defined by Eq. 3.5.

$$\vec{\boldsymbol{S}} = A(\emptyset)\vec{\boldsymbol{u}} \tag{3.5}$$

Where $A(\emptyset)$ is the porosity function and can be defined as:

$$A(\emptyset) = C_{mush}(1-\emptyset)^2/(\emptyset^3 + E) \tag{3.6}$$

Where, C_{mush} denotes mushy zone constant to enhance the suppression effect. This reflects the nature of PCM melting, whose value varies between 10^4 to $10^{7,}$ and 10^5 is taken in the present investigation [202]. Here, E is the small computational constant typically set to be 0.001 to avoid zero in the number [202]. Also, $\emptyset$ is the melt fraction during the solid-liquid phase change over a temperature range of $T_S < T < T_l$ and is defined by Eq. 3.7. Here, the mushy zone allows gradual transition in flow velocity at the interface of liquid and solid during melting. The value $\emptyset$ is defined as:

$$\emptyset = \begin{cases} 0, & T < T_S \\ 1, & T > T_L \\ \dfrac{T - T_S}{T_L - T_S}, & T_L > T > T_S \end{cases} \tag{3.7}$$

The enthalpy(H) can be expressed as:

$$H = h_{ref} + H_{sen} + H_{lat} \tag{3.8}$$

Where h_{ref} is the reference enthalpy at a reference temperature T_{ref} while H_{sen} and H_{lat} can be defined as:

$$H_{sen} = \int_{T_{ref}}^{T} C_p \Delta T \tag{3.9}$$

$$H_{lat} = \emptyset L \tag{3.10}$$

As the melt fraction ranges from 0 to 1, hence the value of the latent heat (H_{lat}) changes from 0 to specific enthalpy L for solid and liquid PCM, respectively.

Initial and boundary conditions:

The initial and boundary conditions are expressed as below:

a) Initial condition: At the beginning of the calculation, the initial temperature of the physical model is set at ambient temperature (27 °C). Also, since at ambient temperature, PCM is in the solid phase hence initial velocity is zero.

$$t = 0, \qquad T(0) = T_i = T_{amb} = 27℃, \qquad \vec{\boldsymbol{u}}(0) = \vec{\boldsymbol{u}}_i = 0 \tag{3.11}$$

b) Boundary condition:

At the bottom and top surface
$$-k\frac{\partial T}{\partial z}\bigg|_{\substack{x=0-100\,mm\\ y=0-100\,mm\\ z=0\,mm}} = q''_{in}\,, \qquad -k\frac{\partial T}{\partial z}\bigg|_{\substack{x=0-100\,mm\\ y=0-100\,mm\\ z=25\,mm}} = 0$$

$$-k\frac{\partial T}{\partial x}\bigg|_{\substack{x=0\,mm\\ y=0-100\,mm\\ z=0-25\,mm}} = 0, \qquad -k\frac{\partial T}{\partial x}\bigg|_{\substack{x=100\,mm\\ y=0-100\,mm\\ z=0-25\,mm}} = 0 \tag{3.12}$$

At side walls
$$-k\frac{\partial T}{\partial y}\bigg|_{\substack{x=0-100\,mm\\ y=0\,mm\\ z=0-25\,mm}} = 0, \qquad -k\frac{\partial T}{\partial y}\bigg|_{\substack{x=0-100\,mm\\ y=100\,mm\\ z=0-25\,mm}} = 0$$

No-slip boundary conditions are adopted at all the walls for velocity.

$$\vec{\boldsymbol{u}}_i = 0 \tag{3.13}$$

Computational methodology:

The numerical solution of the physical problem with the given boundary conditions is obtained using commercial Ansys-fluent software. The finite volume method (FVM) is employed to discretize the computational domain. The pressure-based solver with an implicit solution formulation is utilized to solve the pressure-based Navier stokes equations. Transient formulation involving a first-order implicit time-stepping method is selected. Patankar's SIMPLE algorithm is utilized for coupling the velocity and pressure, and the standard scheme is employed for pressure correction equations [205]. A second-order upwind scheme is employed to discretize the energy and momentum equations. The convergence is checked at each time step and is declared to be converged when residuals of the solution fall below 10^{-5}, 10^{-6}, and 10^{-8} for continuity, momentum, and energy equations, respectively. The maximum 20 iterations for each time step are considered for the present numerical simulation. Moreover, the present simulations are carried out using an Intel Xenon E5, CPU 3.50 GHz, and 32 GB of RAM computer. Each run took between 3-6 days, and thus entire simulation took about three and a half months.

Both grid and time dependency check of the computational model has been carefully carried out to obtain the optimum grid sizes and time step size. Three different grid sizes involving 177000, 215000, and 277000 elements for PCM-based heat sink and different time sizes (0.1 s, 0.5 s, and 0.7 s) are examined. Fig. 3.3(a-b) depicts the variation of heat sink base temperature for different grid sizes and time steps values. The mesh with the quadrilateral grid system is generated and, the mesh involving 215000 elements and a time step of 0.5 s is considered for further numerical simulation.

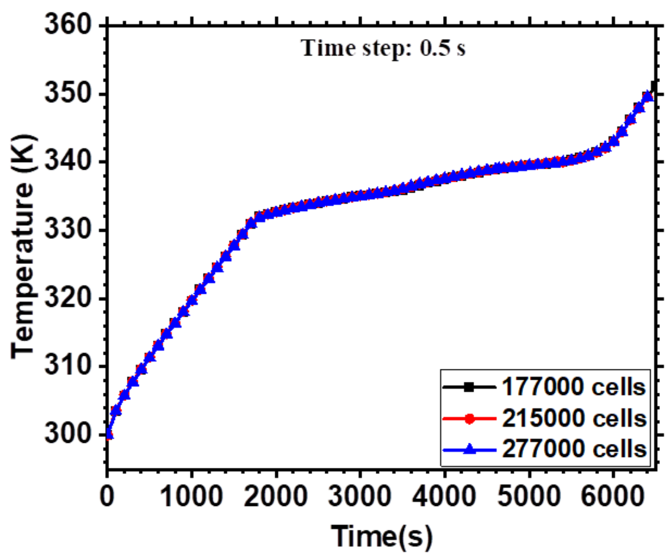

(a)

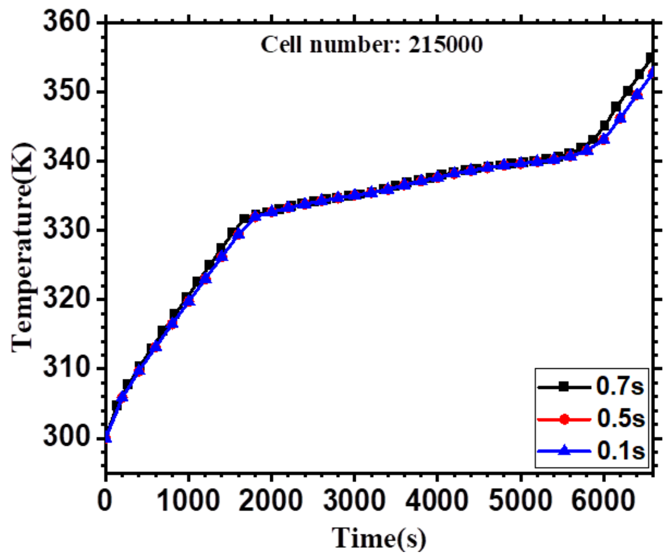

(b)

Fig. 3.3 (a) Mesh independence test with various cell number (177000, 215000, 277000) at a time step of 0.5 s; (b) Time independence test with various time size (0.1 s, 0.5 s, 0.7 s) at cell number of 215000

3.2.3 Results and discussion

As discussed in the previous section (3.1.1), most of the earlier studies focus on the parallel arrangement of plate fins inside the PCM-based heat sink. In the present investigation, different cross fin arrangements of plate fins that form various cavities (1, 4, 9, 16, 25, and 36) filled with paraffin wax as PCM are investigated numerically. Heat flux is varied between 1 and 2 kW/m^2. The results obtained from the present numerical investigation are elaborated in the subsequent sections.

Comparison of present results with available test data from other investigations

Here, the test data of Mahmoud et al. [135] are considered to validate the numerical model (Fig. 3.4). The authors conducted tests of different heat sink designs, namely, single cavity, cross fin arrangement, and parallel fin arrangement, which forms various cavities, and honeycomb structures. Present results are compared to their test data that consider PCM (RT-42) based heat sink with 3 and 9 cavities and subjected to 4 W of heat input. The temperature history of the base of the heat sink is plotted in Fig. 3.4. The maximum difference between present numerical results with test data is found to be less than ± 9 %. The variations in the experimental results and numerical prediction are mainly because of variations in the thermophysical properties of the PCM during the experiments, while the constant value of these properties is used in numerical computations.

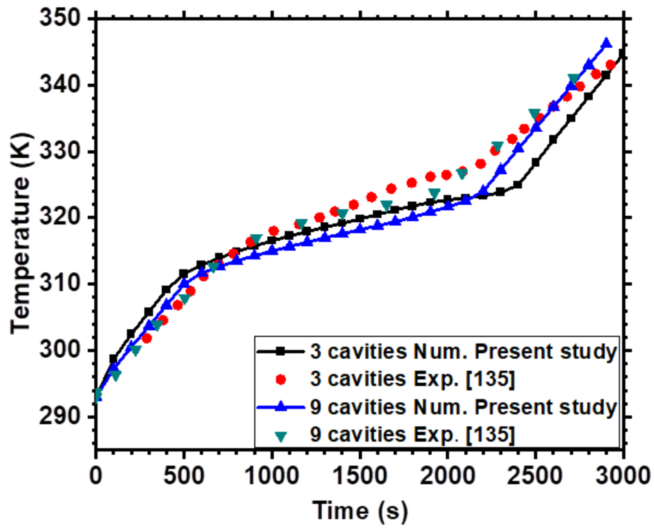

Fig. 3.4 Validations of numerical results with test data of Mahmoud et al. [135]

Validation for PCM phase change process

To ensure the accuracy of the numerical results, the temporal variation of the melt fraction of RT-42 PCM inside a rectangular enclosure with double fins is obtained and compared with the numerical results of Ji et al. [202]. For the studied configuration, a constant temperature boundary condition (70 °C) was applied on the left wall while other walls were maintained at the insulated condition. The initial temperature of the domain was considered to be 30 °C. The heater plate has a thickness of 5 mm, while fins of equal length have a thickness of 2 mm. The comparison of the area-weighted average melt fraction of the present study with the results of Ji et al. [202] is plotted in Fig. 3.5. Fig. 3.5 reveals that the present results show excellent agreement with the numerical results of Ji et al. [202]. The present model reasonably predicts the test data of Mahmoud et al. [135] and numerical results of Ji et al. [202] and therefore can be used for further simulation.

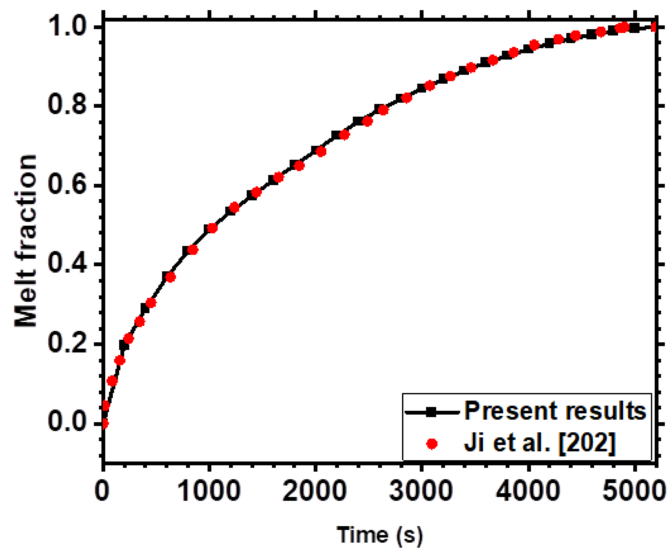

Fig. 3.5 Comparison of present numerical model with Ji et al. [202]

Performance of heat sink with and without PCM

The average temperature of the single cavity heat sink with and without PCM for $q'' = 1.0$ kW/m^2 is compared and shown in Fig. 3.6. Temperature rise for heat sink without PCM is found to be steady and faster, and the average temperature reaches 80 °C (353 K) within 635 s. It may be noted that this situation may influence the reliability and safety of the electronic components. While, the heat sink integrated with PCM (paraffin wax) exhibits a steady temperature rise for the first 1500 s, which represents the sensible heating of PCM. After 1500 s, PCM tends to attain the melting temperature and starts to melt near the base. The melting of PCM continues up to 5000 s. The average temperature of the heat sink is found to be low, from 1500 s to 5000 s. This period of heating is also known as the latent heating phase. For the heat sink module with no PCM, the latent heat storage phase is absent, and therefore sharp rise in temperature is observed for given heat flux. The temperature of the heat sink module involving PCM is maintained close to the melting temperature of PCM throughout the phase transition. This indicates that a PCM-based heat sink needs to be used for cooling of electronic devices for the intermittent condition so that PCM gets enough time for solidification.

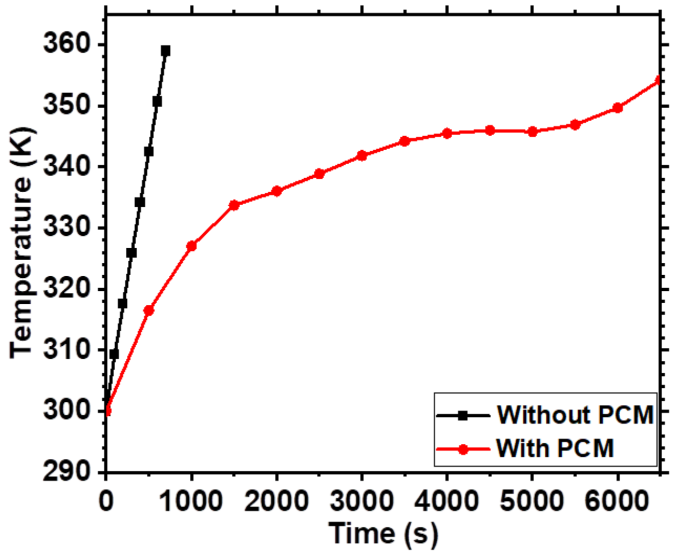

Fig. 3.6 Average temperature variation of heat sink against time with and without PCM

It can be noticed that even though the PCM takes some time to start melting, a rapid temperature rise is observed for the heat sink module with no PCM compared to the heat sink involving PCM. This is because of the higher specific heat value of paraffin wax compared to air. The operating time to attain SPT of 320 K is increased by 220 % for heat sink involving PCM compared to the heat sink without PCM. In a similar study, the operating time to attain the SPT of 320 K is increased by 60 % for heat sink involving PCM compared to the heat sink without PCM [107]. Therefore heat sink involving PCM has enough potential to increase the life and reliability of portable electronics.

PCM melting rate with the addition of cross plate fins

The melting rate of PCM is affected by both heat sink configurations and the amount of heat input to the heat sink. The melting rate is studied by calculating the melt fraction (∅) as given below [202].

$$\emptyset = \iiint \frac{s_{[T>58\,°\mathrm{C}]}}{S} dxdydz \tag{3.14}$$

Here, $s_{[T>58\,°\mathrm{C}]}$ represents the volume of the liquefied PCM when its temperature exceeds 58 °C, and S represents the total PCM volume inside the heat sink cavity. Fig. 3.7(a-c) describes the temporal variation of melt fraction of PCM for various heat sink configurations at different heat flux values ($q'' =$1-2 kW/m^2. Fig. 3.7(a) illustrates the variation of $\emptyset$ with time for different heat sink configurations (1, 4, 9, 16, 25, and 36 cavities) filled with paraffin wax and subjected to $q'' = 1.0\ \mathrm{kW/m^2}$. The melting of the PCM (paraffin wax) begins earlier in the case of the heat sink with a single cavity, while the melting of PCM finishes at last compared to other heat sink configurations. The melting rate of PCM is found to be increased for heat sink assembly involving cross fins and increases with an increase in the number of cross fins. This is due to the higher contact surface area density of PCM with aluminum in the case of a finned heat sink compared to the unfinned heat sink. Similar behaviors are obtained for other heat flux values and are depicted in Fig. 3.7(b-c). The enhancement ratio (ratio of time taken for complete melting of PCM in the finned heat sink to that of unfinned heat sink) for PCM melting inside heat sink involving cross fins is summarized in Table 3.2. The maximum enhancement ratio of 22.67% is obtained for the case of 36 cavities heat sink followed by 25 cavities heat sink (21.33%) at 1.0 kW/m^2. A single cavity heat sink possesses a lower number of heat-conducting paths (walls of the cavity acts as conducting paths) than the heat sink with multiple cavities. The propagation of heat energy occurs from the base of the heat sink to PCM in the case of the single cavity heat sink, while the heat energy flows to different layers of PCM in the case of heat sink involving multiple cavities because of more number of conducting paths. During the initial heating stage, the maximum amount of heat energy flows to PCM through the bottom of the heat sink in the case of a single cavity heat sink. This may be the reason the melting of PCM takes place at a faster rate during the initial stages of melting in the single cavity heat sink. It may be noted that the thermal conductivity of PCM is very low, and therefore PCM at the bottom layer conducts heat to the next adjacent layer at a much slower rate, and it takes a longer time for complete melting of PCM. In the case of multiple heat sink cavities, the heat is conducted to the upper region of the heat sink through fins, and some heat energy is absorbed by fins in the form of sensible heat during the initial period of heating. In such a case, the volume average temperature of PCM does not reach melting temperature, and therefore melting takes place at a slower rate in multiple cavities heat sink. In a similar study, Ji et al. [202] obtained an enhancement ratio of 15% by changing the fin length ratio from 1 to 0.25 for a double fin arrangement in a rectangular enclosure. A closer look at Fig. 3.7 reveals that, with an increase in q'' the energy absorption rate increases, which leads to a higher melting rate of the PCM. With increasing the heat flux values from 1.0 to 2.0 kW/m^2, the melting time of the PCM is reduced by approximately 46.5% in 36 cavities heat sink.

Table 3.2 Enhancement in melting time with the addition of a cross fin

Heat sink	Time for complete melting (s)			Enhancement ratio (%)		
q''(kW/m^2)	1.0	1.5	2.0	1.0	1.5	2.0
1 cavity	7500	5000	3900	-	-	-
4 cavities	6500	4500	3500	13.33	10.00	10.26
9 cavities	6200	4300	3300	17.33	14.00	15.38
16 cavities	6000	4200	3200	20.00	16.00	17.95
25 cavities	5900	4100	3100	21.33	18.00	20.51
36 cavities	5800	4000	3100	22.67	20.00	20.51

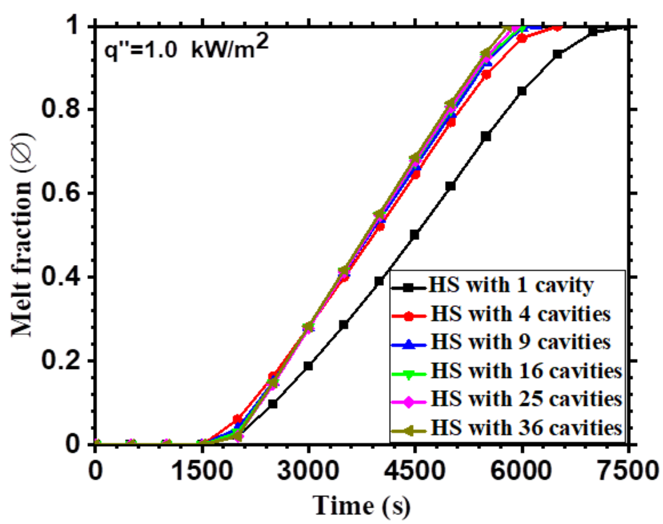

(a)

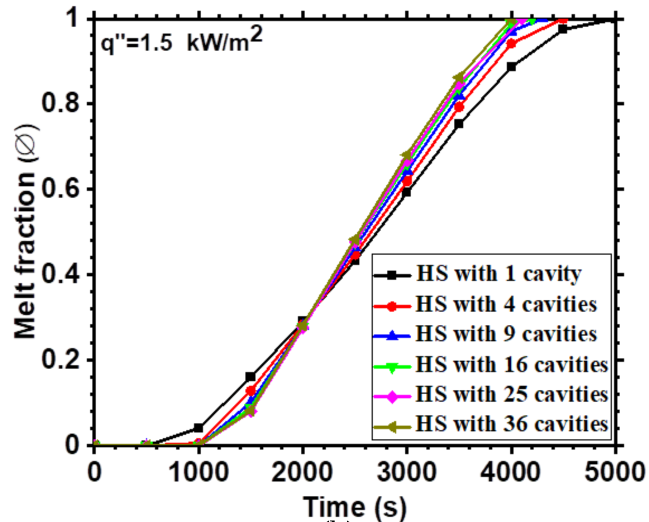

(b)

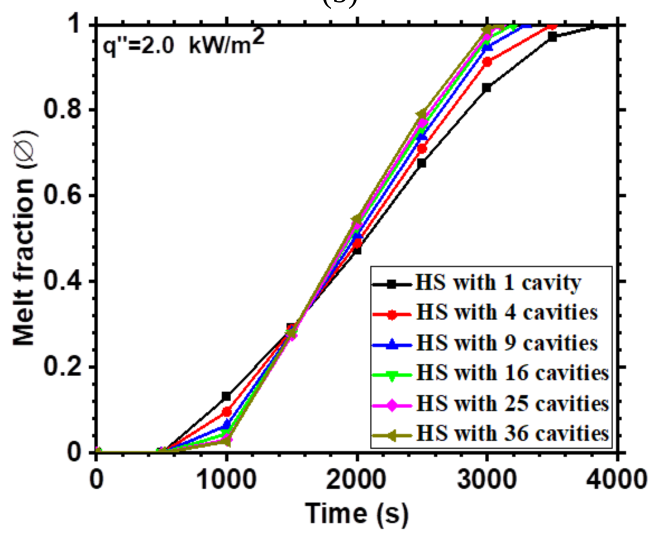

(c)

Fig. 3.7 Variation of ∅ for different heat sinks at (a) $q'' = 1.0$ kW/m^2 (b) $q'' = 1.5$ kW/m^2 (c) $q'' = 2.0$ kW/m^2

Characterization of melting heat transfer mechanism

The mechanism of melting heat transfer induced by the introduction of cross fins can be explored by studying temperature distribution and liquid fraction contours. In addition to this, energy stored by the PCM (latent and sensible) and surface averaged Nusselt number ($\overline{Nu}$) are investigated throughout the melting process of the paraffin wax to study the heat transfer characteristics of LHTESS.

Liquid fraction and temperature distribution

Fig. 3.8 exhibits the transient variation of PCM melt fraction, melting pattern, and strength of convection current of each heat sink configuration taken on the y-z plane. The amount of PCM in all the cases is kept constant. For this, we have varied the thickness of the fins. Heat flux (1.0 kW/m^2) is employed at the base of the heat sink. The heat energy is transferred to PCM through the base, wall, and fin surfaces of the heat sink, and the melting of PCM begins by absorbing latent heat of fusion.

The melting of PCM increases with time. Initially, at t =0, the entire heat sink is filled with solid PCM. After t =2500 s, PCM near the base, side walls, and fin walls begins to melt. As time passes t =3500 s, the PCM layer near the base, side walls, and fins tends to melt, and liquid PCM tends to move due to natural convection. As time elapses, more melting of PCM takes place. The evolution of the solid-liquid interface is influenced by the introduction of cross fins. For the heat sink with a single cavity, melting starts only from the base and side walls and moves upward due to natural convection. When fins are introduced, melting of PCM takes place from all sides of the heat sink. PCM flow motion in the case of a finned heat sink is more active and aggressive. A closer look at Fig. 3.8 reveals that the flow strength during melting of PCM in 25 and 36 cavities heat sink is stronger compared to the other four configurations. PCM flow motion seems to be weaker in the case of the rest four heat sink configurations. It can be noticed from Fig. 3.8 that PCM in 1, 4, 9, and 16 cavities not fully melted even after 5800 s of heating. At the same time, PCM in the case of 25 and 36 cavities heat sink is about to melt completely after 5800 s of heating. After t=5800 s, PCM melts completely, and consequently, convection current tends to be weaker. This indicates the melting rate of PCM is faster in the case of 25 and 36 cavities heat sink. From the above analysis, it can be inferred that heat sink involving cross fins increases the melting rate of PCM due to an increase in natural convection and melt fraction. However, after complete melting, convection heat transfer is weaker in the heat sink with multiple fins than with no fin.

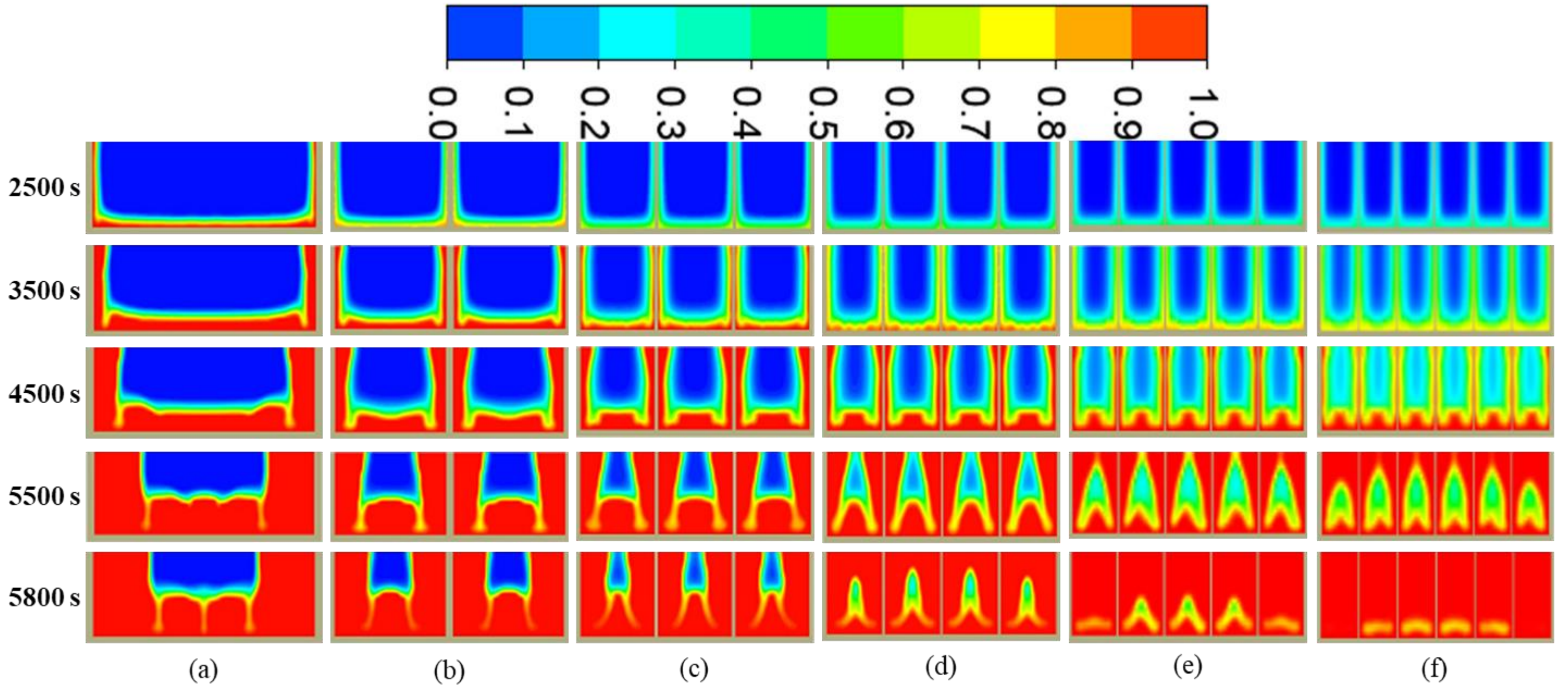

Fig. 3.8 Variation of ∅ at various time periods for different heat sink configurations (a) 1 cavity (b) 4 cavities (c) 9 cavities (d) 16 cavities (e) 25 cavities (f) 36 cavities

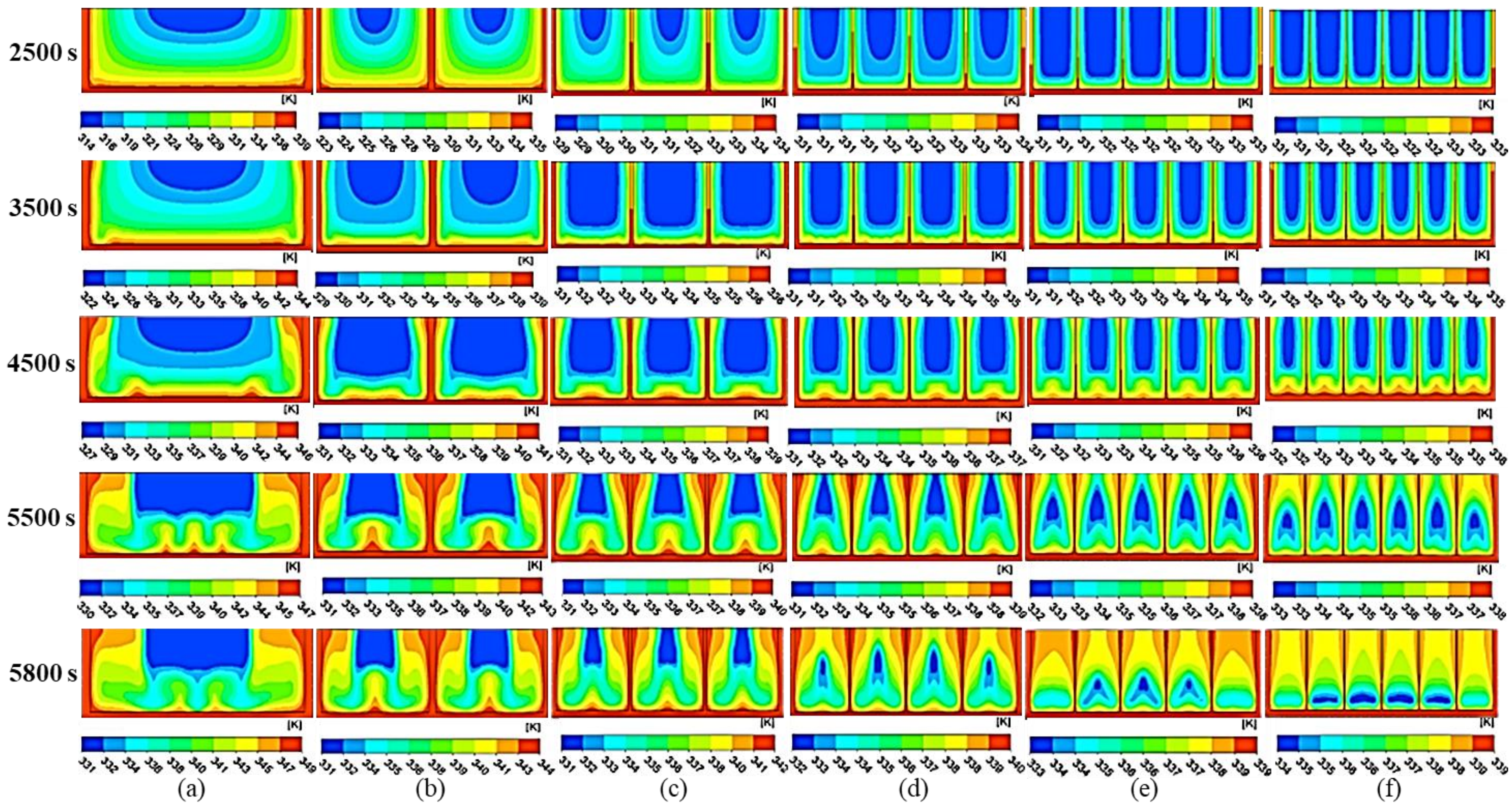

Fig. 3.9 Variation of isotherm contours at various time periods for different heat sink configurations (a) 1 cavity (b) 4 cavities (c) 9 cavities (d) 16 cavities (e) 25 cavities (f) 36 cavities

The heat transfer rate in the PCM integrated cross plate finned heat sink can be studied from isotherm contours presented in Fig. 3.9. Fig. 3.9 presents the temperature distribution of various heat sink configurations on the y-z plane at a different heating time at $q'' = 1$ kW/m^2. It can be noticed that the rise in temperature in the case of no fin heat sink is higher compared to other heat sink configurations. The rise in temperature decreases with the increase in the number of cross fins. It can also be observed from Fig. 3.9 that the uniformity of temperature increases with the increase in the number of the cross fin. The temperature varies from 314 K to 339 K in the case of a single cavity heat sink after 2500 s of heating. Contrarily, it varies from 331 K to 333 K for 25 and 36 cavities heat sink. The peak temperature is also found to be decreased in the case of a finned heat sink. The improvement in heat sink performance in the case of a finned heat sink is because of the reduction in thermal resistance due to the addition of cross fins which leads to augment the heat transfer through the PCM.

Energy stored by the PCM

The energy stored inside the PCM while melting can be expressed in terms of latent (Q_{lat}) and sensible (Q_{sen}) heat. Fig. 3.10 presents the cumulative sensible and latent energy stored at a different time interval during the melting of PCM for $q'' = 1.5$ kW/m^2. It can be noticed that for $t < 2500$ s, the energy absorption rate in the sensible heat curve for the 36 cavities heat sink is higher compared to the single cavity heat sink, while the opposite tendency can be noticed for $t > 2500$ s. In addition, along the latent heat curve, the energy absorption rate for the 36 cavities heat sink is lower than the single cavity for $t < 2000$ s, while the opposite trend can be noticed for $t > 2000$ s. This is because the melting of paraffin wax in a single cavity heat sink starts from 800 s, while in the case of 36 cavities heat sink, melting starts after 1200 s of heating. The volume average temperature of paraffin wax before 2500 s of heating is higher in 36 cavities heat sink compared to the single cavity heat sink. Therefore, sensible heat energy absorbed by PCM in 36 cavities heat sink is higher than single cavity heat sink before 2500 s. After 2500 s, the volume average temperature of paraffin wax in a single cavity heat sink is higher compared to 36 cavities heat sink. Therefore, the sensible heat energy absorbed after 2500 s in the single cavity heat sink is higher compared to the 36 cavities heat sink. In a similar manner, up to 2000 s of heating, Q_{la} for single cavity heat sink is higher since melt fraction value up to 2000 s is higher for single cavity heat sink compared to 36 cavities heat sink. After 2000 s, the melt fraction value of 36 cavities heat sink is higher compared to the single cavity heat sink. It may be noted that the value of $\emptyset$ at 2000 s for a single cavity heat sink is 0.290, and for 36 cavities heat sink is 0.282. While at 2100 s, the value of $\emptyset$ is 0.317 for single cavity heat sink and 0.322 for 36 cavities heat sink, as can be seen in Fig. 3.7(b). Therefore after 2000 s, the latent heat value of 36 cavities heat sink is higher. After complete melting, the energy storage takes place through sensible means.

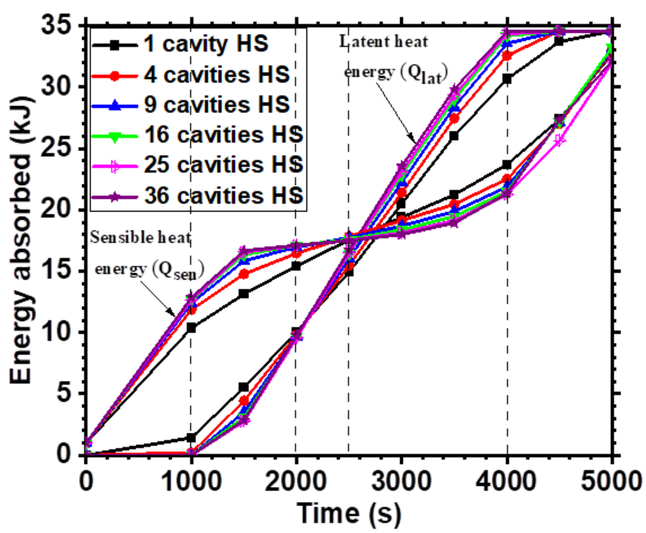

Fig. 3.10 Energy storage rate in terms of sensible and latent heat for various heat sinks at $q'' =$1.5 kW/m^2

Surface averaged Nusselt number $(\overline{\boldsymbol{Nu}})$

The surface averaged Nusselt number $(\overline{Nu})$ is estimated as [202]:

$$\overline{Nu} = \frac{\overline{h} l_c}{k} \tag{3.15}$$

Where, $\overline{h}$ is the surface averaged heat transfer coefficient, l_c is the characteristic length of the PCM container (height of the cavity), and k is the thermal conductivity of the PCM. The $\overline{h}$ can be obtained by the following expression [202]:

$$\overline{h} = \frac{Q_{abs}}{A_{\mathrm{t}}(T_s - T_m)\Delta T} \tag{3.16}$$

Where, Q_{abs} is the heat energy absorbed by paraffin wax in a time interval of ΔT, A_{t} is the overall heat transfer area, including the heat sink and fin surfaces, T_s is surface average temperature and T_m is the mean temperature of the PCM. The variation of surface average Nusselt number with dimensionless time τ of various heat sink configurations for q'' =1.5 kW/m^2 is presented in Fig. 3.11. Fourier number (Fo) alone is not sufficient to express the generalized trend of heat transfer variation because of the effect of the phase change process. The dimensionless time τ is expressed as [109].

$$Fo = \frac{\alpha t}{l_c^2} \tag{3.17}$$

$$Ste^* = \frac{C_p q'' l_c}{kL} \tag{3.18}$$

$$\tau = Fo \times Ste^* \tag{3.19}$$

Where α is the thermal diffusivity of the PCM, t is the time, q'' input heat flux to the heat sink, l_c is the characteristics dimension, and L denotes the specific latent heat of the PCM. Based on the variation of Nusselt number with dimensionless time τ, the melting heat transfer through the PCM can be characterized into different stages such as heat conduction, strong convection, and weak convection.

During the heat conduction stage, the Nusselt number ($\overline{Nu}$) starts from its peak value and drops rapidly. This indicates convection is very weak in this region. The PCM mainly starts to melt by heat transfer through conduction from the base, wall surface, and fins surface. The larger value of $\overline{Nu}$ in the beginning, is mainly due to the smaller thermal resistance. Since in the beginning, the liquid layer of the PCM is very thin, which results in very less thermal resistance. As time elapses, the liquid phase thickness of the PCM increases, which leads to an increase in thermal resistance. Therefore the conduction heat transfer rate gradually decreases. At this point the $\overline{Nu}$ for all fin-PCM cases should necessarily be the same as the total fin length for all the cases are the same.

In the strong convection regime the $\overline{Nu}$ decreases at a slower rate. In this regime, natural convection tends to intensify the heat transfer because of the larger melting rate of PCM. Although resistance to heat conduction continues to increase, but strong convection enhances the heat transfer rate. Therefore, $\overline{Nu}$ still decreases but at a slower rate. From Fig. 3.11, one can observe that $\overline{Nu}$ for heat sink with 25 and 36 cavities shows the slowest decline rate compared to other heat sink configurations. This may be due to the strong convection region throughout the PCM melting.

In the weak convection regime the $\overline{Nu}$ decreases continuously but at a faster rate in comparison to a strong convection regime. This shows a decrease in heat transfer, weakening convection current, and shorter length of the solid and liquid interface.

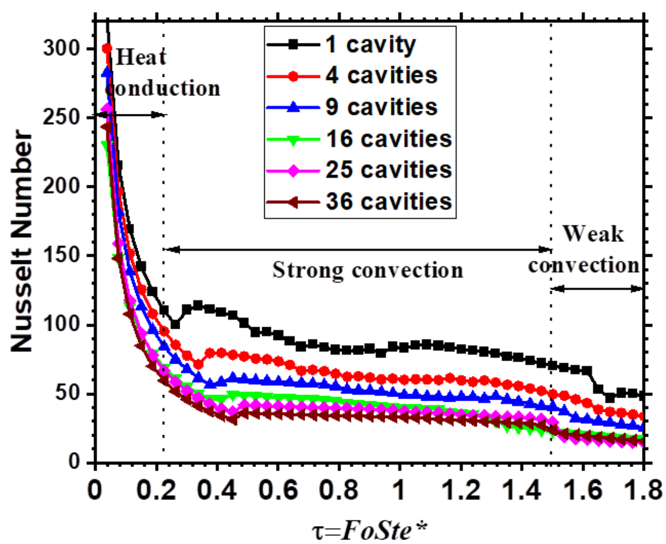

Fig. 3.11 Variation of $\overline{Nu}$ with dimensionless time τ for various heat sink configurations at $q'' =$1.5 kW/m^2

Comparison of transient temperature variation of heat sink base

The above analysis illustrates that introduction of cross plate fins plays a critical role in enhancing the melting of paraffin wax. At this juncture, it is important to compare the transient variation of temperature of different heat sinks involving cross fins. Here, the base temperature is taken as a reference to investigate the effectiveness of the heat sink module involving PCM and cross fins. The variation of heat sink base temperature against time for different heat flux values (1.0, 1.5 kW/m^2) of PCM-based heat sinks with no fin and different cross fin arrangements forming different cavities are shown in Fig. 3.12(a-b). It is observed that an increase in the number of cross fins decreases the heat sink base temperature due to an increase in the localized heat diffusion in the PCM. At $q'' =$1.5 kW/m^2, the heat sink with a single cavity, 25 cavities, and 36 cavities take 765, 1500, and 1500 s, respectively, to achieve the SPT value of 60 °C. While, these heat sink configurations (single cavity, 25 cavity, and 36 cavities) take 1713, 4023, and 4021 s, respectively, to achieve the SPT value of 70°C. This clearly indicates that there exists an optimum number of cross fins for which the maximum reduction in heat sink base temperature takes place, and a further increase in fins does not reduce the base temperature significantly. It may be noted that the effective thermal conductivity of PCM integrated heat sink assembly increases with the increase in the number of cross fins, which increases the melting rate and decreases the base temperature of the heat sink. However, at the same moment, the natural convection heat transfer in post melting is prevented due to the increase in the number of cross fins. This may be the reason that the base temperature in the case of 36 cavities heat sink increases at a faster rate after complete melting of PCM. A similar phenomenon has been observed at different heat flux values for 25 and 36 cavities heat sink. The maximum 10°C of temperature reduction is achieved in the case of 25 cavities heat sink compared to the heat sink with no fin. The SPT is the critical temperature beyond which the thermal performance of electronic components deteriorates or even gets damaged. Table 3.3 depicts the heat transfer performance in terms of SPTs and enhancement ratio in operating time (e_r) for different input heat flux values (1.0-2.0 kW/m^2). The enhancement ratio (e_r) in operating time is determined as the ratio of enhancement in operating time to reach the critical SPT by heat sink with TCE to the time taken by the heat sink without TCE and can be expressed as [202]:

$$(\%)e_r = \frac{t_{SPT\ with\ TCE} - t_{SPT\ without\ TCE}}{t_{SPT\ without\ TCE}} \times 100 \tag{3.20}$$

For 60 °C SPT highest e_r of 139.52 is obtained for 25 cavities heat sink while for 70 °C SPT highest enhancement ratio 171 is achieved for 36 cavities heat sink at $q'' = 2$ kW/m^2 Most of the electronic components have critical SPTs between 60 and 70 °C [128-129]. Therefore, the temperature of 60 °C and 70°C are selected as critical SPTs for the present study. Enhancement in operating time increases with an increase in the number of cross fins. Fig. 3.13(a-b) presents the time required to achieve SPT of 60 °C and 70 °C at various input heat flux values for each heat sink configuration. It may be noted that as the value of heat flux increases, the latent heating phase duration of the PCM is shortened. From the above analysis, it can be inferred that the heat sink with cross fins arrangement can augment the overall thermal performance of PCM integrated heat sink and can improve the reliability and life span of electronic components.

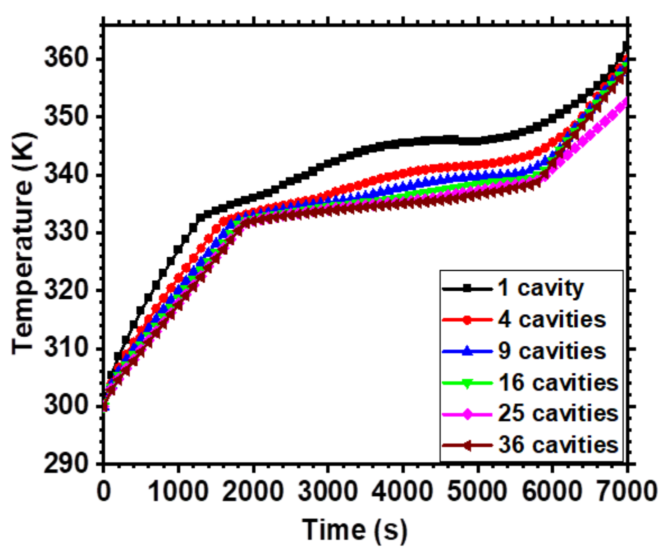

(a)

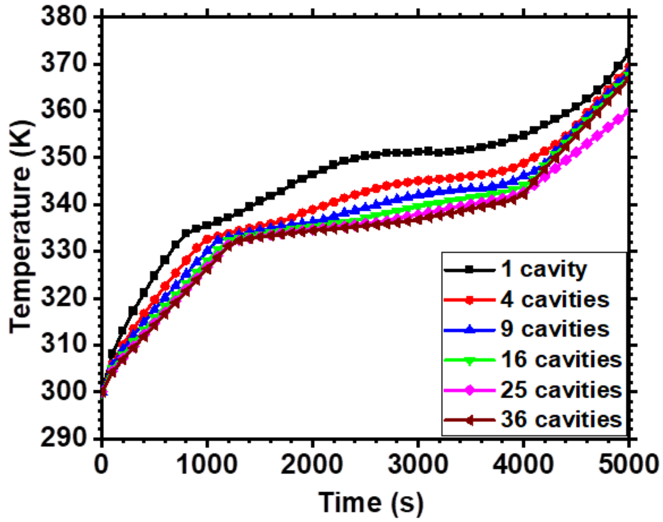

(b)

Fig. 3.12 Variation of heat sink base temperature with time (a) $q'' = 1.0$ kW/m^2 (b) q'' =1.5 kW/m^2

Table 3.3 Enhancement in operating time for various SPTs at different heat flux values

Heat sink	Time to reach SPT of 60 °C (s)						Time to reach SPT of 70 °C (s)					
q''(kW/m^2)	1.0	e_r (%)	1.5	e_r (%)	e_r (%)	e_r (%)	1.0	e_r (%)	1.5	e_r (%)	2.0	e_r (%)
1cavity	1400	-	765	-	501	-	3234	-	1713	-	1079	-
4 cavities	1900	36	1164	52	700	40	5600	73	2535	48.0	1633	51
9 cavities	2100	50	1200	57	804	60	6000	85	3400	98	2023	87
16 cavities	2300	64	1400	83	930	86	6029	86	3900	128	2544	136
25 cavities	2400	71	1500	96	1200	139	6127	89	4023	135	2835	163
36 cavities	2500	79	1500	96	1036	107	6053	87	4021	135	2920	171

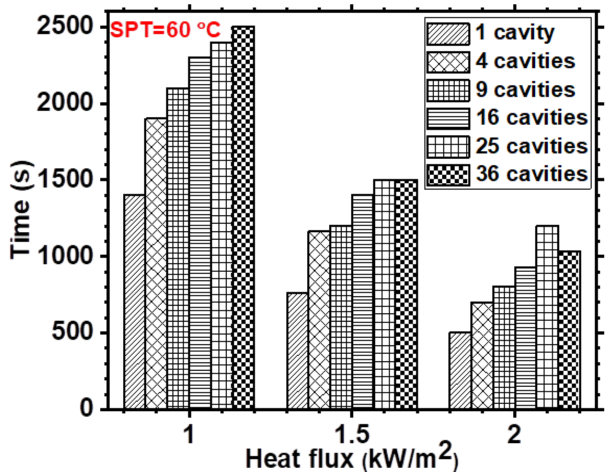

(a)

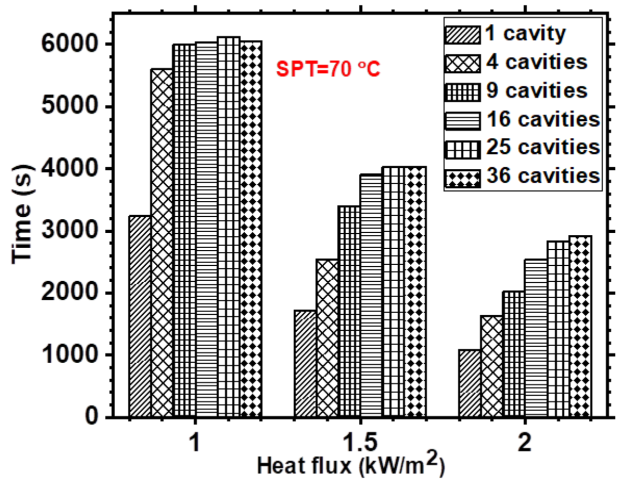

(b)

Fig. 3.13 Time to reach SPT at various heat flux values (a) 60 °C (b) 70 °C

Effect of various PCM

Paraffin wax is the most widely used PCM. Also, from TOPSIS, fuzzy TOPSIS, and VIKOR methods, paraffin wax is selected as one of the most suitable PCM for thermal management applications. Various commercially available PCM whose melting temperature range lies below and close to the melting temperature of paraffin wax are tested using 25 cavities heat sink. Table 3.4 presents the list of the PCM with their thermophysical properties used in the present investigation [172, 206]. It may be noted that PCM-HS29P and PCM-HS34P are inorganic chemicals that constitute the right mix of various additives like salts and other mixtures. These characteristics ensure to maintain equilibrium conditions of various phases (solid and liquid). PCM-OM37P and PCM-OM46P are organic mixtures of fatty acid, various salts, additives, and nucleating agents that appear white waxy flake in a solid phase and combustible at the higher temperature. PCM-HS58P includes a mixture of organic and inorganic materials and exhibits thermal stability and non-flammability characteristics. PCMs HS29P, HS34P, and HS58P include salt and corrosive effect that may affect the material of the heat sink assembly.

Fig. 3.14 presents the comparison of temperature response of different PCM in 25 cavities heat sink at $q'' = 1.5\,\mathrm{kW/m^2}$. The variation of transient temperature of the heat sink base is considered here. PCMs with low melting temperatures such as HS29P and HS34P yield lower base temperatures for a longer duration compared to the HS37P and OM46P. Therefore, HS29P and HS34P can be used for electronic components whose critical SPT is lower than 40 °C. The PCMs such as HS37P and OM46P show a comparable operating temperature to the paraffin wax. The phase change in the case of HS29P, HS34P, and HS58P is almost isothermal because they exhibit a sharp melting point temperature and higher specific and latent heat capacity. PCM-HS58P tends to change phase even after 5300s. Although paraffin wax does not possess a sharp melting point like the others, it usually has better chemical properties and is less costly than inorganic PCMs. Therefore, paraffin wax is ideally suited for those electronic devices which have the critical SPT above 60 °C and below 70 °C and for which other PCMs are not suitable.

Table 3.4 Thermophysical properties of various PCMs [172, 203, 206]

PCM type	Solidus temperature (°C)	Liquidus temperature (°C)	ρ (kg/m^3)	k (W/m-K)	C_p (J/kg-K)	LH (kJ/kg)	μ (Pa.s)
PCM-HS29P	29	29	1840	1.09	2260	190	0.0179
PCM-HS34P	34	34	1980	0.5-0.6	2344.6	150	0.0166
PCM-OM37P	36	37	880	0.16	2550	218	0.0237
PCM-OM46P	45	48	860	0.20	2500	245	0.210
PCM-HS58	57	58	1290	0.65	2500	250	0.0261
Paraffin wax	58	62	900	0.21	2800	193.2	0.0235

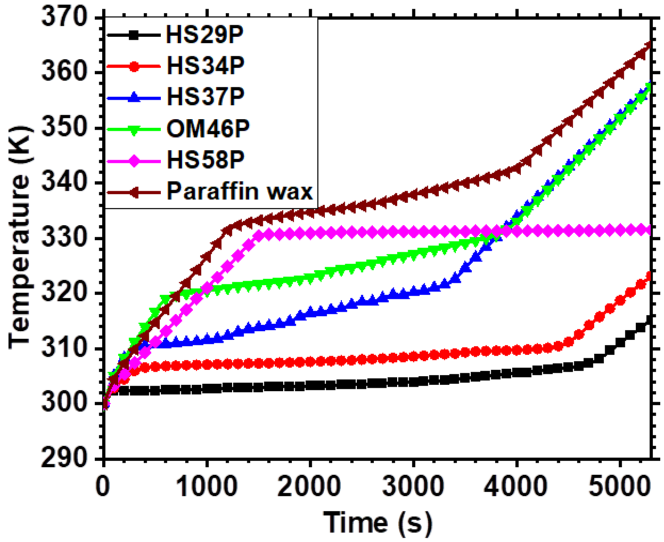

Fig. 3.14 Temperature time response of the base of the 25 cavities heat sink filled with various PCM at $q'' = 1.5$ kW/m^2

3.3 Numerical modeling of PCM based-heat sink with hollow fins as TCE

Numerous studies have been made to analyze the thermal performance of PCM integrated heat sink with plate and pin fins for thermal management of electronic devices. It may be noted that the surface area density of the fins plays a crucial role in the design of the thermal management system. In such a case, one can consider hollow pin fins integrated with PCM for the cooling of portable electronic devices; these configurations may increase the effective thermal conductivity and also decrease the weight of the system. Such studies have not been reported extensively in the literature. Here, an effort has been made to analyze the thermal performance of PCM-based heat sinks involving hollow fins with different configurations (circular and square). The heat transfer performance is analyzed through variation in the heat sink base temperature, melt fractions, solid-liquid interface propagation, and maximum velocity distributions during melting of PCM for a varied range of heat flux values ($q'' = 1.5$-2.0 kW/m^2). The details are elaborated below.

3.3.1 Physical model

The present study considers PCM-based heat sinks involving no fin and hollow fins with square and circular geometry for the analysis (Fig. 3.16a-c). The physical model of the heat sink with square hollow fins is shown in Fig. 3.15. The hollow fins and the heat sinks are made up of aluminum due to lightweight and higher thermal conductivity value. The height of the fins is taken as 22 mm in each case, and the detailed dimensions of the heat sink are presented in Table 3.5. The bottom surface of the heat sink is supplied with a constant heat flux value, and the top and side wall of the heat sink is considered to be adiabatic. Commercially available paraffin wax is used as PCM in this study. The heat sink cavities are filled with PCM while air is considered in the remaining domain. Thermophysical properties of PCM, aluminum heat sink, and air are described in Table 3.6 [202-203].

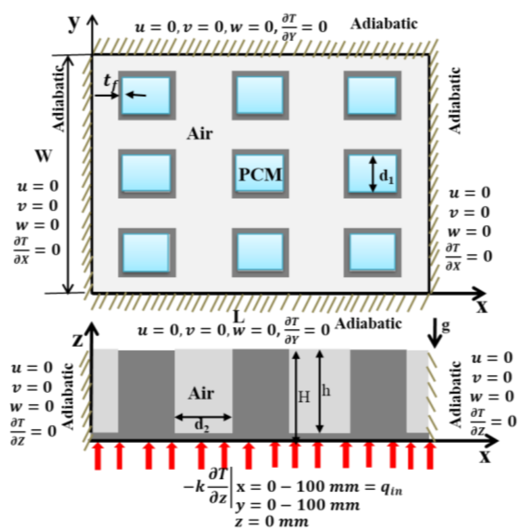

Fig. 3.15 Thermodynamic representation of heat sink with square hollow fins

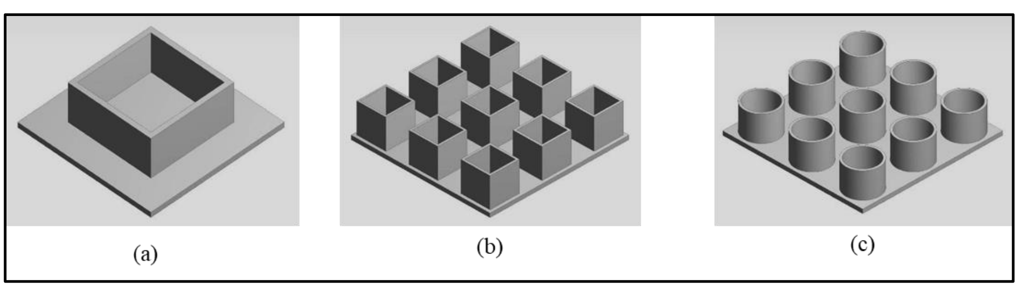

Fig. 3.16 Heat sinks (a) Single Cavity (b) Square hollow (c) Circular hollow

Table 3.5 Dimensions of hollow fin heat sink geometries used

Heat Sink	Dimensions (L×W×H) (mm)	Fins No.	Fin thickness (t_f) (mm)	Cavity dimensions (l×w×h) (mm)	Volume of PCM (mm^3)
No fin	100×100×25	1	--	55.3 ×55.3 ×22	67277.98
Square fins	100×100×25	9	1.25	18.5 × 18.5 ×22	67765.5
Circular fins	100×100×25	9	1.4	ϕ=20.8, h=22	67279.34

Table 3.6 Thermophysical properties of paraffin wax, aluminum, and air

Material	ρ (kg/m^3)	M.P. (K)	k (W/mK)	C_p (J/kg-K)	*L* (kJ/kg)	μ (Pa.s)	β (1/K)
PCM	900	327 to 333	0.21 (s), 0.12 (l)	2890	193.2	0.0235	0.0001
Aluminum	2719	-	202.4	871	-	-	-
Air	1.125	-	0.0242	-	-	1.7894×10^{-5}	-

3.3.2 Mathematical model and computational procedure

The solid-liquid phase transition of PCM is modeled by employing the enthalpy-porosity approach. The solution of the present physical models is obtained using computational fluid dynamic (CFD) Ansys-fluent software. Several assumptions are adopted to model the solid-liquid phase change behavior of PCM and have been illustrated in section 3.2.2. In addition to this, the following assumptions are considered for the analysis.

a) Thermophysical properties of PCM, fins, and air are assumed to be constant.
b) The thermal conductivity of PCM in the solid and liquid phases is varied.
c) The side wall and top edge of the heat sink are considered adiabatic.

The governing equation, initial, and boundary conditions as reported in the earlier section are adopted here. The governing equations such as mass, momentum, and energy are discretized using the finite volume (FVM) technique with double precision. The solutions of governing equations are obtained similar to the procedure explained in section 3.2.2. The grid and time dependency test of the present computational model is carefully tested to avoid their effects on the accuracy of numerical results. Three different mesh sizes involving 248000, 283000, and 328000 elements and three-time steps of 0.3, 0.5, and 0.7 s are considered in the analysis. The results of the transient temperature variation of the heat sink base for each mesh size and time step are presented in Fig. 3.17(a-b). No significant difference in the variation of heat sink base temperature is observed from the results. Based on the analysis, the mesh with 283000 elements and the time step of 0.5 s is considered for further simulations.

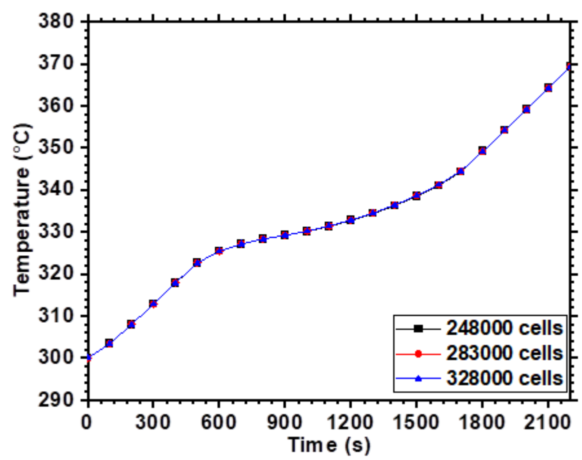

(a)

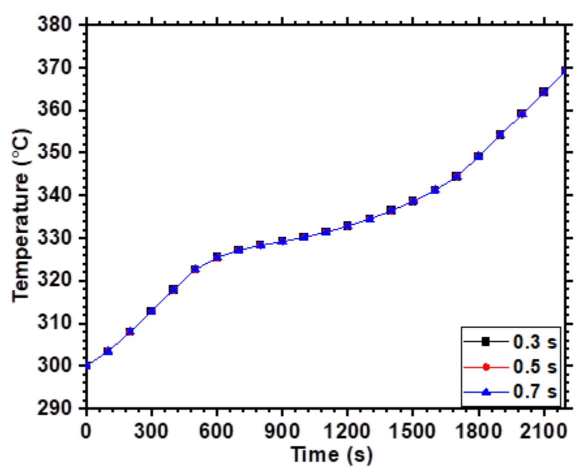

(b)

Fig. 3.17 (a) Mesh independence test (b) Time independence test of hollow fins

3.3.3 Results and discussion

Here, an effort has been made to analyze the thermal performance of various configurations such as heat sink with no fin, heat sink with circular and square hollow fins filled with paraffin wax. The results obtained from the present numerical investigation are elaborated in the subsequent sections.

Model validation

An experimental investigation carried out by Mahmoud et al. [135] on a heat sink with a single cavity integrated with RT-42 PCM is used to compare and validate the present numerical results. The test data and present numerical prediction for transient temperature variation of heat sink base are presented in Fig. 3.18.

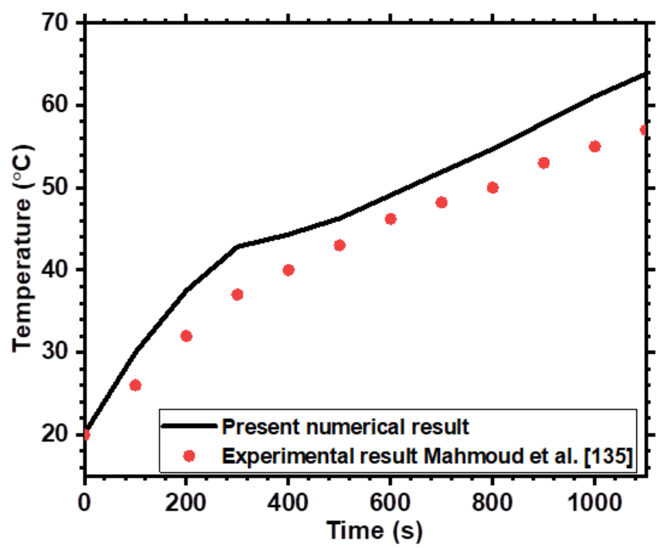

Fig. 3.18 Validation of present numerical results

The average error between the present numerical prediction and the test data of Mahmoud et al. [135] is found to be less than 9%. The variation between present numerical results with the test data of Mahmoud et el. [135] is mainly due to the various assumptions made in the numerical model, such as constant thermophysical properties of PCM while melting and perfect adiabatic conditions applied on the boundary wall. It may be noted that during experiments, the thermophysical properties of PCM may vary with the temperature, and also, there may be heat loss associated with the experiments. Nevertheless, the qualitative trend of the present numerical prediction agrees well with the test data (Fig. 3.18), and therefore, the model has been considered to analyze the thermal performance of PCM-based heat sink for various operating conditions.

Effect of heat flux

Fig. 3.19(a-b) presents the effect of various heat flux (q''= 1.0 1.5 and 2.0 kW/m^2) on the thermal performance of circular and square hollow fin heat sinks. The slope of the time-temperature curve becomes steep for the higher value of heat flux. At a higher value of heat flux, higher energy storage by PCM occurs, and the phase transition time reduces. The variation of melt fractions with time for the circular and square fin heat sink is presented in figure 3.20(a-b), which clearly shows that the increase in heat flux value leads to the early melting of paraffin wax. With the increase in the heat flux value from 1.0 to 2.0 kW/m^2, the melting time is found to reduce nearly by 78.5% for both circular and square hollow fin heat sinks.

The strength of the convection current and propagation of solid-liquid interface of PCM on a cross-sectional plane in a heat sink with no fin, circular and square fin heat sink is illustrated in figure 3.21(a-c).

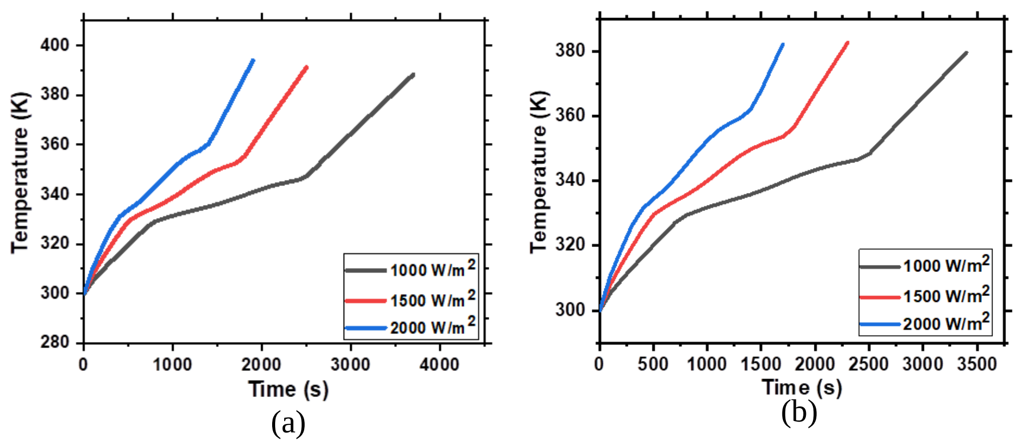

Fig. 3.19 Effect of heat flux for (a) Circular hollow fins (b) Square hollow fins

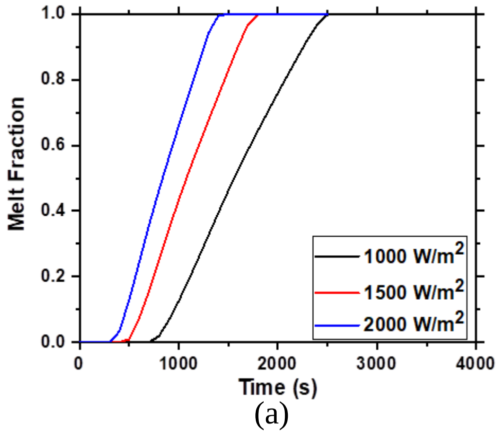

Fig. 3.20 (a) Variation of melt fraction with time for hollow fins (a) Circular (b) Square

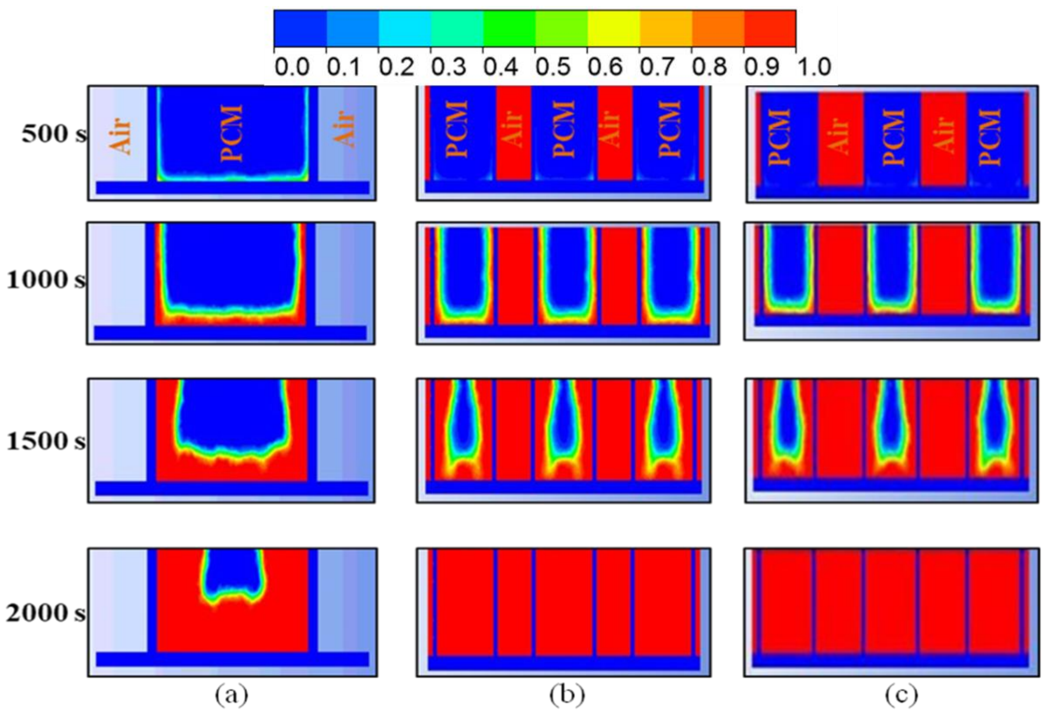

Fig. 3.21 Propagation of solid-liquid interface with time for heat sink with (a) No fin (b) Circular fins (c) Square fins

Initially, the PCM remains in the solid phase, with the progress of time (at t=500), the PCM from the base and side wall of the heat sink cavity starts to melt. Before PCM starts to melt, heat transfer mode is conduction; with the increase in time, the strength of convection current increases and convection heat transfer dominates, leading to the increase in melt fraction. The PCM melts completely after t=2000 s for heat sink with circular and square heat sinks; while, the PCM in the heat sink with no fin remains under phase transition state.

Figs. 3.22(a-c) depict the variation of maximum velocity for different heat sink configurations at different input heat flux values. As the PCM starts to melt, the maximum velocity of PCM is found to increase; subsequently, the velocity decreases gradually, and this trend is observed for all the cases. This shows the maximum velocity is higher in the mushy zone due to enhanced convection current. The maximum velocity is found to be higher for a larger value of heat flux. Also, the maximum velocity is found to be higher for heat sink with no fin; with the absence of fins, the PCM motion becomes stronger. This may be due to the fact that no obstruction occurs to the solid-liquid interface. At q''= 2.0 kW/m^{2,} the maximum velocity is found to be 2.4, 0.73, and 0.65 mm/s for no fin, circular hollow fin, and square hollow fin heat sink, respectively.

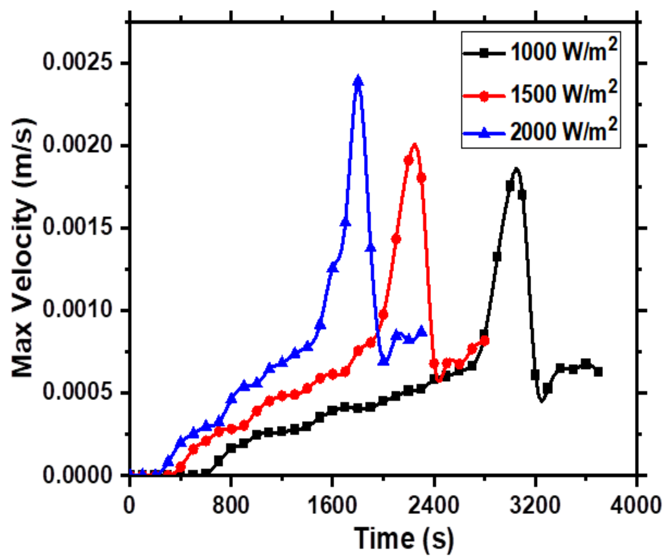

(a)

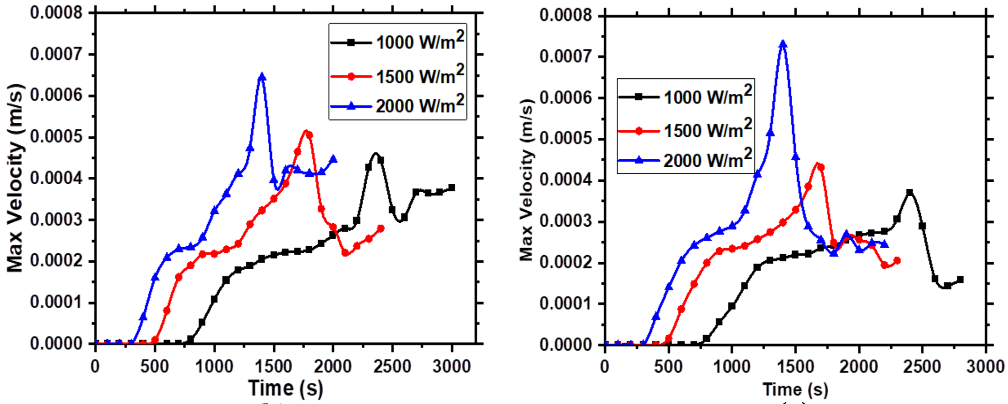

(b) (c)

Fig.3.22 Variation of maximum velocity with time at different heat flux for (a) No fin heat sink (b) Circular hollow fin heat sink (c) Square hollow fin heat sink

Variation of base temperature for different heat sink configurations

Fig. 3.23(a-c) presents the effect of fins on the base temperature of PCM-based heat sinks at various heat flux values (1.0-2.0 kW/m^2). In the case of hollow fins, the heat is conducted to the upper regions of PCM through fins and PCM. In such a case, some energy is absorbed by fins in the form of sensible heat during the initial period. The rise in temperature of the heat sink base for hollow fins is uniform and slower in comparison to the heat sink without fins. Maximum temperature reduction of the heat sink with square hollow fins is found to be 4.19, 5.19, and 5.74%, at q''= at 1.0, 1.5, and 2.0 kW/m^2, respectively, compared to the heat sink with no fin. The higher temperature reduction by square hollow fin is mainly due to higher heat transfer area, which increases the heat transfer rate.

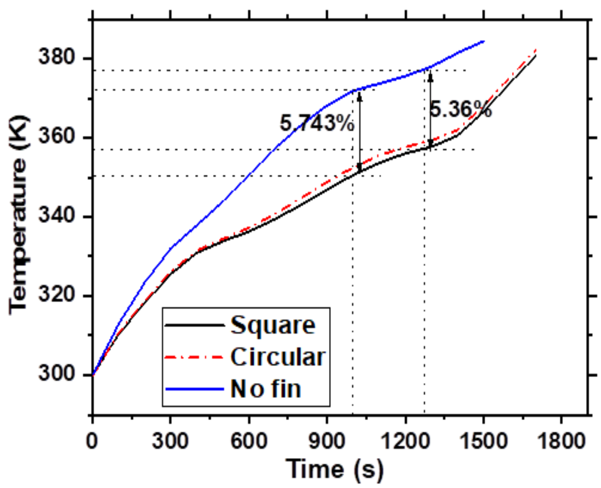

(a)

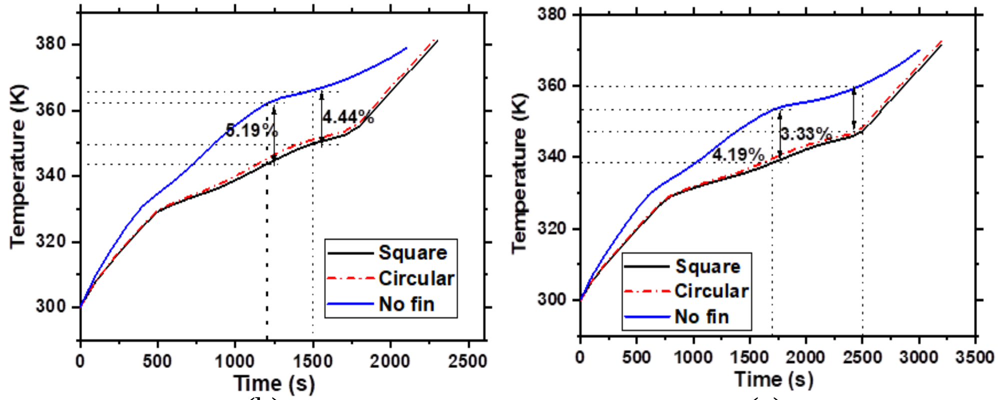

(b) (c)

Fig. 3.23 Variation of base temperature of different heat sink configurations at various heat fluxes (a) 1.0 kW/m^2 (b) 1.50 kW/m^2 (c) 2.0 kW/m^2

3.3 Concluding remarks

In this study, efforts have been made to analyze the thermal performance of heat sink modules with various configurations of fins such as cross plate fins involving various cavities and hollow fins with a circular and square cross-section through numerical investigation. The details are elaborated below.

The first problem considers the heat sink with various cross plate fin arrangements with different cavities and different heat flux values (q''= 1.0, 1.5, and 2.0 kW/m^2) for the analysis. Three-dimensional transient simulations are carried out using Ansys fluent software to simulate the melting process of PCM in the heat sink. The governing equations are solved using the pressure-based finite volume method. The Boussinesq approximation is employed to incorporate the natural convection during the melting of PCM. Validations of the numerical model are carried out with the existing experimental results. The mass and thermal capacity of each heat sink configuration is kept constant. The performance of various cross plate-fin heat sink configurations is evaluated based on the transient temperature variation of heat sink base, PCM melt fraction, average Nusselt number, and energy absorbed by PCM through both latent and sensible heat. The study also investigates the effect of various PCM materials on the thermal performance of heat sinks. Maximum 10°C of temperature reduction is achieved in the case of the heat sink with 25 cavities compared to the heat sink with a single cavity. For the heat sink with 36 cavities, the melting time of the PCM reduces by 46.5% with the increase in the heat flux values from 1.0 to 2.0 kW/m^2. The study on the effect of PCM type reveals that paraffin wax is ideally suited for those electronic devices which have the critical SPT above 60 °C and below 70 °C.

The next problem considers the hollow fins of different configurations (circular and square) for the analysis. Various thermal performance parameters such as PCM melt fraction, maximum velocity of PCM, and variation of heat sink base temperature have been estimated in the investigation. At q''= 2.0 kW/m^2, the maximum velocity is found to be 2.4, 0.73, and 0.65 mm/s for no fin, circular hollow fin, and square hollow fin heat sink, respectively. Maximum temperature reduction of the heat sink with square hollow fins is found to be 4.19, 5.19, and 5.74%, at q''= 1.0, 1.5, and 2.0 kW/m^2, respectively, compared to the heat sink with no fin.

Present numerical investigation reports various thermal performance parameters for PCM-based heat sink assembly. The results obtained from the present investigation can be useful to design the light weight heat sink assembly for cooling of electronic components.

Chapter 4

Experimental investigation of PCM-based heat sink for thermal management of electronic devices

4.1 General background

With increased miniaturization, improved functionality, and higher processing speed of electronic components, the heat generation increases, increasing the operating temperature. It may be noted that a 10-20 °C rise in temperature increases the failure rate of electronic devices by 100% [107]. Passive cooling techniques employing PCM have been utilized to maintain the safe operating temperature of electronic components because of high energy storage capacity and isothermal phase change behavior. However, the PCM possesses a lower value of thermal conductivity that reduces the heat transfer rate and leads to longer charging and discharging time [207-216]. In view of this, high thermal conductivity enhancers (TCEs), namely fin, nanoparticles, and metallic foams (MFs), are embedded in the PCM system to promote the heat transfer rate.

The thermal performance is found to depend on various factors associated with the fins (TCE), such as volume fraction, numbers, cross-section, length, arrangement, and material. In addition to this, the performance of the heat sink varies with input heat flux, orientation, and time required to achieve the SPT. Different factors such as initiation of melting of PCM due to multiple conduction paths, duration of latent heat phase, intense convection to promote heat transfer, and sensible heating in post melting stage are found to affect the performance. It may be noted that heat sink with plate fins not only shows superior performance but also has simpler geometry which leads to lower manufacturing costs. For a fixed weight of fin material, different fin arrangements can be adopted to promote the natural convection effect, number of conduction paths, and surface area density. Limited studies are available on the cross-plate fin arrangement inside the PCM-based heat sink. Studies have been made that consider the inclusion of nanoparticles in PCM (NePCM) to improve thermal performance. The NePCM based finned heat sink can also be explored to improve the thermal performance. At the same time, very limited studies are available that consider the thermal performance analysis of NePCM based heat sinks. In addition to this, it is expected that foams (metal/non-metal) can be explored in PCM-based heat sinks to improve the thermal performance; studies pertaining to PCM-based heat sinks with high conductivity foam material have not been extensively studied in the literature.

Here, a systematic study has been carried out to analyze the thermal performance of PCM-based heat sinks with cross plate fin arrangement. Effect of various cavities (1, 4, 9, 16, 25, and 36) formed by cross fin arrangement (the number of fins, the volume fraction of PCM (φ =0.0-1.0), and effect of different heat flux values (1.5-2.5 kW/m^2) on the thermal performance is analyzed. Also, efforts have been made to analyze the thermal performance of different heat sink configurations such as heat sink with no fin (HSNF), heat sink with rectangular plate fins (HSRPF), heat sink with square pin fins (HSSPF), and heat sink with circular pin fins (HSCPF) integrated with NePCM for a varied range of nanoparticle concentration (γ= 0.5, 1.0, and 3.0) and different heat flux values (q''=1.5, 2.0, 2.5, and 3.0 kW/m^2). In addition, tests are conducted to analyze the thermal performance of various heat sink configurations such as PCM-based heat sinks with copper foam, carbon foam, no fins, circular pin fins, rectangular pin fins, and rectangular plate fins for a wide range of heat flux values (q''=1.5-2.5 kW/m^2) and different TCE values of carbon foam (ξ=5 to 25%).

4.2 Experimental setup and methodology

The schematic and photographic view of the experimental test facility is presented in Fig. 4.1(a-b). It comprises various units such as heat sink support system, PCM-based heat sink assembly, DC power source, digital data acquisition system (DDAS), laptop, and thermocouples. The heat sink assembly consists of a heat sink container, ceramic glass wool, and plate heater placed on the bottom surface of the heat sink. Here, the DC power supply unit (L3260, Aplab, India) having voltage and the current range of 0-32 V and 0-5 A, respectively, is employed to provide the required input heat flux to the heat sink assembly. Calibrated K-type thermocouples are employed to record the temperature at the base and inside the PCM. The heat sink assembly is insulated by employing 25 mm thick ceramic glass wool to minimize the heat loss to the surrounding. Plate heater (Sunrise products, India) of dimension 100×100×4 mm^3, made up of coil type nichrome wire wound on mica sheet, is employed to imitate the heat dissipated by the electronic chips of the electronic devices. The maximum heat flux that can be generated by the plate heater is 15.0 kW/m^2. The DDAS (34972A, Agilent, USA) is connected with thermocouples to measure the temperature at various locations of the heat sink in an interval of 10 seconds. A laptop is used to store the temperature variation data.

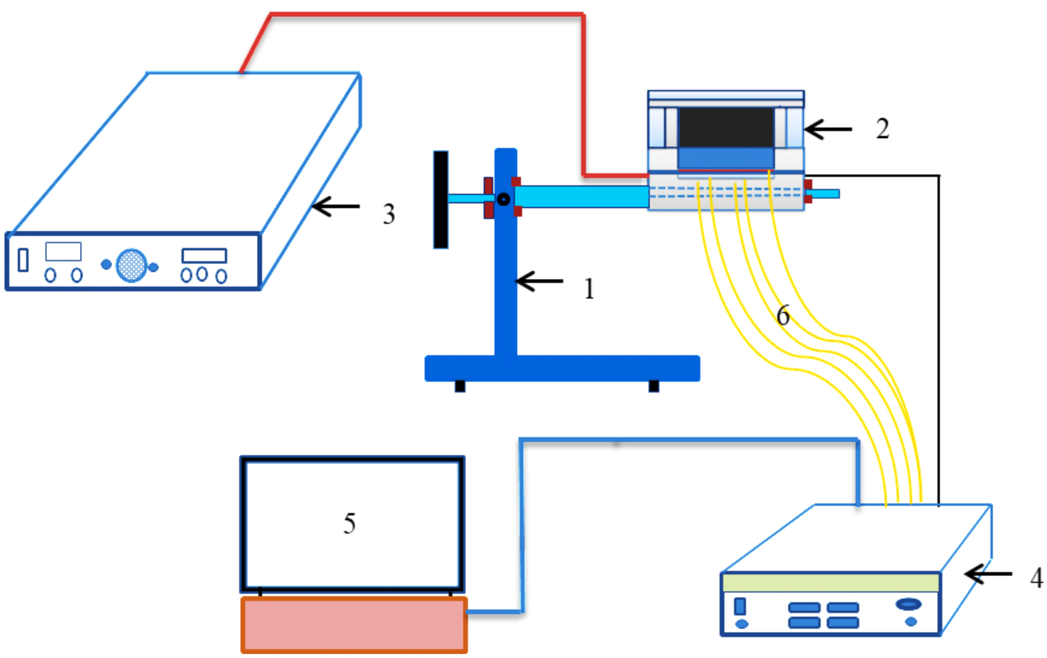

1	Support systems	4	Data acquisition system
2	PCM filled HS assembly	5	Laptop
3	DC power source	6	Thermocouples

(a)

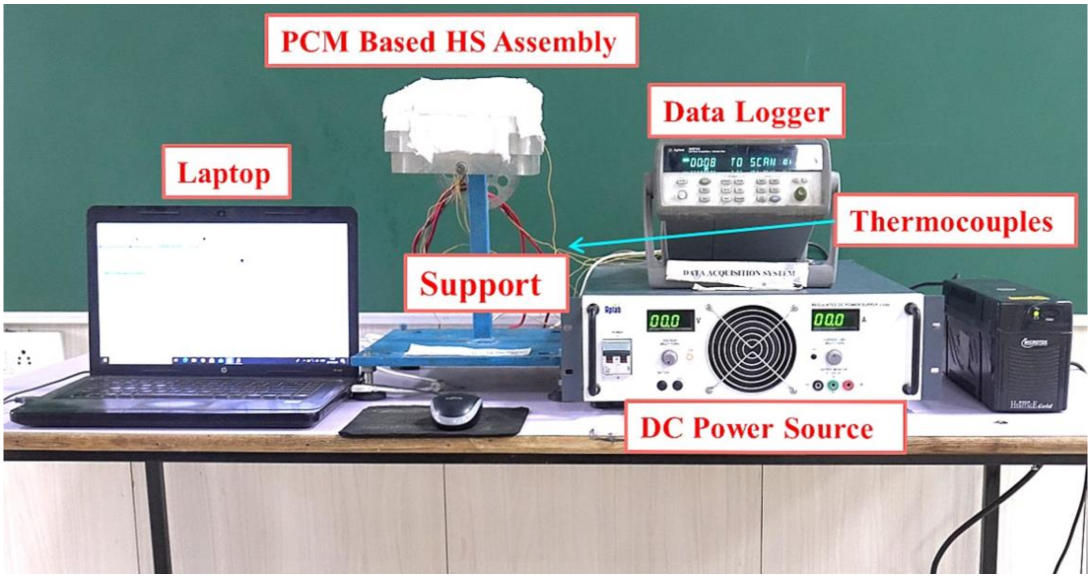

(b)

Fig. 4.1 Experimental setup (a) Schematic view (b) Photographic view

In the present study, Paraffin wax (Sigma Aldrich, USA), having a melting range of 58-62 °C, estimated as one of the optimal PCM from MADM technique is considered as PCM. Ganatra et al. [203] and Kothari et al. [153, 163, 217] have previously utilized paraffin wax) in their research because of various favorable thermophysical and chemical properties such as congruent melting, high specific heat capacity, and enthalpy of fusion on a volumetric basis, corrosion-resistant, thermally and chemically stable and non-toxic. Table 4.1 summarizes the thermophysical parameters of paraffin wax (PCM), aluminum (TCE), plexiglas (heat sink enclosure), and ceramic glass wool (insulator). Various input heat flux values ranging from 1.5-3.0 kW/m^2 are chosen for the present experimental analysis. These are typically the power inputs for portable electronic devices, and they fall within the ranges addressed in many research studies on the thermal performance of PCM-based heat sinks [84, 127, 129, 130, 140, 141, 154, 218].

Table 4.1 Thermophysical properties of paraffin wax, TCE, and insulator

Properties	Paraffin Wax		Aluminum (TCE)	Plexiglas	Ceramic glass wool
	Datasheet	Measured property			
Melting Temperature (^oC)	58-62	61.5	660.37	-	-
Latent heat (kJ/kg)	193.2	202.4	-	-	-
Specific Heat (kJ/kg-K)	2.89	3.74 (at 62^{o}C)	0.896	1.470	-
Density (kg/m^3)	750 (l), 900 (s)	775 (l), 900 (s)	2719	-	128
Thermal Conductivity (W/m-K)	0.12 (l), 0.21 (s)	0.128 (l) 0.233 (s)	218	0.19	0.12

4.2.1 Heat sink configurations and thermocouple location

The present experimental study aims to investigate the thermal characteristics of different heat sink configurations. The overall internal dimension of each heat sink is considered as 100×100×22 mm^3. Because of its superior thermal conductivity, low density, corrosion resistance, and lightweight, aluminum is chosen as the heat sink material. Copper has a better heat conductivity (two times that of aluminum), but it also has a higher density (three times that of aluminum), making it unsuitable for use in portable electronic components. Initially, heat sinks with cross plate fins filled with pure paraffin wax are investigated. Aluminium-6061 is employed to fabricate the heat sink and cross plate fins. Here, a CNC milling machine (Emcomill E350, Emco group, Austria) is utilized to fabricate the heat sinks from an aluminum slab of dimensions 102×102×25 mm^3. Six different heat sink configurations, as shown in Fig. 4.2(a-f), are investigated, and the details of their dimensions are depicted in Table 4.2. The overall dimensions of the heat sink, base thickness, and cavity height are kept constant for each configuration. The wall thickness and thickness of fins are varied to accommodate constant TCE volume fraction (6.60%) in each heat sink configuration.

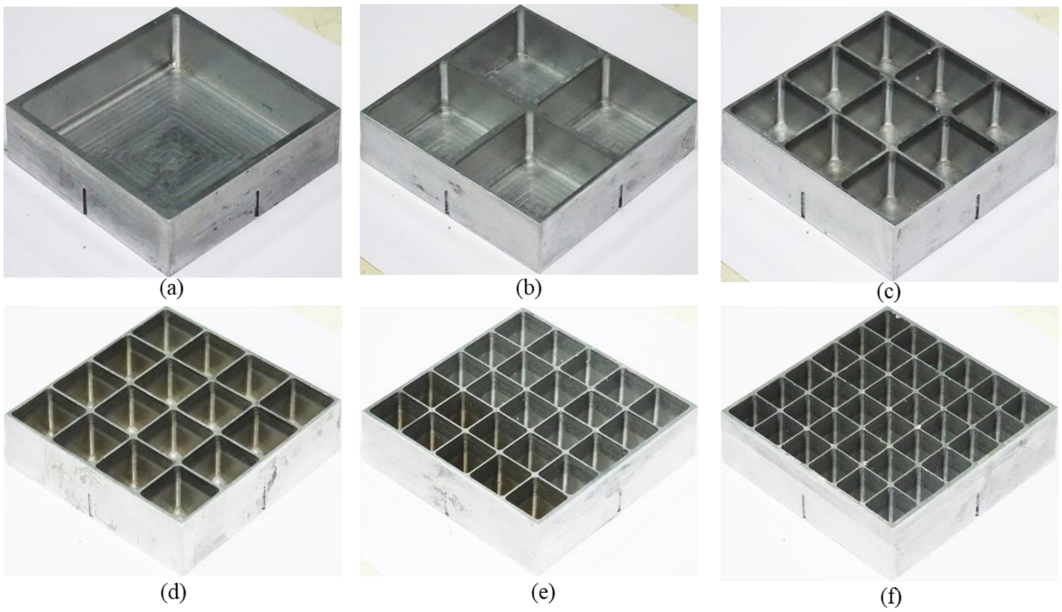

Fig. 4.2 Photographic view of heat sink configurations with (a) 1 cavity (b) 4 cavity (c) 9 cavity (d) 16 cavity (e) 25 cavity (f) 36 cavity

Table 4.2 Dimension of cross plate fin heat sinks

Heat sink	Overall dimensions ($L \times W \times H\ mm^3$)	t_b (mm)	t_w (mm)	t_f (mm)	Cavity dimensions $(l \times w \times h) mm^3$	Fins surface area to volume ratio
1 cavity	100×100×25	2.0	3.5	-	93×93×23	-
4 cavities	100×100×25	2.0	2.0	3.00	46.5×46.5×23	0.043
9 cavities	100×100×25	2.0	2.0	1.50	31×31×23	0.086
16 cavities	100×100×25	2.0	2.0	1.00	23.25×23.25×23	0.129
25 cavities	100×100×25	2.0	2.0	0.75	18.6×18.6×23	0.172
36 cavities	100×100×25	2.0	2.0	0.60	15.5×15.5×23	0.215

In addition, efforts have been made to analyze the thermal performance of different heat sink configurations such as heat sink with no fin (HSNF), heat sink with rectangular plate fins (HSRPF), heat sink with square pin fins (HSSPF), and heat sink with circular pin fins (HSCPF) with paraffin wax and CuO based NePCM for a varied range of nanoparticle concentration (γ = 0.5, 1.0, and 3.0). Taking a cue from other studies, we have considered a 9 % volume fraction [68, 130, 141, 218] and inline configuration [219] of fins for all the cases. The photographic view of heat sinks used in the present investigation is shown in Fig. 4.3(a-d). Heat sinks with 100×100 mm^2 base, and 25 mm height is used. Circular pin fins of diameter 2.95 mm and height 20 mm and square pin fins of dimensions 2×2×20 mm^3 are fabricated by wire electrical discharge machining (ELPULS 15, Ecocut, Electronica India) from an aluminum slab of dimension 101 ×101×25 mm^3. The plate fins of dimensions 100×20×2.5 mm^3 are fabricated by a CNC milling machine. All four sides and the top surface of the heat sink are covered with a 5 mm thick transparent Plexiglas sheet which also acts as an insulator. There is a 2 mm gap left between the top surface of PCM/NePCM and the bottom surface of plexiglas sheet to compensate for the volume expansion of PCM after melting. The dimensions of the material used are listed in Table 4.3.

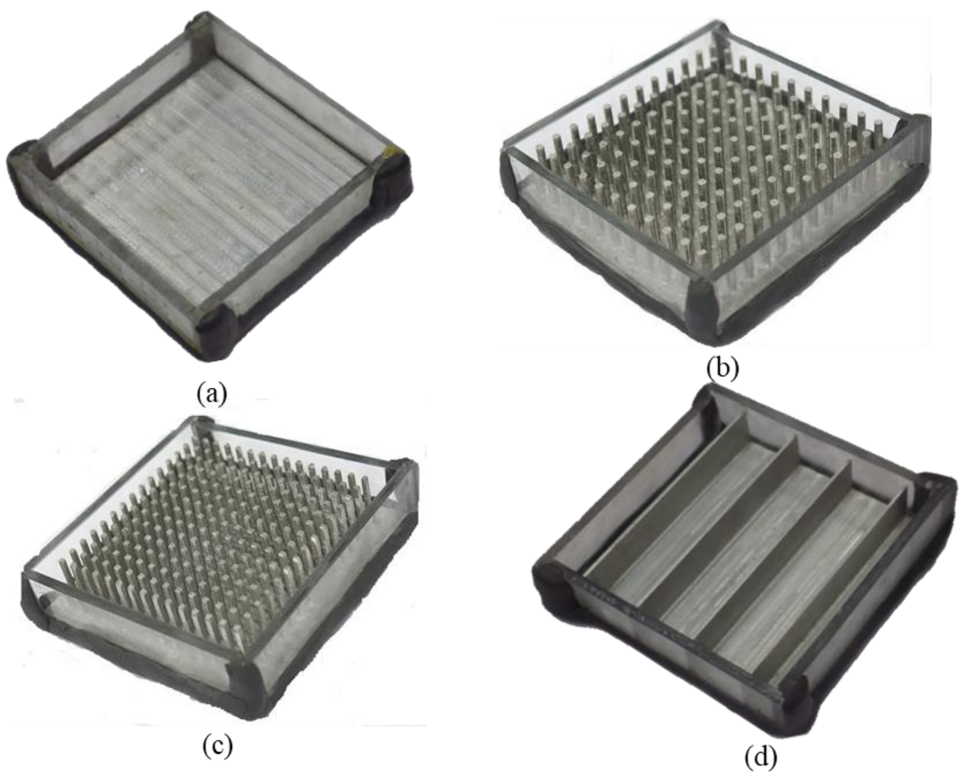

Fig. 4.3 Heat sinks used in the present study (a) HSNF (b) HSCPF(c) HSSPF (d) HSRPF

Table 4.3 Dimensions of the materials used for fabrication of various heat sinks

S. No.	Materials	Dimensions (mm)
1	Plexiglas sheet (Side wall)	100 ×25×5
2	Plexiglas sheet (Top surface)	115 ×115×5
3	Aluminum heat sink base	100 ×100×5
4	Aluminum circular pin fins (132 fins)	2.95×20
5	Aluminum square pin fins (225 fins)	2×2×20
6	Aluminum plate fins (4 fins)	100 ×20×2.25

A study has also been carried out on metallic and non-metallic foam embedded with PCM for electronic cooling applications. The photographic view of the heat sinks is presented in Fig. 4.4(a-b). To reduce thermal resistance between heater and heat sink base, thermal paste (OT-201, OMEGATHERM, Omega India) with thermal conductivity of 2.3 W/mK is used.

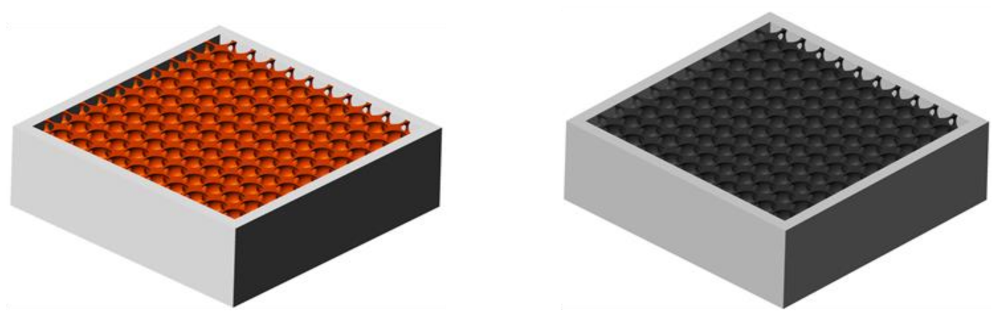

Fig. 4.4 Heat sink configurations (a) Heat sink with copper foam (b) Heat sink with carbon foam

High precision and pre-calibrated thermocouples (K-type) are attached at various locations of the heat sink assembly to measure the temperature during melting of PCM/NePCM, as shown in Fig. 4.5(a-b). Thermocouples B_1 to B_3 are fixed on the base of the heat sink to measure the base temperature. In order to fix the thermocouples, groves of 1.5 mm depth are made that are located 45 mm from heat sink sidewalls. Thermocouples W_1 to W_4 are fixed on the center of the outer wall of the heat sink. Thermocouples T_1 to T_8 are inserted 25 mm inside the PCM/NePCM to analyze the spatial distribution of temperature inside the heat sink. The locations of thermocouples T_1-T_8 from the heat sink bottom surface are shown in the top view (Fig. 4.5b). Thermocouples T_9 and T_{10} are attached on the upper wall of the heat sink and below the heater, respectively. Thermocouples T_{11} to T_{16} are placed on the six outer surfaces of the insulation wall to measure the heat loss during the experiment. Also, a thermocouple is left to the atmosphere to measure the ambient temperature.

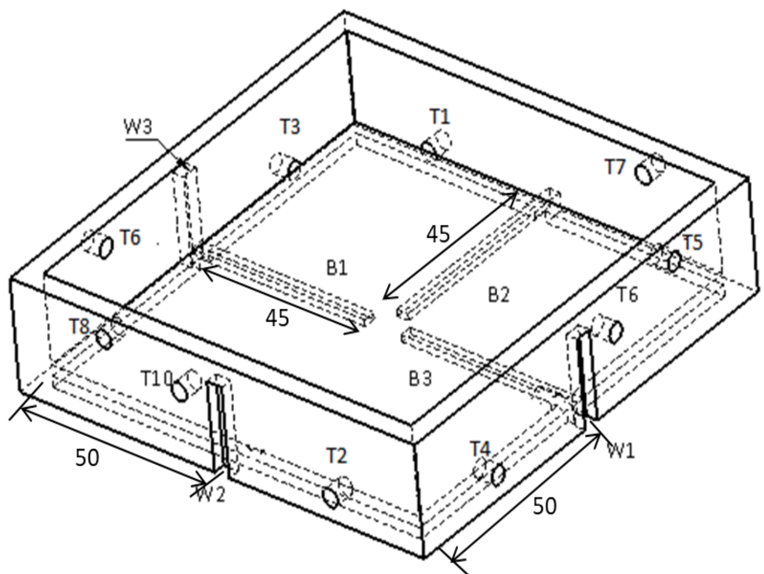

(a)

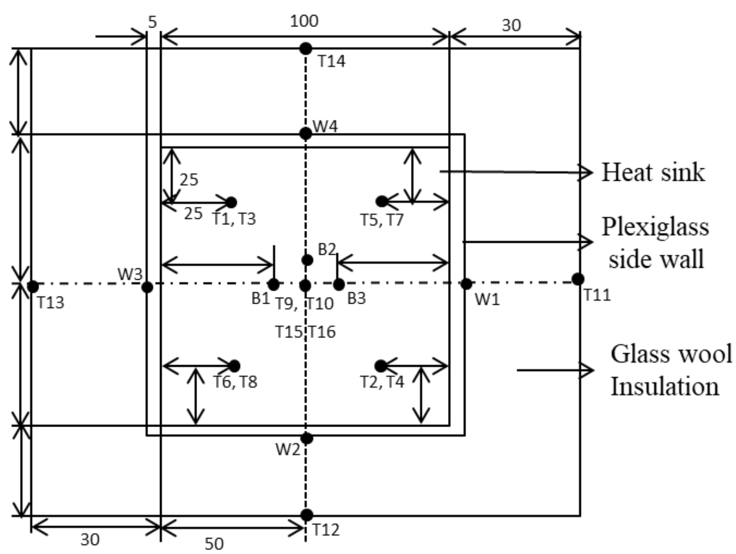

(b)

Fig. 4.5 Position of thermocouples (a) Isometric view (b) Top view

4.2.2 Preparation of nano-enhanced PCM (NePCM)

NePCM is obtained by adding CuO nanoparticles at different mass fractions inside the pure PCM. CuO nanoparticle employed in the present study has an average size of 30-50 nm, 99.9% purity, and 10 m^2/g specific areas and is manufactured by Nano lab India. The thermophysical properties such as specific heat, density, and thermal conductivity of CuO nanoparticles are 551 J/kg-K, 790 $kg/m^{3,}$ and 33 W/m-K, respectively [220]. Initially, the amount of solid PCM and CuO nanoparticles is measured by digital electronic balance (PGB 301, Wensar weighing scale, Chennai, India). The total amount of PCM and CuO nanoparticles is taken as 136.5 gm. After weighing PCM and CuO nanoparticles, the PCM is melted by placing it on a hot plate (Sahil scientific, India) at a constant temperature of 80 °C. CuO nanoparticles are dispersed step by step into liquefied paraffin wax and simultaneously stirred on the magnetic stirrer (REMI, 2MLH, India) for 2 hours at 500 rpm. The magnetic stirrer consists of a permanent magnet DC motor and stainless steel hot plate. Magnetic stirrer provides high accuracy of temperature control, and the speed of the DC motor and the temperature of the hot plate is maintained by supplying heat energy. The temperature of the magnetic stirrer and rpm is maintained properly throughout the operation to ensure uniform mixing of the nanoparticle. Subsequently, an ultrasonic vibrator (USBT-6, RICO Scientific Industries, India) is then used to sonicate the mixture at a constant frequency for 4 hours to ensure uniform distribution of nanoparticles in the PCM. The ultrasonic vibrator runs on 220V/50Hz with a power of 200W and a frequency of 50 kHz. The unit has an internal heating setup and temperature controller that can maintain a constant temperature above the melting point temperature of PCM. The temperature of the ultrasonic vibrator should be maintained above the melting point to avoid PCM solidification. Various researchers adopted a similar methodology to synthesize the NePCM [150, 221]. Fig. 4.6 presents the step by step process involved in the preparation of NePCM. After sonication, NePCM is allowed to solidify at room temperature and used for further analysis.

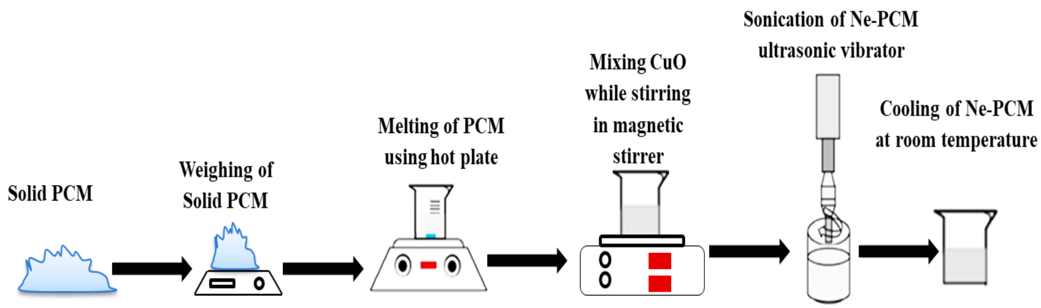

Fig. 4.6 Steps involved in preparation of NePCM

4.2.3 Preparation of foam-PCM composite

The copper foam (CoF) with pore size 10 PPI and 91% porosity is purchased from Nanoshel LLC USA, and carbon foam (CF) with 75% porosity is purchased from CFOAM LLC USA. The Vacuum infiltration technique is used to impregnate the foam with paraffin wax (PCM) which usually provides a higher impregnation ratio compared to the conventional non-vacuum impregnation method. Initially, the original sample (200×200×20 mm^3), provided by the manufacturer is cut into the required size (100×100×20 mm^3) by employing the sharp blade band saw under the tolerance limit of ±0.2 mm. Later on, the lateral surface of the foam is smoothened with the help of a sander. Subsequently, the samples are washed in order with acetone, ethanol, and water before being dried in a vacuum oven at 105 °C for 6 hours and then allowed to cool naturally at room temperature. The foam sample is immersed in liquefied PCM under vacuum, ensuring that any trapped air bubbles are removed from the liquid PCM. The foam-PCM composite is then allowed to cool down and solidify till it reaches the ambient temperature. It should be noted that the exact dimension of foam-PCM composite is obtained by removing the excess PCM surrounding the outer surface of the foam. A similar procedure was followed by Zhu et al. [161] and Kothari et al. [217] to fabricate foam-PCM composite. Due to the high expense of brazing of foam-PCM composite with heat sink, the composite is forced inside heat sink cavity to ensure good contact between heat sink internal surface and foam-PCM composite. Baby and Balaji [84] and Bhattacharya et al. [222] adopted similar procedures in their experimental investigations.

4.2.4 Experimental procedure

Solid PCM/NePCM is first melted in a vacuum furnace and placed into a heat sink container layer by layer, providing enough time for solidification. The process is repeated till the entire heat sink is filled with PCM/NePCM. This assures that no air pockets exist within the PCM integrated heat sink [223]. Tests are performed at room temperature (25/30 °C) and repeated twice to ensure experimental accuracy. Subsequently, the DC power is turned on, and the temperature readings are recorded by using a data acquisition system (Agilent34972A, USA) at regular intervals of 10 s. Heat flux is applied from the DC source by controlling the current and voltage as per ohm's law. The heat sink is kept in a horizontal position throughout the experiments for all the cases. Spirit level is utilized to check the horizontal position of the heat sink assembly. Heat input is stopped during the cooling period, and insulations are removed from all the sides except the bottom surface of the heat sink assembly.

4.2.5 Uncertainty and heat loss in measurement

The readings of current and voltage measurements displayed by the DC power supply are verified using a standard digital multimeter (Mecco 206). The errors associated in the measurement of voltage and current are ±0.1 V and ±0.1 A, respectively. The uncertainty in the measurement of heat flux is calculated by using the approach proposed by Coleman and Steele [224]. The maximum and minimum uncertainty in heat flux calculation is found to be 5.18% and 4.13%, respectively. The uncertainty in measured and calculated parameters is shown in Table 4.4.

Table 4.4 Uncertainty associated with various parameters

S. No.	Parameter	Uncertainty
1	Voltage	± 0.1V
2	Current	± 0.1A
3	Heat flux, max/min	± 5.18/4.13%
4	Temperature	±0.4 °C
5	Length	± 0.2 mm
6	Width	± 0.2 mm
7	Enhancement ratio	± 3.60 %
8	Thermal capacity	± 5.41%
9	Thermal conductance	± 3.60 %

Pre-calibrated Chromel-Alumel thermocouples (K-type) are utilized to measure the temperature at different locations during experiments. Thermocouples are calibrated for the temperature range of 20 to 100 °C following the ASTM standard [225]. A constant temperature bath along with standard mercury in a glass thermometer having a temperature range of 0 to 200 °C and 0.1 °C resolution is used for the calibration of the thermometer. The calibration is performed by immersing one end of all thermocouples into water inside a constant temperature bath (BTI35, Biotechnics, India), and the other end is connected to the data acquisition system (34972A, Agilent Technologies, USA). The temperature data measured by thermocouples are processed and recorded by a data acquisition system connected to the computer. The immersion heater inside the water bath is used to provide necessary heat input to the water, and continuous stirring is carried out to maintain the uniform temperature in the water bath. Subsequently, the temperature rise of water is measured by a thermometer and the thermocouples after a fixed time interval of 5 min. When the water temperature reaches 100 °C, the electric power source is turned off. Subsequently, the drop in the temperature of the water is measured at regular intervals. The maximum error in the temperature measurement is found to be $\pm$0.4 °C.

The Fourier's law for heat conduction can be used to calculate the heat loss as follows: [226].

$$Q_{loss} = \frac{k_{ins} \Delta T}{\Delta z} \tag{4.1}$$

Where, Q_{loss} is the heat loss through the insulation, k_{ins} is the thermal conductivity of insulation material (0.12 W/m-K), ΔT is the temperature difference between the two insulation surfaces, and Δz (0.025 m) is the thickness of the insulation layer. The temperature difference is calculated from the temperature data collected by using different thermocouples employed on both sides. Based on the temperature values of thermocouples (T_{11}-T_{16}), the heat loss to the surroundings is calculated, and the maximum value is found to be 6.27 % of the input heat flux value (3.0 kW/m^2). The value is meaningful, although it might be over-predicted due to the assumption of 1-D heat conduction.

4.3 Characterization and thermophysical properties of PCM, NePCM, and TCE

4.3.1 SEM analysis of aluminum and NePCM

In this study, Aluminum-6061 is used as heat sink material. Initially, field emission scanning electron microscopy (FE-SEM, Supre55, Zeiss, Germany) with Energy Dispersive X-ray Spectroscopy (EDX) is carried out to check the metallurgical composition of the heat sink and fin material. The data obtained from the analysis are presented in Fig. 4.7. It can be observed from SEM-EDX analysis that the heat sink material utilized in this study is pure Aluminium-6061 [227].

Here, SEM analysis is also carried out for NePCM to estimate the nanoparticle distribution inside the pure PCM. Fig. 4.8 shows the uniform distribution of CuO nanoparticles inside pure PCM, and no aggregation is noticed. An open-cell CoF (Nanoshel LLC, USA) and CF (Cfoam LLC, USA) are used as metallic and non-metallic foam, respectively. The microscopic structure of CoF (91% porosity) and CF (75% porosity) is presented in Fig. 4.9.

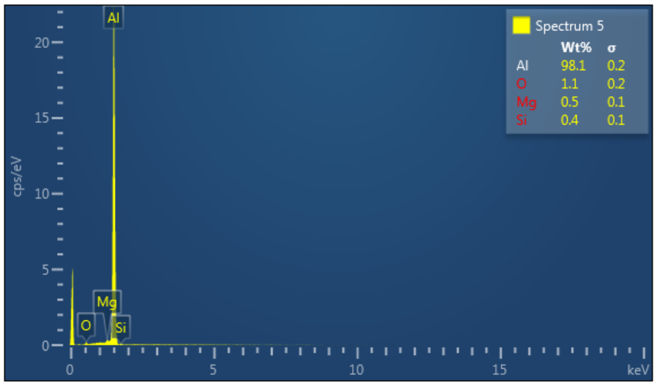

Fig. 4.7 Metallurgical composition of heat sink and fin material

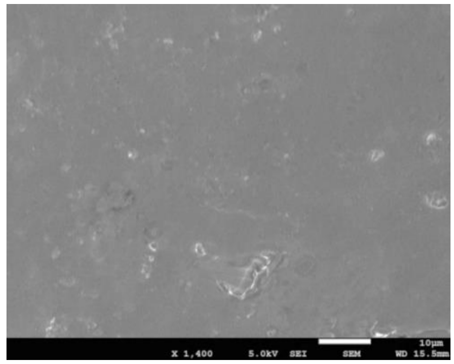

Fig. 4.8 SEM image of paraffin wax/CuO based NePCM

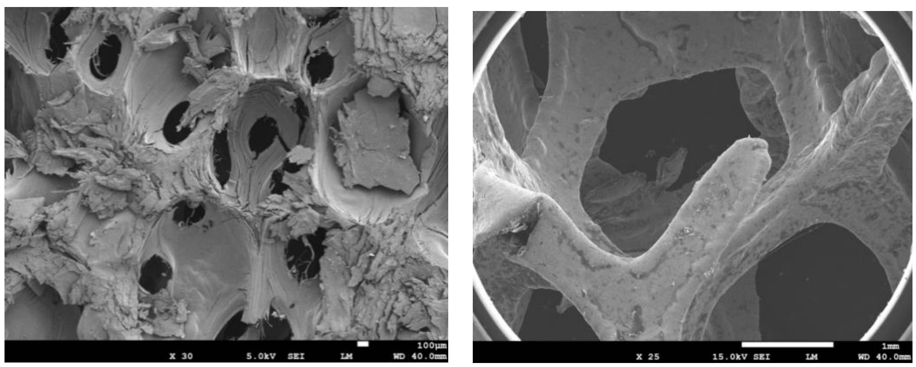

(a) (b)

Fig. 4.9 Microscopic structure (a) Carbon foam 75% porosity (b) Copper foam 91% porosity

4.3.2 Measurement of thermophysical properties of pure PCM

The latent heat, melting temperature range, and freezing temperature range are obtained using the differential scanning calorimetry (DSC) test. The DSC thermal analysis is carried out by PerkinElmer DSC 8000 with 10°C/min heating and cooling rate, and the temperature is varied between 25 °C to 79.97 °C and 79.97 °C to 25°C for the heating and cooling cycle, respectively. Fig. 4.10 presents the DSC curve obtained during heating (endothermic phenomena) and cooling (exothermic phenomena) of paraffin wax. Two peaks can be noticed during the melting and freezing of PCM. The solid-solid phase change is observed by a primary peak that occurs at a lower temperature of ~42 °C. While, the solid-liquid phase change (i.e., melting) is identified by a secondary peak that occurs at a higher temperature of ~59 °C. From the DSC analysis, the peak melting and freezing temperature is found to be 58.9±0.5 °C and 55.2±0.5 °C, respectively.

The secondary peak value obtained by DSC analysis agrees with the value specified by the supplier [Sigma Aldrich, USA]. The latent heat of paraffin wax is obtained by integrating the area under the second peak of the DSC curve and is found to be 153.2 kJ/kg. The specific heat of the paraffin wax is also obtained from DSC analysis and is depicted in Fig. 4.11. The maximum value of specific heat of PCM is found to be 3744 kJ/kgK, and it is measured near the peak melting temperature of PCM.

Here, the thermal conductivity of PCM is measured for a temperature range varying between 25-50 °C with an interval of 5 °C using tempos thermal properties analyzer (Meter Group Inc., USA) by a single needle sensor (KS-3) as shown in Fig. 4.12. It may be noted that thermal conductivity value measured for temperature below the melting point of PCM to avoid the possible natural convection effect in the mushy zone during melting. The measurement is repeated 5 times; the accuracy of thermal conductivity values measured by the KS-3 sensor is found to be ±10%. Table 4.5 presents the thermal conductivity value at each measurement.

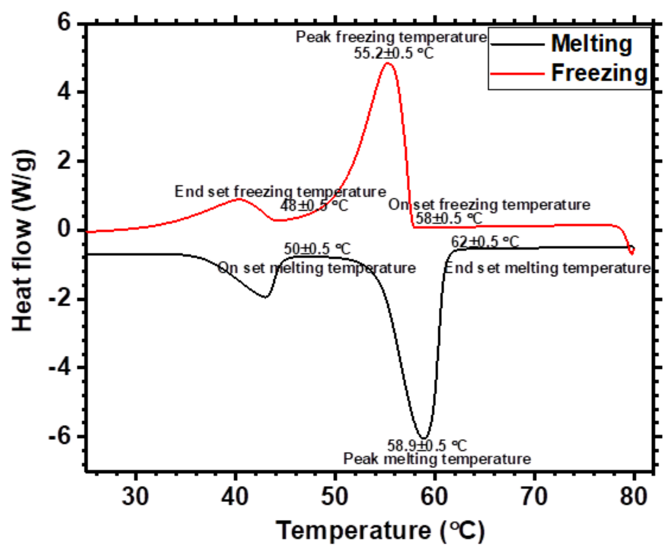

Fig. 4.10 Heating and cooling (DSC) curve of paraffin wax

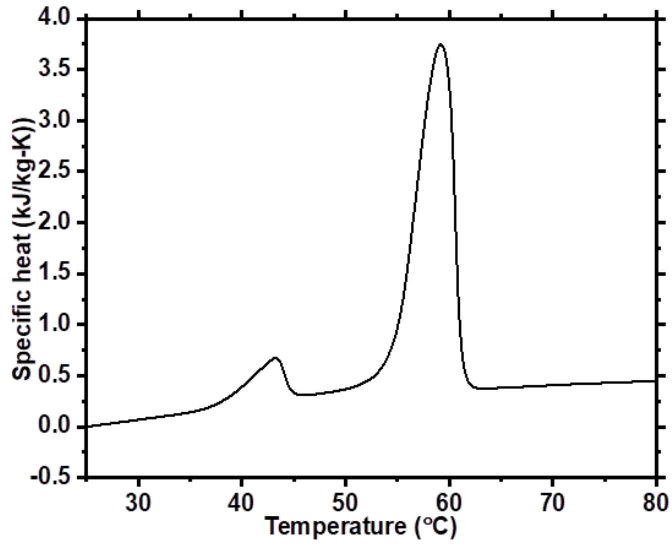

Fig. 4.11 Variation of specific heat during endothermic heating of paraffin wax

Fig. 4.12 Measurement of thermal conductivity of paraffin wax in solid phase

Table 4.5 Measurement of thermal conductivity of paraffin wax

Experiments	Thermal conductivity (W/m-K) at 25 °C (KS-3 sensor)
1	0.2353
2	0.2367
3	0.2302
4	0.2294
5	0.2353
Average	0.2334
Standard deviations	0.0033

To determine the density of PCM, solid paraffin wax is weighed in the appropriate quantity using a digital electronic balance (PGB 301, Wensar weighing scale, Chennai, India) with an accuracy of 0.1 mg. Solid paraffin wax is melted at 80°C on a hot plate (Sahil scientific, India), and liquid PCM is poured into a graduated cylinder. The cylinder is then placed in a water bath at a fixed temperature (BTI35, Biotechnics, India). Readings of change in volume of PCM are recorded at various temperatures and are used to obtain the density of PCM. The maximum volume change during the solid-liquid phase transition is found to be 20%. A similar procedure has been adopted by Shokouhmand and Kamkari [223] to obtain the density of PCM in their experimental investigation. The measured thermophysical properties of PCM are shown in Table 4.1.

4.3.3 Thermophysical properties of NePCM

The melting point and latent heat of fusion for PCM/NePCM with different mass fractions of CuO are obtained with the help of differential scanning calorimetry (DSC 8000, Perkin-Elmer, USA). Fig. 4.13 depicts the heating curve for PCM and NePCM composite at different mass fractions of CuO. It can be noticed that the mixing of CuO nanoparticles inside pure PCM does not affect the melting temperature of PCM significantly. However, the addition of CuO nanoparticles inside pure PCM reduces the latent heat of fusion. Table 4.6 shows the change in latent heat of NePCM composite at a different mass fraction of nanoparticles. It may be noted from the Table that the reduction in the latent heat value is found to be 4.40, 14.43, and 24.75% for nanoparticle loadings of 0.5, 1.0, and 3.0, respectively, compared to pure PCM.

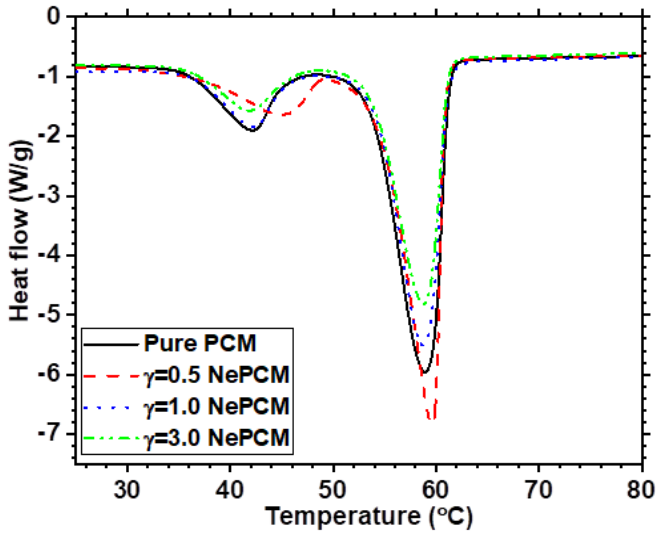

Fig. 4.13 Differential scanning calorimeter heating of PCM dispersed with various nanoparticle concentrations of CuO

Table 4.6 Latent heat variation of NePCMs

Sample	Latent heat (kJ/kg)	Latent heat variation (%)
$\boldsymbol{\gamma} = 0.0$	153.21	-
$\boldsymbol{\gamma} = 0.5$	146.46	4.40
$\boldsymbol{\gamma} = 1.0$	131.09	14.43
$\boldsymbol{\gamma} = 3.0$	115.28	24.75

The variation of thermal conductivity values with temperature for various nanoparticles loading is shown in Fig. 4.14. Here, the thermal conductivity of PCM and NePCM in the solid phase is measured for a temperature range varying between 30-50 °C with an interval of 5 °C by using TEMPOS thermal properties analyzer. The measurement is repeated five times to avoid any discrepancies in the result, and the average value is presented here. The thermal conductivity increases with an increase in nanoparticle mass fraction and remains almost independent of temperature between 30 °C to 45 °C. The maximum increment in thermal conductivity is found to be 150% at γ=3.0. However, as the temperature reaches close to the melting point, the thermal conductivity decreases considerably.

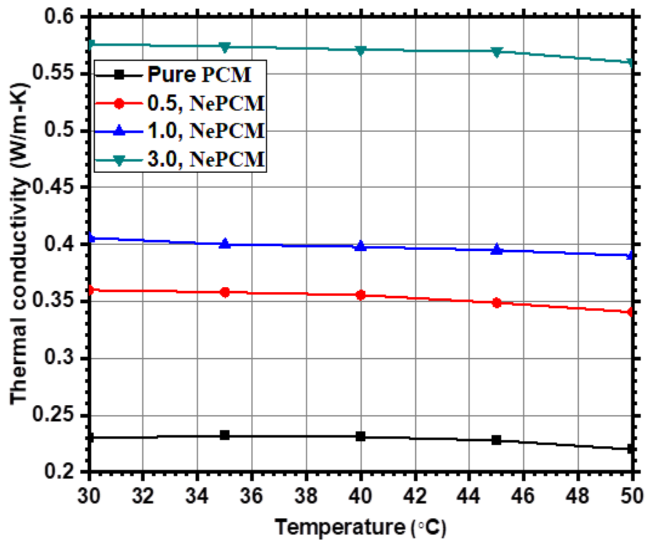

Fig. 4.14 Variation of thermal conductivity of PCM and NePCM with temperature

Here, density, specific heat, and viscosity of NePCM are obtained using standard formulae and correlations for heat transfer analysis. It is assumed that the CuO nanoparticle is distributed uniformly within the pure PCM. In such a case, the effective thermal properties such as density and specific heat of NePCM can be estimated using the mixture rule as below [230-231].

$$\rho_{NePCM} = \gamma\rho_{np} + (1-\gamma)\rho_{PCM} \tag{4.2}$$

$$(\rho c_p)_{NePCM} = \gamma(\rho c_p)_{np} + (1-\gamma)(\rho c_p)_{PCM} \tag{4.3}$$

The viscosity of NePCM is obtained using the correlation provided by Vajjha et al. [232]. It may be noted that the correlation is valid for φ lies between 0.01 and 0.06.

$$\mu_{NePCM} = 0.9197e^{22.8539\psi}\mu_{PCM} \tag{4.4}$$

Where, ψ represents the volume fraction of nanoparticles and can be obtained using the following expression [233].

$$\psi = \frac{\frac{Wt_{np}}{\rho_{np}}}{\frac{Wt_{np}}{\rho_{np}} + \frac{Wt_{PCM}}{\rho_{PCM}}} \tag{4.5}$$

Where, Wt_{np}, and Wt_{PCM} represent the weight of the nanoparticle and the weight of the PCM, respectively. Here, ρ_{np}, and ρ_{PCM} represent the density of nanoparticle and PCM, respectively.

Table 4.7 presents the variation of density, specific heat and viscosity of NePCM at γ= 0.0, 0.5, 1.0 and 3.0. The density of NePCM increases while specific heat decreases with an increase in γ. This is because of the higher density and lower specific heat capacity of CuO nanoparticles compared to pure PCM. It can be seen from Table 4.7 that the density of NePCM increases by 17.45%, and specific heat decreases by almost 14% at γ = 3.0. Also, viscosity increase by 56 % and 100 % at γ =1.0 and γ =3.0, respectively. A similar variation has been obtained by Ho and Gao et al. [228] for Al_2O_3 based NePCM.

Table 4.7 Density, specific heat capacity and viscosity variation of NePCMs

Properties	γ =0.0	γ =0.5	γ =1.0	γ =3.0
Density (kg/m^3)	880	905.6	931.2	1033.6
% change	-	2.91	5.82	17.45
Specific heat	2800	2725.497	2655.09	2408.34
% change	-	2.66	5.17	13.98
Viscosity	0.0235	0.0284	0.0366	0.0470
% change	-	21	56	100

4.4 Data reduction

Various parameters namely, PCM volume fraction (φ), TCE volume fraction (ξ), CuO mass fraction (γ), enhancement ratio in operating time (ε), thermal capacity (δ) in pre and post melting, and thermal conductance (G) are used to study the heat transfer characteristics of different heat sink configurations. These parameters are elaborated and defined below.

PCM volume fraction (φ): It is defined as the ratio of the volume of PCM integrated inside the heat sink to the difference of the total heat sink volume and volume occupied by fins [141].

$$\varphi = \frac{V_{PCM}}{V_{HS} - V_f} \tag{4.6}$$

TCE volume fraction (ξ): It is defined as the ratio of the volume occupied by TCE to the total volume of heat sink (HS) enclosure without fins.

$$\xi = \frac{V_{TCE}}{V_{HS}} \tag{4.7}$$

Nanoparticle (CuO) mass fraction (γ): It is defined as the ratio of the mass of CuO particles to the mass of PCM.

$$\gamma = \frac{m_{CuO}}{m_{PCM}} \tag{4.8}$$

Enhancement ratio in operating time (ε): This is defined as the ratio of the time taken to attain critical SPT by the heat sink with PCM to that of heat sink without TCE and PCM [141].

$$\varepsilon = \frac{t_{Cr\ with\ PCM}}{t_{Cr\ without\ TCE\ and\ PCM}} \tag{4.9}$$

Thermal capacity (δ): It is defined as the amount of energy supplied to the PCM integrated heat sink per unit temperature difference [141].

$$\delta = \frac{H}{\Delta T} \tag{4.10}$$

Thermal conductance (G): It represents the amount of heat transfer from the surface of PCM-based heat sink assembly [141, 234].

$$G = \frac{q''}{T_{max} - T_{amb.}} \tag{4.11}$$

4.5 Comparison of present results with existing studies

In order to validate the experimental setup, present test results are compared with the experimental results of Arshad et al. [129], Mahmoud et al. [135], Kothari et al. [217], Huang et al. [216], and Zhao et al. [235]. Results are compared for both heat sinks with and without PCM subjected to different heat flux values. These studies utilize paraffin wax as PCM, and the melting temperature is found to be 56-58 °C [129] and 58-62 °C [217]. In addition to this, lauric acid with a melting temperature range of 42-44°C and stearic acid having a melting temperature of 68.77 °C are used as PCM by Huang et al. [216] and Zhao et al. [235], respectively. The heat flux value is varied between 1.3-3.0 kW/m^2 in these studies [129, 135, 216, 217, 235], and the initial temperature is considered as 20-30 °C.

In the present investigation, the heat sink has an overall dimension of 100×100×25 mm^{3,} and paraffin wax with a melting temperature range of 58-62 °C is considered as PCM. The heat sink side walls are made up of acrylic sheet of 5 mm thickness. Present test results obtained from heat sink without PCM and heat sink with PCM are compared with the available experimental results as shown in Fig. 4.15(a-b). Fig. 4.15(a-b) reveals that the variation of base temperature in the present study follows a similar pattern as reported by other researchers [129, 135, 216, 217, 235]. The deviation in the results might be due to the variation in their heat sink configuration, type of PCM used, variation in heat flux values, and initial heating condition. The result of a heat sink with a single cavity integrated with paraffin wax are also compared and presented in Fig. 4.15(c). The results of single cavity heat sink also follow a similar pattern as reported by Mahmoud et al. [135], Kothari et al. [217], and Zhao et al. [235.] Based on the qualitative and quantitative agreement, the present test facility is assumed to be validated and can be used for further analysis.

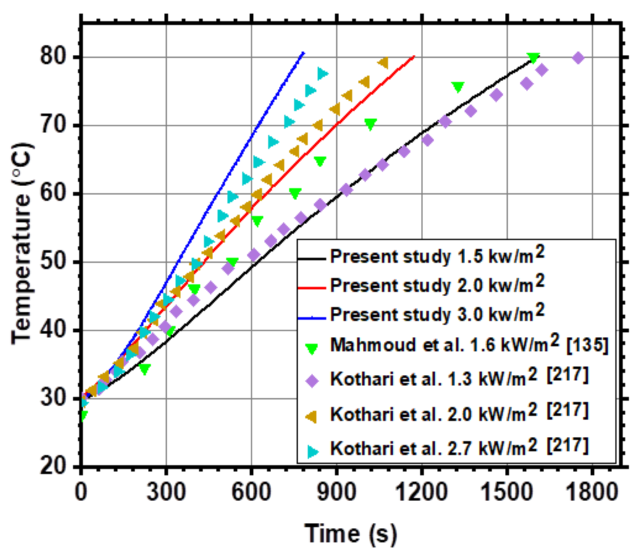

(a)

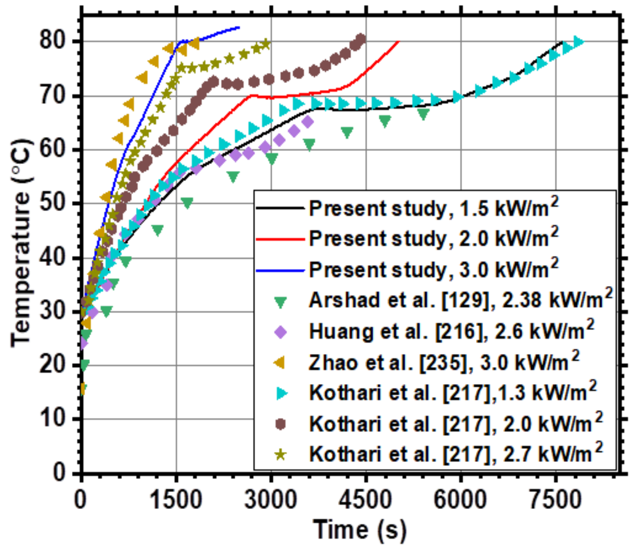

(b)

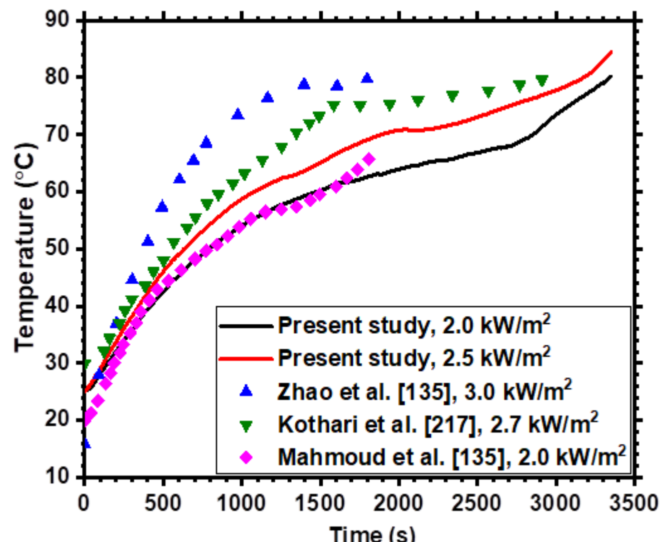

(c)

Fig. 4.15 Comparison of present results with the existing results for (a) Without PCM (b) With PCM (c) Single cavity heat sink with PCM

4.6 Results and discussion

4.6.1 Thermal performance of PCM-based heat sinks with cross plate fins for cooling of electronic components

In this study, tests are performed to study the thermal performance of different PCM embedded heat sinks involving various cavities such as 1, 4, 9, 16, 25, and 36 formed by rectangular cross plate fins as presented in section 4.2.1. Here, the mass of the heat sinks and the amount of PCM are kept constant in each heat sink design which has not been addressed extensively in the literature. Heat flux is varied in the range of 1.5-2.5 kW/m^2. Various heat sink configurations (1, 4, 9, 16, 25, and 36 cavities), as shown in Fig. 4.2, involving organic PCM (paraffin wax), are studied. Effect of heat sink configurations, heat flux (q'') and PCM volume (φ) fractions are analyzed. Results are presented in the form of transient temperature variation of the heat sink base, the time required to reach set point temperature (SPT), enhancement ratio (ε), thermal capacity during pre and post melting (δ), and thermal conductance (G).

Comparison of experimental and numerical results

Initially, the experimental results are compared with the numerical results presented in chapter 3. Fig. 4.16 illustrates the comparison of experimental and numerical results for the case of a 3×3 finned heat sink (16 cavities). The temperature is obtained at the same location as that of the numerical measurements, and heat flux of 1.5 and 2.0 kW/m^2 is considered.

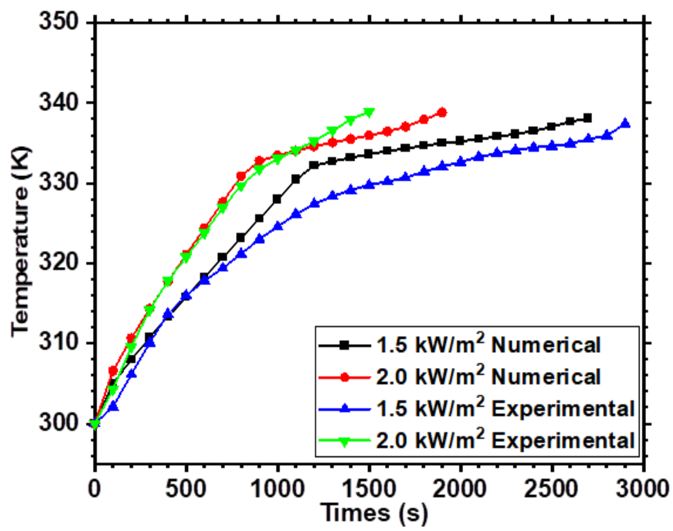

Fig. 4.16 Comparison of experimental and numerical results

From Fig. 4.16, it is observed that experimental results agree well with the numerical results with the maximum variations of less than $\pm$9 %. Variation in the numerical results with the experimental is attributed to the variation thermophysical properties of the PCM with temperature during experimentation which is assumed to be constant in the numerical study. Also, the actual thermophysical properties are different from those used in numerical simulation. For example, the latent heat value used in the numerical simulation is 193.2 kJ/kg, while the calculated latent heat value from DSC analysis is 153.2 kJ/kg.

Effect of PCM volume fraction

Fig. 4.17(a-d) presents the effect of PCM volume fractions (φ= 0.0, 0.5, 0.8, and 1.0) for various heat sink configurations with different cavities (1, 4, 9 and 16) at q''= 2.0 kW/m^2. A rapid increase in temperature is observed at φ= 0.0 for all the heat sink configurations, while a significant enhancement in thermal performance is observed with an increase in φ. Time-temperature variation of the base of the heat sink follows a similar trend for each heat sink configuration integrated with PCM. One can notice that without PCM, the base temperature variation does not change significantly, even with the increase in the number of cavities (1, 4, 9, and 16). While PCM-based heat sink with φ= 1.0 and 16 cavities exhibit better thermal performance than other heat sink designs. The operating time is found to be increased by approximately 30% to attain a temperature of 60 °C in the case of the heat sink with φ= 1.0 and 16 cavities compared to the heat sink with φ= 1.0 and one cavity. This occurs due to the uniform melting of PCM in the presence of TCE.

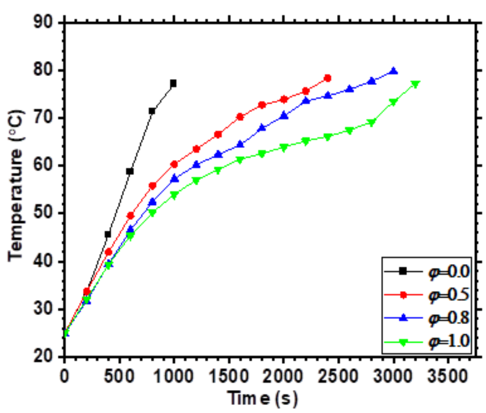

(a)

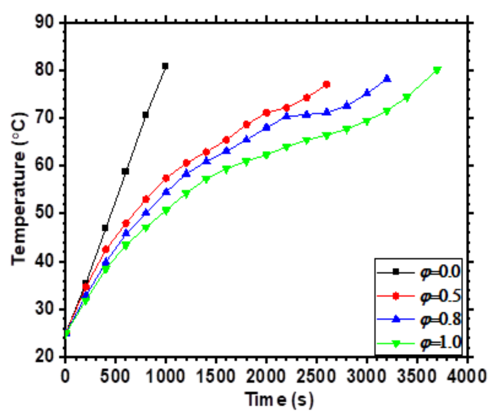

(b)

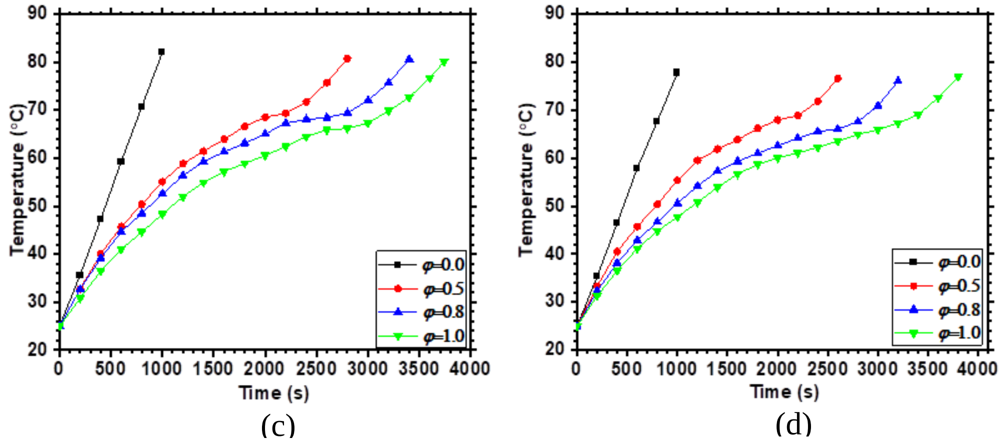

Fig. 4.17 Effect of PCM for different heat sink configurations (a) 1 cavity (b) 4 cavity (c) 9 cavity (d) 16 cavity

Effect of heat sink configurations

The performance of different heat sink configurations (1, 4, 9, 16, 25, and 36 cavities) is shown in Fig. 4.18(a-b) for two different heat flux values for q''= 1.5 and 2.0 kW/m^2 at φ = 1.0. The rise in the base temperature is very sharp for heat sink with one cavity; the rise in temperature takes place at a slower rate for heat sink with more number of cavities. The heat sink with 36 cavities outperforms all other heat sink designs in terms of heat transfer efficacy. For the heat sink with 36 cavities, the maximum temperature drop of 19 and 19.5% is estimated compared to the heat sink with a single cavity at q''= 1.5 and 2.0 kW/m^2, respectively. While, the heat sink with 25 cavities exhibits a 17.2% reduction in base temperature compared to a single cavity heat sink at q''= 1.5 and 2.0 kW/m^2, respectively. It may be noted that the PCM tends to melt from side walls and the bottom surface of the heat sink. Due to the lower value of thermal conductivity (k= 0.23 W/m-K), the heat conduction in the PCM is poor and results in non-uniform melting of PCM in the case of no fins heat sink (single cavity), and the base temperature reaches to the critical limit rapidly. On the contrary, heat sink with Aluminium-6061 as fins material (k = 218 W/m-K), the conduction heat transfer is higher in PCM. Also, with the increase in the number of fins, the surface area to volume ratio increases which leads to uniform heat transfer from heat sink base and walls to PCM and maintains the heat sink base temperature at a lower limit for a longer duration.

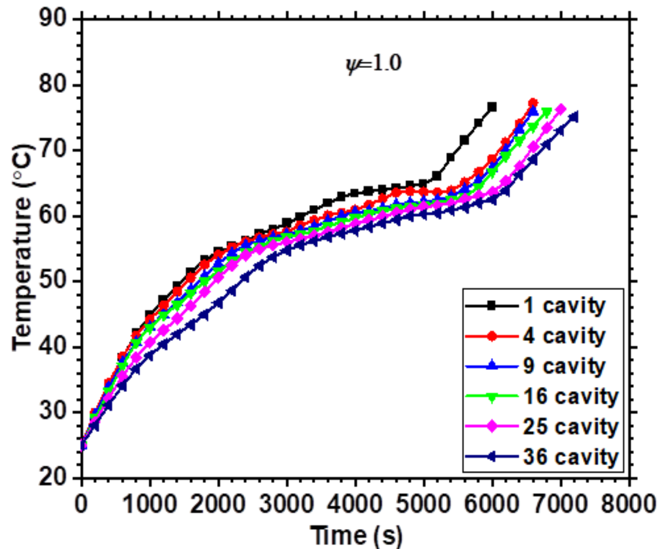

(a)

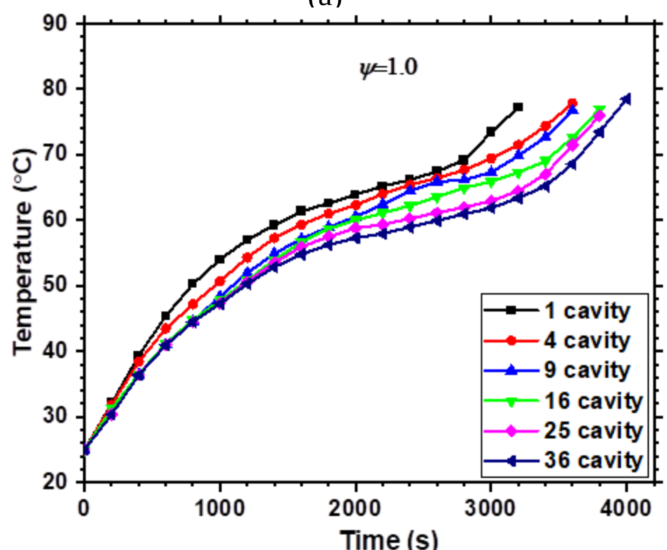

(b)

Fig. 4.18 Effect of heat sink configurations for different heat flux values (a) 1.5 kW/m^2 (b) 2.0 kW/m^2

For the practical application of PCM-based heat sink cooling, it is important to study the solidification time of PCM as PCM needs to be used for the next operation cycle. Fig. 4.19 depicts the solidification time of various PCM-based heat sink assemblies. During the cooling period, heat input is stopped, and insulations are removed from all the sides except the bottom surface of the heat sink assembly. Heat transfer occurs from hot PCM to heat sink through conduction and then to ambient via natural convection. For the heat sink with a single cavity, the solidification time is found to be 15500 s to reach 30 °C, which is significantly higher compared to the melting time of PCM. The solidification time is found to be reduced by 40% for the heat sink with 36 cavities compared to the heat sink with 4 cavities. This can be attributed to the increase in overall thermal conductivity and heat exchange surface area due to the inclusion of cross fins inside the heat sink. From the cooling curve, one can notice that up to the crystallization temperature of PCM, the temperature profile follows the same pattern for each heat sink configuration. The variation in transient temperature during cooling varies for each heat sink configuration in the later part of the cooling, in which the heat transfer occurs due to conduction.

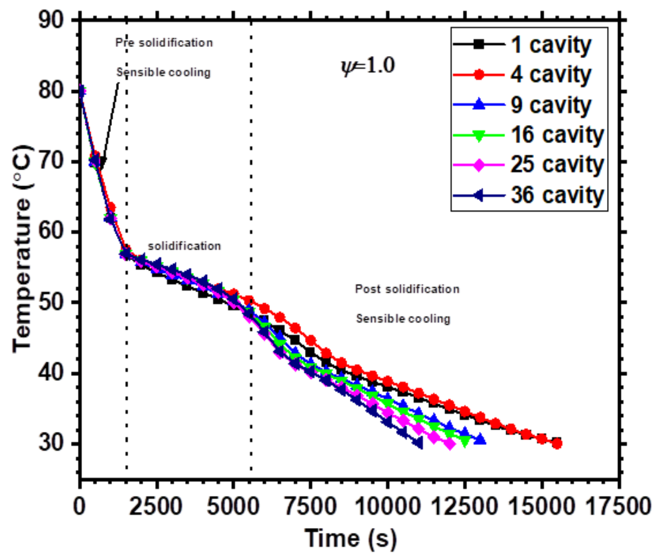

Fig. 4.19 Cooling curve of different heat sink configurations for q'' =2.0 kW/m^2

Study of critical SPT and enhancement ratio (ε)

The thermal efficacy of different heat sink designs integrated with paraffin wax is studied in terms of different values of SPT. Two different temperature values (65 and 75 °C) are chosen as critical SPTs, which are considered the maximum operating temperature for most of the electronic devices [128-129, 217]. The critical SPT is the highest temperature limit for the safe and efficient working of electronic components. Electronic components operating beyond SPTs for a longer period may result in degradation of performance and premature failure. Fig. 4.20(a-b) shows the time required for various heat sink configurations to achieve critical SPTs (65 and 75 °C) for different input heat flux values. The heat sink with 36 cavities takes more time to reach the SPT values. At $q'' = 1.5$ kW/m^2 and heat sink with 36 cavities, the maximum working time is estimated to be 6300 and 7190 s for SPT of 65 and 75 °C, respectively. With an increase in heat flux values, the operating time to reach critical SPT is found to be shorter. For heat flux value (2.5 kW/m^2), the operating time of heat sink with 36 cavities reduces by 2230 and 3190 s for SPT of 65 and 75°C, respectively.

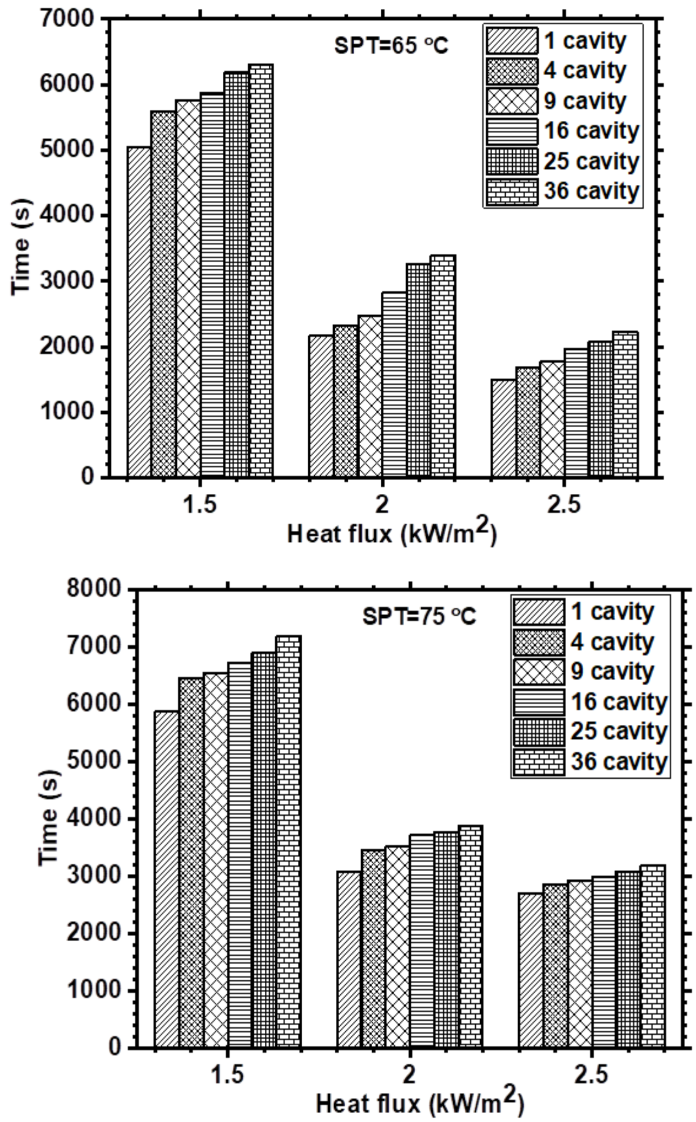

(b)

Fig. 4.20 Time to reach various SPT for different heat sink configurations (a) 65 °C (b) 75 °C

Fig. 4.21(a-b) present the enhancement ratio of various heat sink configurations at different heat flux values for various SPTs (65 and 75 °C). Here, Eq. 4.9 is used to calculate the enhancement ratio. The heat sink with 36 cavities integrated with PCM shows a higher enhancement ratio compared to other heat sink designs. The enhancement ratio decreases with higher input heat flux values and higher SPT values. It is observed that the performance of heat sink depends on various parameters such as heat flux value, PCM type, and SPT value, and fin parameters (arrangement, number of conducting paths, surface area density, and shape). Efforts have been made to compare the maximum enhancement ratio obtained from the experimental investigation with the test results of Ali et al. [132, 141] for circular pin fin heat sink and triangular pin fin heat sink, Arshad et al. [128-129] for circular pin fin heat sink and square pin fin heat sink, Usman et al. [134] for triangular pin fin heat sink, Tariq et al. [150] for NePCM based heat sink with no fins, Kothari et al. [136] for a rectangular plate-fin heat sink. These studies include a wide range of SPT values, heat sink configuration, PCM types, and fin designs (Table 4.8). The maximum enhancement ratio obtained by the present study is found to be higher compared to other studies. The highest enhancement ratio of 6.5 and 5.8 is obtained by heat sink with 36 cavities at q''=1.5 kW/m^2 for SPT of 65 °C and 75 °C, respectively. This shows that the efficient fin design can improve the thermal performance of heat sinks.

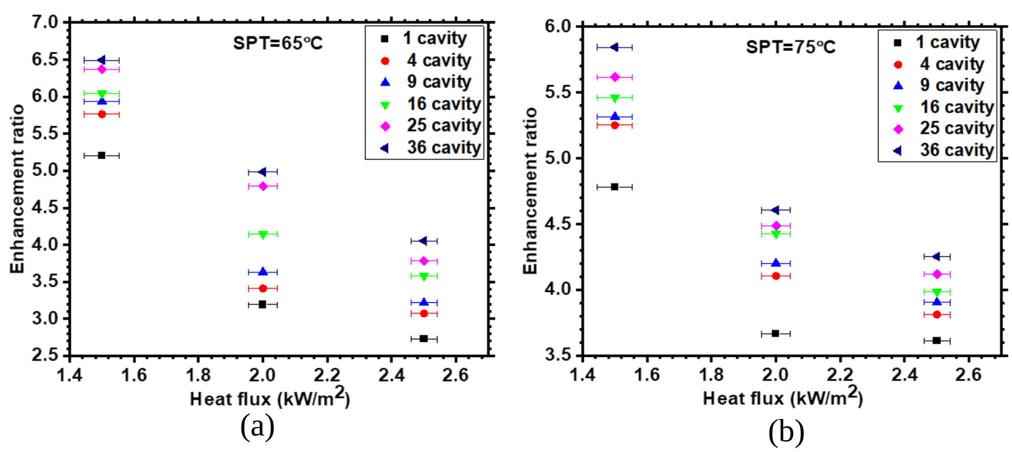

Fig. 4.21 Enhancement ratio for different heat sink configurations for various SPT (a) 65 °C (b) 75 °C

Table 4.8 Comparison of enhancement ratio from the previous studies

Reference	Type of HS	Heat sink overall dimension	SPT (°C)	Maximum enhancement ratio	SPT (°C)	Maximum enhancement ratio
Ali et al. [141]	Circular pin fin HS	114×114×25	40	4.78	50	1.9
Arshad et al. [128]	Circular pin fin HS	114×114×25	60	4.2	70	3.7
Arshad et al. [129]	Square pin fin HS	114×114×25	60	4.30	70	4.0
Usman et al. [134]	Triangular pin fin HS	71×70×25	45	3.4	60	2.24
Tariq et al. [150]	NePCM based HS w/o fins	110×110×25	50	2.61	70	2.5
Kothari et al. [136]	Rectangular plate fin HS	110×110×25	75	4.6	-	-
Ali et al. [132]	Triangular pin fin HS	71×70×25	45	5.0	60	2.2
Present Study	Cross plate fin HS	100×100×25	65	**6.5**	75	**5.8**

Comparison of thermal capacity and thermal conductance

In order to access the thermal performance of PCM integrated heat sink with cross plate fins, the heat capacity during pre-sensible and post-sensible heating is obtained by using Eq. 4.10 and is shown in Fig. 4.22(a-b). In pre-sensible heating, the heat sink with 36 cavities shows the highest heat capacity value of 1.03 and 1.02 kJ/K at q'' = 2.0 and 2.5 kW/m^2, respectively. While, in the post-sensible heating region, the highest values of thermal capacity are found to be 1.63 and 1.28 kJ/K at q'' = 2.0 and 2.5 kW/m^2, respectively. The heat sink with a single cavity exhibits a lower value of heat capacity both in the pre-sensible and post-sensible heating regions, which results in poor thermal performance. The heat sink with 36 cavities has more heat capacity values and can store a large amount of heat which results in lower heat sink base temperature and performs better compared to other heat sink designs.

Fig. 4.23 presents the thermal conductance for different heat sink configurations at q'' = 2.0 and 2.5 kW/m^2. Here, Eq. 4.11 is employed to obtain the thermal conductance values. It refers to the rate of heat transfer from the heat sink base to the PCM assisted by fins per unit temperature difference. The heat sink with 36 cavities exhibits the highest thermal conductance values for each heat flux value which represents the best heat transfer from the heat sink base to the PCM. The heat sink with no fins exhibits the lowest thermal conductance value, which results in poor heat transfer from the heat sink base to the PCM. In such a case, the heat sinks surface temperature increases which are not good for thermal management of electronic components.

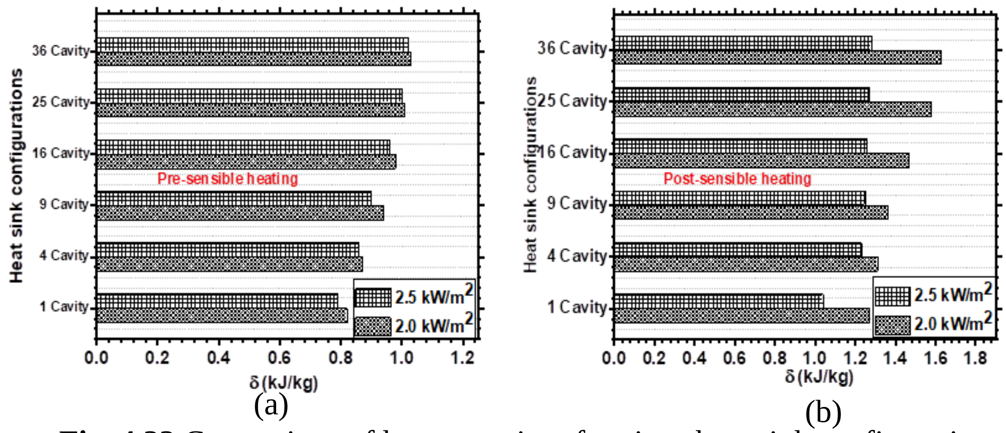

Fig. 4.22 Comparison of heat capacity of various heat sink configurations (a) Pre-melting (b) Post-melting

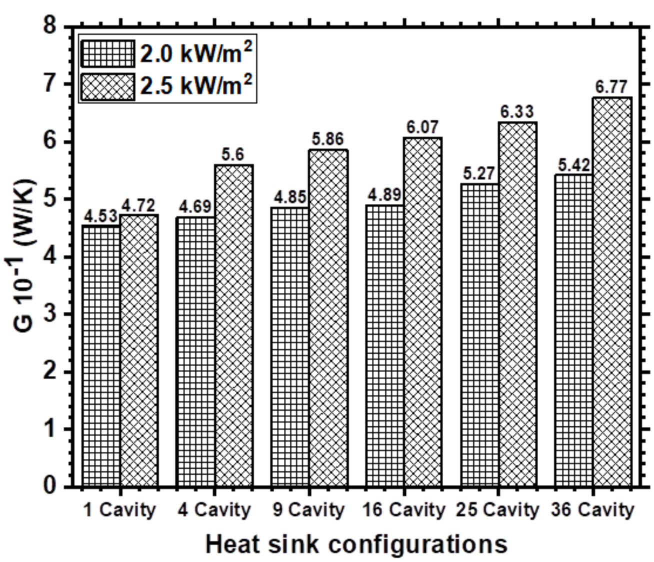

Fig. 4.23 Comparison of thermal conductance of various heat sink configurations for different heat flux values

4.6.2 Thermal performance of heat sink using NePCM for cooling of electronic components

In this study, nano-enhanced phase change material (NePCM) based heat sink thermal energy storage system for cooling of electronic components is investigated. Limited studies have been made that consider the CuO nanoparticle in a PCM-based heat sink thermal energy storage system for cooling of electronic components. Therefore, in the present experimental study, efforts have been made to analyze the thermal performance of different heat sink configurations integrated with NePCM. Here, copper oxide (CuO), paraffin wax, and aluminum are considered as nanoparticles, PCM, and heat sink materials, respectively. Different heat sink configurations such as heat sink with no fin (HSNF), heat sink with rectangular plate fins (HSRPF), heat sink with square pin fins (HSSPF), and heat sink with circular pin fins (HSCPF) as presented in Fig. 4.3 are studied for a fixed volume fraction of fin material. Effect of CuO nanoparticle mass fractions, heat sink configurations, and heat flux are analyzed. The performance of various heat sink configurations is analyzed for different nanoparticle concentrations (γ= 0.5-3.0) and heat flux values (q''= 1.5-3.0 kW/m^2). Results are presented in the form of transient variation of heat sink base temperature, spatial variation of the temperature inside PCM based-heat sink, the time required to attain SPT, enhancement ratio (ε), latent heating phase completion time, and thermal conductance (G).

Effect of mass fraction of CuO nanoparticle

Fig. 4.24(a-d) illustrates the transient temperature variation of NePCM-based heat sink configurations for different mass fraction of CuO (0.0, 0.5, 1.0, 3.0) at constant q''= 1.5 kW/m^2. For all the configurations (HSNF, HSCPF, HSSPF, and HSRPF), the heat sink involving pure PCM exhibits better performance compared to NePCM based heat sinks irrespective of nanoparticle concentration. However, at lower nanoparticle concentration (γ=0.5), NePCM reflects comparable thermal performance to pure PCM. Adding CuO at higher nanoparticle concentrations into the pure PCM increases the thermal conductivity. In spite of that, NePCM-based heat sinks are unable to dissipate more heat compared to pure PCM. This might be due to the various reasons like increase in thermal contact resistance between the heat sink surface and NePCM due to combined properties of PCM and nanoparticle [236], weak convection heat transfer rate in NePCM due to enormous increase in viscosity, especially at higher concentration [142], reduction in latent heat of fusion compared to pure PCM (Table 4.6). It may be noted that at 3.0 mass fractions, the viscosity of NePCM is increased by two times. Sharma et al. [143] also reported experimentally that the variation in transient temperature for unfinned and micro finned heat sinks involving PCM/NePCM is found to be negligible. In another study, Motahar et al. [151] reported that heat sink temperature increases with NePCM involving carbon nanofiber (CNF) as a nanoparticle. They also reported that adding CNF at a higher concentration causes greater heat sink temperature.

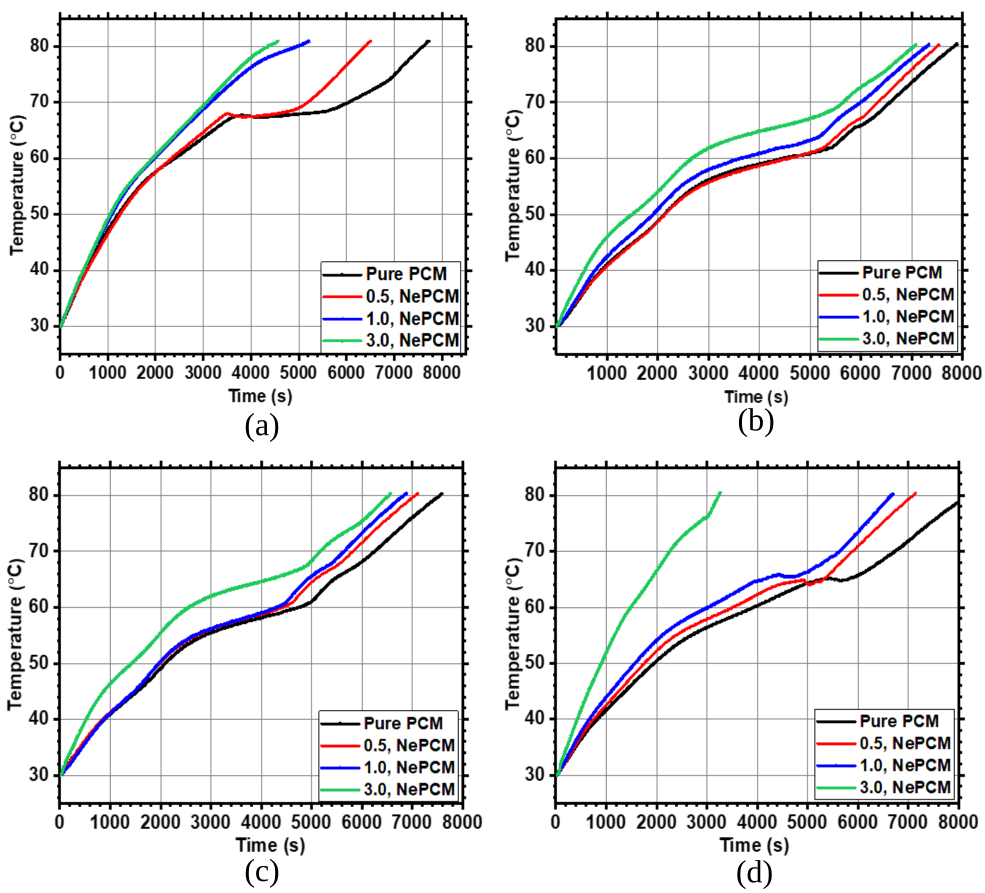

Fig. 4.24 Comparison of time-temperature distribution at different mass fractions of CuO (a) HSNF (b) HSCPF (c) HSSPF (d) HSRPF

Effect of heat flux

Transient temperature variations of various heat sinks at q''=1.5- 3.0 kW/m^2 for γ = 0.5 are presented in the Fig. 4.25(a-d). The average temperature recorded by thermocouples B_1-B_3 is used to plot the average response temperature at each heat flux value. The PCM melting rate increases with an increase in heat flux values. With the increase in input heat flux, the latent heating phase duration decreases, leading to an increase in heat sink base temperature. This is undesirable for PCM-based cooling.

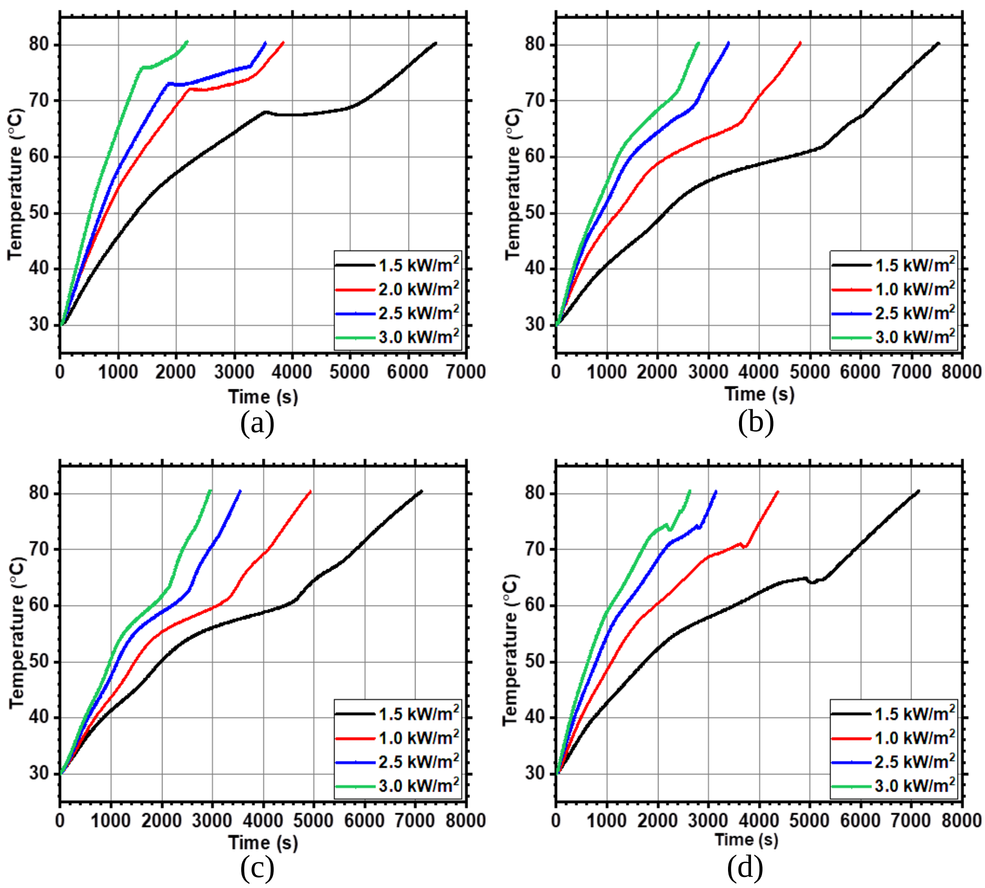

Fig. 4.25 Comparison of transient temperature distribution of heat sink at various heat fluxes (a) HSNF (b) HSCPF(c) HSSPF (d) HSRPF

During the initial period, the PCM undergoes pre sensible heating phase followed by a latent heating phase. After completion of the latent heating phase, the PCM undergoes the post sensible heating phase. For the HSNF, at q''= 1.5 kW/m^2, the sensible and latent heating phase duration is found to be 0 to 3530 s and 3530 to

5050 s, respectively, with a base temperature of 69 °C at the end of the latent heating phase. While for other heat flux values q''= 2, 2.5, and 3.0 kW/m^2, the duration of the latent heating phase continue from 2210 to 3560 s, 1920 to 3250 s, and 1410 to 1980 s, respectively, with the corresponding heat sink base temperature of 76.0, 76.8, and 78.0 °C, respectively at the end of the latent heating phase. With the completion of the latent heating phase, the post melting sensible heating phase continues, and the base temperature increases rapidly. Similar behavior can be seen in the case of other heat sink designs (Fig. 4.25 a-c). A sharp increase in temperature can be seen even in the latent heating phase for heat sink with fins. This might be due to the presence of the number of fins and pitch of the fins [127]. It should be noted that PCM-based heat sink assembly is not encouraged to operate after completion of the latent heating phase as the temperature of the base increases rapidly after post melting.

Effect of heat sink configurations

Fig. 4.26(a-b) compares the time-temperature distribution of different heat sink configurations for pure PCM and NePCM at γ=0.5 subjected to q''= 2.0 kW/m^2. At a 9% volume fraction of fins, HSSPF has the highest heat transfer efficacy in terms of lowering the base temperature, followed by HSCPF, HSRPF, and HSNF. Similarity can be seen for γ =0.5. After the latent heating phase, the difference in base temperature variation between HSCPF and HSSPF is insignificant. This reveals convection current in HSCPF filled with pure PCM is dominant and enhances the heat transfer rate. The lower base temperature in the case of HSSPF before melting may be due to the higher number of fins. With an increase in fin numbers, the heat transfer area increases, which leads to enhance the heat transfer to the PCM/NePCM and keep the base temperature at the lower limit. The surface area per unit volume of square pin fin, circular pin fin, and rectangular plate-fin heat sink is found to be 1.84, 1.27, and 0.8, respectively. Moreover, in the case of HSSPF, fins are thin and closely spaced, which also gives higher fin effectiveness. A maximum temperature reduction of 13 °C and 15 °C is observed for HSSPF filled with pure PCM and NePCM at γ=0.5. At a given volume fraction of TCE, a heat sink involving square pin fins provides better thermal performance compared to a heat sink with rectangular fins and a heat sink with circular pin fins.

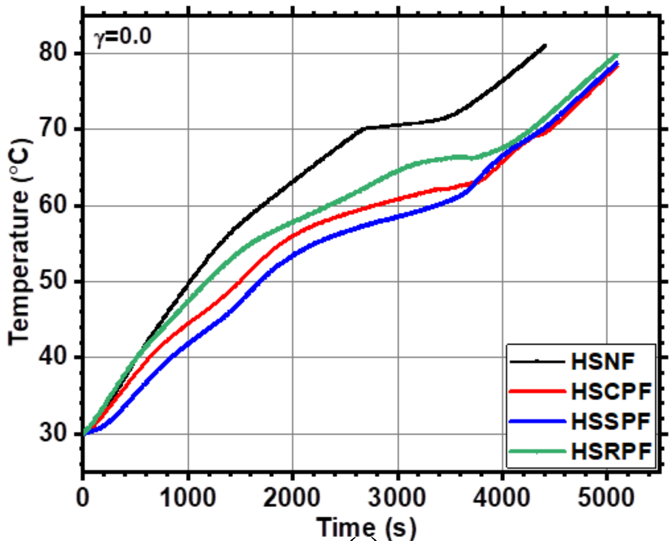

(a)

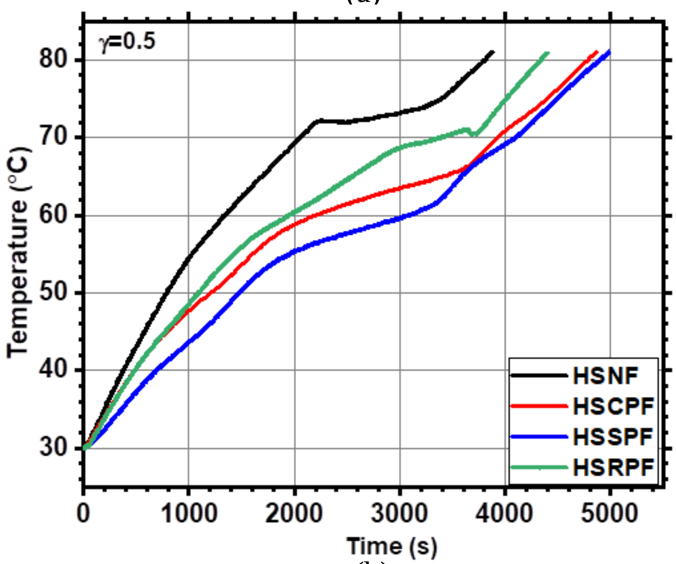

(b)

Fig. 4.26 Comparison of time temperature distribution of different heat sink configurations for 2.0 kW/m^2 (a) Pure PCM (b) γ =0.5 NePCM

Uniformity of temperature inside the heat sink

In order to investigate the temperature uniformity within the PCM-based heat sink, the spatial temperature variation for each heat sink configuration is estimated and shown in Fig. 4.27(a-d). Tests are conducted for q''=2.0 kW/m^2 and γ=0.5. The average temperature of thermocouples T_1 to T_8 recorded after 2000, 3000, and 4000 s is used for the analysis. It is observed that the temperature gradient in the case of HSNF and HSRPF are higher compared to HSCPF and HSSPF, which clearly indicates the non-uniform temperature distribution in HSNF and HSRPF. For HSCPF and HSSPF, the temperature remains almost constant as we move towards the vertical direction from the bottom surface of the heat sink. The non-uniformity in temperature can only be seen at 20 mm of height since PCM remains solid at this height even after 4000 s of heating. Uniform temperature distribution in square and circular pin fin heat sink is because of the higher number of fins, which allow the uniform melting of NePCM from all directions and maintain the uniform temperature gradient inside the heat sink.

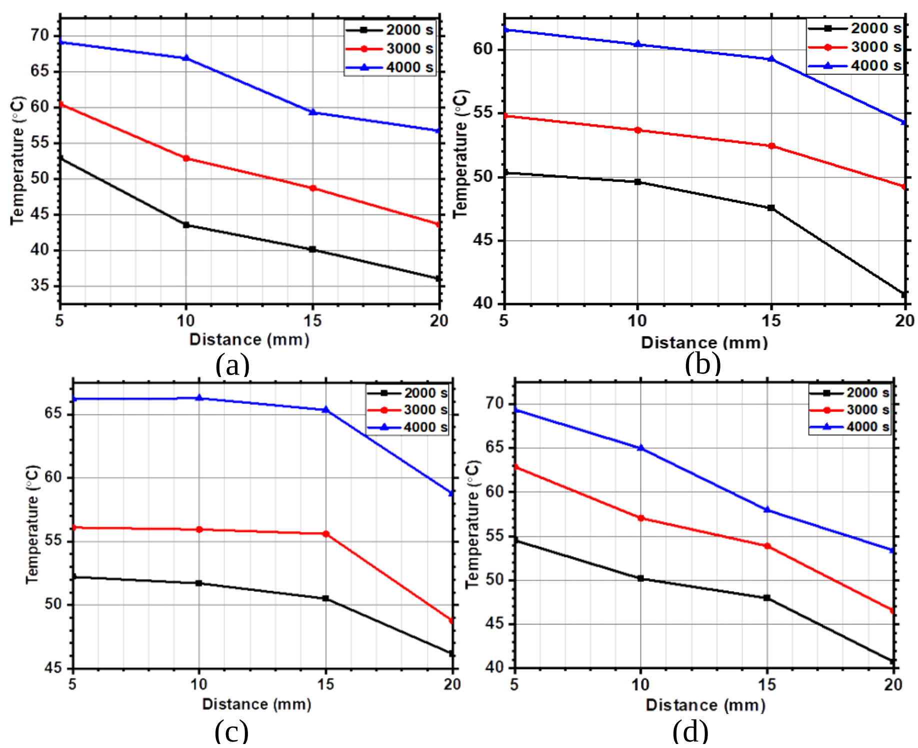

Fig. 4.27 Spatial variation of temperature inside heat sinks for $q''=2.0$ kW/m^2 (a) HSNF (b) HSCPF (c) HSSPF (d) HSRPF

Comparison of latent heating phase and thermal conductance (G)

The heat transfer performance of the PCM integrated heat sink can be studied in more detail by comparing the latent heating phase duration of various heat sink configurations. In view of this, the variation of latent heating phase duration for various heat sink configurations and varied range of input heat flux are shown in Fig. 4.28. The latent heating phase completion time of HSSPF is found to be higher compared to other configurations. A maximum latent heating phase completion time of 2930 s is obtained for HSSPF at q''= 1.5 kW/m^2. Latent heating phase duration decreases with the increase in input heat flux values. This is because of the heat storage rate increases at higher heat flux values. Higher latent heating phase completion time in the case of HSSPF is mainly due to the higher fins surface area, which allows the uniform melting of PCM from all the directions and counterbalances the low thermal conductivity of PCM.

Fig. 4.29 presents the thermal conductance (G) of various heat sink configurations filled with pure PCM for heat flux values varying between 1.5-3.0 kW/m^2. The thermal conductance values of PCM-based heat sink assembly have been estimated by using Eq. 4.11. Thermal conductance basically represents the heat transfer rate per unit temperature difference through the surface of the heat sink in a steady regime. It is found that HSSPF embedded with pure PCM gives higher thermal conductance values followed by HSCPF, HSRPF, and HSNF. The thermal conductance values increase with the increase in heat fluxes.

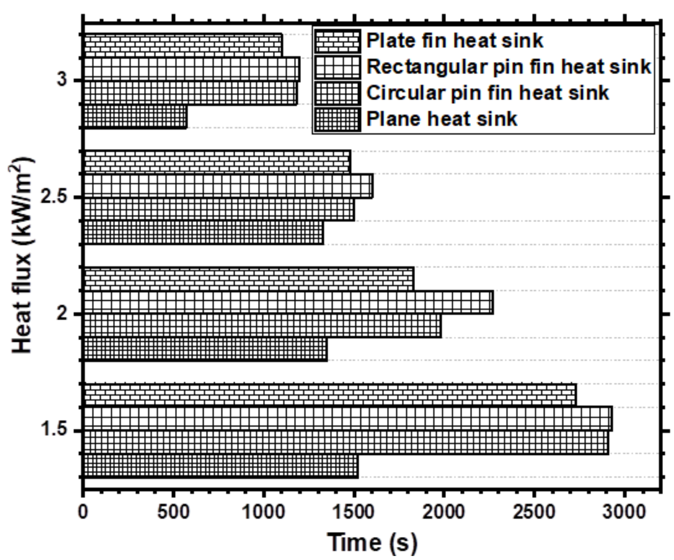

Fig. 4.28 Comparison of latent heating phase of various heat sinks

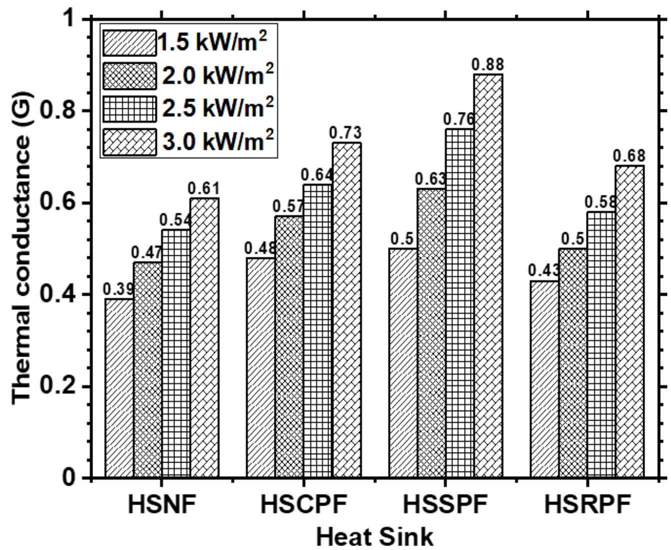

Fig. 4.29 Comparison of thermal conductance of various heat sinks

Enhancement in operating time (ε)

Fig. 4.30(a-d) presents the enhancement in operating time to attain various critical SPTs for different heat sink configurations integrated with pure PCM and γ=0.5 NePCM. Here, the temperature of 65 and 75 °C are selected as critical SPTs. It can be noticed that at q''=1.5 kW/m^2, HSCPF has the highest enhancement ratio for SPT of 65 °C. While for q''= 2.0, 2.5, and 3.0 kW/m^2, HSSPF exhibits the highest enhancement ratio. For SPT of 75 °C, at q''=1.5 kW/m^2, HSRPF exhibits the highest enhancement ratio when the heat sink is filled with pure PCM (Fig. 4.30c). While for γ=0.5 NePCM, HSCPF provides the highest enhancement ratio (Fig. 4.30d). For other heat flux values, HSSPF provides the highest enhancement ratio. The highest enhancement ratio for HSCPF and HSRPF at q''= 1.5 kW/m^2 is mainly due to the variation in latent heating phase completion time. For SPT of 65 °C and q''=1.5 kW/m^2, the maximum value of enhancement ratio is found to be 5.4, and 5.2 for γ=0.0 and γ =0.5, respectively. While for SPT of 75 °C and q''=1.5 kW/m^2, the maximum value of enhancement ratio is found to be 6.5 and 4.65 for γ =0 and γ =0.5, respectively. At lower heat flux (1.5 kW/m^2), HSRPF and HSCPF exhibit the highest value of enhancement ratio for pure PCM and NePCM. While as the heat flux value increases (q''= 2.0, 2.5, and 3.0 kW/m^2), HSSPF provides the highest enhancement ratio. An enhancement ratio of 5.0 is obtained for HSSPF at 2.0 kW/m^2 heat flux value for SPT of 65°C.

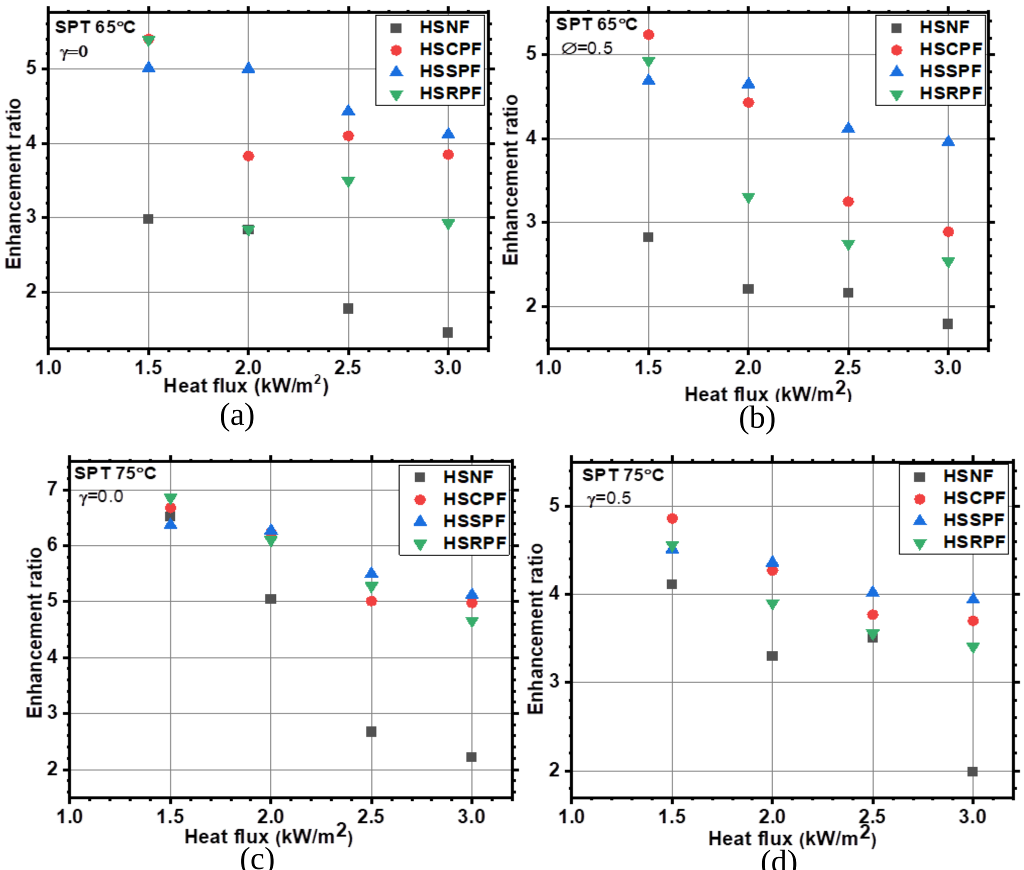

Fig. 4.30 Enhancement ratio at different heat flux (a) SPT 65 °C, γ =0.0 (b) SPT 65 °C, γ =0.5 (c) SPT 75 °C, γ =0.0 (d) SPT 75 °C, γ =0.5

4.6.3 Investigation of foam-PCM composite heat sink and comparison with PCM-based finned heat sink

Here, tests are conducted to investigate the thermal performance of metallic and non-metallic foams embedded with phase change material (PCM) for electronic cooling applications. Highly thermal conductive carbon foam (non-metallic) and copper foam (metallic) are used as thermal conductivity enhancers (TCEs) to outweigh the low thermal conductivity of PCM. Performance of foam-PCM composite heat sinks is compared with PCM-based heat sinks studied in section 4.6.2. Considering the operating condition of several handheld electronic devices, very few studies have been accomplished using high thermal conductivity foam impregnated with PCM. Therefore in this study, copper foam (CoF) and high thermal conductive carbon foam (CF) impregnated with paraffin wax as PCM is investigated for thermal management of electronic components. Effect of heat flux, CF as TCE volume fraction, and heat sink configurations are studied. Performance of heat sink with and without PCM for no fin heat sink is also studied. The performance of different heat sink designs is first compared for a fixed TCE during the PCM charging and discharging. The amount of TCE in CF-PCM based heat sink is then varied from 25 to 5% to estimate the effect of CF as TCEs in PCM-based heat sink.

Comparison of heat sink performance with and without PCM

Here, it is assumed that the base temperature of the heat sink mimics the hot surface of electronic components; in such a case, one needs to keep the base temperature lower than the critical limit for efficient thermal management. The lower temperature of the heat sink base delays the overheating and enhances the lifetime of electronic components. The comparison between heat sink performance with and without PCM at q''=1.5 kW/m^2 is depicted in Fig. 4.31(a-b). The average temperatures measured by thermocouples attached on the bottom surface of the heat sink are utilized to represent the transient temperature variation of the heat sink base. The heat sink without PCM shows a sharp rise in the base temperature and can affect the performance of electronic components. The heating and cooling period in the case of heat sink without PCM can be described as sensible heating and sensible cooling, respectively. While, for PCM-based heat sink, the melting and solidification process can be divided into several regions. These include sensible heating (Region 1; 0-50 min), latent heating (region 2; 50-69 min) and sensible heating post melting (Region 3; 69-110 min); similar regions (Region 4, Region 5, and Region 6) are observed in solidification process in the reverse order. It may be noted that temperature during sensible heating (Region 1 and Region 3) increases rapidly, while in the latent heating stage, the temperature remains nearly constant (stage 2). Here, during solidification, natural convection cooling is considered, and insulations except for the bottom surface of the heat sink are removed during cooling. To reach 80 °C, heat sink without PCM and heat sink with PCM takes 25 min and 110 min, respectively. This reveals that PCM integrated heat sink can protect electronic devices from the high heat flux shock. It is worth noting that stretching the latent heating region is the key parameter for increasing the effectiveness of a PCM-based heat sink. During the cooling process, to attain 35 °C from 80 °C, heat sink with no PCM and heat sink with PCM takes 85 and 250 min, respectively; cooling occurs faster in case of the heat sink with no PCM. It may be noted that for real application cooling rate of PCM integrated heat sink should be faster for efficient thermal management.

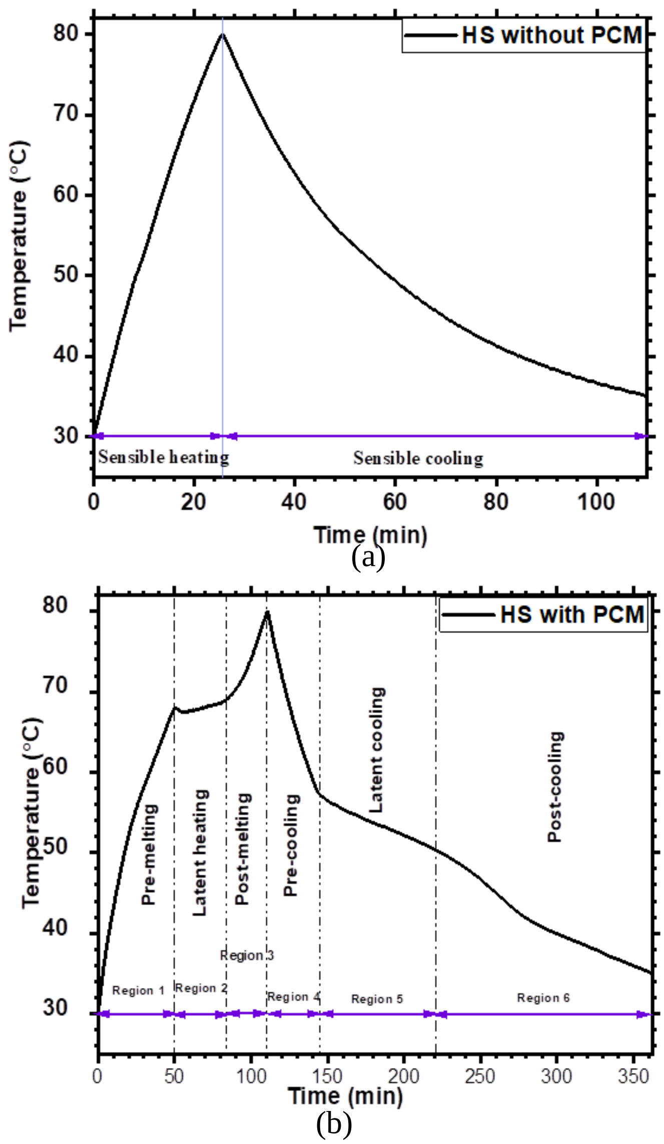

Fig. 4.31 Variation of heat sink base temperature (a) Without PCM (b) With PCM

Effect of various heat sink configurations

Fig. 4.32 depicts the variation of heat sink base temperature for various PCM-based heat sink configurations at q''=1.5 kW/m^2 and 9% TCE volume fraction during both the charging and discharging process. The HSNF with PCM exhibits a sharp rise in the base temperature, while the PCM-based heat sinks with fins and metallic/non-metallic foams exhibit a slower rise in the base temperature; this may be due to an increase in effective thermal conductivity of the PCM system. The performance of HSNF and HSRPF is found to be lower during the charging and discharging process, respectively, compared to other configurations. The heat sink with CF-PCM composite keeps the base temperature lower during charging and also performs satisfactory during discharging process. After heating up to 82 min, the base temperature of CF-PCM composite heat sink, HSCPF, HSRPF, heat sink with CoF-PCM composite, HSSPF, and HSNF attain 61.9, 65.4, 66.12, 66.8, 67.5, and 68.8 °C, respectively. After completing the charging process, the heat sink with CF-PCM composite exhibits an 8.54, 7.83, and 3.34% reduction in base temperature compared to HSSPF, CoF-PCM composite, and HSNF, respectively. During the discharging process, HSSPF, HSCPF, CF-PCM composite, and HSRPF take 216.5, 223.3, 238.1, and 272.3 min, respectively, to reach 35 °C temperature. The finned heat sink keeps the base temperature lower compared to the CoF-PCM composite heat sink. This may be due to the higher PCM melting rate in the case of finned heat sink because of the higher thermal conductivity of aluminum (218 W/m-K) nearly 20 times than copper foam (10.1 W/m-K). The heat transfer is mainly dominated by two factors, namely, conduction in solid PCM and convection at the solid-liquid interface and liquid PCM. Early change in the slope of transient temperature curves is observed in CF-PCM composite and finned-based heat sinks; this may be due to strong conduction heat transfer, which leads to faster melting and maintains lower base temperature. The study shows that the heat sink with CF-PCM composite has not only tremendous potential to enhance the thermal performance but also reduce the significant weight of the system. The liquid PCM remains confined in CF pores, suppressing natural convection and increasing the melting rate, resulting in conduction-dominated heat transfer through the CF-PCM composite. Hence, lower base temperature and better heat transfer performance are achieved for the CF-PCM composite heat sink. Further studies based on the heat sink with CF-PCM composite are illustrated in the subsequent section.

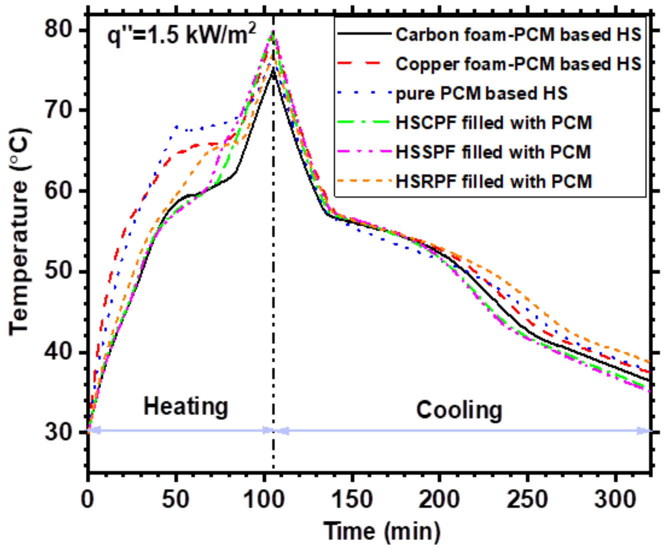

Fig. 4.32 Comparison of various heat sink configurations at q''=1.5 kW/m^2

Effect of CF as TCE at various volume fractions

Fig. 4.33 depicts the thermal performance of heat sink with CF-PCM composite for various volume fractions of TCE (ξ= 5, 9, 15, and 25 %) during the charging and discharging process at q''= 2.0 kW/m^2. To attain the required TCEs volume fraction of CF, various holes are designed and drilled in the CF block [237-238]. It can be noticed from Fig. 4.33 that there is a decline in maximum base temperature with the decrease in ξ. A maximum 17.47% reduction in base temperature can be noticed for 5% of TCE compared to 25% TCE. While, CF with 9 and 15% TCE shows a 13.66 and 9.77% reduction in base temperature, respectively, at the end of the charging process. The enhancement in thermal performance with the decrease in the amount of TCE is attributed to the increase in volume fraction of paraffin wax which increases the latent heat phase duration and keeps the base temperature lower for a longer duration. However, an increase in the amount of PCM also extends the latent heating period during the discharging process and takes more time to solidify. The heat sink with 25, 15, and 9% of TCE takes nearly 221.6 min to attain 35 °C temperature during cooling, while after 221.6 min of cooling, heat sink with 5% TCE reaches to 39.5 °C temperature. Also, heat sink with higher TCE exhibits more conductive material, which supports quicker heat transfer, hence taking a lower time to cool. This indicates that there should be an optimum volume fraction of TCE to augment the thermal performance of PCM-based heat sink assembly.

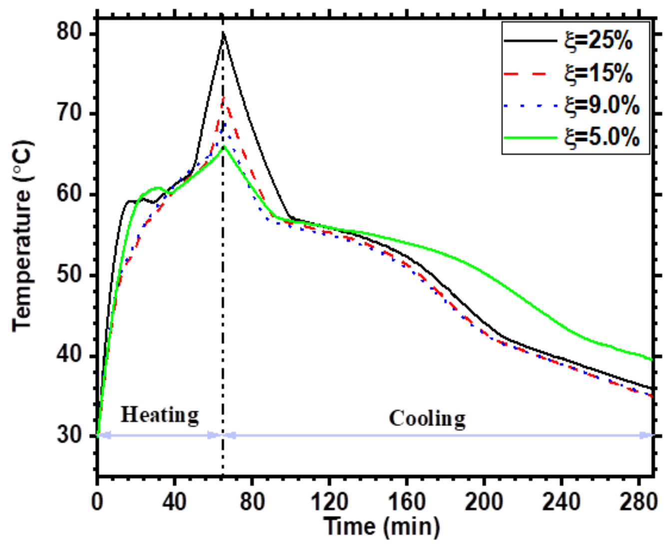

Fig. 4.33 Effect of CF as TCEs on variation of heat sink base temperature

Effect of heat flux

Fig. 4.34(a-b) shows the effect on the base temperature of heat sink for various q''=1.5, 2.0, and 2.5 kW/m^2 for two cases: CF-PCM composite and CoF-PCM composite heat sink with ξ= 9%. The solid-liquid phase change time is found to be 34.5, 22.0, and 17.5 min for q''=1.5, 2.0, and 2.5 kW/m^2, respectively, for the heat sink with CoF-PCM composite; the corresponding maximum temperatures are found to be 66.98, 69.59, and 71.79 °C, respectively at the end of solid-liquid phase change. In addition, the duration of solid-liquid phase change for the heat sink with CF-PCM composite is found to be 36.17, 23.33, 16.33 min for q''=1.5, 2.0, and 2.5 kW/m^2, respectively, while the corresponding maximum temperatures after the completion of the melting process are found to be 62.32, 64.9, and 65.09 °C, respectively. With increasing input heat flux values, the length of the solid-liquid phase transition appears to be shorter.

Before PCM melting, conduction dominates the heat transfer process; however, natural convection takes over once PCM melting begins. PCM attains the melting temperature at higher heat flux with short time duration and melts faster due to intensive natural convention [239].

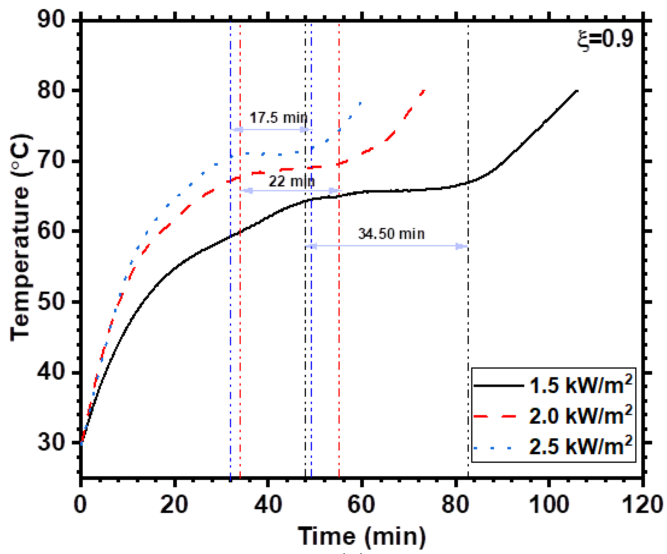

(a)

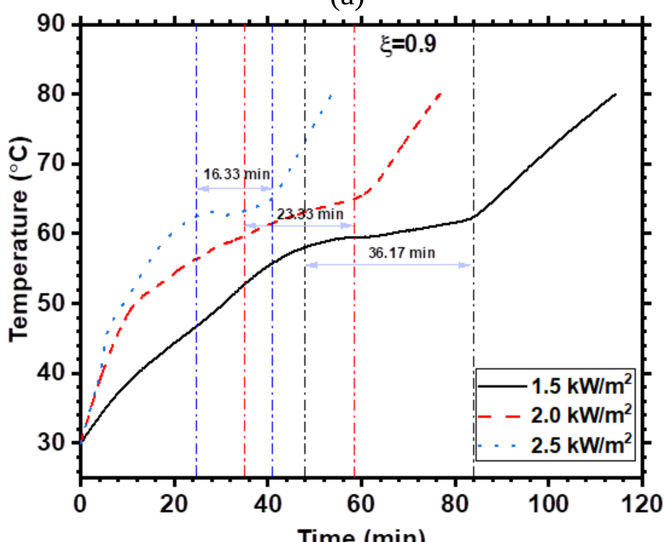

(b)

Fig. 4.34 Effect of heat flux (a) Copper foam-PCM composite (b) Carbon foam-PCM composite

Study of set point temperature

Here, four different SPTs are considered for the analysis. The performance is evaluated for both the charging and discharging period. Fig. 4.35 presents the duration to attain the critical SPT for various heat sink designs at q''=1.5 kW/m^2.

The critical duration of HSNF filled with PCM is lower among all the heat sink configurations. In contrast, the CF-PCM composite heat sink shows the highest critical duration for all the SPTs. HSNF filled with PCM takes only 33.6 min to reach 60 °C SPT while CF-PCM composite heat sink exhibits critical duration nearly two times (66.2 min) to reach 60 °C SPT. On the other hand, HSCPF and HSSPF acquire the same critical duration (66.0 min.), and HSRPF and CoF-PCM composite heat sink exhibit 52.0 and 34.1 min, respectively, for 65 °C SPT. It should be noted that as the critical SPT is increased to 80 °C, the difference between the critical duration of various heat sink configuration decreases. However, heat sink with CF-PCM composite still shows the highest critical duration. Maximum enhancement ratio in operating time for SPT of 65 °C obtained using Eq. 4.9 is found to be 5.5 for heat sink with CF-PCM composite at q''=1.5 kW/m^2. While HSNF filled with PCM shows a minimum enhancement ratio of 2.73 at the same heat flux and SPT values. In addition, for 75 °C SPT at a 1.5 kW/m^2 heat flux value, the maximum and minimum enhancement ratio of 4.8 and 4.4 is obtained for heat sink with CF-PCM composite and HSNF filled with PCM, respectively.

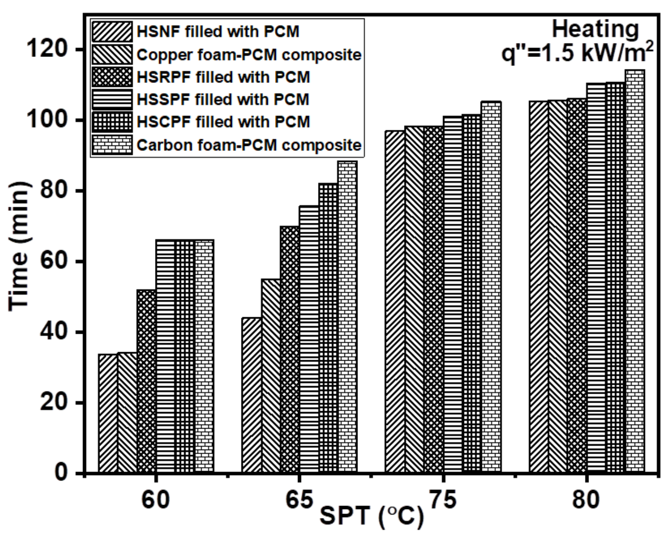

Fig. 4.35 Time to attain SPTs for various heat sink configurations during the charging period

For the practical application of a PCM-based thermal management system, investigation of cooling performance is also necessary. Fig. 4.36 presents the critical duration to reach the critical SPT for various heat sink configurations during cooling. During the cooling period, heat input is stopped, and insulations are removed from all the sides except the bottom surface of the heat sink assembly. The heat transfer from liquid PCM occurs via conduction and natural convection mode. Combined convection and conduction heat transfer occur until PCM reaches crystallization temperature. However, convection dominates the heat transfer in liquid PCM. Once the PCM attain crystallization temperature, only conduction heat transfer occurs. The heat transfer occurs from hot PCM to heat sink through conduction and then to ambient via natural convection. To investigate the cooling efficacy of each heat sink configuration, two SPTs are considered for the analysis. The solidification time depicted in Fig. 4.36 is for heat flux of 1.5 kW/m^2. The time required for discharging process is quite high as compared to the charging phase. Unlike the charging process, HSSPF integrated with PCM is found to be more effective for SPT of 45 and 35 °C. On the other hand, HSRPF filled with PCM is found to be the least effective in terms of cooling efficiency. HSRPF filled with PCM takes approximately 55 min. more time to reach 35 °C than HSSPF filled with PCM. Considering SPT of 45 and 35 °C, it can be observed that CF-PCM composite heat sink shows higher discharging ability compared to CoF-PCM composite heat sink, HSNF filled with PCM, and HSRPF filled with PCM. HSSPF and HSCPF filled with PCM show the highest cooling efficacy because of higher surface area density, the higher thermal conductivity of fin material, and higher fin effectiveness. From the above analysis, it can be observed that the heat sink behavior is found to be different for the charging and discharging process.

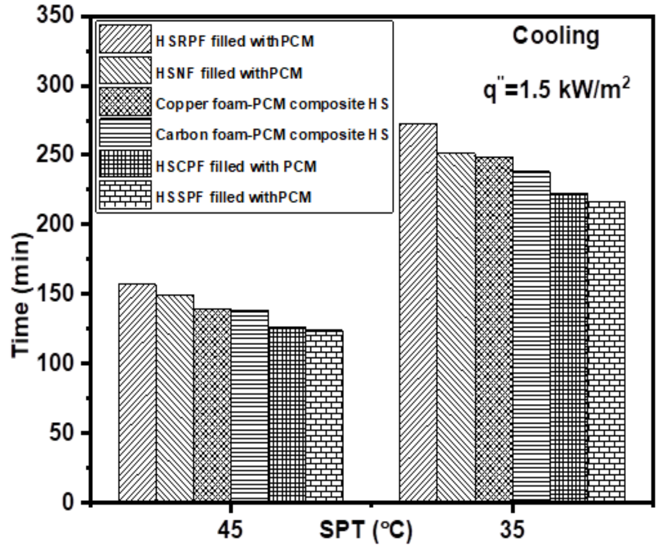

Fig. 4.36 Time to attain SPT for various heat sink configurations during discharging period

4.7 Concluding Remarks

Here, tests are conducted to analyze the thermal performance of various PCM-based heat sink configurations. Paraffin wax with melting temperature range 58-62 °C is utilized as PCM. The heat sinks include various thermal conductivity enhancers (TCEs) such as cross plate fins, parallel plate fins, pin fins, and metallic and non-metallic foams. In addition, nano-enhanced PCM is used to evaluate the thermal performance of the heat sink. The effect of fin types, fin arrangements, foam types, heat flux values, the volume fraction of TCE, volume fraction of PCM, nanoparticle concentration on the thermal performance is analyzed in this chapter.

Initially, tests are performed with a cross plate fin heat sink forming various cavities (1, 4, 9, 16, 25, and 36) for a fixed thermal capacity. The amount of PCM is maintained constant in each heat sink design. Results are presented in the form of transient temperature variation of the heat sink base, the time required to reach SPT, enhancement ratio (ε), thermal capacity during pre and post melting (δ), and thermal conductance (G). The heat transfer performance of the system is found to increase with the increase in the number of cavities. The heat sink with 36 cavities exhibits the maximum 19.5% reduction in temperature at q''= 2.0 kW/m^2 and shows a maximum enhancement ratio of 6.5 for 65 °C SPT. The heat sink with 36 cavities exhibits the maximum heat capacity values of 1.63 during post-sensible heating for q''= 2.0 kW/m^2. The heat sink with 36 cavities exhibits the best thermal performance among all the cross plate fin heat sink designs. The study suggests that solidification time is nearly twice compared to melting time; forced convection cooling needs to be applied to enhance the cooling rate of PCM.

In the next problem, the thermal performance of various heat sinks, namely HSNF, HSCPF, HSSPF, and HSRPF embedded with pure PCM and CuO-based NePCM, is studied for a fixed volume fraction of fins and different nanoparticle concentrations (γ= 0.5-3.0). Also, the effect of CuO nanoparticles on thermophysical properties of PCM such as latent heat, thermal conductivity, specific heat, viscosity, and density are analyzed. For γ= 3.0, thermal conductivity and viscosity of NePCM are found to increase by 150% and 100%, respectively. The HSSPF involving PCM/NePCM exhibits better thermal performance compared to other heat sink configurations. The maximum reduction in temperature is found to be 13°C and 15°C for HSSPF involving PCM and NePCM (γ= 0.5), respectively. The highest enhancement ratio of 5.0 is obtained for HSSPF at q''= 2.0 kW/m^2 for SPT of 65°C. The addition of CuO nanoparticles beyond γ =0.5 decreases the heat sink performance considerably.

In the last problem, tests are performed to study the thermal performance of metallic and non-metallic foams embedded with phase change material (PCM) for electronic cooling applications. Highly thermal conductive carbon foam (non-metallic) and copper foam (metallic) are used as thermal conductivity enhancers (TCE). The effect of TCE volume fraction and heat flux value on the performance of PCM integrated heat sink is studied experimentally. Results indicate that the heat sink with carbon foam (CF)-PCM composite can be utilized for the effective cooling of electronic components. A maximum enhancement ratio in operating time of 5.5 is achieved for heat sink with CF-PCM composite at q''=1.5 kW/m^2. The heat sink with a square pin fin (HSSPF) exhibits 13.7% less time to attain 35 °C SPT compared to HSNF with PCM during the discharging process. In the case of PCM-based heat sink with CF, the reduction in base temperature is found to be 17.47% for 5% TCE compared to 25% TCE.

Present experimental study reveals the thermal performance of PCM-based heat sink configurations involving various fin types, fin arrangements, foam types, heat flux values, the volume fraction of TCE, volume fraction of PCM, and nanoparticle concentration; the results can be useful for the design of heat sink for thermal management applications.

Chapter 5

Summary and conclusions

The present dissertations reports the various issues such as optimal selection of PCM, use of PCM, and estimate the thermal performance in various heat sink configurations through theoretical and experimental investigation. The present study is aimed to analyze the thermal performance evaluation of PCM-based heat sinks as applicable to thermal management of electronic components.

Initially, a theoretical model based on a multi attribute decision making (MADM) approach is employed to rank and select the best PCM for thermal management of electronic devices. Different types of PCMs (organic, inorganic, and eutectics) and the important attributes applicable for thermal management are pre-screened during the analysis. Based on the phase transition temperature, thirty PCMs with melting temperature ranges varying between 28-58 °C and eleven attributes are considered for the analysis. The weight of the attributes is obtained by using analytic hierarchy process (AHP) methodology. Various MADM techniques such as Technique for Order of Preference by Similarity to Ideal Solution (TOPSIS), fuzzy TOPSIS, and VIKOR method are employed to select the best PCM for the efficient design of thermal management module. Next, a three-dimensional numerical model has been proposed to investigate the thermal performance of PCM-based cross plate fin heat sink with a different number of cavities (1, 4, 9, 16, 25, and 36). The thickness of fins and walls is varied to ensure the constant value of mass and thermal capacity of the heat sink module. The performance of various heat sink configurations is evaluated based on the transient temperature variation of the heat sink base, PCM melt fraction, average Nusselt number, and energy absorbed by PCM during both latent and sensible heat stages.

In addition, efforts have been made to study the thermal performance of various heat sink configurations through experimental investigation. The test facility has been developed to analyze the thermal performance of various heat sink configurations. In the first study, heat sinks with cross plate fin arrangement involving various cavities, the different volume fraction of PCM, and various input heat flux values are considered for the analysis. Furthermore, efforts have been made to analyze the thermal performance of different heat sink configurations such as heat sink with no fin (HSNF), heat sink with rectangular plate fins (HSRPF), heat sink with square pin fins (HSSPF), and heat sink with circular pin fins (HSCPF) integrated with PCM/NePCM for a varied range of nanoparticle concentration and different heat loads. In addition, tests are conducted to analyze the thermal performance of various heat sink configurations such as PCM-based heat sinks with copper foam, carbon foam, no fins, circular pin fins, rectangular pin fins, and rectangular plate fins for a wide range of heat flux values and different TCE value of CF. The important findings obtained from the present studies are illustrated in subsequent sections.

5.1 Selection of phase change material for thermal management of electronic devices

A multi-attribute decision making model is proposed for the selection of suitable PCM for thermal management of electronic devices. Three different evaluation models, TOPSIS, fuzzy TOPSIS, and VIKOR are employed to select the best PCM. The AHP method is employed to find the weight of the attributes. The present study considers thirty PCMs (organic and inorganic) and eleven attributes (qualitative and quantitative) for the analysis. The important outcomes obtained from the present analysis are elaborated below.

- Based on the AHP methodology, various attributes such as latent heat, thermal conductivity, density, and incongruent melting are found to be the most important attributes in a thermal management system.
- The consistency ratio is found to be 0.095; therefore, the weight of the attributes obtained from AHP is considered to be logical and consistent.
- The top five alternatives obtained from the TOPSIS method for the thermal management of electronics are RT 44 HC, RT 35, Paraffin wax, n-eicosane, and A-37. While, the top five alternatives obtained from the

fuzzy TOPSIS method include paraffin wax, RT 44 HC, A 37, n- eicosane, and A50.

- VIKOR method estimated RT 44 HC n-octadecene, paraffin wax, and n-eicosane as the top alternatives for PCM-based thermal management of electronic components.
- Based on the analysis, it is found that all the top selected PCMs for thermal management applications belong to the organic category. This may be due to the favorable thermophysical and chemical properties of organic PCM.

5.2 Numerical investigation on the thermal performance of PCM-based heat sink with various fin configurations

This section considers the numerical investigation of various heat sink configurations for a varied range of input heat flux values. Two different problems are considered, and the details are elaborated below.

5.2.1 Numerical modeling to estimate the thermal performance of PCM-based heat sink with cross plate fins

Melting phenomena of phase change material (PCM) in a system of cross plate fin heat sink for passive cooling of electronic devices has been numerically investigated. Six heat sink configurations are investigated involving with and without cross fins. Different number of cavities (1, 4, 9, 16, 25, and 36) formed by cross plate fins arrangement are studied. The mass and thermal capacity of each heat sink configuration is kept as constant. The Boussinesq approximation is employed to evaluate the natural convection during the melting of PCM. Based on the analysis following conclusions are drawn.

- Melt fraction contours reveal that melting of PCM in a cross plate fin heat sink with more number of fins starts later in comparison to a heat sink with less number of fins. Melting time is found to be reduced with the increase in the number of fins.

- An increase in the input heat flux value reduces the latent heating phase change duration and increases the rate of melting of PCM. With the increase in the heat flux values from 1.0 to 2.0 kW/m^2, the melting time of the PCM is reduced by approximately 46.5% in thirty-six cavities heat sink.
- From the variation of Nusselt number with dimensionless time τ, the heat transfer in PCM can be categorized into three stages such as heat conduction, strong convection, and weak convection. In the second stage, the convection current is strengthened, which leads to higher heat transfer.
- The maximum 10 °C of temperature reduction is achieved in the case of twenty-five cavities heat sink compared to the heat sink with no fin.
- The melting time in PCM-based heat sink assembly with twenty-five cavities is reduced by 21.33 % compared to the single cavity heat sink.
- PCM with a sharp melting point temperature can keep the base temperature of the heat sink lower for a longer duration.

5.2.2 Numerical modeling of PCM based-heat sink with hollow fins as TCE

In this study, heat transfer performance of different heat sink configurations such as heat sink with no fins, heat sink with circular and square hollow fins integrated with paraffin wax as PCM is investigated numerically. Numerical simulation has been carried with a different range of heat flux values (q''= 1.0, 1.5, and 2.0 kW/m^2) for a nearly fixed amount of PCM. Thermal performance parameters such as PCM melt fraction, maximum velocity, and variation of base temperature of various heat sinks have been investigated in the investigation. Important conclusions drawn from this study are as follows:

- An increase in heat flux values results in an increased heat sink temperature, the magnitude of maximum velocity, and the melting rate of PCM.

- An increase in the surface area density improves the thermal performance of the heat sink by mitigating its base temperature. Maximum temperature reduction of 4.19, 5.19, and 5.74% are achieved by heat sink with square hollow pin fins at 1.0, 1.5, and 2.0 kW/m^2, respectively.
- Maximum velocity is found to be higher for no fin heat sink as there were no fins, so PCM motion is stronger, and no short obstruction of solid-liquid interface motion is encountered. The maximum velocity of 2.4, 0.73, and 0.65 mm/s is estimated for no fin, circular hollow fin, and square hollow fin heat sink, respectively, at 2.0 kW/m^2.
- The stretching of operating time to attain SPT of 75 °C is found to be 77.74% and 75.2% more for heat sinks with square and circular hollow fins, respectively, compared to the heat sink with no fin (q''= 1.0 kW/m^2).

5.3 Experimental investigation of PCM-based heat sink for thermal management of electronic devices

This section considers the thermal performance analysis of various heat sink configurations through experimental investigation. The investigation considers various heat sink configurations, different input heat flux values, and different PCM volume fractions in the analysis. This is divided into three sections; the details are elaborated below.

5.3.1 Thermal performance of PCM-based heat sinks with cross plate fins for cooling of electronic components

Here, tests are performed to study the thermal performance of various PCM embedded heat sinks involving various cavities (1, 4, 9, 16, 25, and 36) formed by rectangular cross plate fins for a wide range of heat flux q''= 1.5-2.5 kW/m^2. The amount of PCM is maintained constant in each heat sink design. Results are presented in the form of transient temperature variation of the heat sink base, the time required to reach set point temperature (SPT), enhancement ratio (ε), thermal capacity during pre and post melting (δ), and thermal conductance (G). The conclusions obtained from this experimental study are as follows:

- PCM-based heat sink augments the operating time resulting in a lower heat sink base temperature compared to an empty heat sink. An increase in PCM volume fractions and number of fins decreases the heat sink temperature.
- For the heat sink with 36 cavities, the maximum temperature drop is found to be 19 and 19.5% compared to the heat sink with one cavity at q''= 1.5 and 2.0 kW/m^2, respectively. While the heat sink with 25 cavities exhibits a 17.2% reduction in base temperature compared to a single cavity heat sink at 1.5 and 2.0 kW/m^2, respectively.
- The time required to reach critical SPT of 65 and 75 °C is highest for the heat sink with 36 cavities, followed by the heat sink with 25 cavities. The stretching in operating time is found to be higher for heat sink with 36 cavities to reach critical SPT of 65 and 75 °C at 1.5 kW/m^2.
- A maximum enhancement ratio of 6.5 is achieved by heat sink with 36 cavities at q''=1.5 kW/m^2 for SPT of 65 °C. The enhancement ratio is found to decrease with the increase in the amount of heat flux and SPT value.
- The heat sink with 36 cavities exhibits the highest heat capacity and thermal conductance values. The maximum heat capacity value of 1.63 and 1.28 kJ/K is found to be in post-sensible heating for 2.0 and 2.5 kW/m^2, respectively for the heat sink with 36 cavities.
- The time required to melt the PCM is much higher compared to the solidification time of PCM. Solidification time is nearly twice than the melting time. Therefore, forced convection cooling needs to be applied to enhance the cooling rate of PCM.

5.3.2 Thermal performance of heat sink using NePCM for cooling of electronic components

Here, the thermal performance of various heat sinks, namely HSNF, HSCPF, HSSPF, and HSRPF embedded with pure PCM and CuO-based NePCM, is studied for a fixed volume fraction of fins and different nanoparticle concentrations (γ=0.5-3.0) and different input heat flux values (1.5-3.0 kW/m^2). Also, the effect of CuO nanoparticles on thermophysical properties of PCM such as latent heat, thermal conductivity, specific heat, viscosity, and density are analyzed. The important conclusions drawn from the study are presented below.

- The addition of copper oxide nanoparticles inside the pure PCM reduces the value of latent heat of fusion while increasing the thermal conductivity and viscosity. The maximum reduction in latent heat of fusion is found to be 24.75% at γ=3.0. While the maximum enhancement in thermal conductivity and viscosity is found to be 150% and 100%, respectively.
- Based on various parameters such as duration of latent heat phase completion time, thermal conductance, enhancement ratio, and temperature uniformity, HSSPF is found to be superior compared to other heat sink configurations. However, as the melting of PCM/NePCM completes, the difference in temperature variation for HSSPF and HSCPF is insignificant.
- The maximum temperature reduction of 13 °C and 15 °C is observed for HSSPF filled with pure PCM and NePCM at γ= 0.5. At higher heat flux values highest enhancement ratio is obtained for HSSPF. An enhancement ratio of 5.0 is obtained at 2.0 kW/m^2 of heat flux value for SPT of 65°C.
- The addition of CuO nanoparticles beyond γ=0.5 decreases the heat sink performance drastically since heat sink base temperature increases sharply due to an enormous increase in viscosity.

5.3.3 Investigation of foam-PCM composite heat sink and comparison with PCM-based finned heat sink

In this study, tests are performed to study the thermal performance of metallic and non-metallic foams embedded with phase change material (PCM) for electronic cooling applications. Highly thermal conductive carbon foam (non-metallic) and copper foam (metallic) are used as thermal conductivity enhancers (TCE). The effect of TCE volume fraction (5-25%) and various heat flux values (1.5-2.5 kW/m^2) on the performance of PCM integrated heat sink is studied through experimental investigation. The important findings from this study are as follow:

- During the charging process heat sink with CF-PCM composite exhibits better performance for all SPT and heat flux values. HSNF integrated with PCM depicts poor performance among all heat sink configurations for SPT of 65 °C, and heat sink with CoF-PCM composite gives poor performance for SPT of 75 °C for q''=1.5 kW/m^2.
- During discharging process, HSSPF integrated with PCM depicts the best thermal performance followed by HSCPF and heat sink with CF-PCM composite. HSSPF exhibits 13.7% less time to reach SPT of 35 °C in comparison to HSNF filled with PCM.
- A maximum enhancement ratio in operating times of 5.5 is achieved for heat sink with CF-PCM composite at q''=1.5 kW/m^2. While minimum enhancement ratio of 2.73 times is obtained for HSNF filled with PCM at the same heat flux values.
- Effect of CF as TCE volume fraction reveals that decrease in volume fraction of TCE reduces the base temperature. A Maximum 17.47% reduction in base temperature is observed for 5% of TCE compared to 25% TCE of CF.

5.4 Recommendations for further investigation

Due to various advantages such as quasi-isothermal phase change process, high latent heat absorption capacity, phase change materials (PCMs) are widely used for different engineering and industrial applications. The PCM-based heat sink can be utilized for cooling of next-generation electronic devices. It may be noted that very low thermal conductivity is the major challenge of PCM systems for their possible use in different applications. Therefore, high thermal conductivity materials, such as fins, nanoparticles and, metallic/non-metallic foams, are incorporated into the PCM-based heat sink system to improve the thermal conductivity. The results obtained in this research investigation can provide crucial information for the design of heat sinks and further advancement in knowledge in this research area. In view of this, potential directions for future research are outlined below.

- Theoretical models need to be proposed to predict the temperature distribution, solid-liquid interface position, and thermal performance of cascaded PCM-based thermal energy storage devices.
- Significant effort should be made to develop lightweight PCM-based thermal management systems; subsequently, the thermal performance needs to be investigated both through experimental and numerical investigation.
- The study may be useful to propose novel design heat sinks that include the variable cross-section metallic fins as TCE for improving the thermal performance with a reduction in weight of the system and ease of manufacturing.
- The present experimental set-up can be used to study the effect of constant as well as variable thermal loading conditions on the performance of PCM-integrated heat sink to characterize the actual heating conditions of electronic components.
- To counter the leakage associated with solid-liquid PCM, one can employ a solid-solid form stable PCM-based heat sink for thermal management of handheld electronic devices. Present experimental set-up can be employed to perform the experimental study for form stable-PCM based heat sink and characterize the heat transfer.
- The effect of hybrid nanoparticles and the combination of fins, metal foams, and hybrid nanoparticles should be investigated through experimental investigation.
- As the solidification time of PCM is nearly twice the melting time so hybrid PCM-fan based cooling should be investigated during the solidification process.

References

[1] J. D. Plumer, M. Deal, and P. D. Griffin, Silicon VLSI Technology: Fundamentals, Practice, and Modeling. Pearson, Prentice Hall (2000).

[2] M. M. Waldrop, More than Moore. Nature News 530, 145-147 (2016).

[3] U.S. Military, Reliability Prediction of Electronic Equipment, (1992) (MIL-HDBK-217F Notice 1).

[4] L.T.Yeh, "Review of heat transfer technologies in electronic equipment" *J Elect Pack* 117, 333-339, 1995.

[5] A. Arshad, M. Jabbal, and Y. Yan, "Thermal Performance of PCM-based Heat Sink with Partially Filled Copper Oxide Coated Metal-foam for Thermal Management of Microelectronics" *19th IEEE Intersociety Conference on Thermal and Thermomechanical Phenomena in Electronic Systems (ITherm)*, 2020, Orlando, FL, USA,

[6] S. Arora, "Selection of thermal management system for modular battery packs of electric vehicles: A review of existing and emerging technologies" *J Power Sourc* 400, 621-640, 2018.

[7] SimScale, Passive Cooling vs Active Cooling. Assessed on March 1, 2021, from https://www.simscale.com/blog/2017/01/active-and-passive-cooling/.

[8] Electronic Products, assessed on February 28, 2021, from https://www.electronicproducts.com/fundamentals-of-active-vs-passive-thermal-management/#

[9] A. Pinto, Development of paraffin wax as a phase change material for thermal management in electronic systems, Master's thesis, The University of Texas at Arlington, 2016.

[10] Y. Cai, Y. Wang, D. Liu, and F.Y. Zhao, "Thermoelectric cooling technology applied in the field of electronic devices: Updated review on the parametric investigations and model developments" *Appl Therm Eng* 148, 238–255, 2018.

[11] X. Lu, D. Zhao, T. Ma, Q. Wang, J. Fan, and R. Yang, "Thermal resistance matching for thermoelectric cooling systems" *Energy Conv*

Manage, 169, 186–193, 2018.

[12] M. Sajid, I. Hassan, and A. Rahman, “An overview of cooling of thermoelectric devices” *Renew Sustain Energy Rev* 78, 15–22. 2017.

[13] CIGRE. (2010). Experiences in Service with New Insulating Liquids. Accessed on February 27, 2019, from http://static.mimaterials.com/midel/documents/sales/New_Experiences_in_Service_with_New_Insulating_Liquids.pdf.

[14] Z. Nadolny, and G. Dombek, “Thermal properties of mixtures of mineral oil and natural ester in terms of their application in the transformer” *International Conference Energy, Environment and Material Systems (EEMS 2017)* 01040, 2017.

[15] N. Tanteh, D. Yousef, S. Al Liddawi, D. Ssekasiko, and M. Eriksson, “Properties of transformer oil that affect efficiency” Accessed on December 22, 2020, from https://www.diva-portal.org/smash/get/diva2:829952/FULLTEXT01.pdf

[16] A. Ortiz, F. Delgado, F. Ortiz, I. Fernández, and A. Santisteban, “The aging impact on the cooling capacity of a natural ester used in power transformers” Appl Therm Eng 144, 797–803, 2018.

[17] Advanced Cooling Technologies. (2019). Phase Change Material (PCM) Selection. Accessed on December 22, 2020, from https://www.1-act.com/products/pcm-heat-sinks/pcmselection/.

[18] A. Sharma, V.V. Tyagi, C.R. Chen, and D. Buddhi, “Review on thermal energy storage with phase change materials and applications,” *Renew Sustain Energy Rev* 13, 318–345, 2009.

[19] R. Grimes, E. Walsh, and P. Walsh, “Active cooling of a mobile phone handset” *Appl Therm Eng* 30(16), 2363–2369, 2010

[20] Y. Peles, A.K. Ar, C. Mishra, C.J. Kuo, B. Schneider, “Forced convective heat transfer across a pin fin micro heat sink” *Int J Heat Mass Transf* 48(17), 3615–3627, 2005.

[21] K.C Ng, C.R. Yap, and M.A. Chan, “A universal performance chart for

CPU cooling devices" *Heat Transf Eng* 29(7), 651–656, 2008.

[22] E. Walsh, P. Walsh, R. Grimes, and V. Egan, "Thermal management of low profile electronic equipment using radial fans and heat sinks" *J Heat Transf* 130(12), 125001, 2008.

[23] M. Malik, I. Dincer, and M.A. Rosen, "Review on use of phase change materials in battery thermal management for electric and hybrid electric vehicles" *Int J Energy Res* 40, 1011-1031, 2016.

[24] Y.Y. Ganatra, "Passive thermal management using phase change Materials" *Master's thesis*, Purdue University, 2016.

[25] F. Talati, A.H. Mosaffa, and M.A. Rosen, "Analytical approximation for solidification process in PCM storage with internal fins: imposed heat flux" *Heat Mass Transf* 47, 369-376, 2011.

[26] P. Lamberg, and K.Siren, "Approximate analytical model for solidification in a finite PCM storage with internal fins" Appl Mathe Modell 27, 491-513, 2003.

[27] H. Taheri, and A. Sharma. "An Overview of Phase Change Materials for Building Applications" In: Rechargeable Batteries. New Delhi: Springer India, Apr. 2015, pp. 189–213

[28] A. Mathur, R. Kasetty, J. Oxley, J. Mendez, and K. Nithyanandam. "Using Encapsulated Phase Change Salts for Concentrated Solar Power Plant". In: Energy Procedia 49 (2014), pp. 908–915 (cit. on p. 47).

[29] B. Zalba, J.M. Marin, L.F. Cabeza, and H. Mehling, "Review on thermal energy storage with phase change materials heat transfer analysis and applications" *Appl Therm Eng* 23(3), 251-283, 2003.

[30] E. Osterman, V.V. Tyagi, V. Butala, N.A. Rahim, and U. Stritih, "Review of PCM based cooling technologies for buildings" *Energy Build* 49, 37-49, 2012.

[31] G.A. Lane, S. Aboul-Enein, and N. A. Malatidis, "Heat of fusion systems for solar energy storage" Proceed. workshop on solar energy storage 263 subsystems for the heating and cooling of buildings 1975.

[32] C. Herrick, and D. Golibersuch, “Qualitative behavior of a new latent heat storage device for solar heating/cooling systems” General Electric Company Corporate Research and Development, 1977.

[33] A.N. Keshteli, and M. Sheikholeslami, “Nanoparticle enhanced PCM applications for intensification of thermal performance in building: A review” *J Molec Liq* 274, 516-533, 2019.

[34] G. Asefi, A. Habibollahzade, T. Ma, E. Housfar, and R. Wang, “Thermal management of building-integrated photovoltaic/thermal systems: A comprehensive review” *Solar Energ* 216, 188-210, 2021.

[35] B. Xu, P. Li, and C. Chan, “Application of phase change materials for thermal energy storage in concentrated solar thermal power plants: A review to recent developments” *Appl Energ* 160, 286-307, 2015.

[36] M. Liu, Y. Sun, and F. Bruno, “A review of numerical modelling of high-temperature phase change material composites for solar thermal energy storage” *J Energ Stor* 29, 101378, 2020.

[37] C.R. Raj, S. Suresh, R.R. Bhavsar, V.K. Singh, and K.A. Govind, “Influence of fin configurations in the heat transfer effectiveness of Solid solid PCM based thermal control module for satellite avionics: Numerical simulations” *J Energ Stor* 29, 101332, 2020.

[38] T.Y. Kim, B.S. Hyuh, J.J. Li, and J. Rhee, “Numerical study of the spacecraft thermal control hardware combining solid–liquid phase change material and a heat pipe” *Aerosp Sci Techn* 2(1), 10-16, 2013.

[39] K. Kansara, V.K. Singh, R. Patel, R.R, Bhavsar, and A.P. Vora, “Numerical investigations of phase change material (PCM) based thermal control module (TCM) under the influence of low gravity environment” *Int J Heat Mass Transf* 167, 120811, 2021.

[40] J.C. Mulligan, D.P. Colvin, and Y.G. Bryant, “Microencapsulated phase-change material suspensions for heat transfer in spacecraft thermal systems” *J Spacecraf Rock* 33(2), 1996, https://doi.org/10.2514/3.26753.

[41] E. Oro, A. Gracea, A. Castell, M.M. Farid, and L.F. Cabeza, “Review on phase change materials (PCMs) for cold thermal energy storage

applications" *Appl Enery* 99, 513-533, 2012.

[42] A. Gutierrez, L. Miró, A. Gil, J.R. Aseguinolaza, C. Barreneche, N. Calvet, X. Py, A.I. Fernández, M. Grágeda, S. Ushak, and L.F. Cabeza, "Advances in the valorization of waste and by-product materials as thermal energy storage (TES) materials" *Renew Sustain Energy Rev* 59 763–783, 2016.

[43] T. Nomura, N. Okinaka, and T. Yakiyama, "Waste heat transportation system, using phase change material (PCM) from steelworks to chemical plant" *Resour Conser Recycl* 54(11), 1000-1006, 2010.

[44] J. Shon, H. Kim, and K. Lee, "Improved heat storage rate for an automobile coolant waste heat recovery system using phase-change material in a fin–tube heat exchanger" *Appl Energy* 113, 680-689, 2014.

[45] J. Kim, J. Oh, and H. Lee, "Review on battery thermal management system for electric vehicles" *Appl Therm Eng* 149, 192–212, 2019.

[46] A.R.M. Siddique, S. Mahmud, and B.V. Heyst, "A comprehensive review on a passive (phase change materials) and an active (thermoelectric cooler) battery thermal management system and their Limitations" *J Power Sourc* 401, 224–237, 2018.

[47] J. Jaguemont, N. Omar, P.V. Bossche, and J. Mierlo, "Phase-change materials (PCM) for automotive applications: A review" *Appl Therm Eng* 132, 308–320, 2018.

[48] S. Sahoo, M. Das, and P. Rath, "Application of TCE-PCM based heat sinks for cooling of electronic components: A review" *Renew Sustain Energy Rev* 59, 550-582, 2016.

[49] Y. Cai, Y. Wang, D. Liu, and F.Y. Zhao, "Thermoelectric cooling technology applied in the field of electronic devices: Updated review on the parametric investigations and model developments" *Appl Therm Eng* 48, 238-255, 2019.

[50] K. Kant, A. Shukla, A. Sharma, A. Kumar, and A. Jain, "Thermal energy storage based solar drying systems: A review" *Innov Food Sci Emerging Techn* 34, 86–99, 2016.

[51] M.M. Islam, A.K. Pandey, M. Hasanuzzaman, and N.A. Rahim, "Recent progresses and achievements in photovoltaic-phase change material technology: A review with special treatment on photovoltaic thermal-phase change material systems" *Energy Convers Manage*126, 177–204, 2016.

[52] A. Waqas, J. Ji., L. Xu, M. Ali, Zeashan, and J. Alvi, "Thermal and electrical management of photovoltaic panels using phase change materials - A review" *Renew Sustain Energy Reiv* 92, 254–271, 2018.

[53] S.D. Sharma, H. Kitano, and K. Sagara, "Phase change materials for low temperature solar thermal applications" *Res Rep Fac Eng Mie Univ* 29, 31-64, 2004.

[54] T.J. Lu, "Thermal management of high power electronics with phase change cooling" *Int J Heat Mass Transf* 34, 2245–2256, 2000.

[55] A.G. Evans, M.Y. He, and M. Hutchinson, "Temperature distribution in advanced power electronics and effect of phase change materials on temperature suppression during power pulses" J Electronic Package 123, 211–217, 2001.

[56] D.C. Price, "A review of selected thermal management solutions electronics for military system" *Trans Compon Pack Technol IEEE* 26, 26–39, 2003.

[57] R. Kumar, M.K. Misra, R. Kumar, D. Gupta, P.K. Sharma, B.B. Tak, and S.R. Meena, "Phase change materials: Technology status and potential defence application" *Def Sci J* 61, 576–582, 2011.

[58] D.V. Hale, M.J. Hoover, and M.J. O'Neill, "Phase Change Materials Handbook Report No. HREC-5183-2 LMSC-HREC D225138 NASA" Marshal Space Flight Centre, Alabama, 1971.

[59] A.J. Fosset, M.T. Maguire, A.A. Kudirka, F.E. Mills, and D.A. Brown, "Avionics passive cooling with microencapsulated phase change materials" *ASME J Electron Package* 120, 238–242, 1998.

[60] S. Krishnan, and S.V. Garimella, "Analysis of a phase change energy storage system for pulsed power dissipation" *IEEE Trans Compon*

Packag Technol 27, 191–199, 2004.

[61] E.M Alawadhi, and C.H. Amon, “Performance analysis of an enhanced PCM thermal control unit” In: Proceedings of the seventh intersociety conference on thermal and thermomechanical phenomena in electronic systems, ITHERM 2000 (CatNo00CH37069); 2000.p.283–9.

[62] R. Kandasamy, X.Q Wang, and A.S. Mujumdar, “Application of phase change materials in thermal management of electronics” *Appl Therm Eng* 27, 2822–32, 2007.

[63] S. Krishnan, S.V. Garimella, and S.S. Kang, “A novel hybrid heat sink using phase change materials for transient thermal management of electronics” *IEEE Trans Compon Packag Technol* 28, 281–289, 2005.

[64] R. Akhilesh, A. Narasimhan, and C. Balaji, “Method to improve geometry for heat transfer enhancement in PCM composite heat sinks” *Int J Heat Mass Transf* 48, 2759–2770, 2005.

[65] K.C. Nayak, S.K. Saha, K. Srinivasan, and P. Dutta, A numerical model for heat sinks with phase change materials and thermal conductivity enhancers” *Int J Heat Mass Transf* 49, 1833–1844, 2006.

[66] V. Shatikian, G. Ziskind, and R. Letan, “Numerical investigation of a PCM-based heat sink with internal fins” *Int J Heat Mass Transf* 48, 3689–3706, 2005.

[67] S.K. Saha, K. Srinivasan, and P.Dutta, “Studies on optimum distribution of fins in heat sinks filled with phase change materials” *J Heat Transf* 130, 034505, 2008.

[68] S.K. Saha, and P. Dutta, “Heat transfer correlations for PCM-based heat sinks with plate fins” *Appl Therm Eng* 30, 2485–2491, 2010.

[69] G. Setoh, F.L. Tan, and S.C. Fok, “Experimental studies on the use of a phase change material for cooling mobile phones” *Int Commun Heat Mass Transf* 37(9), 1403–1410, 2010.

[70] M. Faraji, H.E.L. Qarnia, U.C. Ayyad, S. Semlalia, and L. De, “Cooling management of a protruding electronic components by using a phase change material heat sink” 2007.(Ic).p.174–7.

[71] X. Lu, L.W. Fan, Y. Zheng, Y.Q. Xiao, X. Xu, and Z.T. Yu, “Effect of the inclination angle on the transient performance of a phase change material-based heat sink under pulsed heat loads” *J Zhejiang Univ Sci A*, 15(10), 789–797, 2014.

[72] M. Alimohammadi, Y. Aghli, E.S. Alavi, and M. Sardarabadi, “Experimental investigation of the effects of using nano/phase change materials (NPCM) as coolant of electronic chipsets, under free and forced convection” *Appl Therm Eng* 111, 271–279, 2017.

[73] F. Bahiraei, A. Fartaj, and G.A. Nazri, “Experimental and numerical investigation on the performance of carbon-based nanoenhanced phase change materials for thermal management applications” *Energy Convers Manag* 153, 115–128, 2017.

[74] K.R.S. Kumar, R. Dinesh, A.A. Roseline, and S. Kalaiselvam, “Performance analysis of heat pipe aided NEPCM heat sink for transient electronic cooling” *Microelectron Reliab* 73, 1–13, 2017.

[75] K. Tumuluri, J.L. Alvarado, H. Taherian, and C. Marsh, “Thermal performance of a novel heat transfer fluid containing multiwalled carbon nanotubes and microencapsulated phase change materials” *Int J Heat Mass Transf* 54, 5554–5567, 2011.

[76] L. Colla, L. Fedele, S. Mancin, L. Danza, and O. Manca, “Nano-PCMs for enhanced energy storage and passive cooling applications” *Appl Therm Eng* 110, 584–589, 2017.

[77] L. Colla, D. Ercole, L. Fedele, S. Mancin, O. Manca, and S. Bobbo, Nano-phase change materials for electronics cooling applications” *J Heat Transfer* 139(5), 52406, 2017.

[78] L. Colla, L. Fedele, S. Mancin, B. Buonomo, D. Ercole, and O. Manca, Nano-PCMs for passive electronic cooling applications” J Phys Conf Ser 655(1), 12030, 2015.

[79] E.M. Alawadhi, and C.H. Amon, “PCM thermal control unit for portable electronic devices: experimental and Numerical studies” *IEEE Trans Compon Packag Technol* 26, 116–125, 2003.

[80] K. Lafdi, O. Mesalhy, and A. Elgafy, “Merits of employing foam encapsulated phase change materials for pulsed power electronics cooling application” *J Electron Packag* 130, 1–8, 2008.

[81] S. Krishnan, J.Y. Murthy, and S.V. Garimella, “A two temperature model for solid–liquid phase change in metal foams” *J Heat Transf* 127, 995–1004, 2005.

[82] K. Chintakrinda, R.D. Weinstein, and A.S. Fleischer, “A direct comparison of three different material enhancement methods on the transient thermal response of paraffin phase change material exposed to high heat fluxes” *Int J Therm Sci* 50, 1639–1647, 2011.

[83] Z.G. Qu, W.Q. Li, J.L. Wang, and W.Q. Tao, “Passive thermal management using metal foam saturated with phase change material in a heat sink” *Int Commun Heat Mass Transf* 39, 1546–1549, 2012.

[84] R. Baby, and C. Balaji, “Experimental investigations on thermal performance enhancement and effect of orientation on porous matrix filled PCM based heat sink” *Int Commun Heat Mass Transf* 46:27–30, 2013.

[85] A. Abhat, “Low temperature latent heat thermal storage” ISPRA course on energy systems and technology, G.Beghi, D. Reidel Publishing Co., Holland;1981.p. 33–91.

[86] R Henze, and J. Humphrey, “Enhanced heat conduction in phase-change thermal energy storage devices” *Int J Heat Mass Transf* 24, 459–474, 1981.

[87] S.K. Sahoo, M.K. Das, P. Rath, Numerical study of cyclic melting and solidification of nano enhanced phase change material based heat sink in thermal management of electronic components, ASME 2016 5th Int. Conf. Micro/Nanoscale Heat Mass Transf. MNHMT2016, Biopolis, Singapore, January 4-6, 2016.

[88] R.K. Sharma, P. Ganesan, J.N. Sahu, H.S.C. Metselaar, and T.M.I. Mahila, Numerical study for enhancement of solidification of phase change materials using trapezoidal cavity” *Powder Tech* 268, 38-47,

2014.

[89] S.S. Sebti, M. Mastiani, H. Mirzaei, A. Dadvand, S. Kashani, and S.A. Hosseini, “Numerical study of the melting of nano-enhanced phase change material in a square cavity” *J Zhejiang University-Science A* (*Applied Physics and Engineering*) 14(5), 307-316, 2013.

[90] L. Fan, and J.M. Khodadadi, “A theoretical and experimental investigation of unidirectional freezing of nanoparticle-enhanced phase change materials” *J Heat Transf* 134, 1-9, 2012.

[91] A. Abhat “Low temperature latent heat thermal energy storage: heat storage materials” *Sol Energy* 30, 313–332, 1983.

[92] I. Sarbu, and C. Sebarchievici, “A comprehensive review of thermal energy storage” *Sustainability* 10:191, 2018.

[93] C. Barreneche, M.E. Navarro, L.F Cabeza, A.I., Fernandez, “New database to select phase change material” *J Energ Stor* 3,18-24, 2019.

[94] C. Granta, University, CES Selector Software, 2012.

[95] S. Khare, M. Dell Amico, C. Knight, and S. McGarry, “Selection of materials for high temperature sensible energy storage” *Solar Energ Mate Solar cells* 115, 144-122, 2013.

[96] M.K. Rathod, and N.V. Kanzaria “A methodological concept for phase change material selection based on multiple criteria decision analysis with and without fuzzy environment” Mat Des 32, 3578-3585, 2011.

[97] L. Socaciu, O. Giuragiu, D. Banyai, and M. Simion, “PCM selection using AHP method to maintain thermal comfort of the vehicle occupants” *Energ Proc* 85, 489-497, 2015.

[98] L.G. Socaciu, and P.V. Unguresan, “Using the Analytic Hierarchy Process to prioritize and select phase change materials for comfort application in buildings” Mathematical Model Civil Eng, 25-32, 2014.

[99] M. Rastogi, A. Chauhan, R. Vaish, A. Kishan, “Selection and performance assessment of phase change materials for heating, ventilation and air conditioning application” *Energ Conver Manage* 89, 260-269, 2010.

[100] G. Zsembinszki, A.G. Fernandez, and L.F. Cabeza, “Selection of the Appropriate Phase Change Material for Two Innovative Compact Energy Storage Systems in Residential Buildings” *Appl Sci* 10, 2116, 2020.

[101] A. Loganathan, and I. Mani, “A fuzzy based hybrid multi criteria decision making methodology for phase change material selection in electronics cooling system” *Ain Shams Eng J* 9, 2943-2950, 2018.

[102] K. Yang, N. Zhu, C. Chang, D. Wang, S. Yang, and S. Ma, “A methodological concept for phase change material selection based on multi-criteria decision making (MCDM): A case study” *Energy* 165, 1085-1096, 2018.

[103] H. Xu, J.Y. Sze, A. Romagnoli, and X. Py, “Selection of Phase Change Material for Thermal Energy Storage in Solar Air Conditioning Systems” *Energy proc* 105, 4281-4288, 2017.

[104] H. Xu, A. Romangoli, J.Y. Sze, and X. Py, “Application of material assessment methodology in latent heat thermal energy storage for waste heat recovery” *Appl Energy* 187, 281-290, 2017.

[105] Y. Wang, Y. Zhang, W. Yang, and H. Ji, “Selection of Low-Temperature Phase-Change Materials for Thermal Energy Storage Based on the VIKOR Method” *Energy Techno* 3(1), 84-89, 2015.

[106] A.D. Brent, V.R. Voller, and K. Reid, “Enthalpy-porosity technique for modeling convection-diffusion phase change: application to the melting of a pure metal Numer” *Heat Transf vol* Part A App pp, 297–318, 1988.

[107] S.F. Hosseinizadeh, F.L. Tan, and S.M. Moosania, “Experimental and numerical studies on performance of PCM-based heat sink with different configurations of internal fins” *Appl Therm Eng* 31(18), 3827-3838, 2011.

[108] N. S. Bondareva, and M. A. Shermet, “Conjugate heat transfer in the PCM based heat storage system with finned copper profile: Application in electronic cooling” *Int J Heat Mass Transf* 124, 1275-1284, 2018.

[109] A. Arshad, M. Jabbal, P. T. Sardari, M. A. Bashir, H. Faraji, and Y. Yan, “Transient simulation of finned heat sinks embedded with PCM for

electronic cooling” *Therm Sci Engg Prog* 18, 100520, 2020.

[110] N.S. Bondareva, B. Buonomo, O. Manca, and M.A. Sheremet, “Heat transfer inside cooling system based on phase change material with alumina nanoparticles” *Appl Therm Eng* 144, 972–981, 2018.

[111] H. Faraji, M. E. Alami, A. Arshad, and M. Faraji, “Numerical simulation of the melting of a NePCM for cooling of electronic components” *Therm. Sci Eng Prog* 21, 100766, 2021.

[112] A. Dadvand,N. H. Boukani, and M. Dawoodian, “Numerical simulation of the melting of a NePCM due to a heated thin plate with different positions in a square enclosure” *Therm Sci Eng Prog* 7, 248-266, 2018.

[113] M. Bayat, M.R. Faridzadeh, and D. Toghraie, “Investigation of finned heat sink performance with nano enhanced phase change material (NePCM)” *Therm Sci Eng Prog* 5, 50-59, 2018.

[114] H. Faraji, M.E. Alami, A. Ali, and Y. Hariti, “Numerical Survey on Performance of Hybrid NePCM for Cooling of Electronics: Effect of Heat Source Position and Heat Sink Inclination” *J Therm Sci Eng Applc* 13, 051010-1, 2021.

[115] P.V.S.S. Srivatsa, R. Baby, and C. Balaji, “Numerical Investigation of PCM Based Heat Sinks with Embedded Metal Foam/Crossed Plate Fins, Num” *Heat Transf Part A Appl* 66, 1131-1153, 2014.

[116] G.K. Marri, and C. Balaji, “Experimental and numerical investigations on the effect of porosity and PPI gradients of metal foams on the thermal performance of a composite phase change material heat sink” *Int J Heat Mass Transf* 164, 120454, 2021.

[117] W.G. Alshaer, S.A. Nada, M.A. Rady, C. Le Bot, and E. Palomo Del Barrio, “Numerical investigations of using carbon foam/PCM/Nano carbon tubes composites in thermal management of electronic equipment” *Energy Convers Manag* 89, 873–884, 2015.

[118] Z. Deng, X. Liu, C. Zhang, Y. Huang, and Y. Chen, “Melting behaviors of PCM in porous metal foam characterized by fractal geometry” *Int J Heat Mass Transf* 113, 1031–1042, 2017.

[119] P.T. Sardari, H.I. Mohammed, D. Giddings, G. S. Walker, M. Gillott, and D. Grant, “Numerical study of a multiple-segment metal foam-PCM latent heat storage unit: Effect of porosity, pore density and location of heat source” Energy 189, 116108, 2019.

[120] X. Yang, S. Tan, Y. Deng, L. Wang, J. Liu, and Y. Zhou, “Experimental and numerical investigation of low melting point metal based PCM heat sink with internal fins” Int. Commun. *Heat Mass Transf* 87, 118-124, 2017.

[121] A. Zehri, M. K. Samani, M.G. Latorre, A. Nylander, T. Nilsson, Y. Fu, N. Wang, L. Ye, and J. Liu, “High porosity and light weight graphene foam heat sink and phase change material container for thermal management” *Nanotechnol* 31, 4244003, 2020.

[122] R. Kalbasi, M. Afrand, J.alsarraf, and M.D. Tran, “Studies on optimum fins number in PCM-based heat sinks” *Energy* 171, 1088-1099, 2019.

[123] S.K. Sahoo, and P. Rath. M.K. Das, “Numerical study of phase change material based orthotropic heat sink for thermal management of electronics components” *Int. J Heat Mass Transf* 103, 855-867, 2016.

[124] C.R. Raj, S. Suresh, S. Vasudevan, M. Chandrasekar, V.K. Singh, and R.R. Bhavsar, “Thermal performance of nano-enriched form-stable PCM implanted in a pin finned wall-less heat sink for thermal management application” *Energy Conv Manage* 226, 113466, 2020.

[125] B. Debich, A.E. Hami, A. Yaich, W. Gafsi, L. Walha, and M. Haddar, “Design optimization of PCM-based finned heat sinks for mechatronic components: A numerical investigation and parametric study” *J Energy Stor* 32, 101960, 2020.

[126] H.M. Ali, A. Arshad, M. Jabbal, and P.G. Verdin, “Thermal management of electronics devices with PCMs filled pin-fin heat sinks: A comparison” *Int J Heat Mass Transf* 117, 1199–1204, 2018.

[127] A. Arshad, H.M. Ali, W.M. Yan, A.K. Hussein, and M. Ahmadlouydarab, “An experimental study of enhanced heat sinks for thermal management using n-eicosane as phase change material” *Appl*

Therm Eng 132, 52–66, 2018.

[128] A. Arshad, H.M. Ali, S. Khushnood, and M. Jabbal, "Experimental investigation of PCM based round pin-fin heat sinks for thermal management of electronics: Effect of pin-fin diameter" *Int J Heat Mass Transf* 117, 861–872, 2018.

[129] A. Arshad, H.M. Ali, M. Ali, and S. Manzoor, "Thermal performance of phase change material (PCM) based pin-finned heat sinks for electronics devices: Effect of pin thickness and PCM volume fraction" *Appl Therm Eng* 112, 143-155, 2017.

[130] R. Baby, and C. Balaji, "Experimental investigations on phase change material based finned heat sinks for electronic equipment cooling" *Int J Heat Mass Transf* 55, 1642–1649, 2012.

[131] M.J. Ashraf, H.M. Ali, H. Usman, and A. Arshad, "Experimental passive electronic cooling: parametric investigation of pin-fin geometries and efficient phase change material" *Int J Heat Mass Transf* 115, 251-263, 2017.

[132] H.M. Ali, M.J. Ashraf, A. Giovanneilli, M. Irfan, T.B. Irshad, H.M. Hamid, F. Hassan, and A. Arshad, "Thermal management of electronics: An experimental analysis of triangular rectangular, and circular pin-fin heat sinks for various PCMs" *Int J Heat Mass Transf* 123, 272-284, 2018.

[133] R. Baby, and C. Balaji, "Thermal performance of a PCM heat sink under different heat loads: An experimental study" *Int J Therm Sci* 79, 240-249, 2014.

[134] H. Usman, H.M. Ali, A. Arshad, M.J. Ashraf, S. Khushnood, M.M. Janjua, and S.N. Kazi, "An experimental study of PCM based finned and un-finned heat sinks for passive cooling of electronics" *Heat Mass Transf* 54, 3587-3598, 2018.

[135] S. Mahmoud, A. Tang, C. Toh, R. AL-Dadah, and S.L. Soo, "Experimental Investigation of Inserts Configurations and PCM type on the Thermal Performance of PCM Based Heat Sinks" *Appl Energy* 112, 1349-1356, 2013.

[136] R. Kothari, S. K. Sahu, S. I. Kundalwal, and S. P. Sahu, "Experimental investigation of the effect of inclination angle on the performance of phase change material based finned heat sink" *J Energy Stor* 37, 102462, 2021.

[137] B. Kamkari, and H. Shokouhmand, "Experimental investigation of phase change material melting in rectangular enclosures with horizontal partial fins" *Int J Heat Mass Transf* 78, 839-851, 2014.

[138] M.Y. Yazici, M. Avci, and O. Aydin, "Combined effects of inclination angle and fin number on thermal performance of a PCM-based heat sink" *Appl Therm Eng* 159, 113956, 2019.

[139] L. Fan, Y. Xiao, Y. Zeng, X. Fang, X. Wang, X. Xu, Z. Yu, R. Hong, Y. Hu, and K. Cen, "Effects of melting temperature and the presence of internal fins on the performance of a phase change material (PCM)-based heat sink" *Int J Therm Sci* 70, 114e126, 2013.

[140] R. Baby, and C. Balaji, "Thermal optimization of PCM based pin fin heat sinks: an experimental study" *Appl Therm Eng* 54, 65–77, 2013.

[141] H.M. Ali, and A. Arshad, "Experimental investigation of n-eicosane based circular pin-fin heat sinks for passive cooling of electronic devices" *Int J Heat Mass Transf* 112, 649–661, 2017.

[142] C.J. Ho, and J.Y. Gao, "An experimental study on melting heat transfer of paraffin dispersed with Al2O3 nanoparticle in a vertical enclosure" *Int J Heat and Mass Transf* 62, 2-8, 2013.

[143] S. Sharma, L. Micheli, W. Chang, A.A. Tahir, K.S. Reddy, and T.K. Mallick, "Nano-enhanced Phase Change Material for thermal management of BICPV" *Appl Energy* 208, 719–733, 2017.

[144] F. Bahiraei, A. Fartaj, and G. Nazri, "Experimental and numerical investigation on the performance of carbon-based nanoenhanced phase change materials for thermal management applications" *Energ Conv Manag* 153, 115–128, 2017.

[145] M. Alimohammadi, Y. Aghli, E.S. Alavi, M. Sardarabadi, and M. Passandideh-Fard, "Experimental investigation of the effects of using

nano/phase change materials (NPCM) as coolant of electronic chipsets, under free and forced Convection" *Appl Therm Eng* 111, 271–279, 2017.

[146] M. Joseph, and V. Sajith, "Graphene enhanced paraffin nanocomposite based hybrid cooling system for thermal management of electronics" *Appl Therm Eng* 163, 114342, 2019.

[147] K.R.S. Kumar, R. Dinesh, A.A. Roseline, and S. Kalaiselvam, "Performance analysis of heat pipe aided NEPCM heat sink for transient electronic cooling" *Microelec Rel* 73, 1-13, 2017.

[148] R. Kothari, S.K. Sahu, and S.I. Kundalwal, "Investigation on thermal characteristics of nano enhanced phase change material based finned and unfinned heat sinks for thermal management system" *Chem Eng Process Proc Intensif* 162, 108328, 2021.

[149] A. Farzanehnia, M. Khatibi, M. Sardarabadi, and M. Passandiedeh, "Experimental investigation of multiwall carbon nanotube/paraffin based heat sink for electronic device thermal management" *Energy Conv Manage* 179, 314-325, 2019.

[150] S.L. Tariq, H.M Ali., M.A. Akram, and M.M. Janjua, "Experimental investigation on graphene based nanoparticles enhanced phase change materials (GbNePCM) for thermal management of electronic equipment" *J Energy Stor* 30, 101497, 2020.

[151] S. Motahar, and R. Khodabandeh, "An experimental assessment of nanostructured material embedded in a PCM based heat sink for transient thermal management of electronics" *Trans Phenom Nano Micro scales* 6 (2), 96-103, 2018.

[152] M. Alimohammadi, Y. Aghli, E.S. Alavi, M. Sardarabadi, and M. Passandideh-Fard, "Experimental investigation of the effects of using nano/phase change materials (NPCM) as coolant of electronic chipsets, under free and forced Convection" *Appl Therm Engg* 111, 271–279, 2017.

[153] R. Kothari, D.V. Vaidya, V. Shelke, S.K. Sahu, and S.I. Kundalwal, "Experimental investigation of thermal performance of nano-enhanced

phase change materials for thermal management of electronic components” *ASME 2019 Power Conference*, POWER2019-1883, July 15-18, 2019, Salt Lake City, UT, USA.

[154] T. ur Rehman, and H.M. Ali, “Experimental study on the thermal behavior of RT-35HC paraffin within copper and Iron-Nickel open cell foams: Energy storage for thermal management of electronics” *Int J Heat Mass Transf* 146, 118852, 2020.

[155] T. ur Rehman, and H.M. Ali, “Thermal performance analysis of metallic foam-based heat sinks embedded with RT-54HC paraffin: an experimental investigation for electronic cooling” *J Therm Anal Calorim* 140, 979–990, 2020.

[156] H. Wang, F. Wang, Z. Li, Y. Tang, B. Yu, and W. Yuan, “Experimental investigation on the thermal performance of a heat sink filled with porous metal fiber sintered felt/paraffin composite phase change material” *Appl Energy* 176, 221–232, 2016.

[157] W.G. Alshaer, S.A. Nada, M.A. Rady, E.P. Del Barrio, and A. Sommier, “Thermal management of electronic devices using carbon foam and PCM/nano-composite” *Int J Therm Sci* 89, 79–86, 2015.

[158] W. G. Alshaer, M. A. Rady, S. A. Nada, E. Palomo Del Barrio, and A. Sommier, “An experimental investigation of using carbon foam–PCM–MWCNTs composite materials for thermal management of electronic devices under pulsed power modes” *Heat Mass Transf* 53, 569–579, 2017.

[159] M. Iasiello, M. Mameli, S. Flippeschi, and N. Bianco, “Metal foam/PCM melting evolution analysis: Orientation and morphology effects” *Appl Therm Eng* 187, 116572, 2021.

[160] K. Lafdi, O. Mesalhy, and S. Shaikh, “Experimental study on the influence of foam porosity and pore size on the melting of phase change materials” *J Appl Phys* 102, 2007.

[161] Z.Q. Zhu, Y.K. Huang, N. Hu, Y. Zeng, and L.W. Fan, “Transient performance of a PCM-based heat sink with a partially filled metal foam:

Effects of the filling height ratio" *Appl Therm Eng* 128, 966–972, 2018.

[162] P. Gimenez, A. Jove, C. Prieto, and S. Fereres, "Effect of an increased thermal contact resistance in a salt PCMgraphite foam composite TES system" *Rene Energy* 106, 321e334, 2017.

[163] R. Kothari, P. Mahalkar, S.K. Sahu, and S. I. Kundalwal, "Experimental Investigations on Thermal Performance of PCM" *Proc. ASME 2018 16th Int. Conf. Nanochannels, Microchannels, Minichannels ICNMM2018 c*, 1–9, 2018.

[164] I.O. Salyer, A.K. Sircar, and R.P. Chartoff, "Analysis of crystalline paraffinic hydrocarbons for thermal energy storage by differential scanning calorimetry" *Part 1, Pure hydrocarbons, 15th North American Thermal Analysis Society Conference, Cincinnati, OH*, 1986.

[165] M. Hadjieva, S. Kanev, and J. Argirov, "Thermophysical properties of some paraffins applicable to thermal energy storage, Solar Energy Mater" *Solar Cells* 27, 181–187, 1992.

[166] J.P. Bardon, E. Vrignaud, and D. Delaunay, "Etude experimentale de la fusion et de la solidification periodique dune plaque de paraffine" *Rev Gen Therm*, 212–213, 1979.

[167] M.M. Farid, "Solar energy storage with phase change" *J Solar Energy Res* 4, 11, 1986.

[168] H.T. EI-Dessouky, W.S. Bouhamra, H.M. Ettouney, and M. Akbar, "Heat transfer in vertically aligned phase change energy storage systems" *J Solar Energy Eng Trans ASME* 121 (2), 98–109, 1999.

[169] R.G. Kemink, and E.M. Sparrow, "Heat transfer coefficients for melting about a vertical cylinder with or without subcooling and for open or closed containment" *Int J Heat Mass Transfer* 24 (10), 1699–1710, 1981.

[170] S. Himran, A. Suwono, and G.A. Mansoori, "Characterization of alkanes and paraffin waxes for application as phase change energy storage medium" *Energy Sources* 16 (1), 117–128, 1994.

[171] Rubitherm, Phase change material, accessed on 27 December 2020 from www.rubitherm.eu.

[172] Pluss, Technology for a better world, accessed on 27 December 2020 from www.pluss.co.in.

[173] Climator, Moving energy in time, accessed on 27 December 2020 from www.climator.com .

[174] S.A. Mohamed, F.A. Al-Sulaiman, N.I. Ibrahim, M.H. Zahir, A. Al-Ahmed, R. Saidur, B.S. Yilbas, and A.Z. Sahin, "A review on current status and challenges of inorganic phase change materials for thermal energy storage systems" *Ren Sustain Energy Rev* 70, 1072-1089, 2017.

[175] S. Nestic, J.F. Lampon, A. Aleeksic, P. Cabanelas, and D. Tadic, "Ranking manufacturing processes from quality management perspective in the automobile industry" *Exp Sys* 36 (6), e12451, 2019.

[176] M.J.J. Wang, and T.C. Chang, "Tool steel materials selection under fuzzy environment" *Fuzzy Sets Sys* 72, 263-270, 1995.

[177] A. Kobryn, and J. Prystrom, "Processing technique of ratings for ranking of alternatives (PROTERRA)" *Exp Sys* 35 (4), e12279, 2018.

[178] J. Roy, K. Chatterjee, A. Bandyopadhyay, and S. Kar, "Evaluation and selection of medical tourism sites: A rough analytic hierarchy process based multi-attributive border approximation area comparison approach" *Exp Sys* 35 (1), e1223, 2017.

[179] A. Noori, H. Bonakdari, K. Morovati, and B. Gharabaghi, "Development of optimal water supply plan using integrated fuzzy Delphi and fuzzy ELECTRE III methods-case study of the Gamasiab basin" *Exp Sys* 37 (5), e12568, 2020.

[180] K. Fayazbakhsh, A. Abedian, B.D. Manshadi, and R.S. Khabbaz, "Introducing a novel method for materials selection in mechanical design using Z- transformation in statistics for normalization of material properties" *Mat Des* 30, 4396-4404, 2009.

[181] T. L. Satty, "The analytic hierarchy process" *Mcgraw-Hill*, 1980.

[182] F.T.S. Chan, and N. Kumar, "Global supplier development considering risk factors using fuzzy extended AHP based-approach" *Omega* 35, 417-431, 1980.

[183] F.T.S. Chan, N. Kumar, M.K. Tiwari, H.C.W. Lau, and K.L. Choy, "Global supplier selection: A fuzzy AHP approach" *Int J Prod Res* 14, 3825-3857, 2008.

[184] Y.H. Chang, and C.H. Yeh, "Application: A survey analysis of service quality for domestic airlines" *Eur J Oper Res* 139, 166-177, 2002.

[185] E. Albayrak, and Y.C. Erensal, "Using analytic hierarchy process (AHP) to improve human performance: An application of multiple criteria decision making problem" *J. Intellig Manuf* 15, 491-503, 2004.

[186] J.J. Wang, and D.L. Yang "Using hybrid multi-criteria decision aid method for information systems outsourcing" *Comp Oper Res* 34, 3691-23700, 2007.

[187] M. Dagdeviren, S. Yavuz, and N. Kilinc "Weapon selection using the AHP and TOPSIS methods under fuzzy environment" *Exp Sys Appl* 36, 8143-8151, 2009.

[188] C.L. Hawang, and K. Yoon, "Multiple attributes decision making: methods and application: a state of-the-art survey" *Springer verlag*, NewYork, 1981.

[189] I. Ertugrul, and N. Karakasoglu, "Performance evaluation of turkey elements firms with fuzzy analytic hierarchy process and TOPSIS method" *Exp Sys Appl* 36, 702-715, 2009.

[190] G.D. Li, D. Yamaguchi, and M. Nagai, "Application of grey-based rough decision-making approach to supplier selection" *J. Model Manage* 2, 1031-142, 2006.

[191] R.V. Rao, "Decision making in the manufacturing environment using graph theory and fuzzy multiple attributes decision making" London, Springer-verlag, 2007.

[192] R.V. Rao, "A decision-making framework model for evaluating flexible manufacturing system using digraph and matrix method" *Int J Adv Manuf Tech* 30, 1101-1110, 2006.

[193] R. Venkatasamy, and V.P. Agarwal, "Selection of automobile vehicle by evaluation through graph theoretical methodology" *Int J Veh Des* 17,449-

471, 1996.

[194] R. Venkatasamy, and V.P. Agarwal, “A digraph approach to quality evaluation of an automobile vehicle” *Qual Eng* 3, 405-417, 1997.

[195] S. Opricovic and G.H. Tzeng, “Compromise solution by MCDM methods: A comparative analysis of VIKOR and TOPSIS” *Eur J Oper Res* 156 (2), 445–455, 2004.

[196] S. Chakraborty, P. Chatterjee, and K. Prasad, “An Integrated DEMATEL–VIKOR Method-Based Approach for Cotton Fibre Selection and Evaluation” *J Inst Eng Ser E* 99 (1), 63–73, 2018.

[197] J.R. San Cristobal, “Multi-criteria decision-making in the selection of a renewable energy project in spain” *The Vikor method Renew Energy* 36 (2), 498–502, 2011.

[198] W.Q. Li, Z.G. Qu, Y.L. He, and W.Q. Tao, “Experimental and numerical studies on melting phase change heat transfer in open-cell metallic foam filled with paraffin” *Appl Therm Eng* 37, 1-9, 2012.

[199] H. Inaba, K. Matsuo, and A. Horibe, “Numerical simulation for fin effect of a rectangular latent heat storage vessel packed with molten salt under heat release process” *Heat Mass Transf* 39 (3), 231-237, 2003.

[200] M. Arici, E. Tutuncu, C. Yildiz, and D. Li, “Enhancement of PCM melting rate via internal fin and nanoparticle” *Int J Heat Mass Transf* 156, 1198454, (2020.

[201] M. Arici, E. Tutuncu, H. Karabay, and A. Campo, “Investigation on the melting rate of phase change material in a square cavity with a single fin attached at the center of the heated wall” *Eur Phys J Appl Phys* 83, 10902, 2018.

[202] C. Ji, Z. Qin, S. Dubey, F.H. Choo, and F. Duan, “Simulation on PCM melting enhancement with double-fin length arrangements in a rectangular enclosure induces by natural convection” *Int J Heat Mass Transf* 127, 255-265, 2018.

[203] R. Ganatra, J. Ruiz, J.A. Howarter, and A. Marconnet, “Experimental investigation of phase change materials for thermal management of

handheld devices" *Int J Therm Sci* 129, 358-364, 2018.

[204] V.R. Voller, and C. Prakash, "A fixed grid numerical modeling methodology for convection-diffusion mushy region phase change-problems" *Int J Heat Mass Transf* 30(8), 1709-1719, 1987.

[205] S.V. Patankar "Numerical heat transfer and fluid flow" *McGraw-Hill Newyork*, 1980).

[206] SavEnrg, Phase change material, accessed on 27 December from http://rgees.com/.

[207] S.H. Tasnim, R. Hossain, S. Mahmud, and A. Dutta, "Convection effect on the melting process of nano-PCM inside porous enclosure" *Int J Heat Mass Transf* 85, 206–210. 2015.

[208] J.M. Khodadadi, and S. F. Hosseinizadeh, "Nanoparticle-enhanced phase change materials (NEPCM) with great potential for improved thermal energy storage" *Int Commun Heat Mass Transf* 34, 534–543, 2007.

[209] S.F. Hosseinizadeh, A.A.R. Darzi, and F.L. Tan, "Numerical investigations of unconstrained melting of nano-enhanced phase change material (NEPCM) inside a spherical container" *Int. J Therm Sci* 51, 77–83, 2012.

[210] N.S. Dhaidan, J. M. Khodadadi, T.A. Al-Hattab, and S.M. Al-Mashat, "Experimental and numerical investigation of melting of phase change material/nanoparticle suspensions in a square container subjected to a constant heat flux" *Int J Heat Mass Transf* 66, 672–683, 2013.

[211] J. Krishna, P.S. Kishore, and A.B. Solomon, "Heat pipe with nano enhanced-PCM for electronic cooling application" *Exp Therm Fluid Sci* 81, 84–92, 2017.

[212] S.K. Mandal, S. Kumar, P.K. Singh, S.K. Mishra, H. Bishwakarma, N. P. Choudhry, R.K. Nayak, and A.K. Das, "Performance investigation of CuO-paraffin wax nanocomposite in solar water heater during night" *Thermochim Acta* 671, 36–42, 2019.

[213] T. ur Rehman, and H. M. Ali, "Experimental investigation on paraffin wax integrated with copper foam based heat sinks for electronic

components thermal cooling” *Int Commun Heat Mass Transf* 98, 155–162, 2018.

[214] Z. Xiangfa, X. Hanning, F. Jian, Z. Changrui, and J. Yonggang, “Pore structure modification of silica matrix infiltrated with paraffin as phase change material” *Chem Eng Res Des* 88, 1013–1017, 2010.

[215] M. Mehrabi-Kermani, E. Houshfar, and M. Ashjaee, “A novel hybrid thermal management for Li-ion batteries using phase change materials embedded in copper foams combined with forced-air convection” *Int J Therm Sci* 141, 47–61, 2019.

[216] Y. Huang, Q. Sun, F. Yao, and C. Zhang, “Experimental Study on the Thermal Performance of a Finned Metal Foam Heat Sink with Phase Change Material” *Heat Transf Eng* 42, 579–591, 2021.

[217] R. Kothari, S.K. Sahu, S.I. Kundalwal, and P. Mahalkar, “Thermal performance of phase change material-based heat sink for passive cooling of electronic components: An experimental study” *Int J Energy Res,* 1-25, 2020.

[218] R. Baby, and C. Balaji, “Thermal management of electronics using phase change material based pin fin heat sinks” *6th European Thermal Sciences Conference. J. of Phys. 2012, IOP Publishing*, 2012.

[219] H.M. Ali, and W. Arshad, “Thermal performance investigation of staggered and inline pin fin heat sinks using water based rutile and anatase TiO2 nanofluids” *Ener Conv Manage* 106, 793-803, 2015.

[220] A.A. Minea, and M.G. Moldoveanu, “Studies on Al_2O_3, CuO, and TiO_2 water based nanofluids: A comparative approach in laminar and turbulent flow” *J Eng Thermo* 26 (2), 291-301, 2017.

[221] R.K. Sharma, P. Ganesan, V.V. Tyagi, H.S.C. Metselaar, and S.C. Sandaran, “Thermal properties and heat storage analysis of palmitic acid-TiO2 composite as nano-enhanced organic phase change material (NEOPCM)” *Appl Therm Eng* 99, 1254–1262, 2016.

[222] A. Bhattacharya, and R.L. Mahajan, “Finned Metal Foam Heat Sinks for Electronics Cooling in Forced Convection” *J. Elec Pack* 124, 155-163,

2002.

[223] H. Shokouhmand, and B. Kamkari, “Experimental investigation on melting heat transfer characteristics of lauric acid in a rectangular thermal storage unit” *Exp Therm Fluid Sci* 50, 201–212, 2013.

[224] H.W. Coleman, and W.G. Steele, “Experimental and uncertainty analysis for engineers” New York, Wiley, 1989.

[225] G.W. Burns, M.G. Scroger, G.F. Strouse, M.C. Croarkin, and W.F. Guthrie. “Temperature electromotive force reference functions and tables for the letter-designated thermocouple types based on the ITS-90” NASA STI/Recon Technical Report N, 1993.

[226] N.S. Effendi, and K. J. Kim, “Orientation effects on natural convective performance of hybrid fin heat sinks, Appl” *Therm Eng* 123, 527–536, 2017.

[227] S. Akilu, A.T. Baheta, and K.V. Sharma, “Experimental measurement of thermal conductivity and viscosity of ethylene-glycol based hybrid nanofluid TiO2-CuO/C inclusions” *J Mol Liq* 246, 396-405, 2017.

[228] C.J. Ho, and J.Y. Gao, “Preparation and thermophysical properties of nanoparticle-inparaffin emulsion as phase change material” *Int Comm Heat Mass Transf* 36, 467–470, 2009.

[229] J. Wang, H. Xie, Y. Li, and Z. Xin, “PW based phase change nanocomposites containing-Al_2O_3” *J Therm Anal Calorimetery* 102, 709–713, 2010.

[230] V. Kumaresan, and R. Velraj, “Experimental investigation of the thermo-physical properties of water-ethylene glycol mixture based CNT nanofluids, Thermochemic” *Acta* 545, 180-186, 2012.

[231] S.M. Peyghambarzadeh, S.H. Hashemabadi, M.S. Jamnani, and S. M. Hoseini, “Improving the cooling performance of automobile radiator with Al2O3 nanofluid” *Appl Therm Eng* 31, 1833-1838, 2011.

[232] R.S. Vajjha, D.K. Das, and P.K. Namburu, “Numerical study of fluid dynamic and heat transfer performance of Al2O3 and CuO nanofluids in the flat tubes of a radiator” *Int J Heat Fluid Flow* 31, 613-621, 2010.

[233] Y.A. Reddy, and S. Venkatachalapathy, “Heat transfer enhancement studies in pool boiling using hybrid nanofluids” Thermochimic*Acta* 672, 93-100, 2019.

[234] S. Gharbi, S. Harmand, and S. B. Jabrallah, “Experimental comparison between different configurations of PCM based heat sinks for cooling electronic components” *Appl Therm Eng* 87, 454–462, 2015.

[235] L. Zhao, Y. Xing, and X. Liu, “Experimental investigation on thermal management performance of heat sink using low melting point alloy as phase change material” *Renew Energy* 146, 1578-1587, 2020.

[236] T.P. Teng, C.M. Cheng, and C.P. Cheng, “Performance assessment of heat storage by phase change materials containing MWCNTS and graphite” *Appl Therm Eng* 50 (1), 637-644, 2013.

[237] X. Yang, P. Wei, G. Liu, Q. Bai, and Y. He, “Performance evaluation on the gradient design of pore parameters for metal foam and pin fin-metal foam hybrid structure” *Appl Therm Energy* 175, 115416, 2020.

[238] Y. Li, L. Gong, M. Xu, and Y. Joshi, “Enhancing the performance of aluminum foam heat sinks through integrated pin fins” *Int J Heat Mass Transf* 151, 119376, 2020.

[239] L.W. Fan, Z.Q. Zhu, Y. Zeng, Y.Q. Xiao, X.L. Liu, Y.Y. Wu, Q. Ding, Z.T. Yu, and K.F. Cen, “Transient performance of a PCM-based heat sink with high aspect-ratio carbon nanofillers” *Appl Therm Eng* 75, 532–540, 2015.

Appendix I

Uncertainty analysis

Here, a test facility has been designed that includes a PCM-based heat sink assembly, power supply scheme, instrumentation scheme, and a solid-liquid interface tracking system. Various parameters such as length, width, and thickness of the heat sink, the temperature of the heat sink base and PCM, supply voltage and current, are measured during the experiment. The deviation in measured quantities initiates error in test results. Therefore, in the present experimental investigation, calibrated instruments are used to minimize errors in measurements.

Following the approach proposed by Cole-man and Steele [I.1], an error analysis method is used to estimate the errors associated with various parameters and explained below.

If R is a dependent variable and is a function of n independent variables, it can be expressed as:

$$R = f(v_1, v_2, v_3, \dots\dots\dots v_n) \tag{I.1}$$

Let the uncertainties associated with independent variables be $e_1, e_2, e_3, \dots\dots\dots e_n$ and resulting uncertainty (e) can be expressed as:

$$e = \left[\left\{\left(\frac{\partial R}{\partial v_1}e_1\right)^2 + \left(\frac{\partial R}{\partial v_2}e_2\right)^2 + \left(\frac{\partial R}{\partial v_3}e_3\right)^2 +.\dots\dots\dots.. \left(\frac{\partial R}{\partial v_n}e_n\right)^2\right\}\right]^{1/2} \tag{I.2}$$

Error in basic quantity

Here, in the experimental investigation, a DC power supply (Aplab L3260, 0-32V/0-60A, India) is utilized to supply the required electrical power to the plate heater. The readings of current and voltage are displayed by the DC power supply and are verified using a standard digital multimeter (Mecco 206). The dimensions of the test sections are measured by using a vernier caliper, and the temperature of the PCM-based heat sink assembly is measured by K-type thermocouples.

The following equation is used to estimate the input heat flux (q'') to the heat sink assembly.

$$\text{q"} = \frac{V \times I}{l \times w} \tag{I.3}$$

Where V is the voltage supplied by the DC power source in volts, I is the current in amps, l is the length of the heater, and w is the width of the heater. The plate heater used in this study has a length and width of 100 mm each.

Table I.1 Error associated with measurement of various parameters

Parameter	**Error**
Length ($\boldsymbol{l}$)	0.02 mm
Width ($\boldsymbol{w}$)	0.02 mm
Height ($\boldsymbol{h}$)	0.02 mm
Temperature ($\boldsymbol{T}$)	±0.2°C
Voltage ($\boldsymbol{V}$)	±0.1 V
Current ($\boldsymbol{I}$)	±0.1 A

Table I.1 shows the individual uncertainties associated with various measuring parameters such as V, I, l, w, h, and T. The uncertainty in the estimated result for heat flux (q") is given below; The uncertainty in heat flux is calculated as follows.

$$q'' = \mathrm{f}(V, I, l, w) \tag{I.4}$$

The errors involved in V, I, l, and w are e_V, e_I, e_l, and e_w, respectively. The uncertainty in supplied heat flux ($e_{q''}$) is calculated by using Eq. (I.2) as:

$$\frac{e_{q"}}{\text{q"}} = \frac{1}{\text{q"}}\left[\left\{\left(\frac{\partial q"}{\partial V} e_v\right)^2 + \left(\frac{\partial q"}{\partial I} e_I\right)^2 + \left(\frac{\partial q"}{\partial l} e_l\right)^2 + \left(\frac{\partial q"}{\partial w} e_w\right)^2\right\}\right]^{1/2} \tag{I.5}$$

$$\frac{e_{q''}}{q''} = \left[\left\{\left(\frac{e_v}{V}\right)^2 + \left(\frac{e_I}{I}\right)^2 + \left(\frac{e_l}{l}\right)^2 + \left(\frac{e_w}{w}\right)^2\right\}\right]^{1/2} \quad (I.6)$$

(a) *Uncertainty in supplied heat flux* $q'' = 1.5\ kW/m^2$

Here, V = 7.9 V, I = 1.9 A, the Eq. (I.6) can be written as:

$$\frac{e_{q''}}{q''} = \left[\left\{\left(\frac{0.1}{7.9}\right)^2 + \left(\frac{0.1}{1.9}\right)^2 + \left(\frac{0.02}{100}\right)^2 + \left(\frac{0.02}{100}\right)^2\right\}\right]^{1/2} \quad (I.7)$$

$$\frac{e_{q''}}{q''} = 0.0541 \quad (I.8)$$

$$e_{q''}\% = 5.41\% \quad (I.9)$$

(b) *Uncertainty in supplied heat flux* $q'' = 2.0\ kW/m^2$

Here, V = 8.7 V, I = 2.3 A, the Eq. (I.6) can be written as:

$$\frac{e_{q''}}{q''} = \left[\left\{\left(\frac{0.1}{8.7}\right)^2 + \left(\frac{0.1}{2.3}\right)^2 + \left(\frac{0.02}{100}\right)^2 + \left(\frac{0.02}{100}\right)^2\right\}\right]^{1/2} \quad (I.10)$$

$$\frac{e_{q''}}{q''} = \left[\left\{\left(\frac{0.1}{9.6}\right)^2 + \left(\frac{0.1}{2.1}\right)^2 + \left(\frac{0.02}{100}\right)^2 + \left(\frac{0.02}{100}\right)^2\right\}\right]^{1/2} \quad (I.11)$$

$$\frac{e_{q''}}{q''} = 0.0450 \quad (I.12)$$

$$e_{q''}\% = 4.50\% \quad (I.13)$$

(c) *Uncertainty in supplied heat flux* $q'' = 2.5\ kW/m^2$

Here, V = 10 V, I = 2.5 A, the Eq. (I.6) can be written as:

$$\frac{e_{q''}}{q''} = \left[\left\{\left(\frac{0.1}{10}\right)^2 + \left(\frac{0.1}{2.5}\right)^2 + \left(\frac{0.02}{100}\right)^2 + \left(\frac{0.02}{100}\right)^2\right\}\right]^{1/2} \tag{I.14}$$

$$\frac{e_{q''}}{q''} = 0.0412 \tag{I.15}$$

$$e_{q''}\% = 4.12\% \tag{I.16}$$

(d) *Uncertainty in supplied heat flux q"* $= 3.0\ kW/m^2$

Here, V = 10.8 V, I = 2.8 A, the Eq. (I.6) can be written as:

$$\frac{e_{q''}}{q''} = \left[\left\{\left(\frac{0.1}{10.8}\right)^2 + \left(\frac{0.1}{2.8}\right)^2 + \left(\frac{0.02}{100}\right)^2 + \left(\frac{0.02}{100}\right)^2\right\}\right]^{1/2} \tag{I.17}$$

$$\frac{e_{q''}}{q''} = 0.0368 \tag{I.18}$$

$$e_{q''}\% = 3.68\% \tag{I.19}$$

The error involved for q''=1.5 kW/m^2, 2.0 kW/m^2 and 2.5 kW/m^2, is found to be 5.41%, 4.50%, 4.12% and 3.96%, respectively (as shown in Eq. I.9, I.13, I.16, and I.19).

Additional Reference

[I.1] H.W. Coleman, and W.G. Steele, Experimental and uncertainty analysis for engineers, New York: Wiley, 1989.

Appendix II

Specifications of equipment

Items	Details	Pictorial View
CNC milling	Make: EMCO MAIER G.M.B.H. AUSTRIA; Model: EMCOMILL E 350; Specifications: Controller: **Sinumerik 828D** from Siemens; X-axis travel: 150 - 300 mm; Y-axis travel: 150 - 300 mm; Z-axis travel: 150 - 300 mm	
Data Acquisition System	Make: Agilent; Model: 34972-A; Maximum up to 60 channels	
Differential Scanning calorimeter	Make: Perkin Elmer; Model: DSC8000 Temp. range: -50 to 700 °C	
DC Power source	Make: Aplab; Model: L3260; Operating voltage: 0-32V; Operating current: 0-60A	

Heater

Make: Sunrise Product:

Maximum heat flux: 15.0 kW/m^2

CNC wire cut EDM

Make: EMCO Electronica India;

Model: ELPULS 15, Ecocut;

Specifications: Controller: **Sinumerik 828D** from Siemens;

X-axis travel: 250 mm;
Y-axis travel: 350 mm;
Z-axis travel: 150 mm

Scanning Electron Microscope (SEM)

Make: Carl ZEISS;

Model: Supra 55

Resolution: 1.0 nm @ 15 kV, 1.7 nm @ 1 kV, 4.0 nm @ 0.1 kV;

Operating voltage range: 0.02-30 kV

Vacuum Oven	Make: MLE make; Model: RS44; Control Logic : PID; Power supply : 90~270 VAC, 50/60 Hz.	
Thermocouple welding machine	Make: Quality Machine Tools; Specification: Welding range: Dia. 1.2×2 (175 J) Charging Voltage: 10-45 V.D.C. Input power: 230 VOLTS 5 AMPS A.C.	

List of Publication

(A) Publication from Ph.D. thesis work:

A1. In Refereed Journals (Accepted/Published)

1. **A. Kumar**, R. Kothari, S. K. Sahu, and S. I. Kundalwal, A comparative study and optimization of phase change material based heat sinks for thermal management of electronic components, *Journal of Energy Storage*, 43 (2021) 103224. *(IF=6.583)* https://doi.org/10.1016/j.est.2021.103224
2. **A. Kumar**, R. Kothari, S. K. Sahu, and S. I. Kundalwal, An experimental study on melting heat transfer of NePCM for thermal management of electronic devices, *Microelectronics Reliability* 121 (2021). *(IF = 1.589)* https://doi.org/10.1016/j.microrel.2021.114144
3. **A. Kumar**, R. Kothari, S. K. Sahu, S. I. Kundalwal, and M.P. Paulraj, Numerical simulation of cross plate fin heat sink filled with PCM for cooling application of portable electronic devices, *International Journal of Energy Research, 45 (2021) 8666-8683. (IF = 5.164)* https://doi.org/10.1002/er.6404
4. **A. Kumar**, R. Kothari, S. K. Sahu, and S. I. Kundalwal, Selection of phase change material for thermal management of electronic devices using multi-attribute decision making technique, *International Journal of Energy Research*, 45 (2021) 2023–2042. *(IF = 5.164).* https://doi.org/10.1002/er.5896
5. **A. Kumar**, R. Kothari, V. Saxena, S.K. Sahu, and S.I. Kundalwal, Experimental investigation on paraffin wax based heat sinks with cross plate fin arrangement for cooling of electronic components, *Journal of Thermal Analysis and Calorimetry*, (2022) (IF=4.626). https://doi.org/10.1007/s10973-022-11223-9

A2. In Refereed Journals (to be submitted)

1. **A. Kumar**, V. Saxena, R. Kothari, S. K. Sahu, S. I. Kundalwal, A. A. Chitre, and A. K. Singh, Numerical investigation of hollow pin fin heat sink integrated with phase change material for cooling application of portable electronic devices.

2. A. Kumar, R. Kothari, Vivek Saxena, Akhalesh Sharma, S. K. Sahu, and S. I. Kundalwal, Sai P. Surapu, Experimental investigation of orthotropic plate fin heat sink integrated with phase change material for cooling application of satellite avionic

A3. In Referred Conferences

1. **A. Kumar**, R. Kothari, S. K. Sahu, and S. I. Kundalwal, Effect of CuO nanoparticle in PCM integrated heat sink for thermal management of electronic component: An experimental study. *25th National and 3rd International ISHMT-ASTFE Heat and Mass Transfer Conference, IHMTC-2019,* IIT Roorkee, December 28-31, 2019.
2. **A. Kumar**, R. Kothari, P. K. Singh, M. P. Paulraj, S. K. Sahu, and S. I. Kundalwal, Numerical simulation of PCM based heat sink with plate fins for thermal management of electronic components. *International Conference on Innovations in Thermo-Fluid Engineering and sciences (ICITFES-2020),* NIT Rourkela, February 10-12, 2020.
3. **A. Kumar**, R. Kothari, P. K. Singh, R. Vaidya, S. K. Sahu, and S. I. Kundalwal, Thermal performance Enhancement of PCM Based Cross Plate Finned Heat Sink for Electronic Cooling, *Proceedings of the 8th International and 47th National Conference on Fluid Mechanics and Fluid Power (FMFP2020-95),* IIT Guwahati, December 09-11, 2020.
4. **A. Kumar**, R. Kothari, S. K. Sahu, S. I. Kundalwal, and A. Sharma, Investigation of phase change material integrated with high thermal conductive carbon foam inside heat sinks for thermal management of electronic components, *Proceedings of the ASME 2021 Power Conference (POWER2021-65569),* Anaheim, CA, USA, July 18-22, 2021. https://doi.org/10.1115/POWER2021-65569 **(*Winner of Qualified Student Award by ASME)***
5. **A. Kumar**, A. A. Chitre, A. K. Singh, R. Kothari, S. K. Sahu, and S. I. Kundalwal, Thermal performance investigation of phase change material based heat sinks with hollow fins for cooling of electronic devices,

International Conference on *"Latest Trends in Civil, Mechanical and Electrical Engineering" (LTCMEE- 257)*, MANIT Bhopal, April 12-13, 2021.

6. **A. Kumar**, A. K. Singh, A. A. Chitre, R. Kothari, V. Saxena, S. K. Sahu, and S. I. Kundalwal, Thermal performance of PCM based heat sink with solid and hollow fins for thermal management of electronics, *Proceedings of the 26th National and 4th International ISHMT-ASTFE Heat and Mass Transfer Conference*, IIT Madras, December 17-20, 2021, (Abstract accepted)

A4. Book Chapters

1. **A. Kumar**, R. Kothari, P. K. Singh., M. P. Paulraj, S. K. Sahu, and S. I. Kundalwal, Numerical simulation of PCM based heat sink with plate fins for thermal management of electronic components, In: F. Cavas-Martinez, F. Chaari, F. Gherardini, M. Haddar, V. Ivanov, Y.W. Kwon, J. Trojanowska (Eds.), Lecture Series in Mechanical Engineering, 2021. https://doi.org/10.1007/978-981-33-4165-4_2

(B) Other publications during Ph.D.:

B1. In Refereed Journals (Under review/to be submitted)

1. V. Saxena, R. Kothari, **A. Kumar**, S. K. Sahu, S. I. Kundalwal, A new prediction model for the effective thermal conductivity of coated metal foams saturated with Phase change material, *International Journal of Energy Research, (EST-D-21-02424) (IF=5.164)* (Under review)
2. M. P. Paulraj, S. S. Chandel, **A. Kumar**, S. K. Sahu, Thermal and flow characteristics of Artificially Roughened Parallelogram Transverse Ribs on an Indirect Type Solar Dryer (ITSD). (To be submitted)

B2. In Refereed Conferences

1. R. Kothari, **A. Kumar**, P. K. Singh, S. K. Sahu, and S. I. Kundalwal, Analytical Model for Melting Process in a Rectangular Phase Change Material

Storage with Internal Fins, *Proceedings of the 25th National and 3rd International ISHMT-ASTFE Heat and Mass Transfer Conference (IHMTC-2019-203),* IIT Roorkee, December 28-31, 2019.

2. P. K. Singh, **A. Kumar**, A. Kishor, A. Shah, S. K. Sahu, P. K. Upadhyay, and S. Singh, Flow and Heat Transfer analysis of an axisymmetric Impinging Synthetic Jet for Electronic Cooling, *Proceedings of the International Conference on Innovations in Thermo-Fluid Engineering and Sciences (ICITFES2020-13724)*, NIT Rourkela, February 10-12, 2020.
3. M.P. Paulraj, A.K. Sharma, **A. Kumar** and S. K. Sahu, Experimental Investigation of Heat Transfer Enhancement on Impinging Jet Cooling Using Surface Laser Treatment, *Proceedings of the 46th national conference on fluid mechanics and fluid power (FMFP-2019),* PSG College of Technology Coimbatore, December 9-11, 2019.
4. J. Sutradhar, R. Kothari, **A. Kumar**, and S. K. Sahu, Study of solidification process of PCM with shrinkage void effect in an annulus, *Proceedings of the 8th International and 47th National Conference on Fluid Mechanics and Fluid Power (FMFP2020-164),* IIT Guwahati, December 09-11, 2020.
5. A. Sharma, R. Kothari, **A. Kumar**, and S. K. Sahu, Effect of fin orientation on PCM melting in a spherical enclosure for latent heat storage, *Proceedings of the ASME 2021 Power Conference (POWER2021-10495)*, Anaheim, CA, USA, July 18-22, 2021. https://doi.org/10.1115/POWER2021-65622
6. V. Saxena, R. Kothari, **A. Kumar**, S. K. Sahu, and S. I. Kundalwal, Theoretical Modeling for the effective thermal conductivity of open-cell metal foams infiltrated with phase change material, *Proceedings of 15th International Conference on Heat Transfer, Fluid Mechanics and Thermodynamic (ATE-HEFAT2021),* Virtual conference, July 25-28, 2021.
7. V. Saxena, H. Dey, **A. Kumar**, A. Sharma, S. K. Sahu, and S. I. Kundalwal, Numerical investigation of a phase change material enhanced Li-ion battery pack using the dual potential multi-scale multi-dimensional (MSMD) approach, *Proceedings of the 26th National and 4th International ISHMT-*

ASTFE Heat and Mass Transfer Conference, IIT Madras, December 17-20, 2021.

B3. Poster Presentation at National and International Symposium

1. **A. Kumar**, R. Kothari, S. K. Sahu, and S. I. Kundalwal, Development of light weight heat sink integrated with phase change material (PCM) for cooling application, Second *International Meeting on Clean Energy Material Innovation challenge (IC6)*, New Delhi, February 2019.
2. **A. Kumar**, R. Kothari, S. K. Sahu, and S. I. Kundalwal, Development of light weight heat sink integrated with phase change material (PCM) for cooling application, *Industry academia conclave on energy storage*, MNIT Jaipur, November 30, 2019.

ANUJ KUMAR

ADDRESS

53/1/A,
Ram Lochan Sayar Street, Belur
Howrah-711202,
West Bengal, India

Mobile: +91 8961728971

Email: kumaranujshaw@gmail.com
phd1801103004@iiti.ac.in

https://www.researchgate.net/profile/Anuj-Kumar-81

https://www.linkedin.com/in/anuj-kumar-031704165/

https://orcid.org/0000-0001-8017-5430

EDUCATION

Indian Institute of Technology Indore **Indore, India**

- ***Ph.D.*** 2018-2021
  Mechanical Engineering
  Advisor: Dr. S. K. Sahu and Dr. S. I. Kundalwal

Indian Institute of Technology (Indian School of Mines) Dhanbad **Dhanbad, India**

- ***Master of Technology*** (CGPA 8.46/10) 2016- 2018
  Mechanical Engineering (Specialization: Thermal Engineering)
  Advisor: Dr. S. K. Ghosh

MCKV Institute of Engineering **Howrah, India**

- ***Bachelor of Engineering*** (8.36/10) 2010- 2014
  Automobile Engineering

Ph.D. OBJECTIVES

- Selection of phase change material (PCM) for thermal management of electronic components employing different multi attributes decision making technique.
- Design and development of a test facility involving various modules such as: test section, the scheme for orientation of the test specimen, the instrumentation scheme: temperature measurement.
- Investigate the thermal performance of heat sinks incorporating the combined effects of fin number, fin shape and heat flux values.

- Study the thermal performance of PCM based heat sinks with combination of different thermal conductivity enhancers (TCEs) such as fins, metal/non-metal foam and nano particles.
- To study the conjugate heat transfer of PCM based heat sinks involving fins through CFD numerical technique.
- Determining the various thermophysical properties of PCM and nano-enhanced PCM.

CURRENT TEACHING ASSISTANCE EXPERIENCE

- Fluid Mechanics and Machinery (ME 204: Spring 2019; tutorial)
- Fluid Mechanics and Machinery Lab (ME 254: Spring 2019; tutorial)
- Fluid Mechanics (ME 203: autumn 2020; tutorial)
- Fluid Mechanics and Machinery (ME 204: Spring 2021; tutorial)
- Fluid Mechanics and Machinery Lab (ME 254: 2021; spring practical)

PAPER PRESENTED IN CONFERENCES

- *25th National and 3rd International ISHMT-ASTFE Heat and Mass Transfer Conference, IHMTC-2019,* IIT Roorkee, December 28-31, 2019.
- *International Conference on Innovations in Thermo-Fluid Engineering and sciences (ICITFES-2020),* NIT Rourkela10-12 February 2020.
- *8th International and 47th National Conference on Fluid Mechanics and Fluid Power (FMFP2020-95),* IIT Guwahati, December 09-11, 2020.
- *ASME 2021 Power Conference (POWER2021-65569), Anaheim, CA, USA, July 18-22, 2021*.
- *International Conference on "Latest Trends in Civil, Mechanical and Electrical Engineering" (LTCMEE- 257),* MANIT Bhopal, April 12-13, 2021.
- *26th National and 4th International ISHMT-ASTFE Heat and Mass Transfer Conference,* IIT Madras December 17-20, 2021.

HONORS AND AWARDS/ACHIEVEMENT

- Contributed in successful completion of **DST, GOI** project entitled "Development of light weight heat sink integrated with phase change material (PCM) for cooling applications"
- Research article selected as **Qualified Student Award Winner** of the student paper competition in the ASME Power conference, *Anaheim, CA, USA, July 18-22, 2021*.
- Co-author in **Qualified Student Award Winner** paper of the student paper competition in the ASME Power conference, *Anaheim, CA, USA, July 18-22, 2021*.

- Qualified GATE 2016, 2017,
- Completed Bachelor of Technology Degree with **2nd rank** in 2014 batch.

COMPUTER SKILLS

Application Softwares:

CAD Packages	AutoCAD, ProE, SolidWorks
Analysis Packages	ANSYS, MATLAB, LAMMPS, Origin Pro, DataFit, Minitab
Programming Languages:	Basic level in C, C++

PERSONAL DETAILS

Date of Birth	June 04, 1992 (Jharkhand, India)
Nationality	Indian
Sex	Male
Religion	Hinduism
Marital Status	Unmarried
Phone	+91-8961728971
Permanent Address	53/1/A, Ram Lochan Sayar Street, Belur, Howrah–711202 (WB), India
Languages known	English, Hindi, Bengali